



2023

Murine Tbk1 is Required by FLT3+ Leukemia Stem Cells Yet Dispensable in Homeostatic Hematopoiesis

Austin Runde
Loyola University Chicago

Follow this and additional works at: https://ecommons.luc.edu/luc_theses

 Part of the [Medicine and Health Sciences Commons](#)

Recommended Citation

Runde, Austin, "Murine Tbk1 is Required by FLT3+ Leukemia Stem Cells Yet Dispensable in Homeostatic Hematopoiesis" (2023). *Master's Theses*. 4467.
https://ecommons.luc.edu/luc_theses/4467

This Thesis is brought to you for free and open access by the Theses and Dissertations at Loyola eCommons. It has been accepted for inclusion in Master's Theses by an authorized administrator of Loyola eCommons. For more information, please contact ecommons@luc.edu.



This work is licensed under a [Creative Commons Attribution-NonCommercial-No Derivative Works 3.0 License](#).
© 2023 Austin Runde

LOYOLA UNIVERSITY CHICAGO

MURINE *TBK1* IS REQUIRED BY FLT3⁺ LEUKEMIA STEM CELLS YET
DISPENSABLE IN HOMEOSTATIC HEMATOPOIESIS

A THESIS SUBMITTED TO
THE FACULTY OF THE GRADUATE SCHOOL
IN CANDIDACY FOR THE DEGREE OF
MASTER OF SCIENCE

PROGRAM IN CELLULAR AND MOLECULAR ONCOLOGY

BY

AUSTIN PATRICK RUNDE

CHICAGO, IL

AUGUST 2023

Copyright by Austin Patrick Runde, 2023
All rights reserved.

ACKNOWLEDGEMENTS

I would like to thank my mentor and someone I have come to know as a dear friend—*Dr. Jiwang Zhang*—for his mentorship, humor, tenacity, and faith in me as he coached me through the entirety of this research and the completion of my degree.

I would like to thank my thesis committee—*Dr. Nancy Zeleznik-Le, Dr. Clodia Osipo, Dr. Mitch Denning, and Dr. Jiwang Zhang*—for their time, attentiveness, responsiveness, and direction.

I would like to thank my Zhang lab colleagues—*Wei Wei, Ryan Mack, Kanak Joshi, MS, Mark Sellin, Allan Youmaran, and Fr. Peter Breslin, S.J., MD/PhD*—for their instruction, advice, and camaraderie.

I would like to thank my current and former MS CMO program directors—*Dr. Maurizio Bocchetta and Dr. Clodia Osipo*, respectively—for their guidance and accepting me into the program.

I would like to thank additional faculty members, staff, friends, and colleagues in the Cardinal Bernardin Cancer Center, LUMC, and the CTRE—*Lorelei Martin, MSW, Sue Niccolai, Kristen Young, Govinda Hancock, Karen Chang, Rachel Mazurek, Nick Achille, Janani Prakash, Lola Badmus, Claudia Rose Keating, Sana Iqbal, Emily Krueger, Saira Khurana, Brenna Flowers, Yoldas Yildiz, Rasa Valiauga, Suzanne Quinn, Oliwia Bochnaka, Annie Sullivan, Pat Simms, Corbin Pomykata, Bert Ladd, Dr. Valerie Chai, Dr. Sean Fanning, Dr. Phong Le, Shubin Zhang, Dr. Ali Vaziri-Gohar, Dr. Bill Adams, Dr. Yee Ling Wu, Dr. Simon Kaja, Susan*

Blatchford, Diane Palmer, Anne Rocconi, Dr. Farshid Azarafrooz, Siobhan Nolan, Rose Buesing, Chrissie Stauton, Lourdcy Pazhampally, Dr. Maria Picken, Dr. Xianzhong Ding, Matt Hejna, MS, Ann Kennedy, Margarita Quesada, Anna Dauzvardis, and finally, Mrs. Mel Bollnow, MS—for their kindness, assistance, and dedication to learning & research.

I would like to thank my first PI—*Dr. Rodney M. Dale*—for introducing me to the field of biological research and constantly pushing me to believe in myself.

I would like to thank my family—*Janet, Dan, & Laney Runde, The Wegman Families, The Brandli Family, The Barr Family, The Runde Families, and Eleanor & Donald Wegman*—and closest friends—*The Grimm Family, Drew Licar, Adan & Cesar Perez, Gracie Sizemore, Chris & Adam Pagan, Eric Santana, Nate Berclaw, Julia Sanchez, Joey Laurx, Jem Hughes, Jerica Cyr, The Needler Family, and Mel Moynihan*—for being and always having been my biggest supporters. I hope all of you know how appreciated and loved you are, and how lucky I am to have you in my life.

Finally—I would like to thank anyone I may have neglected to mention, anyone who has helped me along my journey in any way, directly or indirectly: thank you very much.

Dedicated to my greatest source of inspiration—my family.

It's not whether you get knocked down; it's whether you get up.

Vince Lombardi

PREFACE

Acute myeloid leukemia (AML) is a devastating disease that carries a dismal prognosis. Despite typically being responsive to frontline chemotherapy, AML often returns in the form of a treatment-resistant disease that is fatal without a hematopoietic stem cell transplant (HSCT). While curative, HSCT donors are difficult to find and the transplant process itself exposes patients to chemotherapy and/or radiation. Additionally, a significant portion of AML patients present with refractory disease, failing to respond to frontline chemotherapy altogether.

While targeted therapies are available for select patient populations, these drugs currently serve only to augment chemotherapy and are still inferior to standard-of-care regimens; thus, the search to find the “*Gleevec*® for AML” continues.

Our research is an effort to find a targeted therapy for AML that is effective in all patient populations regardless of mutation status, immunophenotype, and patient fitness. Our goal is to discover a therapy that can serve to augment or replace cytotoxic chemotherapy, sparing patients from the harsh effects of cytotoxic therapy while still helping them achieve and maintain remission.

TABLE OF CONTENTS

ACKNOWLEDGEMENTS	iii
PREFACE	vi
LIST OF FIGURES	xii
LIST OF TABLES	xvi
LIST OF ABBREVIATIONS	xvii
ABSTRACT	xxv
CHAPTER 1: TARGETING THE LEUKEMIA STEM CELL: AN UNMET CLINICAL NEED	1
Introduction	1
Aim 1: Determine if <i>Tbk1</i> is Required for Murine Hematopoiesis	3
Aim 2: Determine if <i>Tbk1</i> Blockade Could be a Means of Anti-AML Therapy	4
CHAPTER 2: LITERATURE REVIEW AND PROJECT RATIONALE	5
Structure of TBK1	5
Genetic and Protein-level Regulation of TBK1	7
Function of TBK1	12
<i>TBK1</i> Mutations in Disease	20
Role of TBK1 in Cancer	23
TBK1 Inhibitors in Cancer Treatment	26
Overview of AML	28
Subtypes of AML	30
Pathophysiology of AML	32
Conventional Treatment of AML	34
Targeted Therapies for AML	36
Targeting TLR Signaling to Treat AML	37
TBK1 as a Molecular Target for AML Treatment	40
CHAPTER 3: AIM 1: DETERMINE IF TBK1 IS REQUIRED FOR MURINE HEMATOPOIESIS	45
Results: Global <i>Tbk1</i> Deletion in Murine Hematopoiesis	45
<i>TBK1</i> mRNA Expression Levels Appear Somewhat Consistent Across the Human and Murine Hematopoietic Systems	45
Development of a Tamoxifen-inducible, Global <i>Tbk1</i> -knockout Mouse	49
<i>Tbk1</i> Deletion is Complete in the Bone Marrow of a 6-week-old Mouse	51
<i>Tbk1</i> ^{NULL} Mice Do Not Display Changes in Levels of Mature Blood Cells nor Erythroid Precursors	53
<i>Tbk1</i> ^{NULL} Mice Display a Significant Increase in the Myeloid-Biased MPP3 Population of HSPCs	56

<i>Tbk1</i> ^{NULL} Mice Do Not Display Changes in Levels of Specific Myeloid Progenitors	58
<i>Tbk1</i> ^{NULL} Mice Display a Significant Increase in Circulating Neutrophils	60
<i>Tbk1</i> ^{NULL} Mice Do Not Display Significant Changes in Spleen nor Thymus Mass	62
<i>Tbk1</i> ^{NULL} Mice Display Histologic Abnormalities in the Spleen and Kidney	63
Results: Competitive Transplantation of <i>Tbk1</i> ^{NULL} Whole Bone Marrow	70
Loss of <i>Tbk1</i> in Whole Bone Marrow Does Not Affect Engraftment Ability of HSPCs	70
Loss of <i>Tbk1</i> in Whole Bone Marrow Does Not Affect Lymphopoiesis	74
Loss of <i>Tbk1</i> in Whole Bone Marrow Transiently Hampers Granulopoiesis but Not Monopoiesis	75
Loss of <i>Tbk1</i> in Whole Bone Marrow Does Not Affect Recovery of Mature Blood Cells nor Erythroid Progenitors	76
Loss of <i>Tbk1</i> in Whole Bone Marrow Does Not Significantly Affect HSPCs	77
Loss of <i>Tbk1</i> in Whole Bone Marrow Does Not Significantly Affect Specific Myeloid Progenitors	78
Loss of <i>Tbk1</i> in Whole Bone Marrow Causes Increased Monocytes	80
<i>Tbk1</i> Deletion is Revealed to be Incomplete at 4 and 7 Months-post-tamoxifen	81
Aim 1 Conclusion: <i>Tbk1</i> is Dispensable in Short-term, Homeostatic Hematopoiesis	84
CHAPTER 4: AIM 2 DETERMINE IF TBK1 BLOCKADE COULD BE A MEANS OF ANTI-AML THERAPY	86
Results	86
MLL-AF9 Induces Increased Expression of <i>Tbk1</i> mRNA	86
<i>Tbk1</i> May Confer a Survival Advantage to <i>MLL-AF9</i> ⁺ HSPCs	88
<i>In Vitro</i> Treatment with 1uM 4-OHT for 4 Days Yields Complete Deletion of <i>Tbk1</i>	92
Based on Morphology, <i>Tbk1</i> ^{NULL} <i>MLL-AF9</i> ⁺ Cells Seem to be More Differentiated	93
<i>Tbk1</i> ^{NULL} <i>MLL-AF9</i> ⁺ HSPCs Proliferate Faster	96
<i>Tbk1</i> ^{NULL} <i>MLL-AF9</i> ⁺ HSPCs Show a Trend Toward Reduced Clonogenicity	99
<i>Tbk1</i> ^{NULL} <i>MLL-AF9</i> ⁺ HSPCs are Sensitized to Serum Starvation	101
c-Kit ⁺ Flt3 ⁺ <i>MLL-AF9</i> ⁺ HSPCs are Resistant to DNO but Not Ara-C	103
<i>Tbk1</i> Regulates <i>MLL-AF9</i> ⁺ LSCs	106
c-Kit ⁺ Flt3 ⁺ <i>MLL-AF9</i> ⁺ cells are Promoted by AMX	108
GSK8612 has Variable Effects on <i>MLL-AF9</i> ⁺ LSCs	110
Loss of <i>Tbk1</i> Causes Increased Expression of c-Fms on <i>MLL-AF9</i> ⁺ HSPCs	112
c-Fms Upregulation Occurs Independently of c-Kit Status on <i>Tbk1</i> ^{NULL} <i>MLL-AF9</i> ⁺ HSPCs	114

Tbk1 and IKK ϵ May Act Oppositely in Regulating c-Fms expression on <i>MLL-AF9</i> ⁺ HSPCs	116
GSK8612 Promotes the c-Kit ⁺ Flt3 ⁺ c-Fms ^{hi} Population of <i>MLL-AF9</i> ⁺ HSPCs	118
Loss of <i>Tbk1</i> in Transplanted <i>MLL-AF9</i> ⁺ HSPCs Causes Chloroma in B6 Mice	120
Aim 2 Conclusion: <i>Tbk1</i> is Required by c-Kit ⁺ Flt3 ⁺ <i>MLL-AF9</i> ⁺ HSPCs and May Prevent Chloroma in <i>MLL-AF9</i> ⁺ AML	137
 CHAPTER 5: DISCUSSION	 139
Summary	139
Future Directions	141
Closing	144
 CHAPTER 6: METHODS	 147
Mice	147
Generation of <i>Tbk1</i> ^{fx/fx} ; <i>Rosa26</i> -CreER ^{T2+} Mice	147
<i>In Vivo</i> Deletion of <i>Tbk1</i>	149
Isolation of CD117/c-Kit ⁺ Mouse BM Cells (HSPCs)	149
Mouse Pre-transplant Conditioning Regimen	150
Mouse Post-transplant Antibiotic Prophylaxis	150
<i>In Vivo</i> AML Mouse Model	151
Harvest of Mouse BM	151
Harvest of Mouse PB	151
Agarose Gel Electrophoresis	152
Bacterial Transformation and Plasmid Isolation	152
Creation of 293T Transfection Reagent	153
293T Transfection and Collection of Retroviral Supernatant	154
Retroviral Transduction (Spinduction/Spinoculation) of Mouse HSPCs	154
<i>Ex Vivo</i> Culture of Mouse HSPCs	155
<i>In Vitro</i> Knockout of <i>Tbk1</i>	156
Growth Curve Analysis	156
Serum Starvation	156
Clonogenicity Assay	157
70% EtOH Fixation and Cell Cycle Analysis	157
Polymerase Chain Reaction (PCR)	158
RNA Isolation	162
DNase I Treatment and Reverse Transcriptase PCR (RT-PCR)	163
Quantitative PCR (qPCR)	164
Isolation of gDNA from Mouse Tails	165
DNA Quantitation	167
DNA Precipitation from H ₂ O	167
Statistical Analyses	168
Cell Counting	168
Western blot/Immunoblot	168
Hematology Analysis of Mouse PB	171

Photographs	171
Histology	171
Cytocentrifuge	172
<i>Hema 3</i> [®] Kit	172
Figures	173
Drug Treatments	173
Drugs	173
Lysis of RBCs/Hemolysis	175
Fluorescence-activated Cell Sorting (FACS [Flow Cytometry]) Analyses	175
MilliQ ddH ₂ O Water	179
Open Researcher and Contributor ID (ORCID) iD	179
REFERENCE LIST	180
VITA	205

LIST OF FIGURES

Figure 1. Schematic depicting the TBK1 Protein and its Domains.	6
Figure 2. Schematic depicting Upstream Regulators and Downstream Substrates/Pathways of TBK1.	13
Figure 3. TBK1 mRNA Expression is Negatively Correlated with AML Prognosis, based on Microarray Data.	42
Figure 4. TBK1 mRNA Expression Level is Somewhat Consistent Across the Human Hematopoietic System.	47
Figure 5. Tbk1 mRNA Expression Level is Somewhat Consistent Across the Murine Hematopoietic System.	48
Figure 6. Tbk1 ^{fx/fx} ;Rosa26-CreER ^{T2+} Mice are Generated.	50
Figure 7. Deletion of Tbk1 is Complete in the Bone Marrow.	53
Figure 8. Tbk1 Deletion Does Not Affect Levels of Mature Blood Cells nor Erythroid Progenitors in the PB or BM.	55
Figure 9. Representative Gating Strategies for FACS Analysis of Mature Blood Cell, Erythroid Precursors, and Megakaryocytes.	56
Figure 10. The MPP3 Population is Significantly Increased Following Tbk1 Deletion.	57
Figure 11. Deletion of Tbk1 Does Not Cause Significant Changes in Myeloid Progenitor Populations.	60
Figure 12. Tbk1 ^{NULL} Mice Display Increased Circulating Neutrophils.	62
Figure 13. Tbk1 ^{NULL} Mice Do Not Display Significant Changes in Spleen nor Thymus Mass.	63
Figure 14. Thymus of Tbk1 ^{NULL} Mouse Appears Grossly Normal.	65

Figure 15. Spleen of Tbk1 ^{NULL} Mouse Appears to Have Maldeveloped Germinal Centers.	66
Figure 16. Kidneys of Tbk1 ^{NULL} Mouse Appear Grossly Normal but Display Slight Proliferation of the Mesangial Cells.	68
Figure 17. Liver of Tbk1 ^{NULL} Mouse may have Mononuclear Cell Infiltration.	69
Figure 18. Schematic Depicting Competitive WBMT Protocol using Tbk1 ^{NULL} WBM and Downstream Analyses.	72
Figure 19. Loss of Tbk1 in WBM Does Not Influence Engraftment of HSPCs in Competitive Transplantation.	73
Figure 20. Representative FACS Gating Strategies for Donor & Mature Cell Analysis of PB-TNCs.	74
Figure 21. Loss of Tbk1 in WBM Does Not Influence Lymphopoiesis in Competitive Transplantation.	75
Figure 22. Loss of Tbk1 in WBM Transiently Hampers Granulopoiesis but Not Monopoiesis in Competitive Transplantation.	76
Figure 23. Loss of Tbk1 in WBM Does Not Affect Reconstitution of Mature Cells nor Erythroid Progenitors in the Bone Marrow.	77
Figure 24. Tbk1 Deletion in WBM Does Not Significantly Affect the Reconstitution of HSPCs.	78
Figure 25. Deletion of Tbk1 in WBM Does Not Affect Reconstitution of Myeloid Progenitors.	80
Figure 26. Loss of Tbk1 in WBM Causes Increased Monocytes and a Trend Toward Increased Lymphocytes and WBCs.	81
Figure 27. Tbk1 ^{fx} Allele is Detected in Mice Presumed to be Tbk1 ^{NULL} .	83
Figure 28. Schematic Depicting the Transfection of 293T cells, Generation of MSCV-puro-MLL-AF9 Retrovirus, and Isolation/Transduction of Mouse HSPCs.	87
Figure 29. MLL-AF9 Induces Increased Expression of Tbk1 mRNA in Mouse HSPCs.	88
Figure 30. Tbk1-retaining Cells are Enriched for in Serial M3434 Culture.	89

Figure 31. $Tbk1^{fx}$ Allele Reappears in MLL-AF9 ⁺ Cells Previously Determined to be $Tbk1^{NULL}$.	91
Figure 32. Treatment with 1uM 4-OHT for 4 Days in Liquid Media Yields Complete Deletion of $Tbk1$.	93
Figure 33. $Tbk1^{NULL}$ MLL-AF9 ⁺ Cells Appear More Differentiated Morphologically.	95
Figure 34. $Tbk1^{NULL}$ MLL-AF9 ⁺ Cells Proliferate Faster than $Tbk1^{WT}$ Counterparts.	98
Figure 35. $Tbk1^{NULL}$ MLL-AF9 ⁺ Cells Show a Trend Toward Reduced Clonogenicity.	100
Figure 36. $Tbk1^{NULL}$ MLL-AF9 ⁺ Cells are Sensitized to 24-hour Serum Starvation.	102
Figure 37. Treatment with Daunorubicin but Not Ara-C Enriches for $c\text{-Kit}^{+}Flt3^{+}$ MLL-AF9 ⁺ Cells.	104
Figure 38. Loss of $Tbk1$ Hampers the $c\text{-Kit}^{+}Flt3^{+}$ and $c\text{-Kit}^{+}CD11b^{lo}$ LSC Subsets of MLL-AF9 ⁺ cells.	108
Figure 39. $c\text{-Kit}^{+}Flt3^{+}$ MLL-AF9 ⁺ Cells are Increased by High-dose AMX.	109
Figure 40. $c\text{-Kit}^{+}Flt3^{+}$ MLL-AF9 ⁺ Cells are Increased with Low-dose GSK8612 and $c\text{-Kit}^{+}CD11b^{lo}$ Cells are Decreased with GSK8612 in a Dose-dependent Manner.	111
Figure 41. Representative Gating Strategies for FACS Analysis of AMX- or GSK8612-treated MLL-AF9 ⁺ Cells.	112
Figure 42. $Tbk1$ Negatively Regulates $c\text{-Fms}$ Expression on MLL-AF9 ⁺ Cells.	114
Figure 43. Increased $c\text{-Fms}$ Expression Following $Tbk1$ Deletion occurs in Both $c\text{-Kit}^{+}$ and $c\text{-Kit}^{-}$ Cells.	115
Figure 44. TBK1 and IKK ϵ May Act in Opposition in Regulating $c\text{-Fms}$ Expression.	117
Figure 45. GSK8612 Upregulates the $c\text{-Kit}^{+}Flt3^{+}c\text{-Fms}^{hi}$ Population of MLL-AF9 ⁺ Cells.	119
Figure 46. Schematic Depicting Models A and B in the In Vivo AML Study.	120

Figure 47. Schematic Depicting Conditioning and Transplant Protocol for our In Vivo Model of MLL-AF9 ⁺ AML.	122
Figure 48. Deletion of Tbk1 Does Not Prevent MLL-AF9 ⁺ AML.	125
Figure 49. Deletion of Tbk1 Ablates the c-Kit ⁺ FIt3 ⁺ Population of MLL-AF9 ⁺ Cells In Vivo.	127
Figure 50. Monocytic Chloroma of the Gallbladder by Alexiev, et al.	129
Figure 51. Tbk1 ^{NULL_A} Mouse Developed a Likely Chloroma, Secondary to MLL-AF9 ⁺ AML.	130
Figure 52. Tbk1 Deletion in AML Cells May Cause Decreased Blasts in the PB of Mice with MLL-AF9 ⁺ AML.	132
Figure 53. Loss of Tbk1 Does Not Prevent Hepatic Infiltration by AML Cells.	133
Figure 54. Loss of Tbk1 Does Not Prevent Splenic Destruction by AML Cells.	134
Figure 55. Tbk1 ^{NULL_B} Mouse Developed a Likely Chloroma, Secondary to MLL-AF9 ⁺ AML.	135
Figure 56. MLL-AF9 Exploits TLR/TNF-TBK1 Signaling to Upregulate Mitophagy.	146

LIST OF TABLES

Table 1. Select Post-translational Modifications of TBK1 and Effect on Protein Function, if Applicable (Adapted from Runde, et al.).	9
Table 2. Tissue Deletion Specificity, Tbk1 Deletion Strategy, and Phenotypes of Tbk1 ^{NULL} Mouse Models (Adapted from Runde, et al.).	17
Table 3. Select TBK1 Mutations, Associated Pathology, Effect on Protein (Mechanism), and Pathway Implicated, if Applicable.	21
Table 4. List of TBK1 Inhibitors (Adapted from Runde, et al.).	27
Table 5. Select Genes, P-value, Correlation with probability of OS in AML (if Applicable), and Microarray Probe Used.	105

LIST OF ABBREVIATIONS

129S5	129S5/SvEvBrd mouse background
4GFS	the Zhang lab's proprietary cocktail of IL-3, IL-6, GM-CSF, and SCF for the culturing of mouse HSPCs
4-OHT	4-hydroxytamoxifen/afimoxifene, a principal metabolite of tamoxifen
7+3	induction phase of AML frontline chemotherapy (7-day delivery of Ara-C + 3-day delivery of daunorubicin/idarubicin)
aa	amino acid(s)
AAALAC	Association for Assessment and Accreditation of Laboratory Animal Care
Ab	antibody
ACSL1	acyl-CoA synthetase long-chain family member 1
AEL	acute erythroid leukemia
AF9	protein AF-9/mixed-lineage leukemia; translocated to, 3 (<i>MLL T3</i>)/MLLT3 Super Elongation Complex Subunit/YEATS3
ALLFTD	ARTFL LEFFTDS Longitudinal Frontotemporal Lobar Degeneration/ NCT04363684
ALS	amyotrophic lateral sclerosis
AML	acute myeloid leukemia/acute myelogenous leukemia; acute non-lymphocytic leukemia (ANLL)
AMML	acute myelomonocytic leukemia
AMML Eo	acute myelomonocytic leukemia with eosinophilia
AMKL	acute megakaryoblastic leukemia
AMoL	acute monoblastic/monocytic leukemia
AML-MRC	AML with myelodysplasia-related changes
AML, NOS	AML, not-otherwise-specified
AMX	amlexanox/Amlx/ <i>Aphthaso</i> [®] /AA-67

ANLL	acute non-lymphocytic leukemia (see “AML”)
APL	acute promyelocytic leukemia (<i>PML-RARA</i> ⁺ AML)
APRIL	A proliferation-inducing ligand/ <i>TNFSF13</i>
Ara-C	cytarabine/cytosine arabinoside/1- β -D-Arabinofuranosylcytosine/ <i>Cytosar-U</i> [®]
Ara-CTP	cytarabine triphosphate/ara-Cytidine-5'-triphosphate
ATM	ataxia-telangiectasia mutated/ATM serine/threonine kinase
ATRA	all-trans retinoic acid/tretinoin/Vesanoid [®]
AZI2	5-azacytidine-induced protein 2/NAP1
B6	C57BL/6 mouse background
BET	Bromodomain and Extra-Terminal motif
BM	bone marrow
BPDCN	blastic plasmacytoid dendritic cell neoplasm
CAC	citric acid cycle/Krebs cycle/tricarboxylic acid cycle (TCA)
CCD	coiled-coil domain
CCL	CC-motif chemokine ligand
ccRCC	clear-cell renal cell carcinoma
CD	cluster of differentiation
CD11b	macrophage-1 antigen (Mac-1)/integrin alpha M (<i>ITGAM</i>)
CD115	proto-oncogene feline McDonough sarcoma (c-FMS)/colony stimulating factor 1 receptor (<i>CSF1R</i>)
CD117	proto-oncogene c-KIT (c-KIT)/stem cell factor receptor (SCFR)
CD135	FMS-like tyrosine kinase 3 (<i>FLT3</i>)
CD150	signaling lymphocytic activation molecule 1 (<i>SLAMF1</i>)/SLAM
CD15s	sialyl-Lewis ^x (sLeX)/SSEA-1
CD62E	E-selectin
CEP170	Centrosomal protein 170kDa
CFU	colony-forming unit

CFU-E	erythroid CFU
CMP	common myeloid progenitor
CTx	chemotherapy
CXCL	CXC-motif chemokine ligand
DA	daunorubicin + Ara-C
DC	dendritic cell
DEPC	diethyl pyrocarbonate/diethyl decarbonate
DMSO	dimethyl sulfoxide
DNO	daunorubicin/ <i>Cerubidine</i> [®]
DSS	dextran sulfate sodium
E	glutamate/glutamic acid
EAE	experimental autoimmune encephalomyelitis
ELN	European LeukemiaNet
EMD	extramedullary disease
ETC	electron transport chain
EtOH	ethanol
EthBr	ethidium bromide
eWAT	epididymal white adipose tissue
FAB	French-American-British
FBS	fetal bovine serum
FLAG-IDA	fludarabine + high-dose Ara-C + G-CSF + idarubicin
FLAMSA	fludarabine + amsacrine + high-dose Ara-C + G-CSF
FTD	frontotemporal dementia
fx	flanked by <i>loxP</i> sites/floxed
G-CSF	granulocyte colony-stimulating factor/CSF3/filgrastim (<i>E. coli</i> -recombinant G-CSF [<i>Neupogen</i> [®]])
gDNA	genomic DNA
GM-CSF	granulocyte-macrophage colony-stimulating factor/CSF2
GMP	granulocyte-monocyte progenitor

H&E	hematoxylin and eosin
H3K4	lysine 4 of histone H3
H3K4me3	trimethylation on lysine 4 of histone H3
Hb	hemoglobin
HFD	high-fat diet
HPC	hematopoietic progenitor cell
HSC	hematopoietic stem cell
HSCT	hematopoietic stem cell transplant
HSE	herpes simplex virus-1 encephalitis
HSV-1	herpes simplex virus-1
HSPC	hematopoietic stem/progenitor cell/c-Kit ⁺ mouse bone marrow cells
HTLV-1	human T-lymphotropic virus type 1
IACUC	Institutional Animal Care and Use Committee
IAV	influenza A virus
IF	immunofluorescence
IFN	interferon
IFN-I	type-I interferon
IHC	immunohistochemistry
IKK	inhibitor of nuclear factor- κ B kinase
IKK ϵ	IKK family member, subunit epsilon/IKKi/ <i>IKBKE</i>
IL	interleukin
IRF	interferon regulatory factor
ITD	internal tandem duplication
JAX	The Jackson Laboratory
K	lysine
KC	keratinocyte chemoattractant/keratinocyte-derived chemokine/CXCL1
KD	kinase domain
KRAS	proto-oncogene Kirsten rat sarcoma virus

Lin	lineage-associated surface antigens (B220, CD3, CD11b, Gr1, TER119, and CD41, unless otherwise specified)
LMPP	lympho-myeloid-primed progenitor (Flt3 ⁺ CD150 ⁻ LSK)
LPS	bacterial lipopolysaccharides
LSC	leukemia stem cell
LK	Lin ⁻ c-Kit ⁺ mouse bone marrow cell
LSK	Lin ⁻ Sca1 ⁺ c-Kit ⁺ mouse bone marrow cell
LUMC	Loyola University Medical Center
M-CSF	monocyte colony-stimulating factor/CSF1
mAb	monoclonal antibody
MAVS	mitochondrial antiviral-signaling protein
MCE	MedChemExpress
MDS	myelodysplastic syndrome
MDSC	myeloid-derived suppressor cell
MEP	myelo-erythroid progenitor
MkP	megakaryocyte progenitor
ML-DS	myeloid proliferations related to Down syndrome
MLKL	Mixed lineage kinase domain like pseudokinase
MLL	Mixed-lineage leukemia 1 (MLL1)/histone-lysine N-methyltransferase 2A (<i>KMT2A</i>)
<i>MLL-AF9</i> ⁺	harboring the MLL-AF9 fusion gene
MMB	momelotinib/CYT387
MLL-r	<i>MLL1</i> -rearranged
moDC:	monocyte-derived dendritic cell(s)
MPP	multipotent progenitor cell
MPN	myeloproliferative neoplasm
MPO	myeloperoxidase
MRD	minimal residual disease
MS	myeloid sarcoma (chloroma)

mtDNA	mitochondrial DNA
MYD88	myeloid differentiation primary response 88
NaOAc	sodium acetate
NASH	non-alcoholic steatohepatitis
NCAM	neural cell adhesion molecule/CD56
NCCN	National Comprehensive Cancer Network
NDP52	nuclear dot protein 52
NSCLC	non-small cell lung cancer
NTG	normal-tension glaucoma
NuMA	Nuclear mitotic apparatus protein 1
OPTN	optineurin
OS:	overall survival
PAS	periodic acid-Schiff
PBS	phosphate-buffered saline
PCR	polymerase chain reaction
PD-L1	programmed cell death-ligand 1
Plts	platelets
pUbn	polyubiquitination
PROTAC	proteolysis-targeting chimera
PTM	post-translational modification
PINK1	PTEN-induced kinase 1
PRR	pattern recognition receptor
qPCR	quantitative PCR
R/R AML	relapsed/refractory AML
RANTES	regulated on activation, normal T cell expressed and secreted/CCL5
RBC	red blood cell(s)/erythrocyte(s)
RIPK1/3	Receptor-interacting serine/threonine-protein kinase 1/3
RLR	RIG-I-like receptor

RNA-seq	RNA sequencing
ROS	reactive oxygen species
RT-PCR	reverse-transcriptase PCR
RXB	ruxolitinib
S	serine
sAML	secondary AML
SC	single cell(s)
SCF	stem cell factor/c-Kit ligand/steel factor
SDD	scaffold dimerization domain/coiled-coil domain 1 [CCD1]
shRNA	small hairpin RNA
SINTBAD	similar to NAP1 TBK1 adaptor/TBK1-binding protein 1 (TBKBP1)
SM-FeSV	feline sarcoma virus-McDonough strain
SPF	specific pathogen-free
SQSTM1	sequestosome 1/p62
STING	stimulator of interferon genes
TAC1	Transmembrane activator and CAML interactor/TNFRSF13B
TAE	tris base-acetic acid-EDTA
T	threonine
t-AML	therapy-related AML
TANK	TRAF family member-associated NF-kappa B activator
TAPE	TBK1-associated protein in endolysosomes/CC2D1A/Freud-1/Aki-1
TBK1	TANK-binding kinase 1/NF- κ B-activating kinase (NAK)/TRAF2-associated kinase (T2K)/Encephalopathy, Acute, Infection-Induced 8 (IIAE8)/Frontotemporal dementia and/or amyotrophic lateral sclerosis 4 (FTDALS4)
TBK1L	zebrafish isoform of TBK1 that lacks the KD and ULD
TBK1s	human/mouse isoform of TBK1 that lacks the KD
TCGA	The Cancer Genome Atlas
Th17	IL-17 ⁺ helper T cells

TICAM-1	TIR domain containing adaptor molecule 1/TIR-domain-containing adapter-inducing interferon- β (TRIF)
TKD	tyrosine kinase domain mutation
TLR	Toll-like receptor
TME	tumor microenvironment
TNC	total nucleated cell(s)
TNF	tumor necrosis factor
ULD	ubiquitin-like domain
ULK1	Unc-51-like autophagy activating kinase 1
UTR	untranslated region
VP3	viral capsid protein 3
WBC	white blood cell(s)/leukocyte(s)
WBM	whole bone marrow
WBMT	WBM transplant
WGCNA	weighted gene co-expression network analysis
WT	wild-type/+
XFG	exfoliation glaucoma
XRT	radiotherapy
Y	tyrosine
YBX1	Y-box-binding protein 1/YB-1

ABSTRACT

The TANK-binding kinase 1 (TBK1) is a cytoplasmic, serine/threonine kinase and a critical activator of the innate immune system. Reports have implicated TBK1 as a promoter of multiple cancer types. Acute myeloid leukemia (AML) is a cancer arising from the hematopoietic stem/progenitor cells (HSPCs). Although ~70% of AML patients achieve complete remission with chemotherapy, at least half will relapse due to the failure to eradicate leukemia stem cells (LSCs). As our previous data indicate the TLR-TAK1/TICAM-1 axes regulate LSCs, we suspect TBK1 also regulates LSCs. To study TBK1 in AML, we generated tamoxifen-inducible, *Tbk1*-knockout (*Tbk1*^{NULL}) mice and *Tbk1*^{NULL} *MLL-AF9*⁺ mouse HSPCs. We found that *Tbk1* deletion ablates the c-Kit⁺Flt3⁺ subset of *MLL-AF9*⁺ HSPCs without perturbing homeostatic hematopoiesis; the loss of *Tbk1* also increases the expression of c-Fms/CD115 on *MLL-AF9*⁺ HSPCs. Our study suggests that TBK1 blockade can selectively and effectively target FLT3⁺ LSCs in AML treatment.

CHAPTER 1

TARGETING THE LEUKEMIA STEM CELL: AN UNMET CLINICAL NEED

Introduction

Acute myeloid/myelogenous leukemia (AML), sometimes called acute non-lymphocytic leukemia (ANLL), is a cancer of the blood-forming (hematopoietic) tissues that reside in the bone marrow (BM) [1, 2]. AML typically occurs in patients aged 65 years or older and necessitates treatment with cytotoxic CTx [3-5]. AML usually responds to frontline CTx, but up to 40% of newly-diagnosed patients present with refractory disease (primary resistance) or cannot tolerate the treatment required to achieved complete remission (CR) [6]. While 60-70% of patients achieve complete remission CR, around half of these patients relapse (acquired/secondary resistance) within 3 years from diagnosis; relapsed AML is often CTx-resistant and necessitates a hematopoietic stem cell (HSC) transplant (HSCT) [4]. Overall, AML still has a dismal long-term prognosis even for patients who initially respond to treatment [7, 8]. Thus, treatments that offer all patients a better chance at achieving sustained CR are urgently needed.

Non-cytotoxic (targeted) therapies for AML are available for patients with specific genetic abnormalities [9, 10]. For example, *PML-RARA*⁺ AML can be virtually cured with the use of tretinoin (all-trans retinoic acid [ATRA]/*Vesanoïd*[®]) and arsenic trioxide (*As₂O₃/Trisenox*[®]), as these agents rapidly and selectively induce the differentiation of *PML-RARA*⁺ cells and cause degradation of the PML-RAR α oncoprotein [11, 12]. Patients harboring mutations in the FMS-like tyrosine kinase 3 (*FLT3*) or isocitrate dehydrogenase 1/2 (*IDH1/2*) genes may be treated with drugs that specifically inhibit the mutated FLT3 receptor (CD135) or IDH1/2 enzyme(s) [10, 13]. Agents targeted against hedgehog signaling (glasdegib [*Daurismo*[®]]) and BCL-2 (venetoclax [*Venclexta*[®]]) are approved for combination use with low-dose CTx in patients who cannot tolerate the frontline regimen [14-19]; while these drugs may be most effective in patients who display overactive hedgehog signaling and/or high BCL-2 expression, pathways both exploited by LSCs, there is not yet a method to determine these parameters clinically. And yet, despite targeting a pathway critical to LSCs, *Daurismo*[®] failed to extend overall survival (OS) in newly-diagnosed AML patients when added to standard daunorubicin + Ara-C CTx (NCT03416179) [20, 21].

Experimental therapies like uproleselan, an E-selectin antagonist, and revumenib, a menin inhibitor for patients with *MLL1* rearrangements or *NPM1c* mutations, have shown promise in clinical trials [22, 23]. However, most targeted therapies for AML (aside from *Vesanoïd*[®] + *Trisenox*[®] for *PML-RARA*⁺ AML) are unable to induce CR alone and must be used in combination with standard or low-dose CTx [16-18]. While targeted therapies can augment cytotoxic CTx to improve response rates, drug

resistance is still a concern [24-27]. Patients treated with any agent—targeted or cytotoxic—can develop resistance and relapse.

Leukemia stem cells (LSCs) AML are responsible for acquired resistance and relapse in AML, and likely even contribute to primary resistance [2, 28]. While it is established that targeting LSCs is the key to preventing relapse, no therapies exist that effectively target LSCs. As such, we seek to discover novel molecular targets that will allow clinicians to target LSCs directly. We believe that TBK1 is critical to the function of LSCs such that TBK1 blockade will sensitize LSCs to cytotoxic CTx, increasing the odds of achieving and maintaining CR in AML.

Aim 1: Determine if *Tbk1* is Required for Murine Hematopoiesis

Blocking the action of TBK1 can be done with small molecules that have been characterized *in vivo* and some of which are orally-bioavailable, such as GSK8612 [29]. However, as there is not yet a way to deliver such drugs to AML cells specifically, TBK1 inhibition occurs systemically. While TBK1 has been studied in cell-specific settings, such as in B cells and dendritic cells, its function in hematopoiesis is unknown and must be determined before TBK1 blockade is pursued clinically [29-31]. To this end, we will use a whole-body (global [via the *Rosa26* promoter]), *Tbk1*-knockout (*Tbk1*^{NULL} [*Tbk1*^{-/-}]) mouse model to determine if the loss of *Tbk1* imparts untoward effects on hematopoiesis.

Aim 2: Determine if *Tbk1* Blockade Could be a Means of Anti-AML Therapy

Based on previous data from our lab, the established & emerging roles of TBK1 in cell physiology, and recent reports examining TBK1 in AML, we anticipate TBK1 is a molecular target for the basis of AML treatment [29, 32-36]. To this end, we will utilize *in vitro* and *in vivo* approaches in the *MLL-AF9*⁺ setting to determine if *Tbk1* blockade holds any promise as a means to treat AML

CHAPTER 2

LITERATURE REVIEW AND PROJECT RATIONALE

Structure of TBK1

The TANK-binding kinase 1 (TBK1; NF- κ B-activating kinase [NAK]/TRAF2-associated kinase [T2K]/IIAE8/FTDALS4) harbors four domains: an N-terminal kinase domain (KD [9-300aa]), a ubiquitin-like domain (ULD [305-383aa]), a scaffold-dimerization domain (SDD/coiled-coil domain 1 [CCD1]; 407-657aa), and a second coiled-coil domain at the C-terminus (CCD2; 659-713aa) [29, 37] (**Figure 1**, adapted from Runde, *et al.*) [29]. The KD harbors the catalytic domain, containing the K38, D135, and S172 residues required for kinase activity; the ULD regulates kinase activity and binding of TBK1 to substrates, such as IRF3/7 [38]; the SDD, harboring a leucine zipper (LZ) and helix-loop-helix (HLH), allows for homodimerization [39, 40]; CCD2 enables interaction of TBK1 with adaptors, such as TBK1-binding protein 1 (TBKBP1; similar to NAP1 TBK1 adaptor [SINTBAD]), TRIF, and OPTN [41, 42].

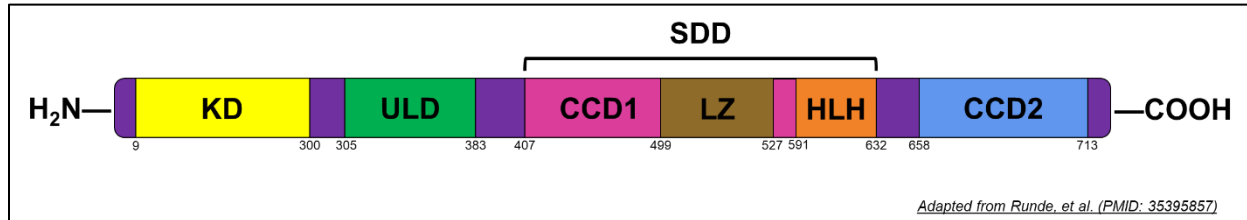


Figure 1. Schematic depicting the TBK1 Protein and its Domains (adapted from Runde, et al. and created with PowerPoint®). TBK1 contains four prototypical domains, from the N- to C-terminus: a KD (9-300aa), a ULD (305-383aa), an SDD/CCD1 (407-657aa), and a CCD2 (659-713aa). The KD harbors the catalytic site (including the S172 necessary for kinase activity); the ULD regulates kinase activity and facilitates binding of TBK1 to its substrates; the SDD/CCD1 (harboring an LZ and HLH) allows for homodimerization; the CCD2 enables interaction of TBK1 with adaptors like SINTBAD and OPTN.

Human/mouse TBK1 is highly homologous to the inhibitor of nuclear factor- κ B kinase (IKK) subunit epsilon (IKK ϵ ; IKKi/encoded by *IKBKE*), sharing 46-64% homology in protein sequence [43-45]. TBK1 and IKK ϵ have such a high degree of homology that they can be inhibited by the same molecules, such as amlexanox (AMX), momelotinib (MMB), BAY985, and BX795 [34, 46-52]. The similarity between the two has led many to investigate whether the kinases are wholly redundant or possess unique functions, and it appears that the kinases are not functionally identical [49, 53, 54]. For example, global deletion of *Tbk1* is embryonic-lethal, whereas global *Ikbke*^{NULL} mice are viable but hypersensitive to respiratory viruses [55]. Thus, while TBK1 and IKK ϵ have overlapping functions, such as mediating IFN- β production, we believe that they each have tissue- and disease-specific functions and are not entirely redundant.

Genetic and Protein-level Regulation of TBK1

TBK1 is a serine/threonine kinase that is a critical activator of the vertebrate innate immune system [56, 57]. TBK1 is 729 amino acids (aa) in length and has a molecular weight of ~84 kDa [58-60]. TBK1 is highly conserved between humans (UniProt: Q9UHD2) and mice (UniProt: Q9WUN2), displaying 94.1% homology in protein sequence [44, 45]. TBK1 is encoded by the *TBK1* gene. In humans, *TBK1* contains 22 exons and resides on chromosome 12q14.2; in mice, *Tbk1* contains 21 exons and resides on chromosome 10D2 [61]. RNA sequencing (RNA-seq) data (PRJEB4337) has revealed that, in addition to innate immune cells, *TBK1* is expressed significantly in nearly all human tissues [59, 62]. Notably, *TBK1* expression is highest in the testis and BM, and lowest in the pancreas.

The transcriptional regulation of *TBK1* has not been well-studied, but splice variants have been reported. In humans and mice, Deng, *et al.* identified TBK1s, a truncated isoform that lacks exons 3-6 [63, 64]. While TBK1s is without a KD, it can compete with the full-length TBK1 for the binding of RIG-I and mitochondrial antiviral-signaling protein (MAVS), thereby inhibiting activation of the downstream pathway and hampering interferon- β (IFN- β) production amid viral infection. In zebrafish, Zhang, *et al.* reported TBK1-like (TBK1L), an isoform that lacks both the KD and ULD [65]. Like TBK1s, TBK1L can disrupt the activation of the RLR-MAVS axis during *Carp spryivirus* infection. While JASPAR predicts *TBK1* to be a target gene of at least 111 transcription factors, including: ARNT, BRCA1, CEBPB, ESR1/2, FOXO3, GATA1/2/3, HLF, HOXA5,

MECOM, MYB, MYC, NFIL3, PAX2/4/5/6, PBX1, RUNX1/2, SOX2/5/9/10/17, SP1, SRY, STAT1/3, TP53/63, ZFX, relatively little is known about the genetic regulation of *TBK1* [66, 67]. However, its regulation at the protein-level has been thoroughly investigated.

At rest, *TBK1* exists as a homodimer in the cytoplasm [68, 69]. *TBK1* is activated by membrane-bound and cytosolic pattern-recognition receptors (PRRs), such as Toll-like receptors (TLRs) and RIG-I-like receptors (RLRs), which initiate the innate immune response. Activation of PRRs leads to the production of inflammatory cytokines, such as TNF, IL-6, IL-1 β , and IL-12, as well as the production of type-I interferon (IFN-I) [70]. *TBK1* is activated by the following PRRs: TLR3/4/7/8/9, cyclic GMP-AMP synthase (cGAS), DAI, DDX41, AIM2, MDA5, LGP2, and RIG-I [56]. In addition to PRRs, *TBK1* can be induced by the stimulator of interferon genes (STING), tumor necrosis factor (TNF) family of ligands and receptors (e.g, APRIL and TACI [*TNFRSF13B*]), other kinases (e.g., IKK β), 5-azacytidine-induced protein 2 (AZI2; NAP1), cytokines (e.g., IL-1, CXCL4, GM-CSF) and even the oncogenic KRAS^{G12} GTPase [29, 30, 71-77].

The activation and function of *TBK1* involves a multi-step process of post-translational modifications (PTMs) at various residues spanning the protein [29, 69, 78]. PTMs govern both the enzymatic activity of *TBK1* and its interaction with adaptor proteins (**Table 1**).

Table 1. Select Post-translational Modifications of TBK1 and Effect on Protein Function, if Applicable (Adapted from Runde, et al.) [29].

PTM	Site	Mediators	Function	References
Phosphorylation	Y354; Y394	Lck/Hck/Fgr	Inhibitory	[79]
Phosphorylation	S510	AKT1	Inhibitory	[80]
Phosphorylation	Y179	SRC	Activating	[81]
Phosphorylation	S716	PKC θ	Activating	[82]
Phosphorylation	S172	TBK1 (trans-autophosphorylation) ; ULK1; IKK β ; PINK1/PARKIN; GSK3 β —can be reversed by PPM1B	Activating (rate-limiting, enables kinase activity)	[69, 76, 83-86]
K27-linked pUbn	K344	NEDD4	Activating (enables association with NDP52)	[87]
K33-linked pUbn	K670	E3 ligase is unknown—can be reversed by USP38/NLRP4	Activating	[88, 89]
K48-linked pUbn	K670	DTX4/TRIP	Inhibitory	[88-90]
K48-linked pUbn	K251; K372	Siglec1/TRIM27	Inhibitory	[91]
K63-linked pUbn	K30; K401	MIB2; TRAF2/3/6; NRDP1; RNF128 E3 ligases—can be	Activating (precedes S172)	[40, 58, 68, 92, 93]

		blocked by the RNF144B E3 ligase	phosphorylation; required for downstream IRF3/7 activation; promotes association with AZI2, NDP52, SINTBAD, and NEMO)	
Ubiquitination	K69; K154; K372		Activating	[94]
Acetylation	K241; K692; additionally, K30, K154, K236, K251, K607, K646, & K691 are proposed)	Acetyltransferases are unknown—can be reversed by HDAC3/4/9	Variable (HDAC3 and HDAC9/DNMT3A promote TBK1 activity, whereas HDAC4 inhibits it)	[95-97]

SUMOylation	K694	SUMO1/2/3 (trans-SUMOylation)—can be blocked by Gam1	Activating (enables association with AZI2, SINTBAD, and TANK)	[98]
S-nitrosylation	C423	Spontaneous—can be reversed by GSNOR		[99]
Hydroxylation	P48	EGLN1	Inhibitory (TBK1 becomes substrates for pVHL and PPM1B)	[100]

By determining which adaptors TBK1 can associate with, PTMs also govern the subcellular localization of TBK1, further regulating its function. For example, localization to the Golgi will allow interaction with STING and optineurin (OPTN), localization to the centromere will allow interaction with nuclear mitotic apparatus protein 1 (NuMA) and centrosomal protein 170kDa (CEP170), and localization to the mitochondria will allow interaction with PINK1/PARKIN, p62/sequestosome 1 (SQSTM1), and acyl-CoA synthetase long-chain family member 1 (ACSL1) [101-108]. Distinct domains/motifs spanning TBK1 allow interaction with a wide array of adaptor proteins.

Function of TBK1

TBK1 is best known for being a master activator of the innate immune system, mediating IFN-I production in response to viral/bacterial infection or, in the case of TLR7/8, stimulation by an imidazoquinolone such as imiquimod [*Aldara*[®]] (**Figure 2**, adapted from Runde, *et al.*) [29, 109]. Upon PRR stimulation, a cascade involving adaptor proteins will facilitate the activation of TBK1 [29]. Common TBK1 adaptors include: TIR domain containing adaptor molecule 1 (TICAM-1; TIR-domain-containing adapter-inducing interferon- β [TRIF]), mitochondrial antiviral-signaling protein (MAVS), myeloid differentiation primary response 88 (MYD88), TBK1-associated protein in endolysosomes (TAPE; CC2D1A/Freud-1/Aki-1), TRAF family member-associated NF-kappa-B activator (TANK), and nuclear dot protein 52 (NDP52) [29, 32, 110-113].

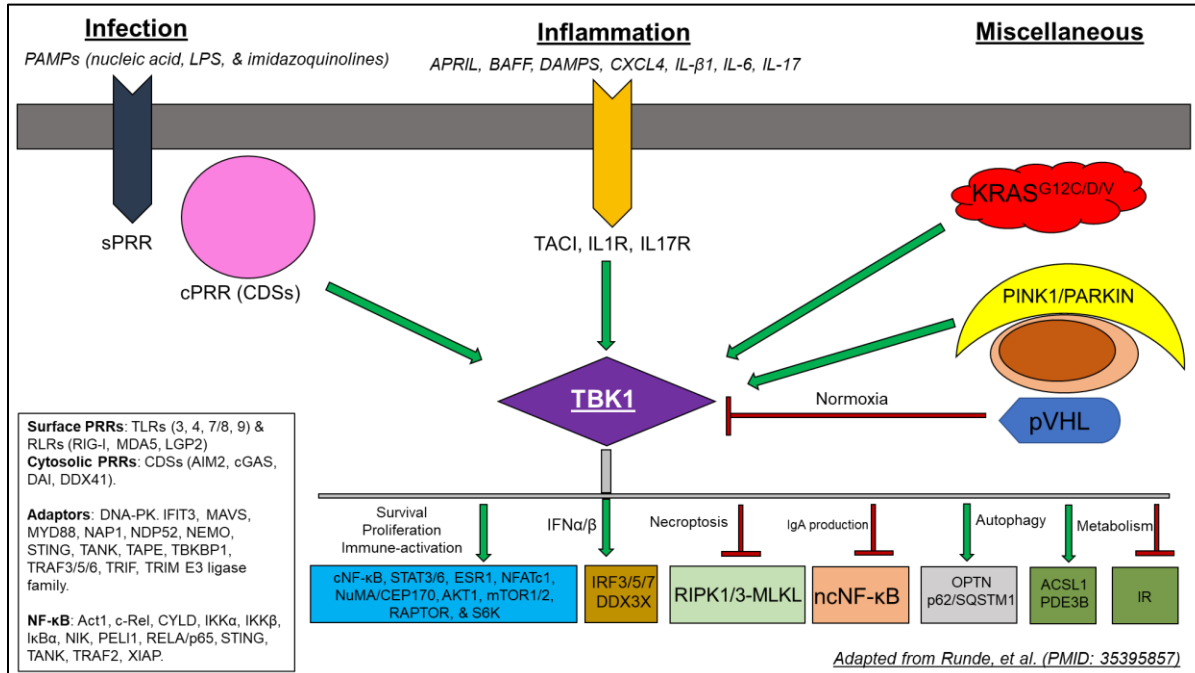


Figure 2. Schematic depicting Upstream Regulators and Downstream Substrates/Pathways of TBK1 (adapted from Runde, et al. and created with PowerPoint®). TBK1 is activated by PRRs that reside on the cell membrane (sPRR) and those that function within endosomes (cPRR/cytosolic DNA sensors [CDSs]), as well as inflammation-associated receptors and miscellaneous proteins, like the oncogenic KRAS^{G12} and mitochondria-associated PINK1/PARKIN; TBK1 is negatively regulated by pVHL under normoxic conditions. Following activation, TBK1 governs a wide array of cellular processes, including those involved in survival and proliferation, metabolism, and IgA production.

Activated TBK1 initiates the production of IFN-I, like IFN- α and IFN- β , by phosphorylating transcription factors of the interferon regulatory factor (IRF) family. TBK1 most often phosphorylates and activates IRF3 (S386/S398/T404) and IRF7 (S425/S426/S437/S438), as well as IRF5 (S158/S309) in certain contexts. In response to *Pneumoviridae* but not LPS, TBK1 stimulates the activation of IRF1 by phosphorylating p65/RELA (S536), promoting IFN- β production; IFN- β production itself

stimulates IRF1 activity in an autocrine manner via IFNAR1/2-STAT1 [68, 114-119]. Recent reports have also shown that zebrafish, but not human, TBK1 phosphorylates IRF6—whether mouse *Tbk1* interacts with IRF6 has not been investigated [115, 116]. TBK1 can also act on behalf of the innate immune system in an IRF-independent manner, antagonizing various *Picornaviridae* infections by serving as an E3 ligase against viral capsid protein 3 (VP3) [120]. Recently, TBK1 has been implicated in the adaptive immune system as well: Lee, *et al.* demonstrated that B-cell *Tbk1* is required for germinal center formation in mice, and Xiao, *et al.* reported a role for TBK1 in the crosstalk between T cells and dendritic cells [31, 121].

Non-immune functions of TBK1 have also been identified. For example, TBK1 regulates metabolism by inhibiting the insulin receptor (IR) via phosphorylation on S994 and promotes the activity of the estrogen receptor α (ER α ; *ESR1*) via phosphorylation on S305 [122, 123]. TBK1 regulates cell survival by inhibiting the TNF- α -RIPK1/3-MLKL axis and modulating the production of cytokines such as granulocyte-macrophage colony-stimulating factor (GM-CSF; colony-stimulating factor 2 [CSF2]), TNF- α , IL6/8, CCL2/20/26, CCL5 (Regulated on Activation, Normal T cell Expressed and Secreted [RANTES]), and CXCL1 (keratinocyte chemoattractant [KC]/keratinocyte-derived chemokine) [102, 124-129]. TBK1 is also a master regulator of PINK1/PARKIN-driven mitophagy. Mitophagy is a quality control process critical to the health of virtually all cells. In this process, damaged and/or redundant mitochondria are degraded by the autophagosome [102, 124, 130, 131].

At designated mitochondria, PINK1/PARKIN recruits TBK1 and mediates its activation. The interaction between TBK1 and PINK1/PARKIN allows TBK1 to recruit and stabilize the receptors required for mitophagy, such as OPTN, NDP52, and p62/SQSTM1. The interaction between TBK1 and PINK1/PARKIN doubles as a “fail-safe”, forcing G2/M arrest if a cell attempts to divide during mitophagy: upon activation by PINK1/PARKIN, TBK1 is prevented from localizing to the centromere and thus cannot activate NuMA/CEP170 to enable cell division [106, 107, 124].

Mitophagy is a means by which cells can control levels of reactive oxygen species (ROS). As mitochondria emit ROS from normal metabolism and after having sustained damage, mitophagy can be utilized to reduce the cell's ROS burden [132]. ROS can lead to cancer as they increase the risk of incurring mutations from oxidative DNA damage [131, 133]. As mitophagy is an effective mechanism by which ROS can be reduced, it is crucial to the viability of stem cells, as ROS can cause them to differentiate and forfeit their tissue-renewal capabilities [131, 132, 134-138]

While mitophagy serves to prevent cancer, it can be exploited by cancer cells to adopt a more aggressive phenotype and resist CTx [133, 139-144]. In fact, chemotherapies are noted to exert their anticancer effects at least in part by increasing mitochondrial ROS production and dysfunction [145]. Targeting mitochondrial metabolism (*e.g.*, citric acid cycle [CAC]) may be a promising anticancer strategy, as the CAC inhibitor devimistat (CPI-613®; *Cornerstone Pharmaceuticals, Inc.*) has made it to clinical trials for pancreatic cancer (NCT03504423) and R/R AML (NCT01768897)

[146-148]. As such, while not explored in the scope of this thesis, targeting TBK1 to block mitophagy could be a means of anticancer treatment.

Furthermore, kinase-independent/non-enzymatic functions of TBK1 have been reported. For example, TBK1 promotes β -oxidation by sequestering ACSL1 at the mitochondria, preventing its translocation to the endoplasmic reticulum, and induces the degradation of IKK ϵ by preventing it from binding TANK [104, 122, 123, 149]. Thus, TBK1 is not merely an activator of the immune system but rather is a highly versatile regulator of cell physiology.

The functions of TBK1 have been studied in knockout-mouse models. Many tissue-specific, *Tbk1*-knockout mice have been developed (**Table 2**, adapted from Runde, *et al.*) [29]. Global *Tbk1*^{NULL} models present a challenge, as the germline loss of *Tbk1* is embryonic-lethal in C57BL/6 (B6) mice [150]. Global *Tbk1*^{NULL} B6 mice die of liver failure near embryonic day 14.5 due to RIPK1/3-MLKL-driven cell death, as the loss of *Tbk1* allows necroptosis to occur amid basal levels of TNF- α [151]. However, germline *Tbk1*^{NULL} 129S5/SvEvBrd (129S5) mice are viable (although born at a reduced Mendelian frequency) as they are deficient in *Tnfr2* [127]. B6 mice can only be used as global *Tbk1*^{NULL} models if they also lack either *Tnfa* or *Tnfr1*, or if *Tbk1*-deletion is controlled temporally such as with the *Rosa26*-CreER^{T2} or *Mx1*-Cre system [152]. Deletion of exon 2 has been the most common *Tbk1*-knockout strategy.

Table 2. Tissue Deletion Specificity, *Tbk1* Deletion Strategy, and Phenotypes of *Tbk1*^{NULL} Mouse Models (Adapted from Runde, et al.) [29].

Genotype	Deletion strategy	Phenotype	Reference
B6-germline <i>Tbk1</i> ^{NULL}	ES cell-targeting: loss of most of exon 1, all of intron 1, and all of exon 2	Embryonic lethality; death near E14.5 due to liver degeneration.	[150]
129S5-germline <i>Tbk1</i> ^{NULL}	<i>Prm1</i> -Cre: exon 2 (<i>Tbk1</i> deleted in parental sperm)	Reduced IFN- β /RANTES secretion and IRF3 activity in macrophages, increased circulating monocytes, inflammatory skin changes, increased serum levels of TNF α /GM-CSF/IL-6/CXCL1, and increased sensitivity to LPS. <i>Increased</i> insulin-sensitivity on high-fat diet (HFD) [153].	[127]
B6-global <i>Tbk1</i> ^{NULL}	<i>Rosa26</i> -CreER	Increased number of splenic memory CD4 ⁺ T cells (CD44 ^{hi} CD62L ^{lo}) at the expense of naïve CD4 ⁺ T cells (CD44 ^{lo} CD62L ^{hi}); no changes in CD4 ^{+/-} /CD8 ^{+/-} thymocyte populations.	[152]

Neuron- <i>Tbk1</i> ^{NULL}	<i>Nestin-Cre</i>	Cognitive and locomotor deficits consistent with an ALS/FTD-like pathology.	[154]
Adipocyte- <i>Tbk1</i> ^{NULL}	<i>Adiponectin-Cre</i>	On HFD: adipose tissue inflammation, <i>decreased</i> insulin-sensitivity, reduction in HFD-induced obesity, and increased AMPK activity.	[85]
Myeloid- <i>Tbk1</i> ^{NULL} (neutrophils retain <i>Tbk1</i>)	<i>LyzM-Cre</i>	<p>Increased survival due to decreased immune response in influenza A virus (IAV) infection model.</p> <p>Increased progression of ALS-like pathology in mouse model of ALS [155].</p> <p>Mice developed spontaneous hypertrophy of epididymal white adipose tissue (eWAT) and increased M1 macrophage infiltration, and mice on HFD developed NASH-like pathology and increased sensitivity to DSS-induced colitis [77].</p>	[156]
T cell- <i>Tbk1</i> ^{NULL}	<i>CD4-Cre</i>	Increased activation of AKT-mTORC1 axis leading to impaired T-cell egress from	[152]

		lymph nodes and decreased symptoms in experimental autoimmune encephalomyelitis (EAE).	
B cell- <i>Tbk1</i> ^{NULL}	<i>CD19</i> -Cre	Unrestrained production of IgA and accumulation in the kidneys, leading to development of an IgA nephropathy-like pathology, and increased NF- κ B activation.	[30]
Dendritic cell- <i>Tbk1</i> ^{NULL}	<i>CD11c</i> -Cre	Upregulation of costimulatory molecules imparting better T-cell priming abilities of dendritic cells, development of autoimmune-like pathology, enhanced antitumor immunity, increased IFNAR activity.	[31]
Intestine epithelia- <i>Tbk1</i> ^{NULL}	<i>Villin</i> -Cre	Increased production of MT1, increased number of Th17 cells in lamina propria, increased production of IL-1 β by macrophages, increase in both number and size of intestinal tumors.	[157]
Hepatocyte- <i>Tbk1</i> ^{NULL}	<i>Albumin</i> -Cre	Increased lipid accumulation in liver, reduced β -oxidation, and reduction in	[104]

		mitochondrial-localization of ACSL1.	
--	--	--------------------------------------	--

***TBK1* Mutations in Disease**

As *TBK1* regulates a remarkable array of cellular processes, alterations in *TBK1* function have been implicated in several disease states. In fact, over 100 mutations in *TBK1* have been associated with neurological, immunological, ophthalmological, and hematological pathologies (**Table 3**) [29, 40, 158-164].

In amyotrophic lateral sclerosis (ALS)/frontotemporal dementia (FTD), loss of *TBK1* function is believed to compromise mitophagy, contributing directly to neuronal dysfunction and degeneration [158, 165]. In fact, *TBK1* mutations are so strongly associated with ALS/FTD that the ALLFTD cohort study (NCT04363684) lists “*TBK1* gene mutation” on the inclusion criteria [166].

In herpes simplex virus-1 (HSV-1) encephalitis (HSE), loss of *TBK1* function hampers the innate immune response to HSV-1 infection [160, 167]. Without *TBK1*, TLR3 signal transduction is impeded and IFN production is insufficient; as a result, HSV-1 can replicate excessively, leading to HSE in both pediatric and adult patients.

Similarly, in severe COVID-19, loss of *TBK1* function blunts TLR3 signal transduction and the production of IFN-I, allowing undue replication of SARS-CoV-2 and worsened infection [168]. Conversely, in a single pediatric patient with COVID-19, co-existing *TBK1* and *TNFRSF13B* (TACI) mutations are believed to have caused the overzealous, fatal immune response to SARS-CoV-2 [169].

Table 3. Select *TBK1* Mutations, Associated Pathology, Effect on Protein (Mechanism), and Pathway Implicated, if Applicable.

Aberration	Pathology	Mechanism [170]	Pathway affected	References
D50A	HSE	Decreased protein stability (hypomorphic)	Defective TLR3 signaling	[160]
G159A	HSE	Kinase-dead (amorphic)	Defective TLR3 signaling	[160]
Duplication/ Triplication	NTG	Increased gene dosage (hypermorphic)	Hyperactive autophagy in retinal ganglion cells	[161, 162, 171, 172]
Duplication	XFG	Increased gene dosage (hypermorphic)	?	[173]
E653fs; L688Rfs*14	ALS/FTD	Impaired interaction with OPTN (hypomorphic)	?	[174]
E696K	ALS/FTD	Impaired interaction with OPTN (hypomorphic)	Defective mitophagy	[175, 176]
R357Q; I450K; M559R; Q565P	ALS/FTD	Ablated homodimerization (amorphic)	Defective mitophagy?	[176]
G217R; M559R	ALS/FTD	Kinase-dead (amorphic)	Defective mitophagy?	[176]

R47H	ALS/FTD	Near total loss of kinase activity (hypomorphic)	Defective mitophagy?	[176]
Q565P	ALS/FTD	Reduced kinase activity (hypomorphic)	Reduced p62, IRF3, and NF- κ B phosphorylation?	[177, 178]
E643del	ALS/FTD	Reduced protein levels (hypomorphic)	Defective autophagy?	[179]
T79del	ALS/FTD	Reduced protein levels, possibly reduced kinase function (hypomorphic)	Defective autophagy?	[180]
N489I; 3'-UTR (2 distinct substitutions); N63S (also found in ALS/FTD [180])	Multiple myeloma	?	?	Multiple Myeloma CoMMpass Study (TCGA) [181]
S206N	Acute myeloid leukemia	?	?	TCGA AML Dataset [182]
Skipping of exon 16	COVID-19, fatal	Truncation leading to partial loss of	Autoimmunity complicated	[169]

(homozygous ; predicted to yield truncated/R5 74Sfs*11 isoform)		SDD and ablation of CCD2 (hypomorphic)?	by accompanying loss-of-function mutation in <i>TNFRSF13B</i> ?	
F24S; R308* (heterozygous with WT)	COVID-19, severe	? (hypomorphic)	Impaired TLR3 signaling/type I IFN production?	[168]

Role of TBK1 in Cancer

In addition to these pathologies, TBK1 is becoming increasingly implicated in the pathogenesis of cancer [29, 72, 122, 182-192]. Specifically, TBK1 contributes to cancer by promoting cell proliferation and blunting antitumor immune responses. However, other mechanisms are becoming evident.

TBK1 has come to light as a promoter of several cancer types and predictor of metastasis risk and thus, a possible molecular target for the basis of cancer treatment. Recent reports have suggested that TBK1 promotes prostate cancer [183, 193, 194], thyroid cancer [195], head/neck squamous cell carcinoma [196, 197], non-small cell lung cancer (NSCLC) [72, 101, 186, 198, 199], diffuse large B-cell lymphoma (DLBCL) [126, 200-202], AML [33, 34], cervical cancer [203], multiple myeloma/plasma cell leukemia [204], ccRCC [100], and pancreatic cancer [185]. In ER⁺ breast cancer, while it is established that TBK1 stabilizes the ER α , the role of this interaction in disease

pathogenesis is not yet clear: TBK1 can facilitate tamoxifen-resistance by activating the $E\alpha$ yet, the loss of TBK1 promotes invasion/migration following $E\alpha$ destabilization [122, 205]. However, in HER2⁺ breast (and colorectal) cancer, TBK1 promotes disease progression [80, 206, 207]

While *TBK1* mutations are not yet routinely reported in cancer, 138 mutations have been identified in different cancer types across 127 patients with The Cancer Genome Atlas (TCGA) [208]. Notably, almost $\frac{1}{4}$ th of the patients harboring *TBK1* mutations had endometrial cancer (30 out of 127).

TBK1 can promote cancer in a cell-intrinsic manner by modulating internal signaling pathways. TBK1 can drive cell division through its interaction with NuMA/CEP170 at the centrosome and by facilitating activation of the AXL/AKT3, AXL/KRAS^{G12}/RALB, STAT3, PI3K/AKT/mTOR1, MYC, p62, and NF- κ B/BCL-X_L pathways. [34, 74, 108, 150, 209].

TBK1 has been observed to exploit STAT3 across multiple cancer types, albeit through distinct mechanisms. In dendritic cells (DCs), activation of STAT3 decreases the expression of costimulatory molecules on DCs, abrogating their ability to stimulate T cells [31]. In DLBCL cells, activation of STAT3 induces production of protumor cytokines, such as IL-10 and CCL3/4 [200]. In human T-lymphotropic virus 1 (HTLV-1)-transformed T cells, TBK1 is co-opted by Tax to induce activation of STAT3 and maintain the survival of HTLV-1⁺ cells [202]. However, while TBK1 can be exploited by cancer cells to drive their survival and proliferation, reliance on TBK1 also sensitizes certain cells to TBK1 inhibition.

In cancer cells with certain mutations, such as KRAS^{G12}-mutated NSCLC and VHL^{NULL} ccRCC, TBK1 becomes hyperactivated [72, 100, 210]. While such hyperactivation enhances cell proliferation, it simultaneously imparts a vulnerability such that KRAS-mutated and VHL^{NULL} cells are killed by TBK1 inhibition [72, 81, 211]. TBK1 blockade may even sensitize such tumors to treatment and, in the case of NSCLC, may augment KRAS^{G12C} inhibitors like sotorasib (*Lumakras*[®]) and adagrasib (*Krazati*[®]) [212, 213]. In mouse models of KRAS^{G12D}-mutated lung cancer, addition of JQ1, a Bromodomain and Extra-Terminal motif (BET) protein inhibitor, re-sensitized cancer cells to combination TBK1/MEK inhibition by blocking IGF1 and YAP1 signaling [214].

Additionally, AML cell lines that display high MYC activity, such as the MOLM14, OCIAML5, HL-60, and KASUMI-1, and NRAS-mutated melanoma cells are also sensitive to pharmacologic TBK1 inhibition [34, 72, 100, 210, 214]. Despite largely being a promoter of cancer, TBK1 acts as a tumor suppressor in specific intestinal cells.

It was discovered that TBK1 has tissue-specific, tumor-suppressive roles when a Villin-specific deletion of *Tbk1* led to accelerated formation of intestinal polyps in *Apc*^{Min/+} mice [157]. The loss of *Tbk1* in villin⁺ cells allows for the increased production of metallothionein 1 (MT1) in the lamina propria, promoting increased IL-1 β production from resident macrophages. IL-1 β stimulates the proliferation of inflammatory Th17 cells which produce cytokines such as IL-17 and IL-22; thus, loss of *Tbk1* allows for the expansion of Th17 cells and ensuing inflammation from Th17-secreted IL-17 and IL-22. Mechanistically, *Tbk1* restrains MT1 production by inhibiting NF- κ B in villin⁺ intestinal epithelia.

TBK1 can also promote cancer by modulating the tumor microenvironment (TME) and the behavior of T cells locally and distantly. Within tumor cells, TBK1 induces the production of immunosuppressive cytokines, such as IL-6 and RANTES, which act in autocrine and paracrine fashions to facilitate tumor growth [190, 209, 215]. Additionally, TBK1 stimulates tumor cells to upregulate expression of PD-L1, an immune checkpoint molecule that protects them from destruction by antitumor T cells [82, 203, 216, 217]. Locally, TBK1 can act within tumor-infiltrating CD4⁺ and CD8⁺ T cells to restrain the production of antitumor cytokines, such as IL-2 and IFN- γ [217]. Outside the TME, TBK1 acts within dendritic cells to hamper their ability to prime T cells [82, 190, 216, 217]. As a proof-of-concept, pharmacologic inhibition of TBK1 has been proven to slow tumor growth and enhance the effectiveness of immune checkpoint blockade, providing evidence that TBK1 blockade has anticancer efficacy [217].

TBK1 Inhibitors in Cancer Treatment

Several small-molecule inhibitors and proteolysis-targeting chimeras (PROTACs) against TBK1 have been characterized and tested in an array of *in vitro* and *in vivo* cancer models (**Table 4**, adapted from Runde, *et al.*) [29]. AMX and MMB have even made it to clinical trials for the treatment of metabolic disorders and myelofibrosis/lung cancer, respectively [50, 218, 219]. TBK1 inhibitors may be TBK1-selective or have additional activity against IKK ϵ ; IKK ϵ -selective inhibitors have not been characterized. Additionally, some TBK1 inhibitors also block the action of other proteins. Many TBK1 inhibitors show good druglikeness and appear to be promising candidates for the

treatment of solid and liquid tumors. We hypothesize that combination use with immune checkpoint blockade and/or cytotoxic CTx would be of the greatest benefit.

Table 4. List of TBK1 Inhibitors (Adapted from Runde, et al.) [29].

Molecule	Target(s) Inhibited	Clinical Trial (if Applicable)	Reference(s)
Amlexanox (AMX; <i>Aphthaso</i> [®] /Amlx/AA-673)	TBK1/IKK ϵ	NCT01842282; NCT01975935	[50, 85, 104, 153, 183, 204, 220-224]
AZ13102909/AZ909	TBK1	-	[225]
BAY985	TBK1/IKK ϵ	-	[51]
BX795	TBK1/IKK ϵ ; Aurora B; NUAK1; PDK1	-	[52, 226, 227]
Compound I	TBK1/IKK ϵ	-	[216]
Compound II	TBK1/IKK ϵ	-	[192, 228]
DMX14	TBK1/IKK ϵ	-	[229]
GSK8612	TBK1	-	[33, 230]
MDK10496	TBK1/IKK ϵ	-	[187]

Momelotinib (MMB)/CYT387/GS03 87	TBK1/IKKε; ACVR1; ALK2; JAK1/2	NCT02101021; NCT02206763; NCT02258607; NCT04173494/MOMENTUM; NCT01969838/SIMPLIFY1; NCT02101268	[34, 218, 219, 231- 235]
MPI0485520	TBK1/IKKε	-	[236]
MRT67307	TBK1/IKKε	-	[84]
MRT68601	TBK1	-	[52]
UNC6587 (Cereblon PROTAC)	TBK1	-	[100]
15a	TBK1/IKKε; Aurora A; GSK3β	-	[237]
200A	TBK1/IKKε	-	[189]
3i (VHL PROTAC)	TBK1	-	[238]

Overview of AML

In AML, a clone of cancerous myeloid cells expands in the BM [1, 2, 239]. AML cells consume resources as they proliferate, hampering the function of normal HSPCs and eventually spilling into the bloodstream. A hematologic neoplasm is evident when a high blast percentage in the BM or blood is detected, and AML is diagnosed when ~20% of cells in the BM or peripheral blood (PB) are myeloid blasts; the normal blast

percentage in the BM is less than 5% and close to 0% in the blood [240]. AML cells can extravasate from the vasculature to enter the spleen, destroying its normal architecture, and AML cells can also infiltrate extramedullary sites such as the kidneys, skin and gums (leukemia cutis), and spine, brain, abdomen, and mouth where they can even form solid tumors (chloroma/myeloid sarcoma [MS]) [1, 241, 242]. As normal hematopoiesis is increasingly disturbed, AML patients experience fatigue (due to anemia), infection (due to leukopenia [chiefly, neutropenia]), and bruising (due to thrombocytopenia). As AML cells are inert in terms of infection-fighting abilities, AML patients are at high risk of infection despite presenting with high white blood cell counts, sometimes exceeding 100 K/uL [239, 243, 244]. AML progresses rapidly and an AML burden of 10^{12} cells is fatal [245].

While a rare cancer overall, accounting for ~1% of all cancer cases in the US, AML is the most common type of leukemia [9]. In the US in 2023, it is estimated that 20,380 people will be newly-diagnosed with AML and around 11,310 people will die from the disease [3, 4]. Risk factors for AML include: male sex (~34% increase in risk), age, tobacco exposure, ionizing radiation exposure, previous CTx treatment (namely, anthracyclines, alkylating agents, and epipodophyllotoxin derivatives [etoposide/teniposide]), some genetic disorders (e.g., Fanconi anemia, Down syndrome [specifically, the M7 subtype], and Li-Fraumeni syndrome), and myelodysplastic syndrome (MDS; 1/3rd of MDS patients will develop AML) [246-249]. Benzene exposure is a unique risk factor for AML: following hepatic metabolism, benzene metabolites are

transported to the BM and undergo further oxidation by myeloperoxidase (MPO), yielding a mutagenic benzoquinone metabolite in myeloid cells [250, 251].

Prognosis is strongly and inversely associated with age, mostly because older patients often have comorbidities that preclude the use of standard CTx [7, 8, 19, 252, 253]. As well, older patients are more likely to present with drug resistance and unfavorable cytogenetics, specifically with alterations to chromosomes 5, 7, and 17 [252]. Aside from *PML-RARA*⁺ AML, the 5-year survival rates are 69% and 27% for patients below and above age 20, respectively [9, 254].

Subtypes of AML

AML is not one cancer, but a complex, highly heterogenous group of myeloid neoplasms [255]. Several AML subtypes exist, each with unique clinical presentations and molecular classifications (immunophenotypes) [256]. As such, AML can be classified by the World Health Organization (WHO) into any one of seven subtypes [241, 257, 258]:

- AML with recurrent genetic abnormalities (*e.g.*, *MLL1-AF9*⁺, *PML-RARA*⁺, *RUNX1-ETO*⁺, *NPM1*-mutated, *CEBPA*-mutated [biallelic], ETC.)
- AML with myelodysplasia-related changes (AML-MRC)
- Therapy-related AML (t-AML)
- AML, not otherwise specified (AML, NOS)
- Myeloid sarcoma (*noted by Burns in 1811 [259]; described as “chloroma” in 1853 by King, as the tumors appeared green due to the MPO of the myeloid cells [242, 260]*)

- Myeloid proliferations related to Down syndrome (*e.g.*, transient abnormal myelopoiesis and myeloid leukemia associated with Down syndrome)
- Blastic plasmacytoid dendritic cell neoplasm (BPDCN)

AML can arise *de novo*, that is, in patients who have not been previously treated with CTx/XRT nor have a history of MDS/myeloproliferative neoplasms (MPN) [261]. In contrast, AML can arise secondarily (sAML), resulting from the progression of MDS/MPN or previous CTx/XRT treatment. Patients with *de novo* AML, AML-MRC, and t-AML each present with distinctive mutations and cytogenetics [262].

In cases of AML, NOS, the French-American-British (FAB) classification system can be used to aid diagnosis based on cell morphology [239, 256, 263]. While the FAB system has largely been replaced by more sensitive techniques, like flow cytometry and genome sequencing, it is still used to complement molecular methods. The FAB classification consists of nine major subtypes, some of which have additional subclassifications based on differentiation status [264]:

- M0 (undifferentiated acute myeloblastic leukemia)
- M1 (acute myeloblastic leukemia with minimal maturation)
- M2 (acute myeloblastic leukemia with maturation)
- M3 (acute promyelocytic leukemia [APL]/*PML-RARA*⁺ AML)
- M4 (acute myelomonocytic leukemia [AMML])
- M4eos (acute myelomonocytic leukemia with eosinophilia [AMML Eo])
- M5 (acute monoblastic/monocytic leukemia [AMoL])
 - M5a (monocytic without differentiation [acute monoblastic leukemia])

- M5b (monocytic with differentiation [acute monocytic leukemia])
- M6 (acute erythroid leukemia [AEL])
- M7 (acute megakaryoblastic leukemia [AMKL])

While not listed under the FAB classification, acute basophilic leukemia (ABL) and acute panmyelosis with myelofibrosis (APMF) are recognized by the WHO as rare subtypes of AML, NOS [258, 265].

Pathophysiology of AML

AML encompasses a diverse group of cancers that arise when a hematopoietic stem/progenitor cell (HSPC) incurs an AML-initiating mutation, such as rearrangement of *mixed-lineage leukemia 1 (MLL1; hereafter referred to as MLL)*, biallelic loss of *CEBPA*, or *FLT3* mutation [28, 266]. An excellent report by Chopra, *et al.* posits that AML can arise through one of two mechanisms: either an HSC incurs an AML-initiating mutation that enables rapid proliferation, or a myeloid progenitor gains aberrant self-renewal capacity [28, 267]. In both cases, a myeloid cell with a survival advantage and self-renewal capacity results.

The t(9; 11)(p22; q23) translocation is an AML-driving event that produces the *MLL-AF9* oncogene and is present in nearly 1/3rd of AML patients [268]. *MLL-AF9* encodes MLL-AF9, an abnormal transcription factor wherein the N-terminus of MLL is fused to the C-terminus of AF9 [269, 270]. Normally, the MLL epigenetic modifier (*KMT2A* on chromosome 11) facilitates the expression of development- and hematopoiesis-related genes, such as *HOXA9* and *MEIS1* (whose ectopic expression alone can cause leukemia) [271]. MLL is a histone methyltransferase, an epigenetic

“writer”, that installs methyl groups on K4 of histone H3 (H3K4); namely, MLL trimethylates H3K4 (H3K4me3) [271, 272]. However, upon fusion with AF9 (*MLLT3* on chromosome 9), MLL loses its ability to correctly regulate target genes and becomes a potent driver of high-risk, acute leukemias [269, 273]. The *MLL-AF9* translocation is found in both pediatric and adult AML, is associated with cases of t-AML (specifically after treatment with etoposide [*Vepesid*®]/teniposide [*Vumon*®]), and imparts an increased risk of relapse [247, 270, 271, 274-276].

FLT3 mutations, such as the internal tandem duplication (ITD) and tyrosine kinase domain (TKD) mutations, are also common drivers of AML [277-282]. Mutations in *FLT3* are detected in 25-30% of all AML cases; the *FLT3*-ITD accounts for approximately 83% of *FLT3* mutations in AML [281, 283]. These mutations cause the FLT3 receptor tyrosine kinase to become constitutively active, leading to the aberrant growth/survival of afflicted cells. Although, it is reported that even unmutated FLT3 (*FLT3*^{WT}) is overexpressed in almost all cases of AML [277, 279, 280] and can facilitate leukemogenesis in the presence of certain driver mutations. For example, *FLT3*^{WT} is exploited in *MLL-AF9*⁺ AML to promote disease progression through the *FLT3*^{WT}-JAK3/STAT3 axis [276-281, 284-286]. Expectedly, *MLL-AF9*⁺ AML is worsened by *FLT3* mutations [276, 287].

Despite harboring the same driver mutations, the cells comprising the AML liquid tumor are heterogenous, with some being more or less differentiated than their counterparts [2, 267, 288, 289]. The more-differentiated, most abundant AML cells are referred to as “blasts” and, while being responsible for AML symptoms, they are not

believed to possess leukemogenic abilities; if transplanted, AML blasts are unable to reconstitute the disease. The less-differentiated, less abundant AML cells that initiate and maintain the disease are the LSCs; if transplanted, LSCs will reconstitute the disease.

Conventional Treatment of AML

Untreated AML constitutes a medical emergency [253, 290]. Aside from the M3 subtype, the frontline CTx regimen for newly-diagnosed/previously-untreated AML typically employs cytotoxic CTx and consists of two phases [10, 257, 291]. First, in the “7+3” or “induction” phase, cytarabine (Ara-C [*Cytosar-U*®]) is given in combination with daunorubicin (DNO [*Cerubidine*®]), sometimes abbreviated as the “DA” protocol. Occasionally, idarubicin (*Idamycin*®) will be used instead of DNO. Then, in the “consolidation” phase, Ara-C is dose-escalated and used alone [292-295]. The 7+3 phase of frontline CTx is primarily used as “cytoreduction”, a means of rapidly clearing AML blast cells from the body to help restore normal hematopoiesis and alleviate symptoms, whereas consolidation is used to prevent relapse, ideally killing any remaining LSCs [10, 293, 296-298]. While there is not currently an established treatment regimen for relapsed/refractory AML (R/R AML), a combination of fludarabine, high-dose Ara-C, G-CSF, and idarubicin (**FLAG-IDA** protocol) yields CR in approximately half of R/R AM patients CR [4, 299]. Additionally, amsacrine in combination with fludarabine, high-dose Ara-C, and G-CSF (FLAMSA protocol) can be used to prepare eligible R/R AML patients for an allogenic HSCT [300].

Mechanistically, Ara-C is a prodrug of cytarabine triphosphate (Ara-CTP), a nucleoside analog that causes chain termination and S-phase arrest upon incorporation into DNA [294, 301-303]. DNO is an anthracycline-type drug that exerts antineoplastic effects through multiple mechanisms. Chiefly, DNO blocks the relegation action of topoisomerase II during DNA replication, which leads to the accumulation of DNA double-stranded breaks and activation of the ATM/p53-mediated DNA damage response [144, 304-306]. Additionally, DNO damages DNA via intercalation, which causes histone eviction, and causes ROS formation upon reaction with O₂. While Ara-C and DNO are effective, AML cells possess mechanisms to counter their effects. AML cells can resist Ara-C by expressing SAMHD1, a hydrolase that degrades Ara-CTP, the active metabolite of Ara-C [26, 27]. AML cells can overexpress ABC transporters, such as P-glycoprotein and ABCG2, to efflux intracellular DNO [307].

Cytogenetics, whole-genome sequencing, and immunophenotyping are becoming increasingly valued in the diagnosis, risk stratification, and treatment planning of AML [308]. AML risk-stratification by genetics is indicated by 2023 National Comprehensive Cancer Network (NCCN) and 2022 European LeukemiaNet (ELN) guidelines; for example, *MLL-AF9*⁺ AML carries a better prognosis versus *TP53*-mutated AML [309, 310]. Although, despite vast knowledge of the genetics and pathophysiology of AML, precision medicine and targeted therapies are lacking. Cytotoxic CTx remains the standard-of-care for most AML patients despite their typically advanced age and frailty.

Targeted Therapies for AML

Targeted therapies are available but currently limited to patients harboring specific genetic signatures [14, 295]. Inhibitors specific to mutated *FLT3* (midostaurin [*Rydapt*®] & gilteritinib [*Xospata*®]) and *IDH1/2* (ivosidenib [*Tibsovo*®]/enasidenib [*Idhifa*®]) are available, and an antibody-drug conjugate can be used for patients with CD33⁺ AML cells (gemtuzumab ozogamicin [*Mylotarg*®]).

Recently, following promising results from the AUGMENT-101 clinical trial (NCT04065399), revumenib (SNDX-5613, *Syndax*) displayed efficacy in acute leukemia patients harboring *MLL* rearrangements (*MLL*-r [e.g., *MLL-AF9* or *MLL-AF6*]) or *NPM1* mutations that cause *NPM1* to translocate to the cytoplasm (*NPM1c*) [22, 311]. Revumenib disrupts the interaction between *MLL* and menin (*MEN1*), thereby preventing *MLL* from inducing transcription of leukemia-promoting genes like *HOXA9*, *PBX3*, and *MEIS1*.

Expectedly, *MEN1* mutations have been reported in patients who progress on revumenib monotherapy, highlighting the necessity of combination regimens even with targeted agents. However, combination/targeted therapy requires the discovery of feasible targets and development of molecules [24]. Recent research has suggested that various components of TLR signaling, including TICAM-1 and RIPK1/3, are feasible molecular targets for the treatment of *MLL-AF9*⁺ AML. While targeted therapies applicable to a larger cohort of AML patients are emerging, such as E-selectin antagonists (uproleselan [phase III: NCT03616470]; *GlycoMimetics, Inc.*) and p53-restoring agents (eprenetapopt/APR-246; *Aprea Therapeutics, Inc.*), all cases of non-

M3 AML still necessitate cytotoxic CTx [23, 312]. Thus, there is dire need for the discovery of novel molecular targets [19, 23, 312].

Targeting TLR Signaling to Treat AML

TLRs are expressed on many cell types, including normal HSPCs and AML cells. In normal hematopoiesis, HSPCs express varying levels of TLR2/4/7/8/9 [313]. Activation of TLRs causes HSPCs to produce inflammatory cytokines and skews them towards myeloid fate (myelopoiesis) at the cost of lymphoid fate (lymphopoiesis). Stimulation of TLR7/8 on human CD34⁺ HSCs causes them to produce IL-1 β , IL-6, IL-8, TNF- α , and GM-SCF, and further promotes their differentiation into macrophages and monocyte-derived dendritic cells (moDCs) [314]. In addition, stimulation of TLR7 on common myeloid progenitors (CMPs) promotes their fate as monocyte/macrophages, and this effect is enhanced in by IFN-I. Activation of TLR2/4 promotes cycling and myeloid differentiation of murine Lin⁻Sca1⁺c-Kit⁺ cells (LSK cells [LSKs]), mediated largely through MYD88-dependent signaling. The effect of TLR stimulation on HSPCs may be illustrated by the “left shift” (bandemia) observed clinically in patients with severe infections [315]. Bandemia indicates emergency granulopoiesis and increased G-CSF production, likely mediated at least in part by TLR activation on HSPCs [316, 317].

TLRs are also expressed differentially on AML cells. Specifically, TLR2/4/7/8 are expressed highly, TLR1/5/9/10 to a lesser degree, and TLR3 expression is undetectable. Relevant to our study, the AML subtypes commonly driven by *MLL-AF9* (M4 and M5) express markedly higher levels of TLR4 and TLR7 [274, 318].

The role of TLR signaling in AML appears somewhat pleiotropic, however. While AML cells have been thoroughly demonstrated to rely on TLR signaling for their survival and leukemogenicity, TLR agonism has been shown to be an effective anti-AML strategy in mouse models [319-321]. While *TLR2* and *TLR4* mRNA levels are reported to inversely correlate with OS of AML patients, selective TLR stimulation has been shown to possess antileukemic effects, specifically in *MLL-AF9*⁺ AML models [322, 323]. While TLR1 is required for the survival of *MLL-AF9*⁺ mouse HSPCs, TLR1/2 agonism reduces leukemogenicity of transplanted *MLL-AF9*⁺ cells by promoting their differentiation [324]. Moreover, TLR4/7 stimulation induces increased expression of CD54, CD80, and CD86 on AML M4/M5 cells, enhancing their susceptibility to T cell-mediated clearance [325].

Our group and others have demonstrated that blockade of TLR signaling, genetic and pharmacologic, has anti-AML effects *in vitro* and *in vivo*. Specifically, our lab has demonstrated that blocking TLR and TLR-related signaling hampers the leukemogenicity of *MLL-AF9*⁺ cells in human cell lines and mouse models.

Volk, *et al.* demonstrated the necessity of TNF signaling in *MLL-AF9*⁺ mouse cells and human AML cell lines [35]. It was determined that while normal HSPCs do not require TNF for their survival, several human AML cell lines (HL-60, ML2, NB4, and THP-1) rely on autocrine TNF, which activates their JNK-AP1 and NF- κ B axes. Notably, not only does TNF promote the survival of AML cells also proves toxic to local HSPCs. Thus, AML cells may “weaponize” TNF as a strategy to overtake the BM. Blocking JNK

or NF- κ B signaling delays leukemogenesis in a mouse model of *MLL-AF9*⁺ AML, supporting the targeting of TNF/JNK/NF- κ B signaling as a means of AML treatment.

Xin, *et al.* showed that *MLL-AF9*⁺ cells rely on RIPK1/RIPK3, serine/threonine kinases that mediate TNF- and IFN-I-induced cell death, for their survival [36, 326]. It was determined that pharmacologic blockade of RIPK1/3 sensitizes AML cells to IFN- γ -induced differentiation, leading to a reduction in AML cell growth and clonogenicity. In addition, the loss of either kinase alone significantly delays leukemogenesis in an *MLL-AF9*⁺ AML mouse model, and this benefit is strongly augmented by the addition of IFN- γ . These data provide further support for the targeting of TNF- and RIPK1/3-associated cellular machinery as anti-AML therapy.

Most recently, Cannova determined that *MLL-AF9*⁺ mouse LSCs (c-Kit⁺CD11b^{lo}) rely on MYD88 and TICAM-1 for leukemogenesis [32]. Following TLR stimulation, TICAM-1 recruits TBK1 and is phosphorylated by TBK1 on its S210, S212, and T214 residues [29, 327]. An activated TICAM-1 will recruit IRF3 to facilitate its phosphorylation by TBK1. TBK1 is an integral component of TLR signaling, as TBK1 is required for the TICAM-1-mediated activation of IRF3 [328]. Subsequent studies suggested that TBK1 is a feasible target for AML treatment, as pharmacologic inhibition with BX795 hampers the clonogenicity of *MLL-AF9*⁺ mouse HSPCs; however, shRNA knockdown of *Tbk1* in the same cells failed to recapitulate the effects seen with BX795. It is possible that the knockdown of *Tbk1* was insufficient, but it is also possible that the other targets of BX795 (IKK ϵ , Aurora B, NUA1, and PDK1) are involved in the clonogenicity of these cells. Regardless, *Tbk1* warrants further investigation [32].

These data together strongly demonstrate that TLR signaling is critical to the survival and leukemogenicity of AML LSCs. However, while preliminary data support the targeting of TBK1—a transducer of TLR3/4/7/8/9 and TICAM-1 signaling—for AML treatment, the role of TBK1 has yet to be determined [29, 320].

TBK1 as a Molecular Target for AML Treatment

Considering previous data and being a critical component of TLR signaling, we hypothesize that TBK1 is a molecular target that can be employed for AML treatment. Specifically, just as targeting TICAM-1 did, targeting TBK1 may antagonize the p27^{Kip1}-quiescent AML cells that are CTx-resistant and responsible for relapse: LSCs (c-Kit⁺CD11b⁺). In addition to Cannova's preliminary data, recent reports provide additional evidence that TBK1 blockade has anti-AML effects.

In 2018, Liu, *et al.* demonstrated that human AML cells that rely on the YBX1-MYC axis for their survival (MOLM14, OCIAML5, HL-60, and KASUMI-1) also require TBK1 and/or IKK ϵ ; although, it was not determined if just one or both kinases are required for survival [34]. This finding was recapitulated in a mouse xenograft model using MOLM-14 cells, which are *MLL-AF9*⁺ and *FLT3-ITD*⁺ [34, 282]. MMB, a TBK1/IKK ϵ inhibitor, dose-dependently reduced the leukemia burden and spleen sizes of xenografted mice. While MMB also inhibits JAK1/2, ACVR1, and ALK2, its antileukemic effects were determined to be specific to TBK1/IKK ϵ , at least in MOLM-14 cells, independent of JAK1/2, ACVR1, or ALK2 blockade.

Mechanistically, MMB exerts its effects by dampening YBX1 phosphorylation (S102), causing a dose-dependent reduction in MYC protein levels [34]. Although, TBK1 and IKK ϵ are not anticipated to directly interact with YBX1, but rather facilitate its interaction with an unidentified kinase; the authors ruled-out the involvement of AKT. While MMB also reduces the clonogenicity of AML cells more significantly than healthy CD34⁺ HSCs, the control cells were not unaffected; thus, the authors cautioned that prolonged blockade of TBK1/IKK ϵ could be harmful to normal hematopoiesis.

Additionally, the authors mined cDNA microarray datasets from 2004 (GSE1159) and 2009 (GSE13159). As such, while *IKBKE* expression (204549_at) is slightly/positively correlated ($p = 0.04$) with the OS of AML patients, *TBK1* expression (218520_at) has no bearing (p -value unlisted) [34, 329-331]. However, Liu, *et al.* only reported on the 2004 dataset when investigating *TBK1*. In contrast, *BloodSpot* mined the 2009 dataset when they reported that *TBK1* expression is strongly/negatively correlated ($p = 0.00227$) with OS of AML patients while *IKBKE* expression is not predictive ($p = 0.327$) [332-336] (**Figure 3**). Thus, further research regarding *TBK1* and *IKBKE* expression in AML is required, with RNA-seq now being the gold-standard for determining the prognostic value of gene expression.

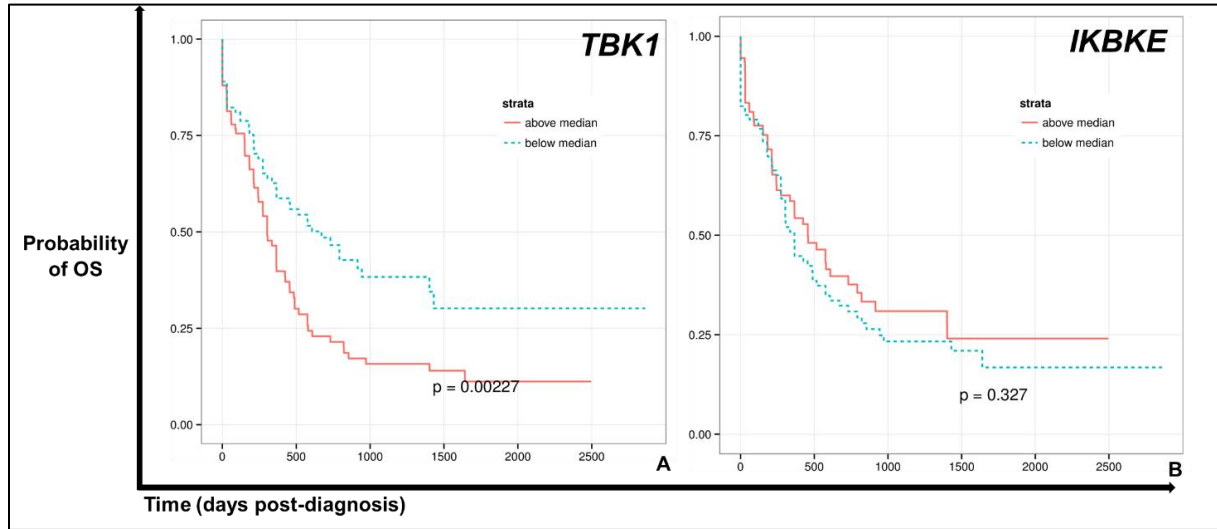


Figure 3. *TBK1* mRNA Expression is Negatively Correlated with AML Prognosis, based on Microarray Data. Kaplan-Meier curves generated by *BloodSpot* based on median expression of (A) *TBK1* or (B) *IKBKE* mRNA in human AML patients. Based on cDNA microarray data from 2009, *TBK1* mRNA level is significantly/negatively correlated ($p = 0.00227$) with probability of OS whereas *IKBKE* mRNA is not correlated ($p = 0.327$). Above-median expression of *TBK1* mRNA portends decreased probability of OS in AML.

In 2021, Chen, *et al.* demonstrated that pharmacologic *TBK1* blockade sensitizes human AML cells to CTx [33]. Specifically, treatment with GSK8612, a *TBK1*-selective inhibitor, sensitizes human AML cell lines (HL-60 and KASUMI-1) and patient samples to 100nM DNO. Notably, the *MLL-AF9*⁺ THP-1 cell line was not sensitized by GSK8612, possibly due to a decreased expression of *TBK1* compared to HL-60 and KASUMI-1 cells. Mechanistically, inhibiting *TBK1* dampens activation of CDK2, promoting G0/G1 arrest. It was determined that *TBK1* activates CDK2 through AKT1/2, such that pharmacologic inhibition of AKT1/2 sensitized cells to DNO similarly to GSK8612. Specifically, *TBK1* or AKT1/2 blockade augments the apoptosis-inducing ability of DNO.

The authors also found that TBK1 protein is significantly increased in the BM of AML patients compared to healthy controls. Notably, R/R AML patients displayed significantly higher levels of TBK1 compared to AML patients who achieved CR; this finding could suggest that TBK1 contributes to treatment-resistance in AML.

It was determined that the upregulation of inflammation-associated genes drives resistance to FLT3 inhibitors in *FLT3*-ITD⁺ AML cells [277, 337]. Specifically, MV4-11 cells are observed to upregulate inflammatory gene sets as they develop resistance to quizartinib (GSE116432). Although, treatment with the glucocorticoid dexamethasone resensitizes both MV4-11 cells and *FLT3*-ITD⁺ patient samples/xenograft models to quizartinib. Mechanistically, dexamethasone induces increased expression of the proapoptotic BIM and degradation of the antiapoptotic MCL-1, leading to increased cell death in *FLT3*-ITD⁺ but not *FLT3*^{WT} human AML cells.

Subsequently, after mining the RNA-seq data from Gebru, et al., Wooten's group utilized an *in silico* approach (weighted gene co-expression network analysis [WGCNA]) to identify possible therapeutic targets to counter drug-resistance in *FLT3*-ITD⁺ AML [283, 337]. The authors posited that TBK1 upregulates a set of genes in response to dexamethasone in quizartinib-resistant, MV4-11 cells. Specifically, genes hypothesized to be regulated by TBK1 are associated with extracellular matrix remodeling and collagen synthesis. While the significance of this finding is unknown, it suggests that TBK1 functions in opposition to dexamethasone in quizartinib-resistant, *FLT3*-ITD⁺ AML cells. Furthermore, midostaurin (*Rydapt*[®])—a staurosporine derivative used in the treatment of *FLT3*-mutated AML—was recently demonstrated to inhibit TBK1 with an

IC₅₀ of 9 nM [338, 339]. While the significance of this finding is unknown, TBK1 blockade may contribute to the antileukemic activity of midostaurin (*Rydapt*[®]).

While these reports support the targeting of TBK1 as a means of AML treatment, the role of TBK1 in normal hematopoiesis has yet to be determined. For TBK1 blockade to be an effective anti-AML strategy, any untoward effects on normal hematopoiesis must be minimal and, ideally, TBK1 inhibition should preferentially afflict AML cells.

CHAPTER 3

AIM 1: DETERMINE IF TBK1 IS REQUIRED FOR MURINE HEMATOPOIESIS

Results: Global *Tbk1* Deletion in Murine Hematopoiesis

***TBK1* mRNA Expression Levels Appear Somewhat Consistent Across the Human and Murine Hematopoietic Systems**

The ideal CTx would selectively kill cancer cells while sparing the normal, healthy counterparts. Most conventional chemotherapies show some degree of selectivity as they preferentially afflict the most rapidly dividing cells, which includes but is not limited to cancer cells [340]. Cells of the gastrointestinal mucosa, hair follicle, and especially hematopoietic system also divide rapidly, hence the side effects characteristic of cytotoxic CTx (e.g, diarrhea, non-androgenic alopecia, and myelosuppression, respectively). Similar to antibiotics, which target the 70S ribosome or other proteins unique to bacteria, selectivity can be conferred to anticancer drugs by targeting a gene/protein unique to or overexpressed by cancer cells; excellent examples of this are the targeting of *BCR-ABL1* in CML or HER2 (trastuzumab [*Herceptin*®]) in HER2⁺ breast cancer [341, 342]. While TBK1 seems to be a promising target for AML treatment, we sought to determine if targeting TBK1 may selectively afflict AML cells.

To this end, we examined RNA-seq datasets catalogued on *Haemosphere/Haemopedia* to investigate *TBK1* expression across the human (GSE115736) and murine (GSE116177) hematopoietic systems [343]. We believe that increased expression of *TBK1* would suggest an increased reliance on its protein product, thus making cells with high *TBK1* expression more sensitive to TBK1 inhibition.

From the RNA-seq data examined, *TBK1* appears to be expressed at similar levels across cells of the human (**Figure 4**) and murine (**Figure 5**) hematopoietic systems, aside from some select populations where it is expressed at relatively lower levels, such as reticulocytes (likely at least partially due to enucleation), NK cells, and plasma/plasmacytoid dendritic cells. However, this conclusion was based on a visual inspection of $\log_2(\text{tpm}+1)$ -plotted expression levels and can only be interpreted as such; obviously, a statistical comparison would be more reliable.

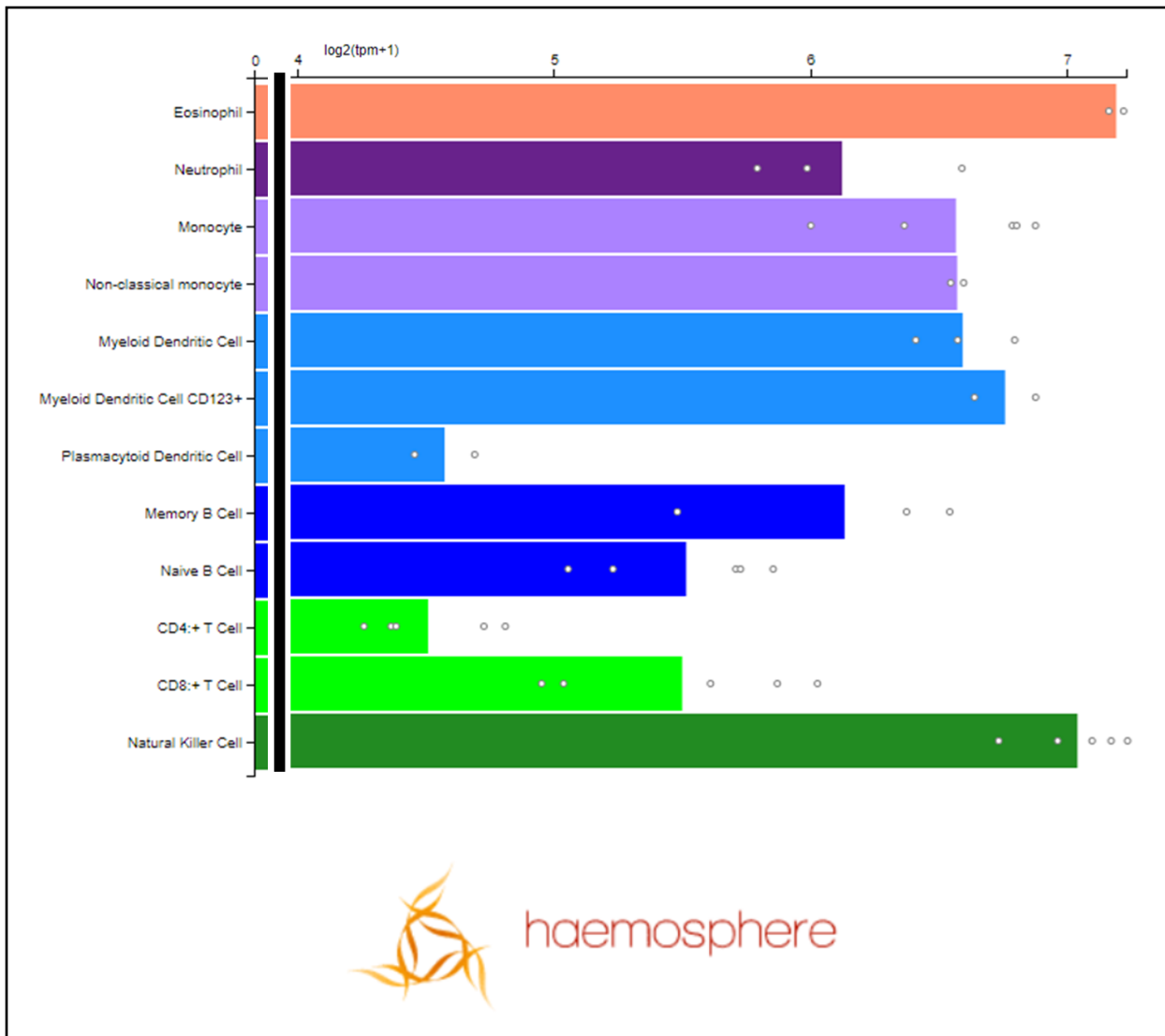


Figure 4. *TBK1* mRNA Expression Level is Somewhat Consistent Across the Human Hematopoietic System. The RNA-seq data catalogued by *Haemosphere* (GSE115736 [Haemopedia-Human-RNASeq]) from human hematopoietic cells was $\log_2(\text{tpm}+1)$ -plotted and visually inspected. Between the select cell types depicted therein, *TBK1* mRNA level appears roughly consistent (aside from decreased levels in plasmacytoid dendritic cells and CD4⁺ T cells). NOTE: graph has been broken (black bars) between 0 and 4 to allow for better visualization.

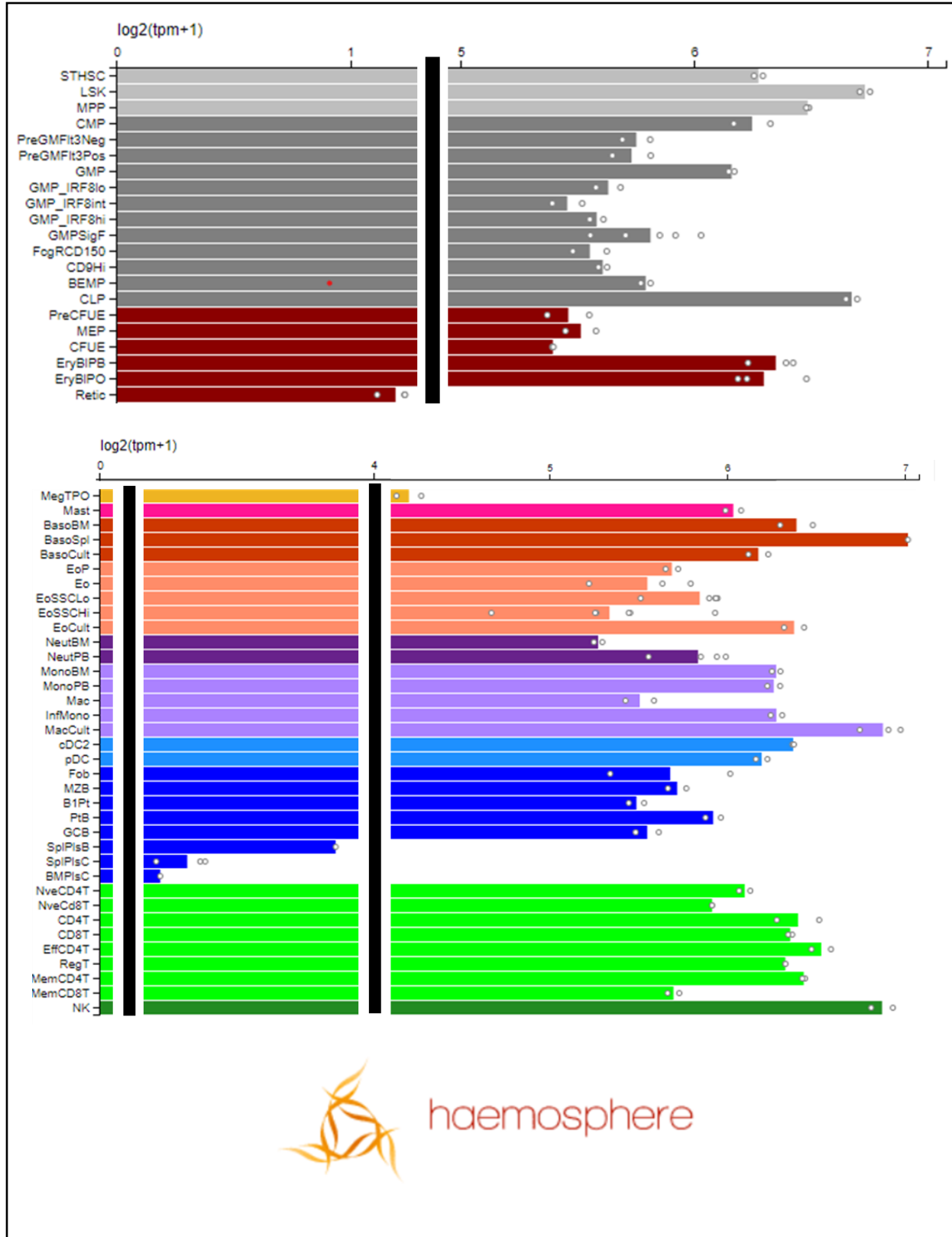


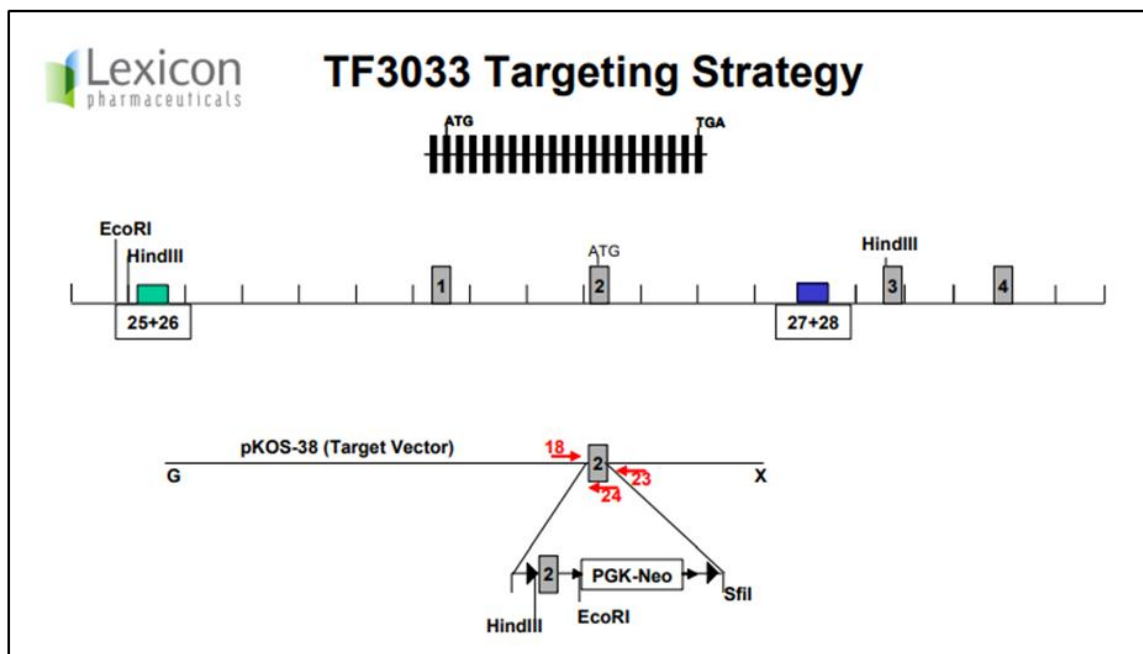
Figure 5. *Tbk1* mRNA Expression Level is Somewhat Consistent Across the Murine Hematopoietic System. The RNA-seq data catalogued by *Haemosphere* (GSE116177 [Haemopedia-Mouse-RNASeq]) from murine hematopoietic cells was $\log_2(\text{tpm}+1)$ -plotted and visually inspected. Between the select cell types depicted therein, *Tbk1* mRNA level appears roughly consistent (aside from decreased levels in reticulocytes and plasma cells). NOTE: graphs have been broken (black bars) to allow for better visualization.

Development of a Tamoxifen-inducible, Global *Tbk1*-knockout Mouse

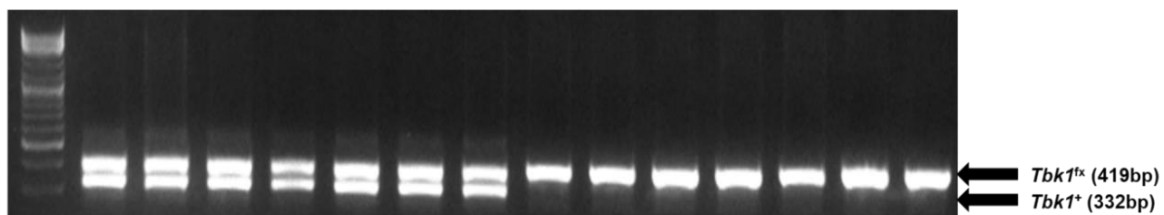
To study the role of *Tbk1* in normal and malignant hematopoiesis, we generated tamoxifen-inducible, global *Tbk1*-knockout (*Tbk1*^{NULL}) mice. All mice were maintained on the B6 background.

The *Tbk1*-deletion strategy employed was adapted from Marchlik, *et al.* and produced by Lexicon Pharmaceuticals (Lexicon; **Figure 6A**) [127, 344]. The deletion strategy involved flanking exon 2 of *Tbk1* with *loxP* sites (floxing; *Tbk1*^{fx}). Floxed-homozygous (*Tbk1*^{fx/fx}) mice were crossed with *Rosa26-CreER*^{T2+} mice until *Tbk1*^{fx/fx};*Rosa26-CreER*^{T2+} mice were generated (**Figures 6B and 6C**). *Tbk1*^{fx/fx} mice NOT harboring *Rosa26-CreER*^{T2} were used as “wild-type” (WT) controls to control for tamoxifen exposure. In addition, *Tbk1*^{+/fx};*Rosa26-CreER*^{T2+} mice were bred as floxed-heterozygous controls; however, time did not allow for analysis of these mice within the scope of this thesis.

A



B



C

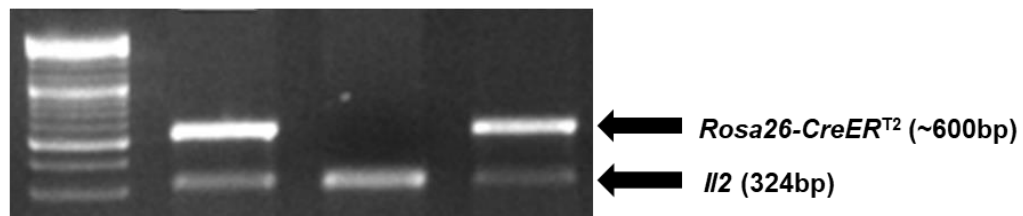


Figure 6. $Tbk1^{fx/fx};Rosa26-CreER^{T2+}$ Mice are Generated. $Tbk1^{fx/fx}$ mice were purchased from Lexicon using a floxing strategy previously indicated by Marchlik, *et al.* $Tbk1^{fx/fx}$ mice were crossed with $Rosa26-CreER^{T2+}$ mice until $Tbk1^{fx/fx};Rosa26-CreER^{T2+}$ progeny were generated. (A) Schematic depicting $Tbk1$ -floxing/knockout strategy adapted from Marchlik, *et al.* and produced by Lexicon. Homologous recombination results in floxing of exon 2 and consequent insertion of *PGK-Neo*; red arrows depict PCR primers indicated by Lexicon. “ATG” indicates the $Tbk1$ start codon contained in exon 2. (B) Results from 3% agarose gel electrophoresis/ $Tbk1$ PCR-genotyping depicting $Tbk1^{fx/fx}$ and $Tbk1^{+/fx}$ mice. Each lane corresponds to an individual mouse, left-most lane contains 1kB DNA ladder, and Lexicon primers #18 and #24 were used to determine *loxP* status. (C) Results from 3% agarose gel electrophoresis/ $Rosa26-CreER^{T2}$ PCR-genotyping depicting $Rosa26-CreER^{T2+}$ and $Rosa26-CreER^{T2-}$ mice. Each lane corresponds to an individual mouse, left-most lane contains 1kB DNA ladder. Murine interleukin 2 gene (*Il2*) primers added as reaction/internal control.

***Tbk1* Deletion is Complete in the Bone Marrow of a 6-week-old Mouse**

Under basal conditions, the $CreER^{T2}$ recombinase resides in the cytoplasm, inactive, sequestered by heat-shock protein 90 (Hsp90) [345, 346]. Upon exposure to 4-hydroxytamoxifen (4-OHT), a principal metabolite of tamoxifen, $CreER^{T2}$ is released from Hsp90 and allowed to enter the nucleus for its recombinase activity. Notably, especially for *in vitro* deletion, $CreER^{T2}$ is unresponsive to tamoxifen and requires 4-OHT for activation. As tamoxifen is metabolized to 4-OHT, intraperitoneal delivery of tamoxifen is acceptable as it will undergo hepatic metabolism following movement across the peritoneal mesothelium and absorption into the bloodstream [347].

Following a regimen indicated by Zhong, *et al.*, mice were injected at 6-8 weeks of age with 100mg/kg tamoxifen for 4 days consecutively (**Figure 7A**; hereafter, referred

to as “tamoxifen regimen”) [348]. Deletion was checked via PCR of genomic DNA (gDNA).

In 6-week-old mice, *Tbk1* is deleted efficiently in c-Kit⁺ and c-Kit⁻ BM cells (**Figure 7B**) by 12-days post-tamoxifen regimen; tail and other hematopoietic tissues were not analyzed. All mice in our study underwent the tamoxifen regimen between 6 and 8 weeks of age, unless otherwise specified. As such, it was anticipated that the deletion would be complete in subsequent mice, and mice were not individually assessed for deletion until later in the study. As the BM gives rise to the entire hematopoietic system, it was presumed that a complete deletion of *Tbk1* in the BM was sufficient for our analyses. As turnover of the murine hematopoietic system occurs approximately every 16 weeks, a “washout” period of 3-6 months was allowed between the tamoxifen regimen and analysis, to allow for complete regeneration of the—now *Tbk1*^{NULL}—hematopoietic system. It was believed that deletion of *Tbk1* need only occur in HSPCs to achieve a *Tbk1*-deficient hematopoietic system, so *Tbk1*-deletion was not routinely checked in following mice.

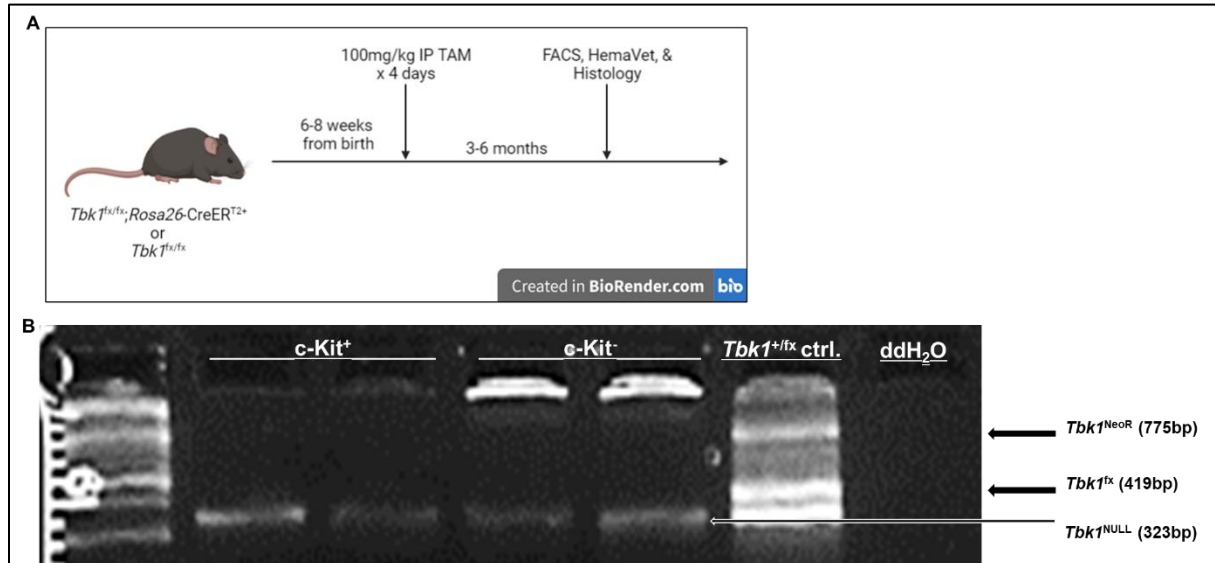


Figure 7. Deletion of *Tbk1* is Complete in the Bone Marrow. To determine the efficacy of our tamoxifen-inducible, *Tbk1*-knockout system, a 6-week-old male mouse ($n = 1$) was injected with 100mg/kg tamoxifen IP for 4 consecutive days (standard tamoxifen regimen) and the deletion of *Tbk1* was checked 12 days after the final tamoxifen dose (PCR using c-Kit⁺ and c-Kit⁻ bone marrow cells). (A) Schematic depicting tamoxifen-induced deletion of *Tbk1*; created with BioRender.com. (B) Results from 2-3% agarose gel electrophoresis/*Tbk1* PCR. gDNA template from c-Kit⁺ and c-Kit⁻ bone marrow cells (ran in duplicate) from a 6-week-old mouse that underwent tamoxifen regimen 12 days prior to analysis; left-most lane contains 1kB DNA ladder and Lexicon primers #18, #23, and #24 were used to determine *Tbk1* status; untreated *Tbk1*^{+/flx} gDNA (positive) and water (negative) controls are shown.

***Tbk1*^{NULL} Mice Do Not Display Changes in Levels of Mature Blood Cells nor Erythroid Precursors**

To determine if *Tbk1* is required to produce mature hematopoietic cells in the BM and PB, as well as erythroid progenitors in the BM, BM and PB were harvested from *Tbk1*^{NULL} mice at approximately 3-5-months post-deletion. Mice were age-matched (5-6

months old) and compared to *Tbk1*^{fx/fx} controls that underwent the same tamoxifen regimen; sex-matching was not performed.

The harvested tissues were analyzed via FACS, and relevant populations measured as percentage of total nucleated cells (TNCs) in the PB (PB-TNCs; **Figure 8A**) or BM (BM-TNCs; **Figure 8B**); doublets eliminated by gating on single cells (SC). B cells (B220⁺), T cells (CD3⁺), monocytes (CD11b⁺Gr1⁻), granulocytes (Gr1⁺), megakaryocytes (CD41⁺), and erythroid progenitors (Ter119⁺) were analyzed. Representative FACS gating strategies are shown (**Figures 9A** and **9B**). Statistics could not be performed to the low number of mice analyzed (n = 2 of each). While several other batches of mice were analyzed, technical issues with staining and sample preparation precluded them from our analysis.

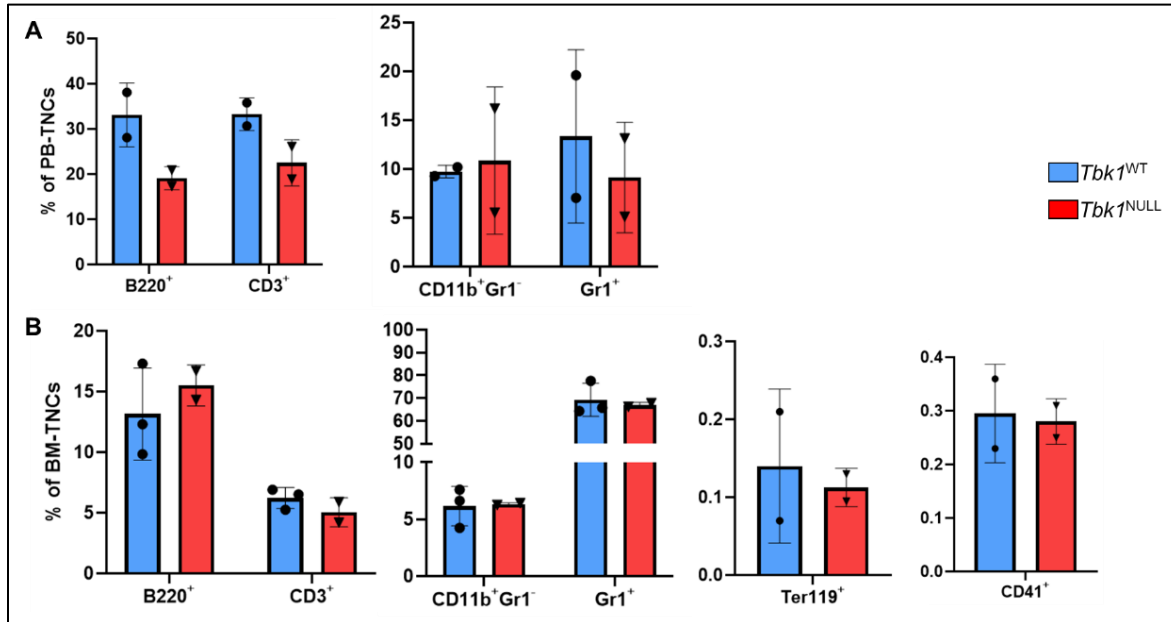


Figure 8. *Tbk1* Deletion Does Not Affect Levels of Mature Blood Cells nor Erythroid Progenitors in the PB or BM. To determine if the loss of *Tbk1* affects homeostatic hematopoiesis, the levels of mature cells in the PB and BM, as well as erythroid progenitors and megakaryocytes in the BM, were analyzed via FACS. The data were quantified, though statistical analyses could not be performed due to insufficient numbers of mice ($n = 2$ *Tbk1*^{WT}, 2 *Tbk1*^{NULL}). (A) PB-TNCs. (B) BM-TNCs.

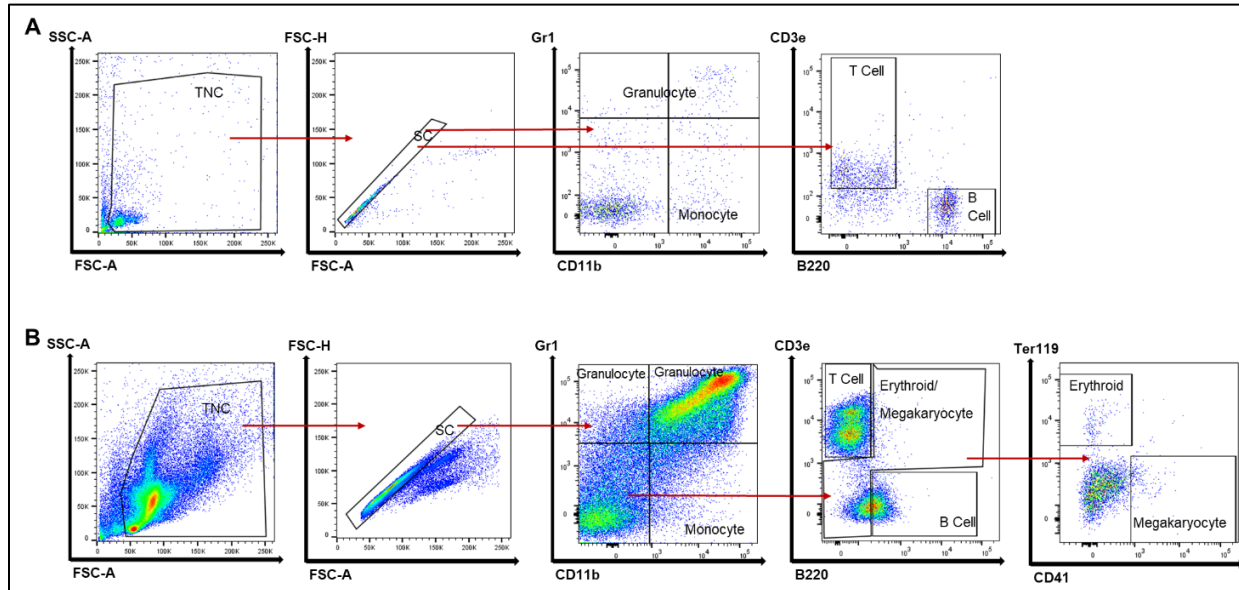


Figure 9. Representative Gating Strategies for FACS Analysis of Mature Blood Cells, Erythroid Precursors, and Megakaryocytes. After gating on TNCs and eliminating doublets (SC gating), B cells (B220⁺), T cells (CD3⁺), monocytes (CD11b⁺Gr1⁻), granulocytes (Gr1⁺), megakaryocytes (CD41⁺), and erythroid progenitors (Ter119⁺) were analyzed. (A) PB-TNCs and (B) BM-TNCs.

Notwithstanding the low sample size, it appears that *Tbk1* is not required for the production of mature cells in the BM or PB, nor is *Tbk1* required for the function of erythroid progenitors.

***Tbk1*^{NULL} Mice Display a Significant Increase in the Myeloid-Biased MPP3 Population of HSPCs**

To determine if *Tbk1* is required for the function of select HSPCs, BM was harvested from *Tbk1*^{NULL} mice at approximately 3-5-months post-deletion. Mice were age-matched (5-6 months old) and compared to *Tbk1*^{fx/fx} controls that underwent the same tamoxifen regimen; sex-matching was not performed. The harvested tissues were

analyzed via FACS, and relevant populations measured as percentage of BM-TNCs.

Representative FACS gating strategy is shown (**Figure 10D**). All murine HSPCs are Lin⁻c-Kit⁺ (LK cells [LKs]), but only some are also positive for Sca1⁺ (LSK cells [LKSs]).

Thus, all HSPCs reside within the LK compartment of the BM, which includes both LKs and LSKs.

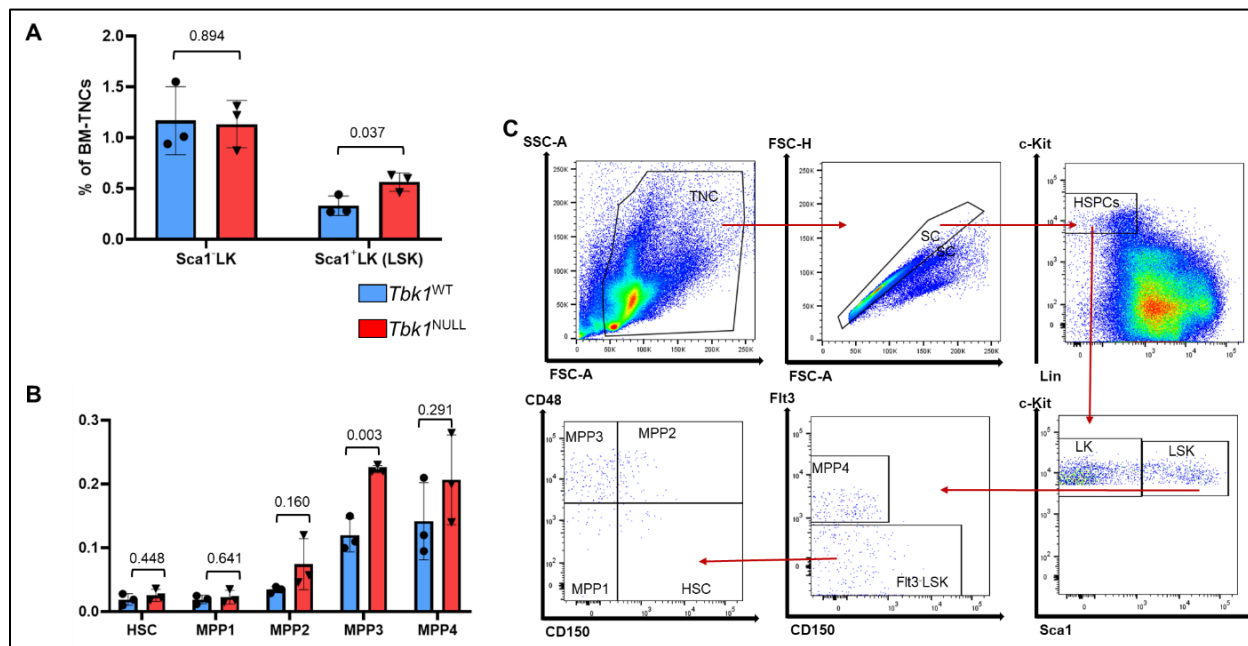


Figure 10. The MPP3 Population is Significantly Increased Following *Tbk1* Deletion. To determine if the loss of *Tbk1* affects HSPCs, the levels of HSPCs in the BM were analyzed via FACS. The data were quantified and unpaired t-test used for all statistical analyses ($n = 3$ *Tbk1*^{WT}, 3 *Tbk1*^{NULL}). (A) LK compartment (LKs + LSKs); LSK, $p = 0.037$. (B) MPP4/LMPP (Flt3⁺CD150⁻ LSK) and Flt3⁻ LSKs, separated by CD48 and CD150; MPP3 (Flt3⁻CD150⁻CD48⁺ LSK), $p = 0.003$. (C) Representative gating strategy for FACS analysis. After gating on TNCs and eliminating doublets (SC gating), the HSC and MPP1-MPP4 subsets were analyzed.

I observed that the loss of *Tbk1* does not affect the size of the LK compartment as percentage of BM-TNCs (**Figure 10A**). However, deletion of *Tbk1* does lead to an

increase in the number of LSKs within the LK compartment, though not at the cost of LK cells ($p = 0.037$; **Figure 10A**). To determine the nature of this increase, the LSK subset was examined further using Flt3 and CD150.

I found that the loss of *Tbk1* leads to an increase in the number of Flt3⁻ LSKs ($p = 0.005$; **Figure 10B**). Following this observation, Flt3⁻ HSPCs were examined using CD150 and CD48, wherein it was revealed that the MPP3 (Flt3⁻CD150⁻CD48⁺ LSK), population was increased significantly ($p = 0.003$; **Figure 10C**). In addition, while not significant, a trend towards increased ($p = 0.160$; **Figure 10C**) MPP2 was observed. From these data, it was determined that the increase in LSK cells in *Tbk1*^{NULL} mice was most likely due to an increase in the MPP3 population. This suggests that *Tbk1* promotes the differentiation of HSPCs, such that loss of *Tbk1* causes an accumulation of HSPCs at the MPP3 stage or increase in the size of the MPP3 compartment, and possibly also the MPP2 stage.

***Tbk1*^{NULL} Mice Do Not Display Changes in Levels of Specific Myeloid Progenitors**

To determine if *Tbk1* is required for the function of specific myeloid progenitors, BM was harvested from *Tbk1*^{NULL} mice at approximately 3-5-months post-deletion. Mice were age-matched (5-6 months old) and compared to *Tbk1*^{fx/fx} controls that underwent the same tamoxifen regimen; sex-matching was not performed. The harvested tissues were analyzed via FACS, and relevant populations measured as percentage of BM-TNCs. Representative FACS gating strategy is shown (**Figure 11D**).

No significant changes were observed in granulocyte/monocyte progenitors (GMP/CFU-GM), common myeloid progenitors (CMP/CFU-GEMM), differentiated precursors (DP) (**Figure 11A**), megakaryocyte progenitors (MkP [Lin⁻Kit⁺CD41⁺CD150⁺]; **Figure 11B**), pre-colony-forming units-erythroid (Pre CFU-E), colony-forming units-erythroid (CFU-E), pre-megakaryocyte-erythroid progenitors (Pre-MegE), or pre-myeloid-erythroid progenitors (Pre-MEP) (**Figure 11C**) populations in *Tbk1*^{NULL} mice. These data indicate that *Tbk1* does not regulate the aforementioned myeloid progenitors.

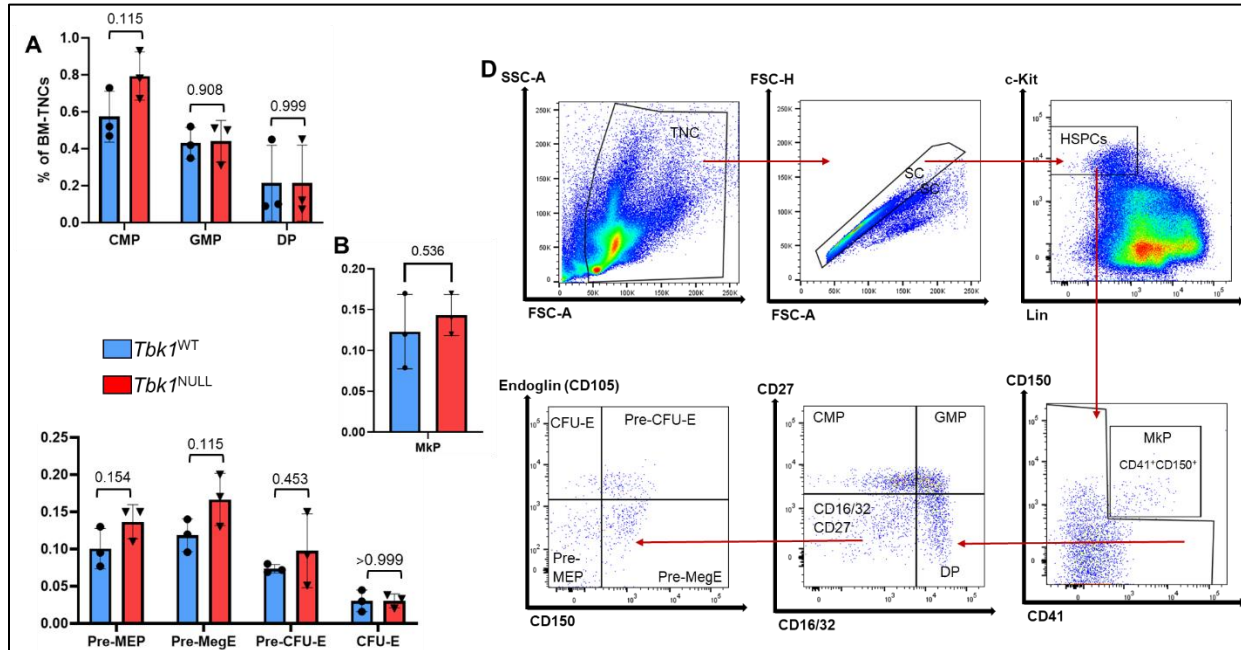


Figure 11. Deletion of *Tbk1* Does Not Cause Significant Changes in Myeloid Progenitor Populations. To determine if the loss of *Tbk1* affects myeloid progenitors, the levels of myeloid progenitors in the BM were analyzed via FACS. The data were quantified and unpaired t-test used for all statistical analyses ($n = 3$ *Tbk1*^{WT}, 3 *Tbk1*^{NULL}). (A) Non-MkP HSPCs. (B) MkPs (Lin⁻c-Kit⁺CD41⁺CD150⁺). (C) CD16/32⁻CD27⁻ Non-MkPs. (D) Representative gating strategy for FACS analysis. After gating on TNCs and eliminating doublets (SC gating), the myeloid progenitor subsets were analyzed.

Tbk1^{NULL} Mice Display a Significant Increase in Circulating Neutrophils

To determine if *Tbk1*^{NULL} mice displayed abnormalities in blood-cell counts, PB was isolated via cardiac puncture (post-mortem) and analyzed using *HemaVet*[®]. PB herein was isolated from *Tbk1*^{NULL} mice approximately 6-months post-deletion, making them ~7-8 months of age. Mice were age-matched and compared to *Tbk1*^{fx/fx} controls that underwent the same tamoxifen regimen; sex-matching was not performed.

Tbk1^{NULL} mice displayed a trend towards increased ($p = 0.067$) total white blood cells (WBCs)/leukocytes (**Figure 12A**) and a significant increase ($p = 0.008$) in neutrophils (**Figure 12B**); no changes were observed in red blood cells (RBCs), hemoglobin (Hb), platelets (Plts) (**Figure 12A**) or other leukocytes (**Figure 12B**). These data indicate that *Tbk1* negatively regulates the production of neutrophils and seems to, overall, restrain WBC production. In contrast to Marchlik, *et al.*, no differences were observed in circulating monocytes ($p = 0.136$), however, differences in mouse background (129S5/B6) and *Tbk1*-deletion strategy (germline/tamoxifen-inducible) confound comparisons between our model and Marchlik, *et al.*'s [127].

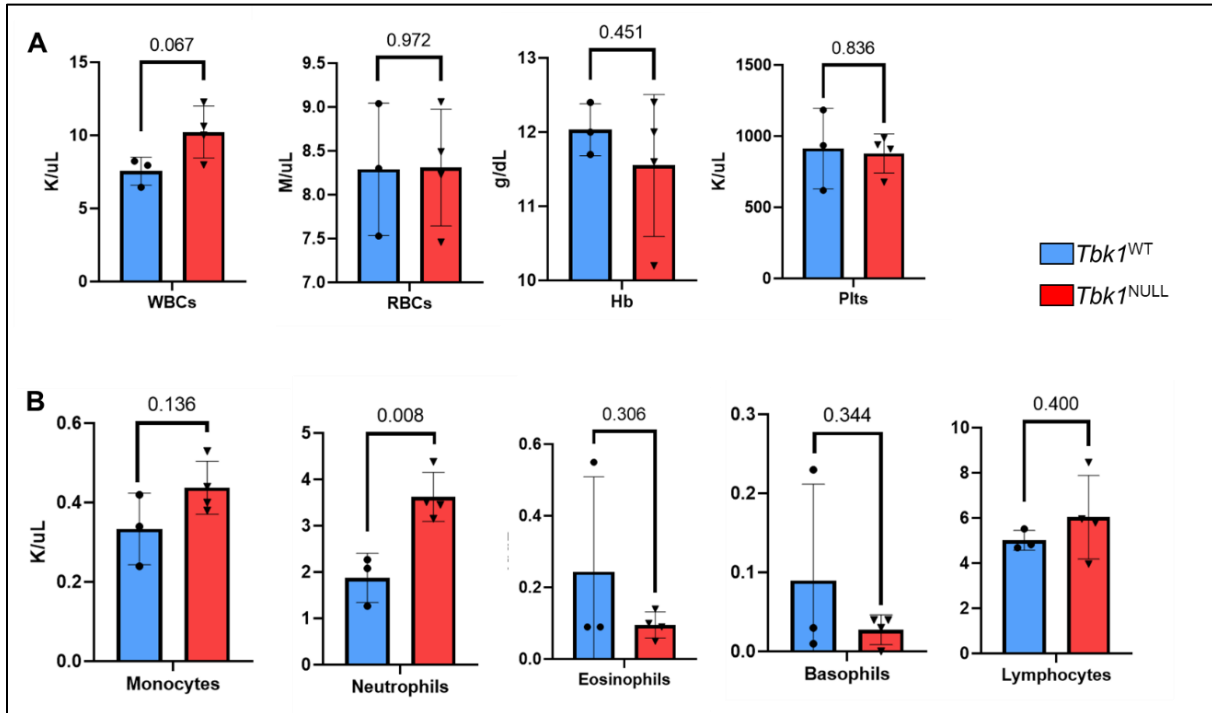


Figure 12. $Tbk1^{NULL}$ Mice Display Increased Circulating Neutrophils. To determine if $Tbk1$ deletion affects hematologic parameters, PB from mice 6-months-post-deletion was analyzed using *HemaVet*[®] hematology analyzer. The data were quantified and unpaired t-test used for all statistical analyses ($n = 3$ $Tbk1^{WT}$, 4 $Tbk1^{NULL}$). (A) WBCs ($p = 0.067$), RBCs, Hb, and Plts. (B) WBC differential: monocytes, neutrophils ($p = 0.008$), eosinophils, basophils, and lymphocytes.

$Tbk1^{NULL}$ Mice Do Not Display Significant Changes in Spleen nor Thymus Mass

Given the alterations observed in leukocyte counts, it was hypothesized that there may be an increase in the mass of primary (thymus) and/or secondary (spleen) lymphoid tissue in $Tbk1^{NULL}$ mice. Spleen and thymus herein were isolated from $Tbk1^{NULL}$ mice approximately 6-months post-deletion, making them ~7-8 months of age. Mice were age-matched and compared to $Tbk1^{fx/fx}$ controls that underwent the same tamoxifen regimen; sex-matching was not performed. No significant differences in

spleen or thymus mass were observed, but a trend towards increased ($p = 0.099$) spleen mass was noted (**Figure 13**) Regardless, these data suggest that the loss of *Tbk1* does not significantly affect the mass of primary or secondary lymphoid tissue.

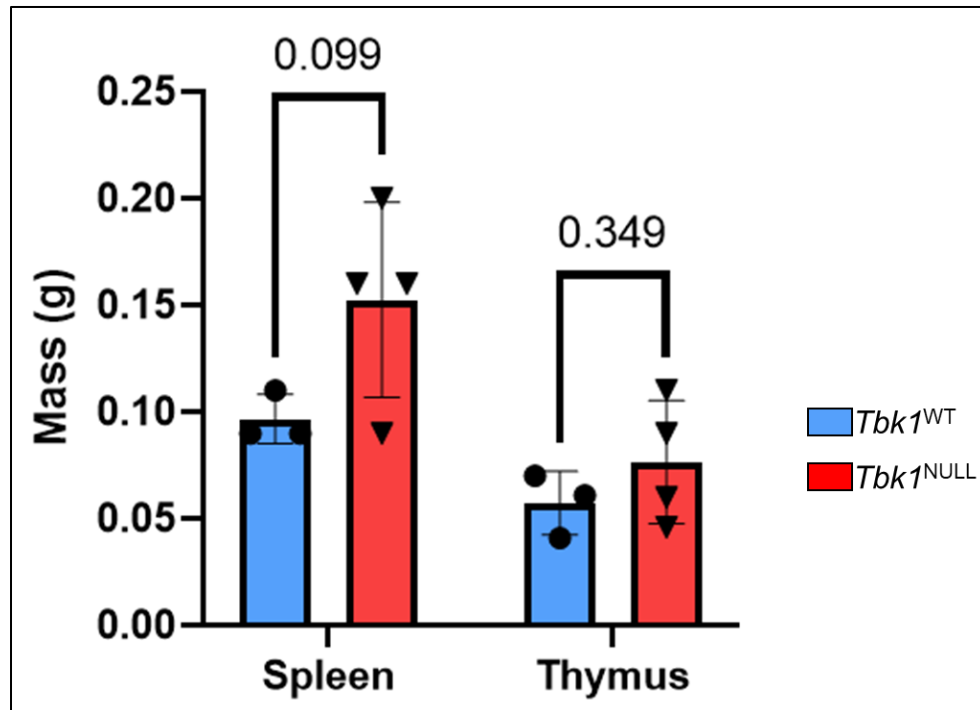


Figure 13. *Tbk1*^{NULL} Mice Do Not Display Significant Changes in Spleen nor Thymus Mass. To determine if *Tbk1* deletion affects the size of secondary (spleen) and primary (thymus) lymphoid tissue, organs from mice 6-months-post-deletion were harvested and weighed. The masses were quantified and unpaired t-test used for both statistical analyses ($n = 3$ *Tbk1*^{WT}, 4 *Tbk1*^{NULL}). Significant differences were not observed in spleen nor thymus mass between mice.

***Tbk1*^{NULL} Mice Display Histologic Abnormalities in the Spleen and Kidney**

To further characterize the phenotype of *Tbk1*^{NULL} mice, histologic analysis was performed on several tissues. In addition, while tissues were harvested and prepped from many mice, the images shown have been selected to account for sex-matching

(male), age-matching (~8 months old), and post-tamoxifen regimen-matching (~6 months post-injection) mice (n = 1).

As the hematopoietic phenotype of *Tbk1*^{NULL} mice is of primary interest, thymus and spleen were analyzed, as well as the liver due to its propensity to reflect hematologic abnormalities such as hemolytic anemia, disseminated intravascular coagulation (DIC), and neoplasms, including AML [349]. Kidney tissue was analyzed additionally, following Jin, *et al.*'s observation of an IgA nephropathy-like pathology in mice with *Tbk1*^{NULL} B cells [30]. Of note, kidneys were isolated from a different pair of 8-month-old, male mice that were ~4 months-post-tamoxifen. The Department of Pathology & Laboratory Medicine at Loyola University Medical Center (LUMC) performed tissue embedding/cutting/staining and assisted with analysis.

The thymus isolated from a *Tbk1*^{NULL} mouse appeared largely normal (**Figure 14B**), although an increased amount of red blood cells and possible dendritic cells were noted compared to the thymus of the control mouse (**Figure 14A**). However, these findings could be benign and thus cannot yet be ruled as pathologic.

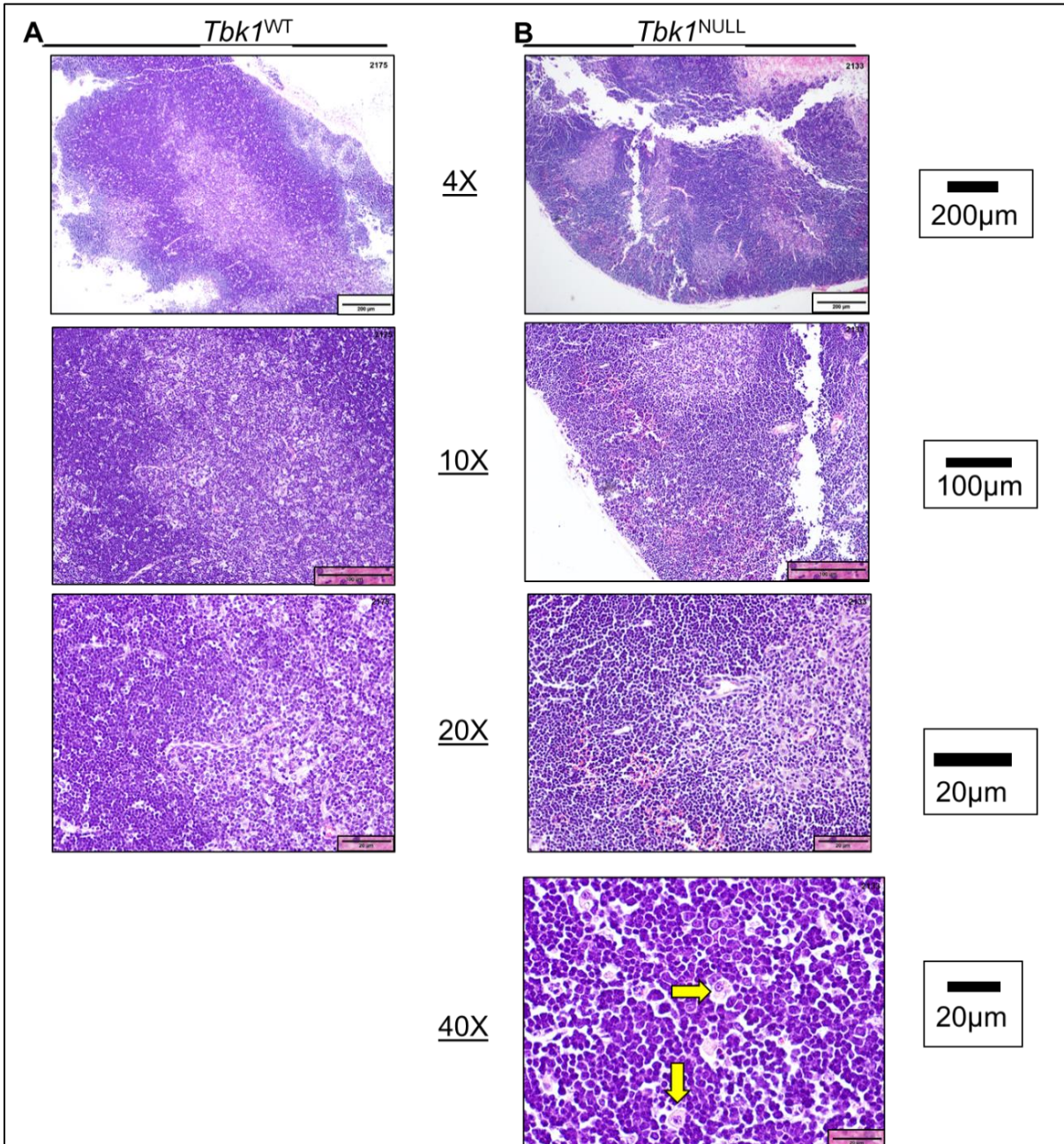


Figure 14. Thymus of *Tbk1*^{NULL} Mouse Appears Grossly Normal. To determine if *Tbk1* deletion affects thymic architecture, histologic analysis was performed. Thymi were isolated from mice, H&E-stained, and morphology was inspected. Yellow arrows indicate possible dendritic cells. (A) *Tbk1*^{WT} mouse (n = 1). (B) *Tbk1*^{NULL} mouse (n = 1). Objective magnification is indicated with scale bars.

The spleen isolated from a *Tbk1*^{NULL} mouse (**Figure 15B**) appeared to have poorly developed and less abundant germinal centers compared to *Tbk1*^{WT} mice (**Figure 15A**). However, the disrupted architecture may be due to aggressive harvesting/preparation of spleen tissue. While it is the opinion of the author that the altered spleen morphology is due to *Tbk1* deletion, this requires further validation.

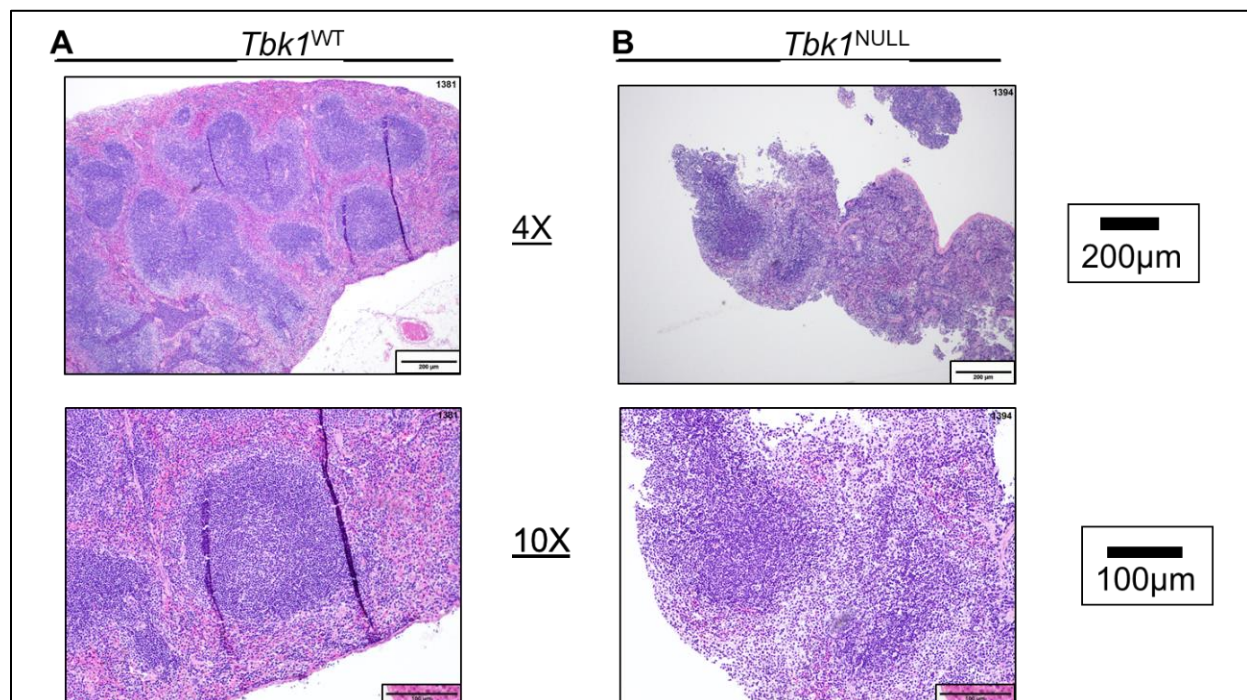


Figure 15. Spleen of *Tbk1*^{NULL} Mouse Appears to Have Maldeveloped Germinal Centers. To determine if *Tbk1* deletion affects splenic architecture, histologic analysis was performed. Spleens were isolated from mice, H&E-stained, and morphology was inspected. (A) *Tbk1*^{WT} mouse (n = 1). (B) *Tbk1*^{NULL} mouse (n = 1). Objective magnification is indicated with scale bars.

As loss of B cell-intrinsic *Tbk1* leads to uncontrolled IgA production and nephropathy in the mouse, kidney tissue from a *Tbk1*^{NULL} mouse was examined. While immunohistochemistry (IHC) or immunofluorescence (IF) is required to confirm IgA deposition, periodic acid-Schiff (PAS) staining can be used to detect proliferation of mesangial cells in the glomerulus (mesangial hypercellularity). While not specific to IgA nephropathy, mesangial hypercellularity can occur in response to IgA deposition and can thus provide a basis for pursuing IHC/IF [350, 351]. As such, anti-IgA IHC/IF was withheld pending the PAS staining results.

PAS staining revealed the kidneys to be grossly normal. Though, in consultation with LUMC, it was noted that there appears to be a slight increase in the number of mesangial cells of *Tbk1*^{NULL} mice. However, the increase is subtle and has not been quantified, and did not constitute mesangial hypercellularity. However, these data mandate further investigation to assess IgA deposition in the kidneys of *Tbk1*^{NULL} mice. **(Figure 16B).**

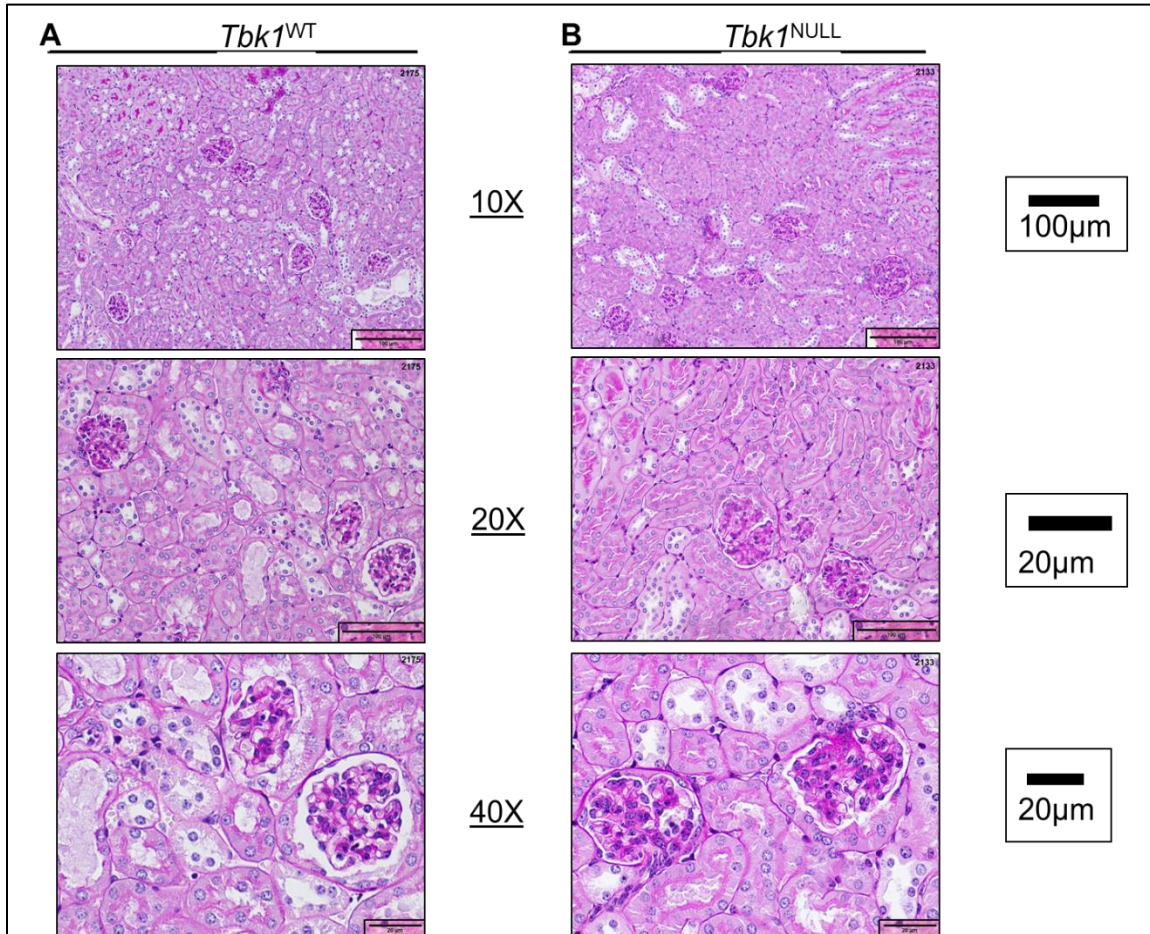


Figure 16. Kidneys of *Tbk1*^{NULL} Mouse Appear Grossly Normal but Display Slight Proliferation of the Mesangial Cells. To determine if *Tbk1* deletion affects kidney architecture, histologic analysis was performed. Kidneys were isolated from mice, PAS-stained, and morphology was inspected. (A) *Tbk1*^{WT} mouse (n = 1). (B) *Tbk1*^{NULL} mouse, slight expansion of mesangial cells can be observed (n = 1). Objective magnification is indicated with scale bars.

It appeared that the livers of *Tbk1*^{NULL} mice contained a significant number of mononuclear infiltrates, particularly around the vasculature; however, some control mice also displayed similar infiltration, which may be a result of the tamoxifen regimen (Figure 17). However, it was observed *Tbk1*^{NULL} mice seemed to have more infiltrates, though these were not quantified. Additionally, 3 *Tbk1*^{NULL} mice displayed hemosiderin-

containing/“pigment-laden” macrophages in the liver [352]. However, sufficient samples were not available to account for sex- and age-matching, so a conclusion cannot be made. Further examination of the *Tbk1*^{NULL} liver is recommended.

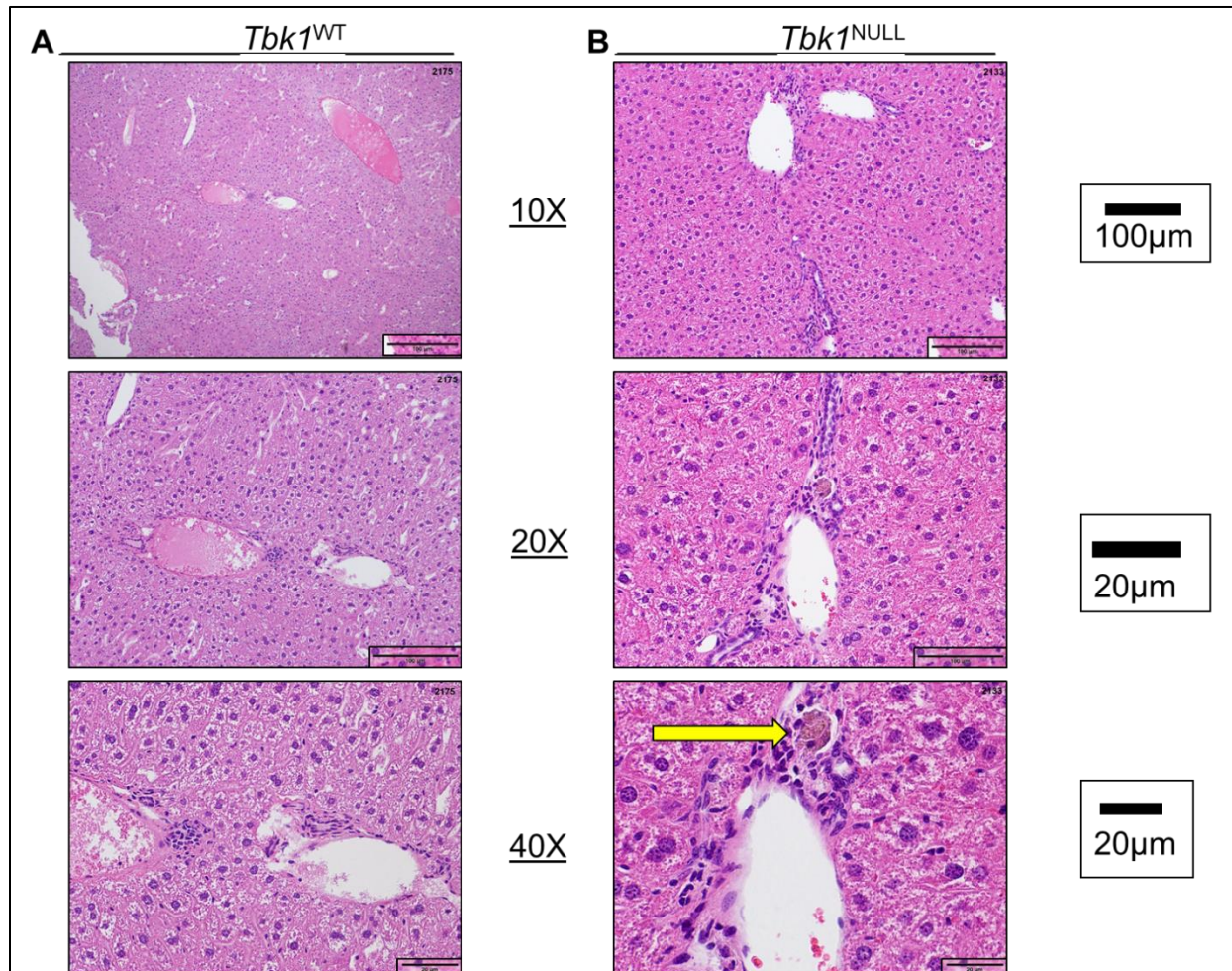


Figure 17. Liver of *Tbk1*^{NULL} Mouse may have Mononuclear Cell Infiltration. To determine if *Tbk1* deletion affects liver architecture, histologic analysis was performed. Livers were isolated from mice, H&E-stained, and morphology was inspected, which revealed mononuclear cell infiltrates in both groups, with a possible increase in *Tbk1*^{NULL} mice, though this requires quantification. Yellow arrow indicates suspected pigment-laden macrophage. (A) *Tbk1*^{WT} mouse (n = 1). (B) *Tbk1*^{NULL} mouse, (n = 1). Objective magnification is indicated with scale bars.

Results: Competitive Transplantation of *Tbk1*^{NULL} Whole Bone Marrow
Loss of *Tbk1* in Whole Bone Marrow Does Not Affect Engraftment Ability of HSPCs

The physiology and fate of cells are governed by both cell-*intrinsic* and -*extrinsic* factors. For example, in the BM, the self-renewal capacity of HSPCs is largely maintained by sustained activation of c-KIT, a receptor tyrosine kinase found on the surface of HSPCs [353]. BM stromal cells express transmembrane and soluble c-KIT ligand (stem cell factor [SCF], KIT-ligand [KL], and steel factor) to nourish and maintain the stemness of local HSPCs. Without continuous the activation of c-KIT, which typically occurs via direct contact with stromal cells, HSPCs lose their self-renewal and hematopoietic abilities [354].

Thus, the BM provides an excellent example of how cell-intrinsic (c-KIT on HSPCs) and cell-extrinsic (SCF on stromal cells) factors regulate physiology. Similarly, TBK1 can act to promote cancer in tumor cell-intrinsic and -extrinsic roles. For example, TBK1 acts within the KRAS^{G12}-mutated NSCLC cell to activate cell survival pathways. Additionally, TBK1 can act within TME-infiltrating T cells to negate the production of antitumor cytokines, acting to promote cancer in a tumor cell-extrinsic role.

To determine if *Tbk1* has BM-intrinsic functions, whole BM (WBM) transplantation (WBMT) was employed. Initially, two WBMT experiments were planned: a non-competitive (replacement with donor *Tbk1*^{NULL} WBM) and competitive (replacement with

WBM consisting of half *Tbk1*^{NULL} donor WBM and half wild-type support WBM).

Unfortunately, too many mice were lost to busulfan (*Busulfex*[®]) conditioning prior to transplant, so only competitive transplantation could be performed (n = 11 [*Tbk1*^{WT} = 5 & *Tbk1*^{NULL} = 6]).

To this end, *Tbk1*^{WT} and *Tbk1*^{NULL} WBM were isolated from CD45.2⁺ (donor [*Ptprc*^b]) mice. The isolated WBM were then mixed in an approximate 1/1 ratio (1.0 x 10⁶ WBM cells total [5.0 x 10⁵ of each]) with WBM isolated from a wild-type, CD45.1⁺ (support [*Ptprc*^a]) mouse (**Figure 18**). Cell mixtures were then delivered in 200uL 1X PBS to lethally-conditioned, CD45.1⁺ recipient (host) mice and FACS analysis was performed on PB (cheek bleed) at 2 and 5 months post-WBMT. Mice were sacrificed at 8 months post-WBMT, and PB and BM was analyzed. Mice were age-matched (~6 weeks old) and sex-matched (male); mice received WBM cells in an approximate 1/1 combination of either [*Tbk1*^{WT} donor + WT support] OR [*Tbk1*^{NULL} donor + WT support].

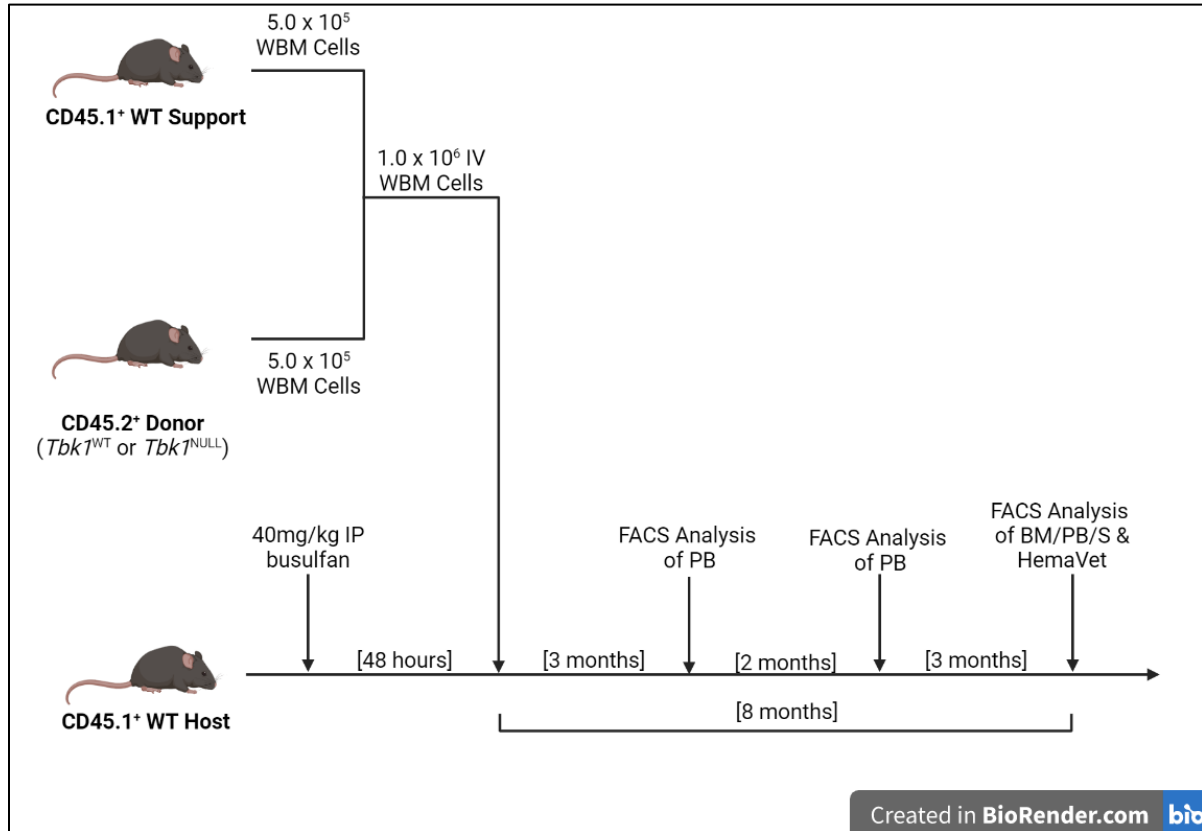


Figure 18. Schematic Depicting Competitive WBMT Protocol using $Tbk1^{NULL}$ WBM and Downstream Analyses. To determine if $Tbk1$ regulates the engraftment of transplanted WBM cells and if $Tbk1$ has WBM-intrinsic functions, competitive WBMT was performed ($n = 5$ $Tbk1^{WT}$, 6 $Tbk1^{NULL}$); created with BioRender.com.

To determine if $Tbk1$ regulates the engraftment of transplanted WBM cells, the amount of donor (CD45.2+ [CD45.1-]) cells in the PB was analyzed via FACS as percentage of PB-TNCs (**Figure 19**). Differences were not observed in the level of circulating donor cells, which suggests that $Tbk1$ does not influence the engraftment ability of transplanted WBM. Representative FACS gating strategy is shown (**Figure 20**).

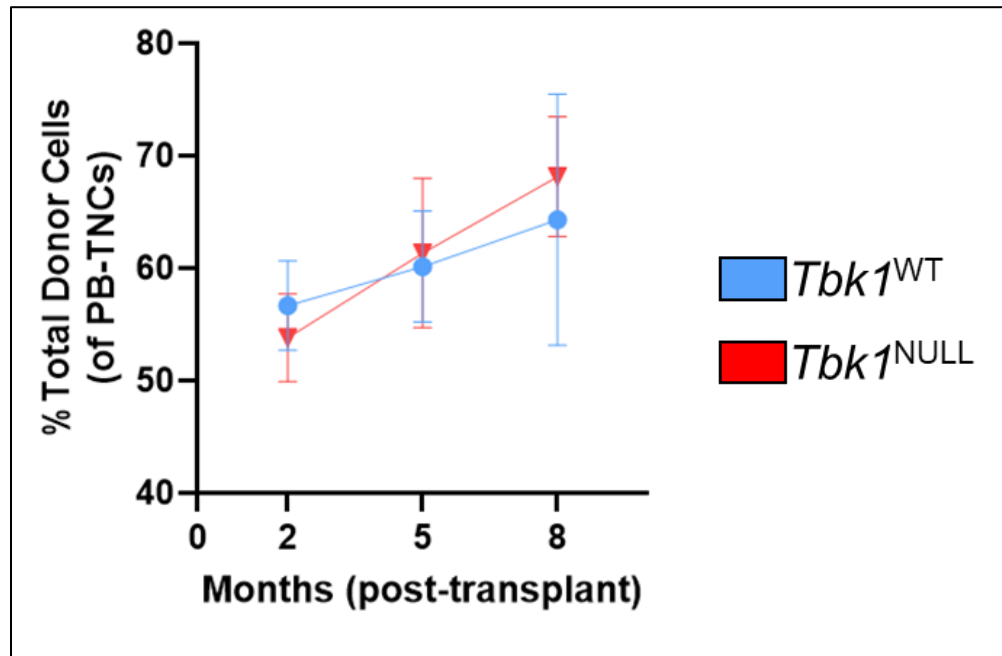


Figure 19. Loss of *Tbk1* in WBM Does Not Influence Engraftment of HSPCs in Competitive Transplantation. To determine if *Tbk1* governs the engraftment ability of transplanted HSPCs, the percentage of donor cells (CD45.2⁺ [CD45.1⁻]) in the PB was checked via FACS at 2, 5, and 8 months-post-WBMT. The data were quantified and unpaired t-test used for all statistical analyses (between *Tbk1*^{WT} [n = 5] and *Tbk1*^{NULL} [n = 6] mice at each timepoint). Percentage of donor (CD45.2⁺ [CD45.1⁻]) cells of PB-TNCs. NOTE: as CD45.1⁺ support cells were used in WBMT, CD45.2⁺ cells cannot display 100% engraftment (*i.e.*, remaining 30-40% of PB-TNCs are CD45.1⁺).

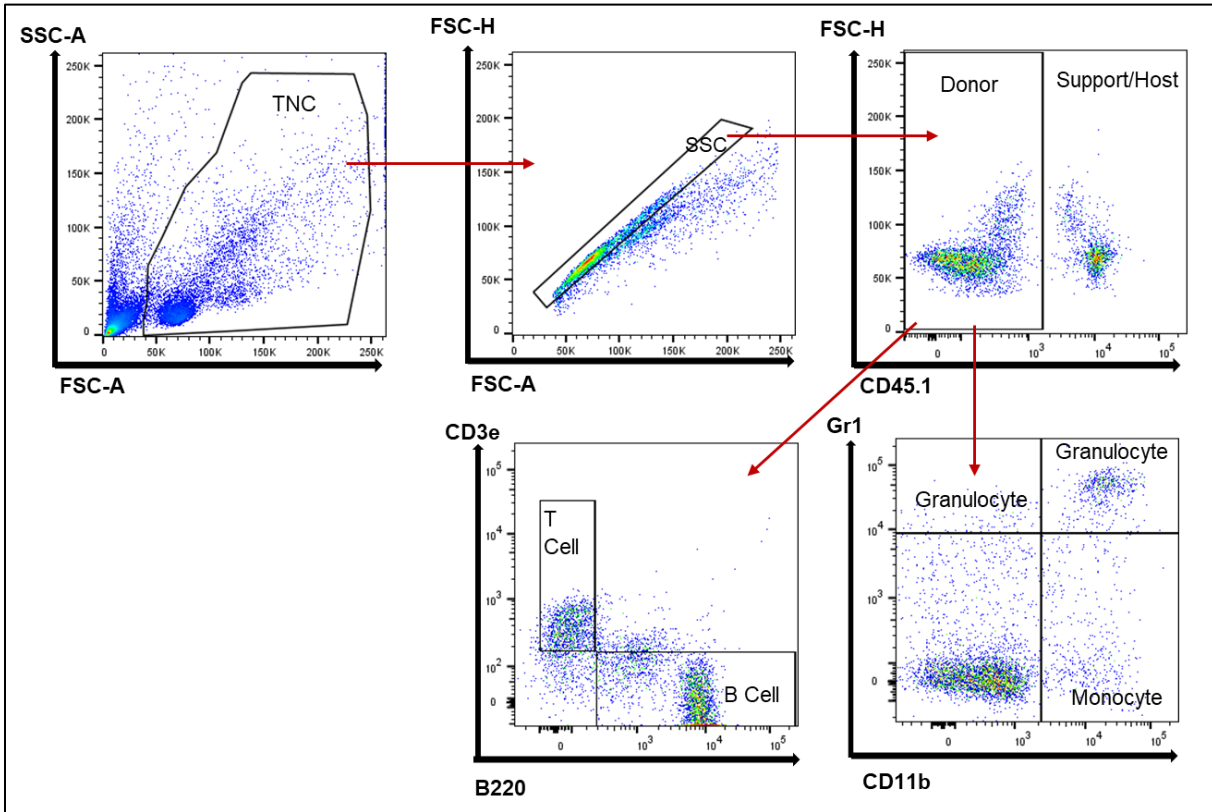


Figure 20. Representative FACS Gating Strategies for Donor & Mature Cell Analysis of PB-TNCs. After gating on TNCs and eliminating doublets (SC gating), total donor cells (CD45.2⁺ [CD45.1⁻]), donor B cells (CD45.2⁺B220⁺), donor T cells (CD45.2⁺CD3⁺), donor monocytes (CD45.2⁺CD11b⁺Gr1⁻), and donor granulocytes (CD45.2⁺Gr1⁺) were analyzed as percentage of PB-TNCs.

Loss of *Tbk1* in Whole Bone Marrow Does Not Affect Lymphopoiesis

To determine if *Tbk1* has lineage-specific effects, lymphocytes were measured similarly. The loss of *Tbk1* has no effect on the reconstitution of circulating B (CD45.2⁺B220⁺; **Figure 21A**) and T cells (CD45.2⁺CD3⁺; **Figure 21B**), which suggests that WBM-intrinsic *Tbk1* does not regulate the production of circulating lymphocytes. Representative FACS gating strategy is shown (**Figure 20**).

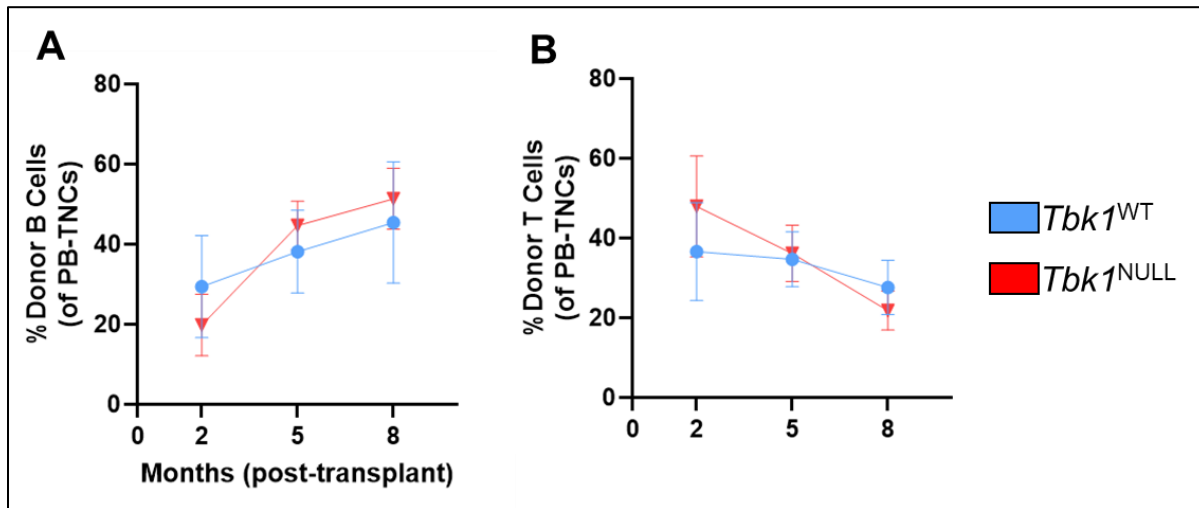


Figure 21. Loss of *Tbk1* in WBM Does Not Influence Lymphopoiesis in Competitive Transplantation. To determine if *Tbk1* governs the ability of transplanted WBM to produce lymphocytes, the percentage of donor B (CD45.2⁺B220⁺) and T (CD45.2⁺CD3⁺) cells in the PB was checked via FACS at 2, 5, and 8 months-post-WBMT. The data were quantified and unpaired t-test used for all statistical analyses (between *Tbk1*^{WT} [n = 5] and *Tbk1*^{NULL} [n = 6] mice at each timepoint). (A) B cells. (B) T cells.

Loss of *Tbk1* in WBM Transiently Hampers Granulopoiesis but Not Monopoiesis

To determine if *Tbk1* has lineage-specific effects, myeloid cells were measured similarly. The loss of *Tbk1* has no effect on the reconstitution of circulating monocytes (CD45.2⁺CD11b⁺Gr1⁻; **Figure 22A**), but temporarily impedes granulopoiesis (CD45.2⁺Gr1⁺; **Figure 22B**). Specifically, while both groups of mice displayed a transient decrease in granulocytes between 2 and 5 months post-WBMT, *Tbk1*^{NULL} mice displayed a more significant decrease ($p = 0.038$) at 5 months. Although, by 8 months post-WBMT, all mice displayed comparable recovery of granulocyte counts following WBM transplant. These data indicate that while the loss of *Tbk1* in WBM can delay

count recovery of granulocytes, this temporary delay resolves with time. Representative FACS gating strategy is shown (Figure 20).

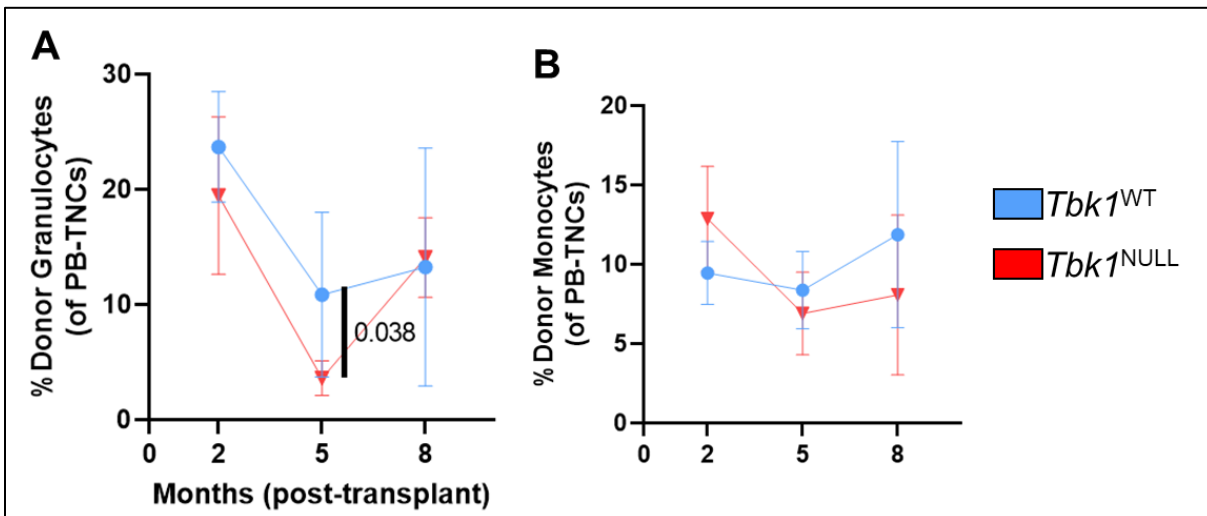


Figure 22. Loss of *Tbk1* in WBM Transiently Hampers Granulopoiesis but Not Monopoiesis in Competitive Transplantation. To determine if *Tbk1* governs the ability of transplanted WBM to produce myeloid cells, the percentage of donor granulocytes (CD45.2⁺Gr1⁺) and monocytes (CD45.2⁺CD11b⁺Gr1⁻) cells in the PB was checked via FACS at 2, 5, and 8 months-post-WBMT. The data were quantified and unpaired t-test used for all statistical analyses (between *Tbk1*^{WT} [n = 5] and *Tbk1*^{NULL} [n = 6] mice at each timepoint). (A) Granulocytes (p = 0.038 at 5 months post-WBMT) displayed a significant but transient delay in reconstitution in *Tbk1*^{NULL} WBMT. (B) Monocytes.

Loss of *Tbk1* in Whole Bone Marrow Does Not Affect Recovery of Mature Blood Cells nor Erythroid Progenitors

It was not known how the loss of *Tbk1* in WBM affects the BM itself. To this end, BM was harvested and analyzed via FACS; relevant populations measured as percentage of BM-TNCs. In terms of lymphocytes, myeloid cells, erythroid progenitors,

and megakaryocytes in the BM, the loss of *Tbk1* in WBM had no effect on these populations (**Figure 23A**). Representative FACS gating strategy is shown (**Figure 23B**).

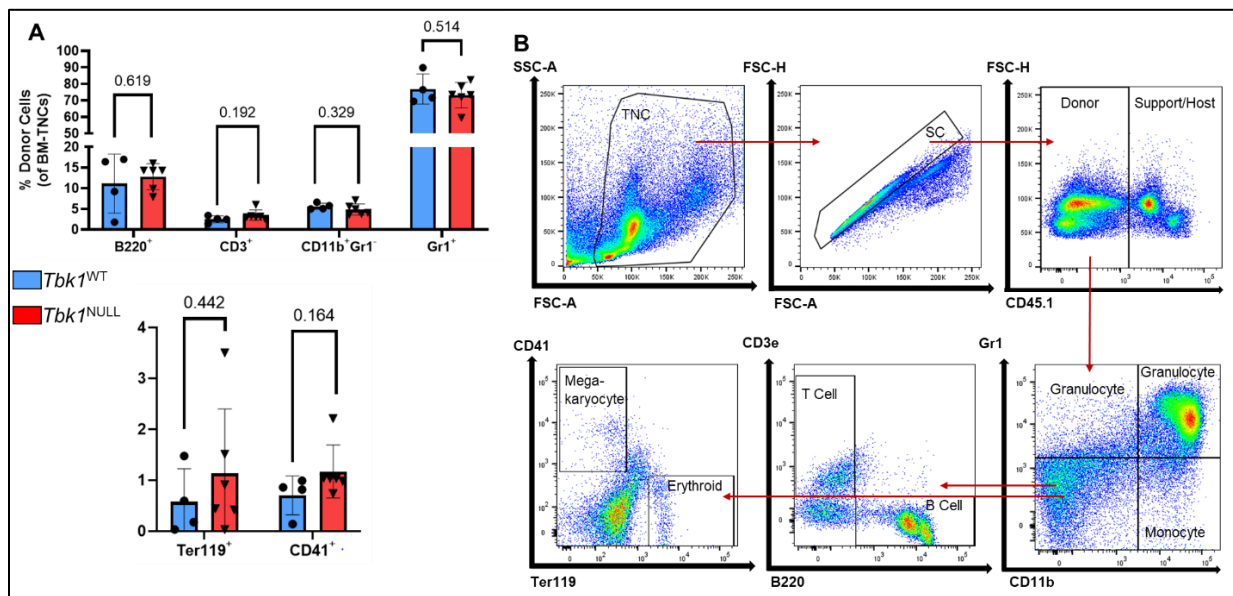


Figure 23. Loss of *Tbk1* in WBM Does Not Affect Reconstitution of Mature Cells nor Erythroid Progenitors in the Bone Marrow. To determine if the loss of *Tbk1* affects homeostatic hematopoiesis, the levels of mature cells in the PB and BM, as well as erythroid progenitors and megakaryocytes in the BM, were analyzed via FACS at 8-months-post-WBMT. The data were quantified and unpaired t-test used for all statistical analyses ($n = 5$ *Tbk1*^{WT}, 6 *Tbk1*^{NULL} mice). (A) Donor cells as percentage of BM-TNCs. (B) Representative gating strategy for FACS analysis. After gating on TNCs and eliminating doublets (SC gating), donor B cells (CD45.2⁺B220⁺), donor T cells (CD45.2⁺CD3⁺), donor monocytes (CD45.2⁺CD11b⁺Gr1⁻), and donor granulocytes (CD45.2⁺Gr1⁺) were analyzed.

Loss of *Tbk1* in Whole Bone Marrow Does Not Significantly Affect HSPCs

HSPCs (**Figure 24A-B**) were also analyzed as percentage of BM-TNCs, and representative FACS gating strategies are shown (**Figures 23C**). Differences in HSPC populations were not significantly different (CD45.2/CD45.1 sorting was not available for

this analysis). While a trend may exist towards increased HSPCs in *Tbk1*^{NULL} mice, any difference herein was not significant.

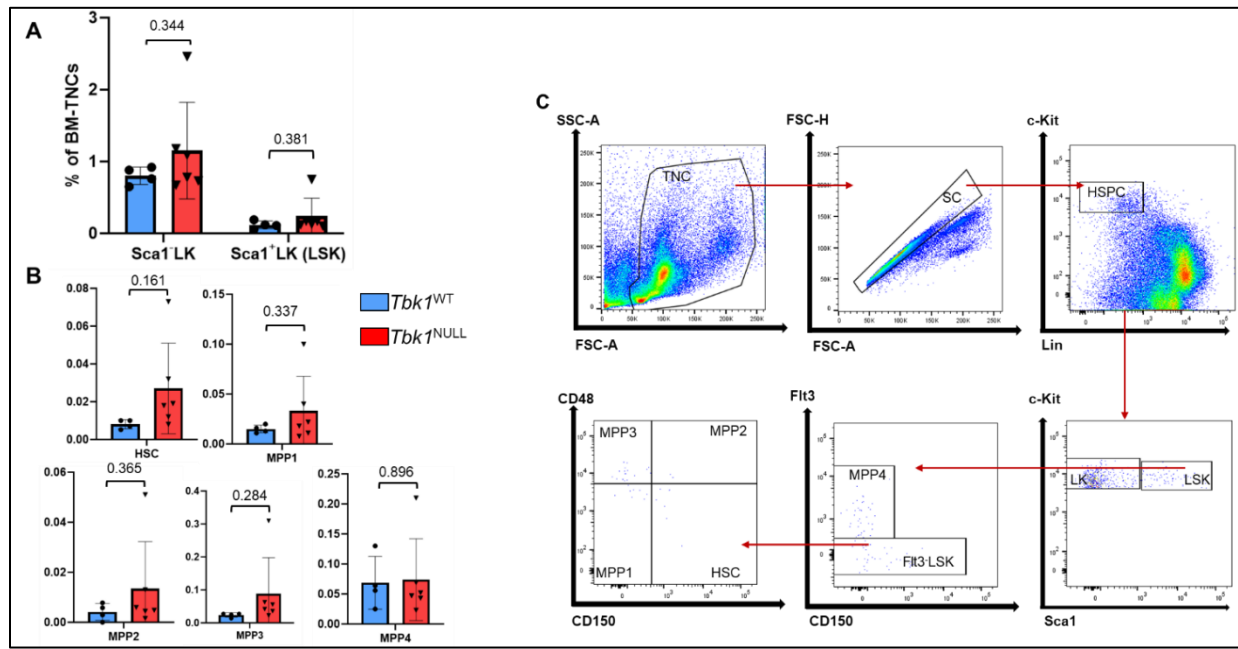


Figure 24. *Tbk1* Deletion in WBM Does Not Significantly Affect the Reconstitution of HSPCs. To determine if the loss of *Tbk1* affects HSPCs, the levels of HSPCs in the BM were analyzed via FACS at 8-months-post-WBMT. The data were quantified and unpaired t-test used for all statistical analyses ($n = 5$ *Tbk1*^{WT}, 6 *Tbk1*^{NULL}). (A) HSPC compartment (LKs + LSKs). (B) MPP4/LMPP and Flt3⁻ LSKs (HSC and MPP1-MPP3). (C) Representative gating strategy for FACS analysis. After gating on TNCs and eliminating doublets (SC gating), the HSC and MPP1-MPP4 subsets were analyzed.

Loss of *Tbk1* in Whole Bone Marrow Does Not Significantly Affect Specific Myeloid Progenitors

Additional myeloid progenitors were also analyzed as percentage of BM-TNCs, and representative FACS gating strategies are shown (Figures 25D). It was determined

that, similar to global deletion, the loss of *Tbk1* in WBM did not impart significant changes in any of the assayed myeloid progenitors (GMP, DP, CMP, MkP [Lin⁻c-Kit⁺CD41⁺CD150⁺], CFU-E, Pre-CFU-E, Pre-MegE, and Pre-MEP; **Figure 25A-25C**). However, a trend towards increased Pre-CFU-E (CD41⁻CD16/32⁻CD27⁻CD150⁺Endoglin⁺) and Pre-MegE (CD41⁻CD16/32⁻CD27⁻CD150⁺Endoglin⁻) HPCs was observed in *Tbk1*^{NULL} mice (**Figure 25C**). Despite not reaching significance, the trend observed herein indicates the WBM-intrinsic role of *Tbk1* in regulating myeloid progenitor populations warrants further investigation. CD45.2/CD45.1 sorting was not available for this analysis.

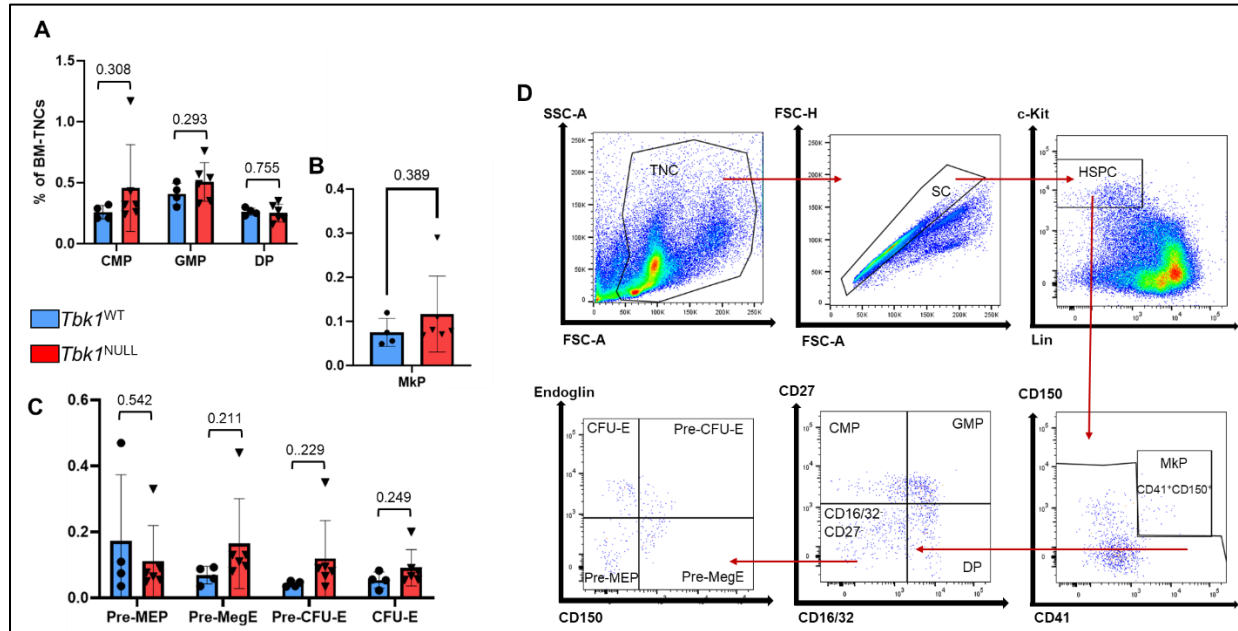


Figure 25. Deletion of *Tbk1* in WBM Does Not Affect Reconstitution of Myeloid Progenitors. To determine if the loss of *Tbk1* affects myeloid progenitors, the levels of myeloid progenitors in the BM were analyzed via FACS at 8-months-post-WBMT. The data were quantified and unpaired t-test used for all statistical analyses ($n = 5$ *Tbk1*^{WT}, 6 *Tbk1*^{NULL}). (A) Non-Mkp HSPCs. (B) MkPs (Lin⁻c-Kit⁺CD41⁺CD150⁺). (C) CD16/32⁻CD27⁻ Non-MkPs. (D) Representative gating strategy for FACS analysis. After gating on TNCs and eliminating doublets (SC gating), the myeloid progenitor subsets were analyzed.

Loss of *Tbk1* in Whole Bone Marrow Causes Increased Monocytes

To determine if the loss of *Tbk1* in WBM causes hematologic abnormalities, PB was isolated via cardiac puncture (post-mortem) and analyzed using *HemaVet*[®]. At 8 months post-WBMT, *Tbk1*^{NULL} recipients displayed a trend towards increased ($p = 0.051$) total WBCs, lymphocytes ($p = 0.062$), and neutrophils ($p = 0.097$) (**Figure 26A**), and a significant increase ($p = 0.021$) in monocytes (**Figure 26B**); no changes were observed in red blood cells (RBCs), hemoglobin (Hb), platelets (Plts) (**Figure 26A**) or

neutrophils, eosinophils, basophils, nor lymphocytes. Spleen and thymus mass were not analyzed.

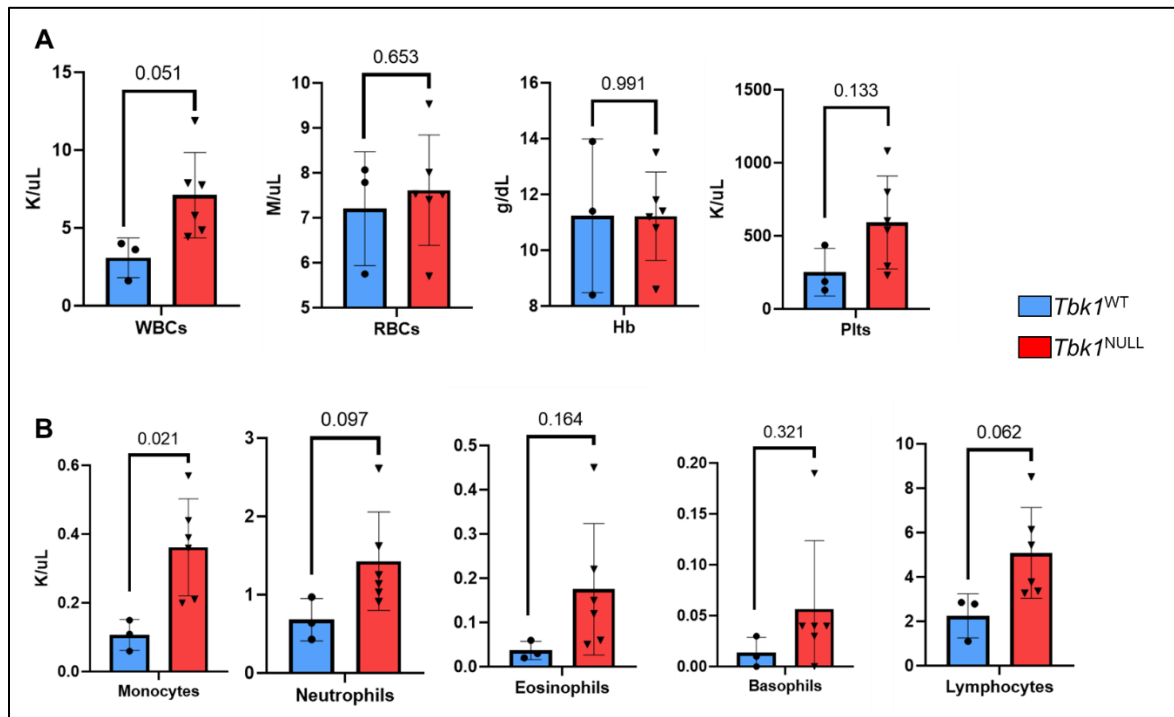


Figure 26. Loss of *Tbk1* in WBM Causes Increased Monocytes and a Trend Towards Increased Lymphocytes and WBCs. To determine if *Tbk1* deletion in WBM affects hematologic parameters, PB from mice 8-months-post-WBMT was analyzed using *HemaVet*[®] hematology analyzer. The data were quantified and unpaired t-test used for all statistical analyses ($n = 3$ *Tbk1*^{WT}, 6 *Tbk1*^{NULL}). (A) WBCs ($p = 0.051$), RBCs, Hb, and Plts. (B) WBC differential: monocytes ($p = 0.021$), neutrophils ($p = 0.097$), eosinophils, basophils, and lymphocytes ($p = 0.062$).

***Tbk1* Deletion is Revealed to be Incomplete at 4 and 7 Months-post-tamoxifen**

The deletion of *Tbk1* was previously confirmed in a 6-week-old mouse, 12 days after the tamoxifen regimen; PCR was used to confirm a complete deletion of *Tbk1* in c-Kit⁺ and c-Kit⁻ BM cells (**Figure 7B**). As the BM gives rise to the entire hematopoietic system, it was presumed that complete deletion of *Tbk1* in the BM was sufficient for our

purposes. Thus, PCR to confirm deletion in subsequent mice was not routine, and mice were presumed to be *Tbk1*^{NULL} following results from the “test” mouse.

However, upon re-evaluation, it was decided that PCR should be used to confirm *Tbk1* status of all analyzed mice. Much to our surprise, PCR indicated that the deletion of *Tbk1* was not complete in hematopoietic tissues and the tails of mice that had undergone the tamoxifen regimen both 4 (**Figure 27A**) and 7 (data not shown) months prior. *Tbk1*^{fx} alleles were clearly evident in the spleen (S), thymus (Thy), and PB of two age-matched (+/- 2 weeks) *Tbk1*^{fx/fx};*Rosa26*-CreER^{T2+} mice that underwent the same tamoxifen regimen as the initial “test” mouse. More surprising is the fact that the WBM of both sampled mice still displayed a near-complete deletion of *Tbk1*, while the PB displayed a clearly incomplete deletion; as the BM produces cells that move directly to the PB, this result cannot be explained at this time. It may be that either the hematopoietic system had not yet fully turned over, that a small fraction of *Tbk1*-retaining HSPCs (“escapers”) were able to repopulate sufficiently, and/or that other cell types, such as epithelia, are responsible for the observed heterozygosity. False positivity was ruled-out, however, as the negative control resulted as expected. It is not known whether the cells harboring the *Tbk1*^{fx} allele are *Tbk1*^{NULL/fx} or *Tbk1*^{fx/fx}.

The deletion was initially assessed only in the BM of a 6-week-old male mouse (**Figure 7B**). As such, the deletion was re-assessed using a second “test” mouse (**12-week-old female**), this time with S, Thy, PB, WBM, and tail included in PCR; BM was not separated based on c-Kit status. *Importantly, the only mouse available was a 12-week-old female, in contrast to the 6-week-old male used in the initial test.* Tissues were

harvested 11 days post-tamoxifen regimen, PCR was performed, and it was learned that while deletion in the thymus appeared complete, *Tbk1^{fx}* alleles were detected in tail, WBM, PB, and S (**Figure 27B**). Non-specific amplification (false positive) of the PCR results was ruled-out, as the negative control (ddH₂O) resulted as expected. Interestingly, the deletion efficiency observed in the PB herein was comparable to that of the WBM (**Figure 27B**), in stark contrast to the deletion in PB in the mice 4-months post-tamoxifen regimen (**Figure 27A**). These data are perplexing and cannot be explained at this time, aside from supporting the notion that *Tbk1* confers a survival advantage to mouse cells.

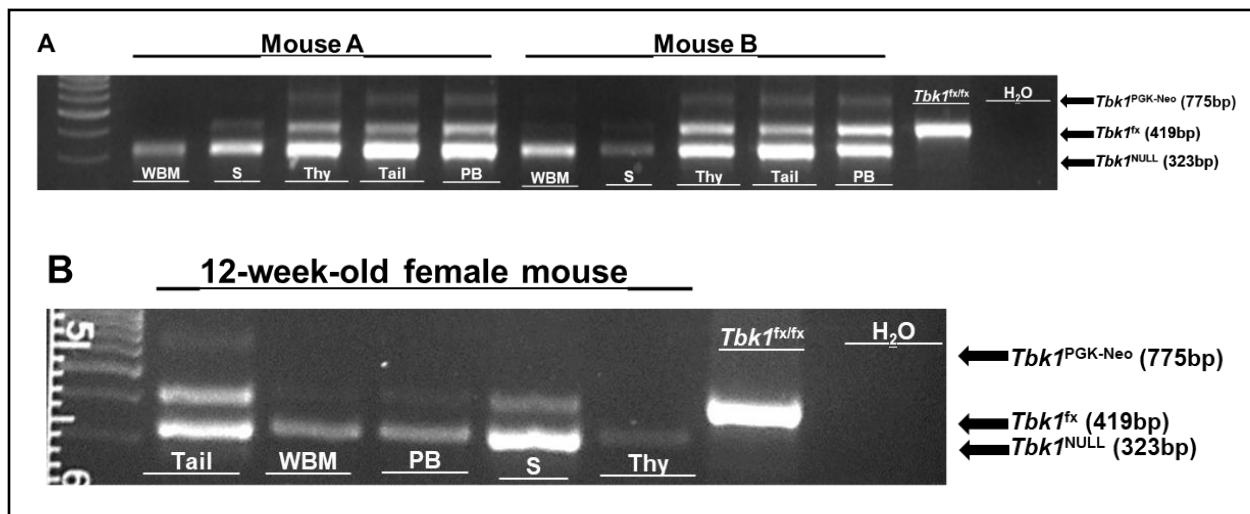


Figure 27. *Tbk1*^{fx} Allele is Detected in Mice Presumed to be *Tbk1*^{NULL}. (A) Results from 3% agarose gel electrophoresis/*Tbk1* PCR. gDNA templates from mice presumed to be *Tbk1*^{NULL} (4-months post-tamoxifen regimen) used as templates (n = 2), left-most lane contains 1kB DNA ladder, and Lexicon primers #18, #23, and #24 were used to determine *Tbk1* status; untreated *Tbk1*^{fx/fx} gDNA (positive) and water (negative) controls are shown. (B) Results from 3% agarose gel electrophoresis/*Tbk1* PCR. gDNA template from indicated tissues from a 12-week-old “test” mouse (n = 1) that underwent tamoxifen regimen 11 days prior to analysis; left-most lane contains 1kB DNA ladder, and Lexicon primers #18, #23, and #24 were used to determine *Tbk1* status; untreated *Tbk1*^{fx/fx} gDNA (positive) and water (negative) controls are shown.

Should mice need to be injected past 8 weeks of age, intensification of the regimen is recommended. As well, it is not known if sex affects the tamoxifen-mediated induction of CreER^{T2}. A larger dosage and/or longer duration of tamoxifen may be necessary, especially as mice increase in age and mass. Yu, et al. employed the *Rosa26*-CreER system and induced deletion with 2mg IP tamoxifen for 4 consecutive days [152]. However, the authors only provided evidence that the deletion was relatively complete in thymic T cells 2 weeks after injection, and—to our knowledge—did not specify the mass nor age of the injected mice.

Aim 1 Conclusion: *Tbk1* is Dispensable in Short-term, Homeostatic

Hematopoiesis

The genetic loss of *Tbk1* in the adult mouse does not lead to overt, untoward effects on the hematopoietic system nor animal overall—no mice died from anything other than suspected tamoxifen toxicity, which was deemed cause-of-death for mice that died during the regimen or within 7 days following the last dose and do not display

a clear alternative cause (mice that die from tamoxifen toxicity often display yellow-pale livers and/or intestinal hemorrhage [unpublished observations, Zhang lab]). While *Tbk1* restrains leukocyte production and has roles in regulating the MPP3 population in the BM, *Tbk1* regulates the production of mature blood cells, including platelets and erythrocytes, only minimally, at least in a short-term timeframe (3-6 months in B6 mice). However, as our mice are housed in specific pathogen-free (SPF) facilities, and as we did not challenge them with pathogen or vaccine, the effect of global *Tbk1*-knockout on the immune system is unknown and requires exploration. While the loss of *Tbk1* may cause a differentiation block, causing the accumulation of HSPCs at the MPP3 stage, hematologic abnormalities suggestive of blocked differentiation (e.g., anemia, thrombocytopenia, leukopenia, ETC.) were not observed. However, these abnormalities may only become apparent after more time (6+ months) has elapsed following *Tbk1* deletion. Nonetheless, in terms of life-sustaining (homeostatic) hematopoiesis, *Tbk1* appears to be dispensable for at least 6 months, suggesting short-term blockade of *Tbk1* is safe. Although, the long-term effect of *Tbk1* deletion on hematopoiesis, immunity, and homeostasis overall requires investigation.

CHAPTER 4

AIM 2: DETERMINE IF TBK1 BLOCKADE COULD BE A MEANS OF ANTI-AML THERAPY

Results

MLL-AF9 Induces Increased Expression of *Tbk1* mRNA

As it was determined that *Tbk1* minimally regulates homeostatic hematopoiesis in the adult mouse, we sought to determine if *Tbk1* blockade may be a useful strategy in the treatment of AML. To this end, we elected to study *Tbk1* in *MLL-AF9*⁺ cells, as this is an aggressive, clinically relevant model of AML. The *MLL-AF9* oncogene drives high-risk leukemias in humans, specifically in pediatric patients and cases of t-AML, and aggressive disease in mouse models [247, 270, 271, 274-276]. Our lab has previously generated an *MLL1-AF9*-containing plasmid using the MSCV-puro backbone (MSCV-puro-*MLL-AF9*). Transfection of 293T cells and transduction of mouse HSPCs is depicted (**Figure 28**)

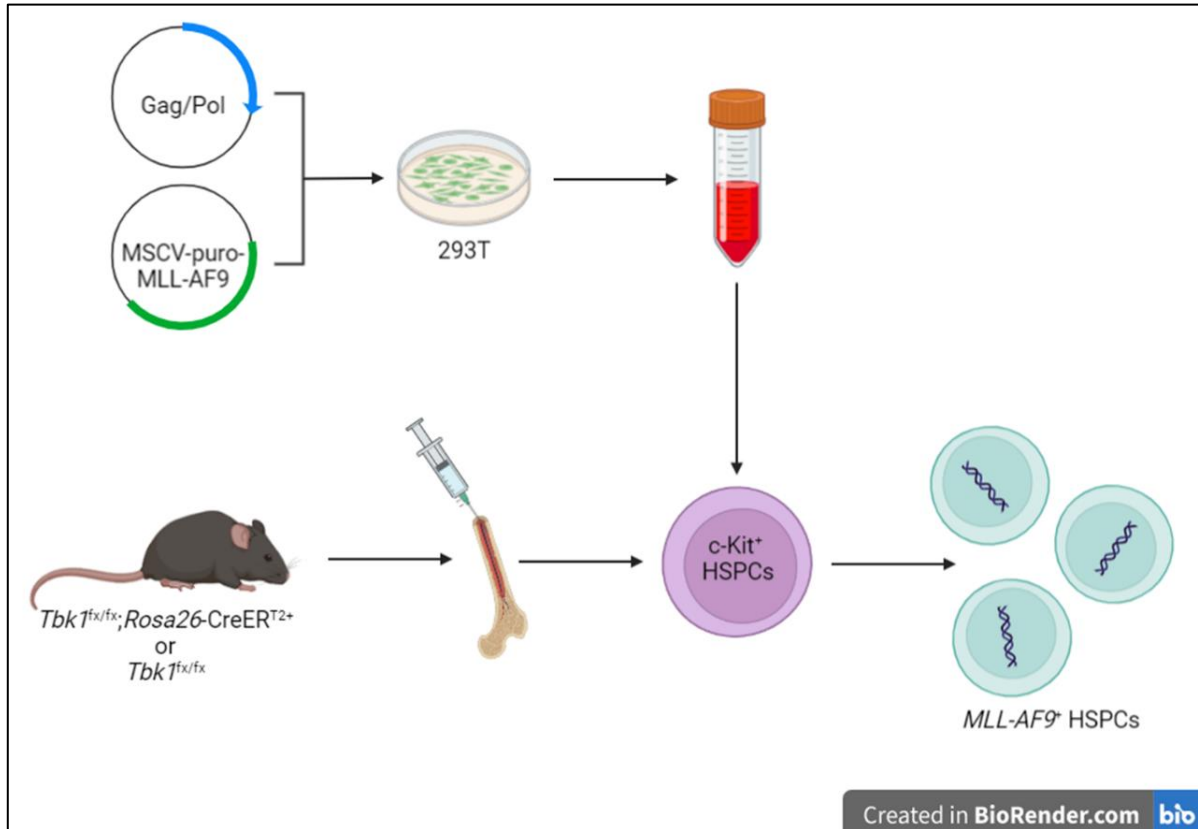


Figure 28. Schematic Depicting the Transfection of 293T cells, Generation of MSCV-puro-MLL-AF9 Retrovirus, and Isolation/Transduction of Mouse HSPCs; created with BioRender.com.

Forty-eight hours after transduction, to allow for production of the puromycin N-acetyltransferase (*pac*), cells were treated with puromycin to select for *MSCV-puro-MLL-AF9*⁺ cells. Following puromycin selection, RNA was isolated from *MLL-AF9*⁺ HSPCs. Then, all isolated RNA (wild-type [*WT*^{c-Kit⁺}] and *MLL-AF9*⁺ HSPCs) was reverse-transcribed into cDNA and subjected to multiplex, quantitative PCR (qPCR). This entire procedure was performed twice, separately (n =2 [biological duplicate]).

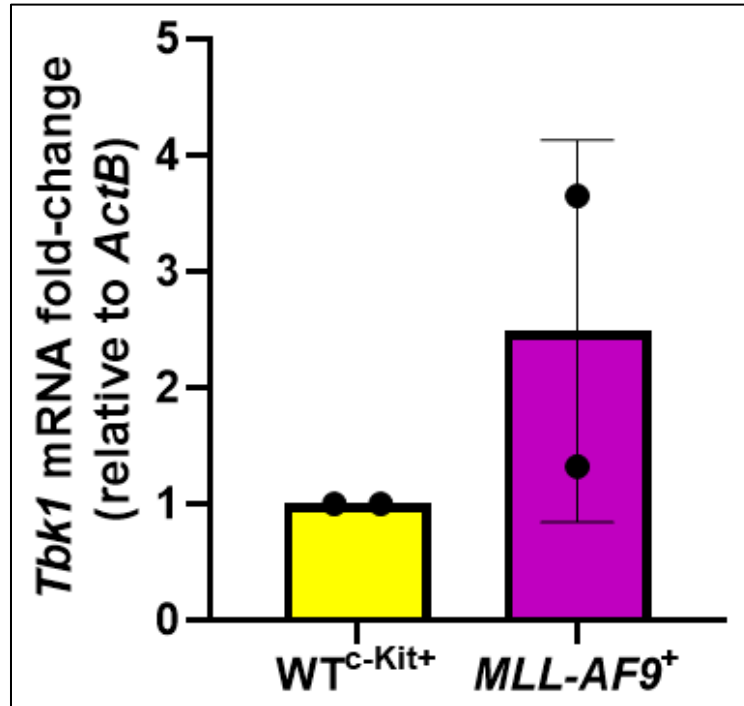


Figure 29. MLL-AF9 Induces Increased Expression of *Tbk1* mRNA in Mouse HSPCs. To determine if *MLL-AF9*-transformation affects *Tbk1* mRNA levels, RNA was isolated from WT HSPCs and *MLL-AF9*⁺ HSPCs, reverse-transcribed into cDNA, and subjected to multiplex qPCR with *ActB* used as internal control. Four replicates were performed for each group (n = 2). Data were collected via comparative C_T method and analyzed via the 2^{-ΔΔCT} method.

While this study was not sufficiently powered, it appears that *MLL-AF9*⁺ mouse HSPCs express greater levels of *Tbk1* mRNA (Figure 29). While these data may indicate that *MLL-AF9*⁺ HSPCs rely on *Tbk1* more than wild-type counterparts, ideally making *MLL-AF9*⁺ cells more sensitive to *Tbk1* inhibition, the increased *Tbk1* mRNA may simply be an artifact of the faster cycling rate of leukemic cells.

***Tbk1* May Confer a Survival Advantage to *MLL-AF9*⁺ HSPCs**

To further study *Tbk1* in *MLL-AF9*⁺ cells, *Tbk1*^{NULL} *MLL-AF9*⁺ cells were desired. To this end, *Tbk1*^{fx/fx}; *Rosa26-CreERT2*⁺ *MLL-AF9*⁺ cells were treated with 200nM 4-

OHT, to induce deletion of *Tbk1* *in vitro*. However, at least in this protocol, it was learned thereafter that 200nM 4-OHT is insufficient to induce complete deletion of *Tbk1*. Specifically, if CreER^{T2} is incompletely induced, escapers are enriched for via plating in *MethoCult*TM M3434 methylcellulose (M3434) (**Figure 30**). Single-colony PCR would be required to determine whether escapers are *Tbk1*^{NULL/fx} or *Tbk1*^{fx/fx}. It should be addressed that two bands are visualized in the PCR positive control shown in **Figure 30**—this is due to an untreated, floxed-heterozygous (*Tbk1*^{+/fx}) gDNA template being used. As the *Tbk1*⁺ and *Tbk1*^{NULL} bands differ by only 9bp (332bp and 323bp, respectively), untreated *Tbk1*^{+/fx} gDNA can easily be mistaken for *Tbk1*^{NULL/fx} gDNA.

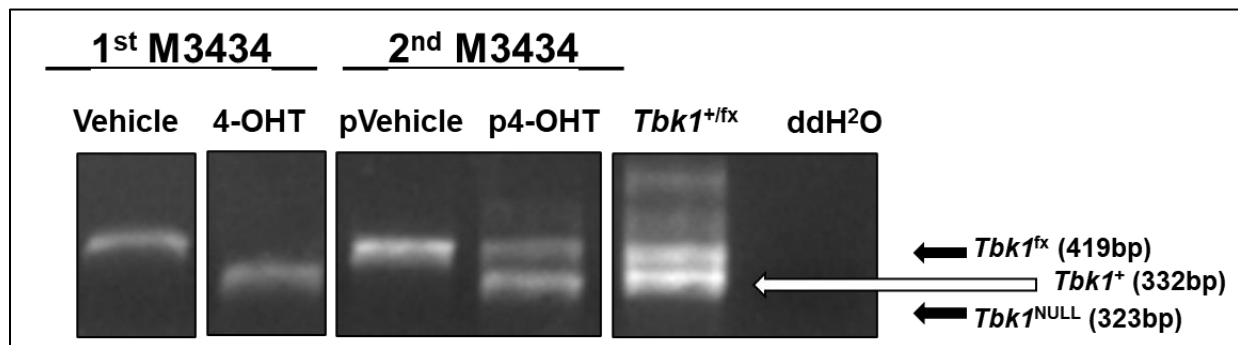


Figure 30. *Tbk1*-retaining Cells are Enriched for in M3434 Culture. Results from 3% agarose gel electrophoresis/*Tbk1* PCR. Lexicon primers #18, #23, and #24 were used to determine *Tbk1* status. gDNA templates from *Tbk1*^{fx/fx}; *Rosa26*-CreER^{T2}+ *MLL-AF9*⁺ cells treated with 200nM 4-OHT or vehicle in 1st M3434 and washed into liquid media after 6 days (Vehicle & 4-OHT). Following re-plating in M3434 without 4-OHT or vehicle (2nd M3434; pVehicle & p4-OHT) and re-sampling of DNA, PCR indicates re-emergence of the *Tbk1*^{fx} allele. Untreated *Tbk1*^{+/fx} gDNA (positive) and ddH₂O (negative) controls are shown. Vertical spacing between lanes indicates image cropping.

Following recommendations from other investigators, 3,000 *Tbk1*^{fx/fx}; *Rosa26-CreER*^{T2+} *MLL-AF9*⁺ cells were plated in M3434 media (1st M3434) for colony forming unit (CFU) analysis with either 200nM 4-OHT (4-OHT) or EtOH-PBS (vehicle) (**Figure 31A**). After 6 days, cells were washed and transferred to liquid media for 48 hours, allowing for *in vitro* expansion and DNA sampling for *Tbk1* PCR; subsequent PCR suggested the deletion of *Tbk1* was virtually complete (**Figure 31B**).

After 48 hours in liquid media, 3,000 cells were isolated from each liquid culture and plated again in M3434 (2nd M3434), without the addition of 4-OHT (p4-OHT) or vehicle (pVehicle) (**Figure 31D**). After 6 days, cells were washed and transferred to liquid media for 48 hours, to allow for similar *in vitro* expansion and DNA sampling for *Tbk1* PCR. Herein, subsequent PCR herein indicated a re-emergence of the *Tbk1*^{fx} allele in the cells previously believed to be *Tbk1*^{NULL} (**Figures 31E**). Considering this finding, DNA was re-sampled from the cells that had been washed from the 1st M3434 which, at this point, had been maintained in liquid media for 2-3 weeks; subsequent *Tbk1* PCR indicated that these cells now displayed a similar re-emergence of the *Tbk1*^{fx} allele (**Figure 31C**).

Notably, in cells that had been maintained in liquid media, the *Tbk1*^{fx} banding was of significantly lesser intensity compared to the *Tbk1*^{NULL} banding (**Figure 31C**); this contrasted with the banding intensities observed in cells following the 2nd M3434 (**Figure 31E**). This indicates that M3434 exerts a stronger selection pressure than liquid media in favor of *Tbk1*-retaining cells. As M3434 more strongly selects for LSCs than liquid media, wherein most *MLL-AF9*⁺ cells are blasts, we believe these data suggest

that *Tbk1* is more critical in *MLL-AF9*⁺ LSCs compared to blast counterparts [355].

Deletion of *Tbk1* would be expected to most significantly afflict the cells that *Tbk1* is most required by, which we believe are *MLL-AF9*⁺ LSCs.

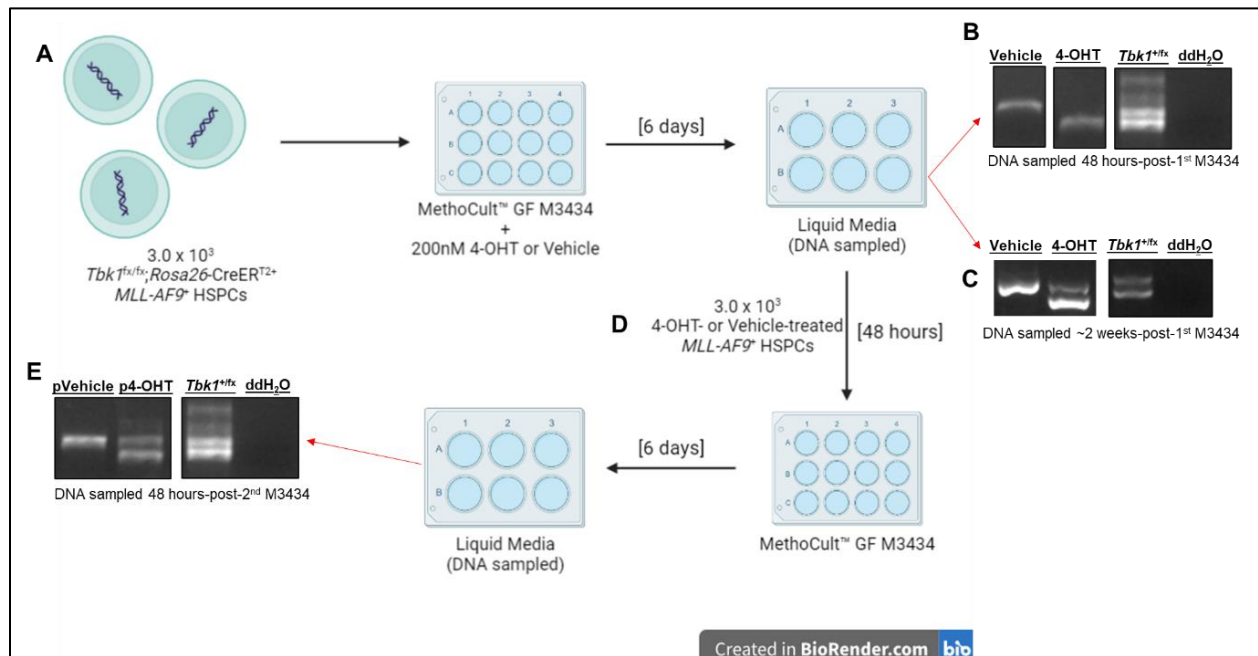


Figure 31. *Tbk1*^{fx} Allele Reappears in *MLL-AF9*⁺ Cells Previously Determined to be *Tbk1*^{NULL}. Schematic depicting initial attempt to delete *Tbk1* *in vitro*; created with BioRender.com. Lexicon primers #18, #23, and #24 were used to determine *Tbk1* status in all PCRs. Untreated *Tbk1*^{+/fx} gDNA (positive) and ddH₂O (negative) controls are shown. Vertical spacing between lanes indicates image cropping. (A) 3,000 *Tbk1*^{fx/fx}; *Rosa26-CreERT2*⁺ *MLL-AF9*⁺ cells are plated in M3434 with either 200nM 4-OHT or vehicle. (B) DNA sampled from cells washed into liquid media from initial M3434 plating and cultured for 48 hours; results from 3% agarose gel electrophoresis/*Tbk1* PCR. (C) Cells from initial M3434 plating were cultured for 2-3 weeks in liquid media and PCR was performed again; results from 3% agarose gel electrophoresis/*Tbk1* PCR. (D) After 48-hour culturing in liquid media, cells were plated in a 2nd M3434 assay without added 4-OHT or vehicle, then transferred to liquid media similarly after 6 days. DNA was sampled for PCR after cells had been in liquid media for 48 hours. (E) Results from 3% agarose gel electrophoresis/*Tbk1* PCR.

These data indicate that if induction of CreER^{T2} is incomplete, *Tbk1*^{fx} escapers will re-emerge after culturing in M3434 or liquid media; thus, the *in vitro* deletion protocol requires optimization. Moreover, these data suggest that *Tbk1* confers a survival advantage to *MLL-AF9*⁺ cells, although the mechanism is not yet known.

In Vitro* Treatment with 1uM 4-OHT for 4 Days Yields Complete Deletion of *Tbk1

It was determined that 200nM 4-OHT was insufficient to induce complete deletion of *Tbk1* in *MLL-AF9*⁺ cells. To this end, the *in vitro* deletion protocol was intensified, with both the dosage of 4-OHT and duration of treatment escalated.

Tbk1^{fx/fx}; *Rosa26-CreER*^{T2+} *MLL-AF9*⁺ and *Tbk1*^{fx/fx} *MLL-AF9*⁺ control cells were treated with 1uM 4-OHT in liquid media for 4 days. After 48 hours, cells were passaged, media was swapped, and 4-OHT re-added again for a final concentration of 1uM. Following 4 days of 1uM 4-OHT treatment, cells were transferred to fresh, liquid media (without 4-OHT) and DNA was sampled 48 hours later for *Tbk1* PCR. Similar to the initial deletion attempt, PCR herein suggested the deletion was also complete.

However, to confirm that *Tbk1* was completely deleted, two, serial M3434 platings were conducted; DNA was sampled for *Tbk1* PCR after cells were transferred to liquid media following the 2nd plating. PCR subsequently confirmed that *Tbk1* was completely deleted with the intensified regimen (**Figure 32A and 32B**). Notably, serial M3434 platings were performed twice, in independent experiments, confirming the intensified regimen induces complete deletion of *Tbk1*. Furthermore, western blot, performed by Allan Youmaran, BS of our group, confirms the loss of total *Tbk1* protein in *Tbk1*^{NULL} *MLL-AF9*⁺ cells and (**Figure 32B**).

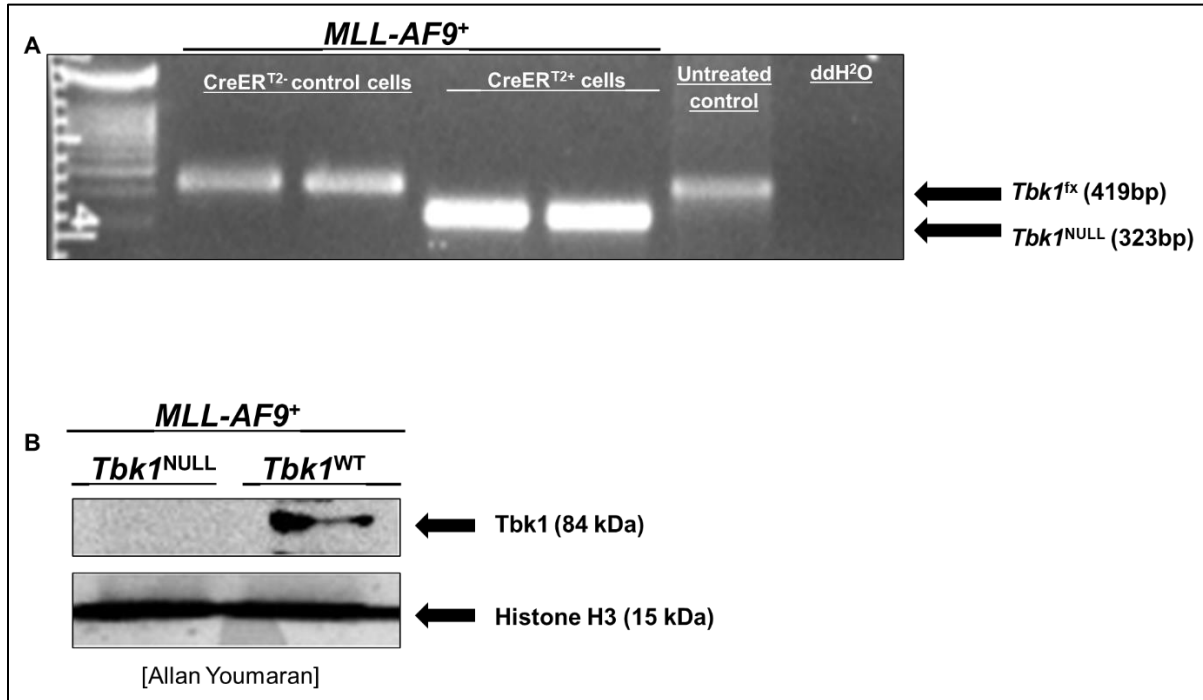


Figure 32. Treatment with 1uM 4-OHT for 4 Days in Liquid Media Yields Complete Deletion of *Tbk1*. To determine if the intensified 4-OHT regimen could induce complete deletion of *Tbk1*, PCR and western blot were used to confirm deletion following 2 consecutive M3434 assays. (A) Results from 3% agarose gel electrophoresis/*Tbk1* PCR. gDNA templates are from *Tbk1*^{fx/fx} (CreER^{T2-} control cells) and *Tbk1*^{fx/fx}; *Rosa26*-CreER^{T2+} (CreER^{T2+} cells) *MLL-AF9*⁺ cells treated with 1uM 4-OHT for 4 days (ran in duplicate). Left-most lane contains 1kB DNA ladder, Lexicon primers #18, #23, and #24 were used to determine *Tbk1* status, untreated *Tbk1*^{fx/fx} gDNA (positive) and ddH₂O (negative) controls are shown. Image is representative of two, independent experiments. (B) Western blot depicting total *Tbk1* protein expression in *Tbk1*^{NULL} *MLL-AF9*⁺ cells and *Tbk1*^{WT} counterparts, histone H3 used as loading control; performed by Allan Youmaran, BS of our group. Horizontal spacing between lanes indicates image cropping.

Based on Morphology, *Tbk1*^{NULL} *MLL-AF9*⁺ HSPCs Seem to be More Differentiated

Cell morphology is used to aid in the diagnosis and classification of AML, especially in cases of AML, NOS [239, 256, 263]. Lobularity and size of the nucleus are strong indicators of differentiation in normal and malignant myeloid cells: cells with with

larger, rounder nuclei are typically less differentiated than those with smaller, more lobular/kidney-shaped nuclei [356, 357]. Clinically, and not specific to AML, cancer cells that are less differentiated are almost invariably more aggressive than differentiated counterparts [358, 359]. As such, inducing the differentiation of AML cells is an extremely effective therapeutic strategy, such in cases of *IDH1/2*-mutated or *PML-RARA*⁺ AML [10, 13, 291]. However, while morphology can aid in the diagnosis of AML, morphology alone cannot provide an accurate diagnosis or determination of disease aggressiveness.

To determine if *Tbk1* regulates cell morphology, and possibly differentiation, H&E staining was performed on *Tbk1*^{WT} *MLL-AF9*⁺ (**Figure 33A**) and *Tbk1*^{NULL} counterparts (**Figure 33B**) that had been cultured in liquid media.

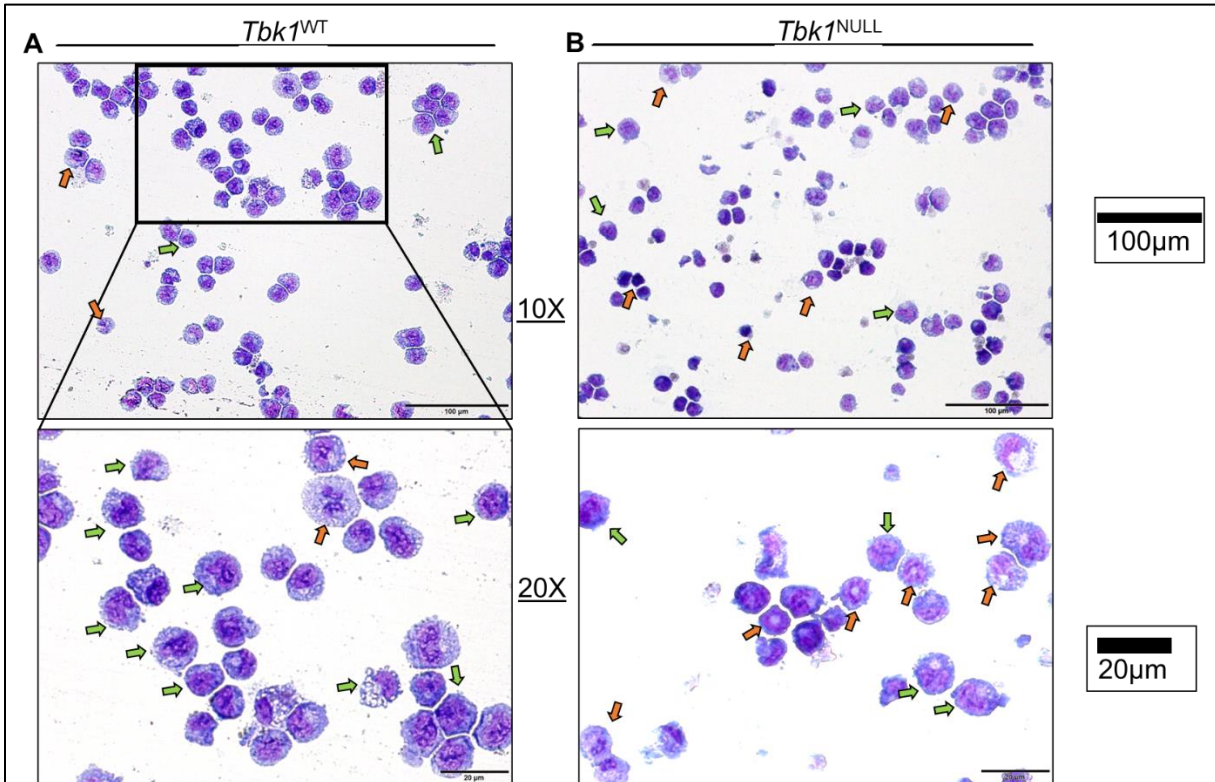


Figure 33. *Tbk1*^{NULL} *MLL-AF9*⁺ Cells Appear More Differentiated Morphologically. To determine if the loss of *Tbk1* affects the morphology of *MLL-AF9*⁺ cells, the morphology of cells was inspected. Cells were isolated from liquid culture, cytocentrifuged onto glass slides, methanol-fixed and H&E-stained (*Hema 3*[®] kit, Fisher). Green arrows indicate what are likely less-differentiated, LSC-like cells and orange arrows indicate what are likely more-differentiated, blast-like cells (some of which are actually mature cells, indicated by donut-shaped nuclei). (A) *Tbk1*^{WT} (n = 1). (B) *Tbk1*^{NULL} (n = 1). Objective magnification is indicated with scale bars.

As the AML liquid tumor is highly heterogeneous, cells will differ in their differentiation status, and differentiation must be considered generally, as opposed to an all-encompassing determination of all cells. With this, based on morphology alone, it appears that the *Tbk1*^{NULL} culture is generally more differentiated than the *Tbk1*^{WT} culture. The loss of *Tbk1* seems to increase the number of differentiated cells within the

MLL-AF9⁺ culture, but this observation was not quantified as it was in a report by Somerville, *et al.* [360]. Clinically, ~500 cells will be assessed and quantified, and the differentiation status of the disease will be determined as a percentage of differentiated cells/total cells assessed (per Jiwang Zhang, MD/PhD). While morphology can only be used to support more definitive measures, such as flow cytometry, it appears that *Tbk1* regulates the morphology of *MLL-AF9*⁺ cells, which provides rationale for confirming if *Tbk1* regulates these cells' differentiation. Although, these observations in AML cells are consistent with a PDAC model wherein *Tbk1*^{NULL} tumor cells are more differentiated than *Tbk1*^{WT} counterparts [185].

***Tbk1*^{NULL} *MLL-AF9*⁺ HSPCs Proliferate Faster**

Observations by lab personnel suggested that there is a difference in the growth rates of *Tbk1*^{WT} *MLL-AF9*⁺ cells and *Tbk1*^{NULL} counterparts. Specifically, *Tbk1*^{NULL} *MLL-AF9*⁺ cells seem to proliferate faster, thereby exhausting culture media more quickly than *Tbk1*^{WT} counterparts. To further interrogate these observations, growth rate/curve analysis was performed.

To this end, 10,000 cells of each type were seeded (4 replicates); cells were counted every 24 hours via trypan blue-exclusion. While there was initially no difference in the growth rate of the cells, *Tbk1*^{NULL} *MLL-AF9*⁺ cells show a significantly increased ($p < 0.0001$) growth rate at 96 hours post-seeding (**Figure 34A**). The raw cell count was log-transformed and plotted (**Figure 34B**) to further analyze the data, as it was surprising to see the difference in growth rate only apparent after several days. However, based on observations and reports from other labs, it is estimated that only

15-25% of *MLL-AF9*⁺ cells in bulk culture are LSCs, with the remaining being blast cells [360]. As *Tbk1*^{NULL} *MLL-AF9*⁺ cells differ in growth rates only after several days, this could suggest that *Tbk1* regulates a less-abundant, LSC population of *MLL-AF9*⁺ cell in culture, at least more so than it does the more-populous blast cells, though this interpretation requires further validation.

Following results of the growth curve analysis, cell cycle analysis was performed. To assess the cells in the conditions they were most often maintained in, cells were simply isolated from bulk, media-replete culture conditions (not seeded specifically for cell cycle analysis). Time and resources only allowed for a single analysis, so the results are interpreted cautiously (n = 1).

However, the results from cell cycle analysis (Dean-Jett-Fox algorithm; **Figure 34C and 34D**) support both our observations and the results of the growth curve analysis. Specifically, *Tbk1*^{NULL} *MLL-AF9*⁺ cells were more likely to exist in S or G2/M phase than *Tbk1*^{WT} cells at any given time, suggesting an increase in cycling rate.

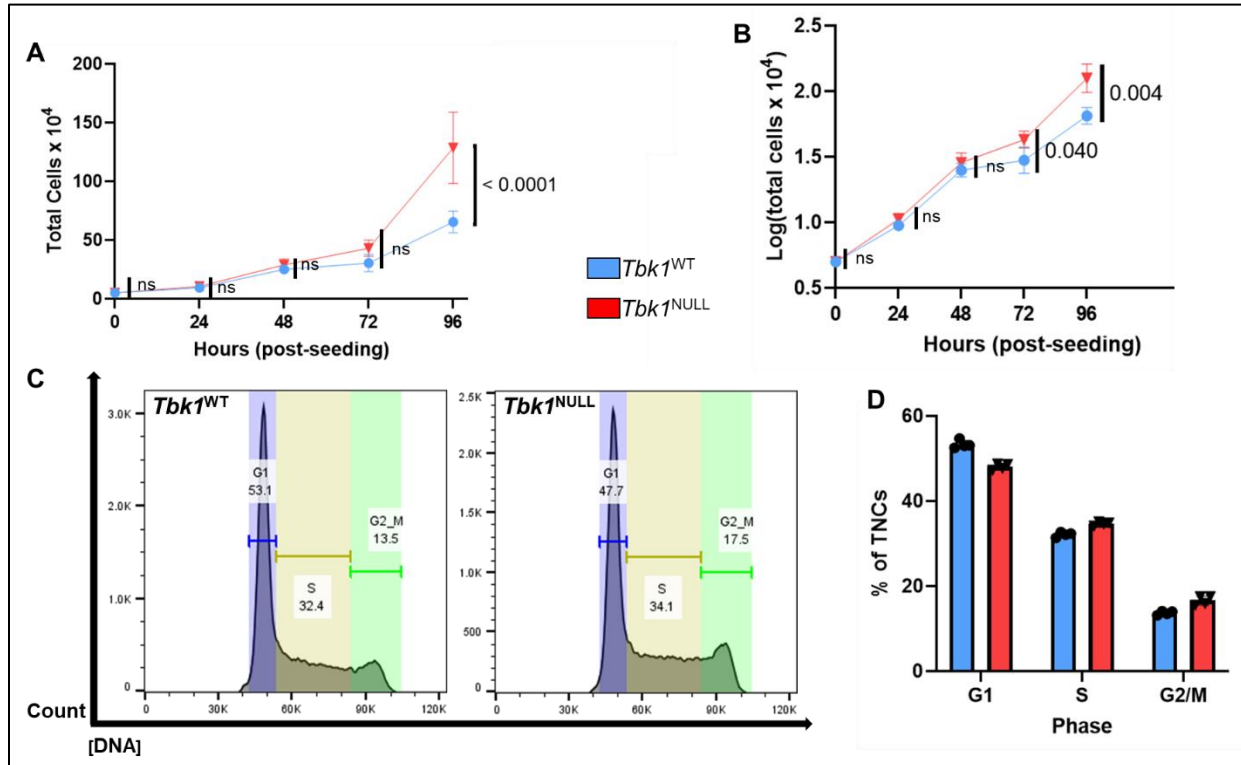


Figure 34. *Tbk1*^{NULL} MLL-AF9⁺ Cells Proliferate Faster than *Tbk1*^{WT} Counterparts. To quantify the observation that *Tbk1* deletion caused MLL-AF9⁺ cells to grow faster, growth rate/curve analysis and cell cycle analysis (using PI) were performed. (A) 10,000 cells were plated (3 replicates) and counted daily via trypan blue-exclusion. Cultures were homogenized and half volume discarded, then fresh media + growth factor added at 48 and 72 hours to prevent cell exhaustion. Raw cell counts plotted as [total cells x 10⁴]. Unpaired t-test used for all statistical analyses (between *Tbk1*^{WT} and *Tbk1*^{NULL} cells at each timepoint; p < 0.0001 at 96 hours-post-seeding). (B) Log transformation of [total cells x 10⁴] from Figure 33A to assess the rate-of-change in cell growth. Unpaired t-test used for all statistical analyses (between *Tbk1*^{WT} and *Tbk1*^{NULL} cells at each timepoint; p = 0.040 and 0.004 at 72 and 96 hours-post-seeding, respectively). (C) Representative histograms of cell cycle analyses and use of Dean-Jett-Fox algorithm for analysis. (D) Quantification of FACS data (n = 1).

***Tbk1*^{NULL} *MLL-AF9*⁺ HSPCs Show a Trend Toward Reduced Clonogenicity**

Given the alterations in cell morphology and cycle rate, we further sought to investigate the functional characteristics of *Tbk1*^{NULL} *MLL-AF9*⁺ cells. To this end, colony-forming unit (CFU)/clonogenic ability (clonogenicity) assays, an established surrogate measure for stemness and leukemogenicity, were performed [355].

In 2 independent experiments, cells were plated in M3434 for 7 days, manually counted and washed, then cultured in liquid media overnight and replated in M3434 again before manual counting again after 7 days. Results from the initial experiments cannot be interpreted accurately, as the positive control (*Tbk1*^{WT} *MLL-AF9*⁺) did not result as expected (**Figure 35**). Specifically, *MLL-AF9*⁺ cells are expected to maintain clonogenicity over several platings; ours did not and, instead, decreased significantly ($p = 0.0012$ and 0.0043) in the second plating of each experiment, mostly invalidating the results. However, while both cell types had reduced clonogenicity in each 2nd plating, *Tbk1*^{NULL} cells seemed to form fewer colonies, though this requires confirmation with a positive control (*Tbk1*^{WT} *MLL-AF9*⁺) that results correctly.

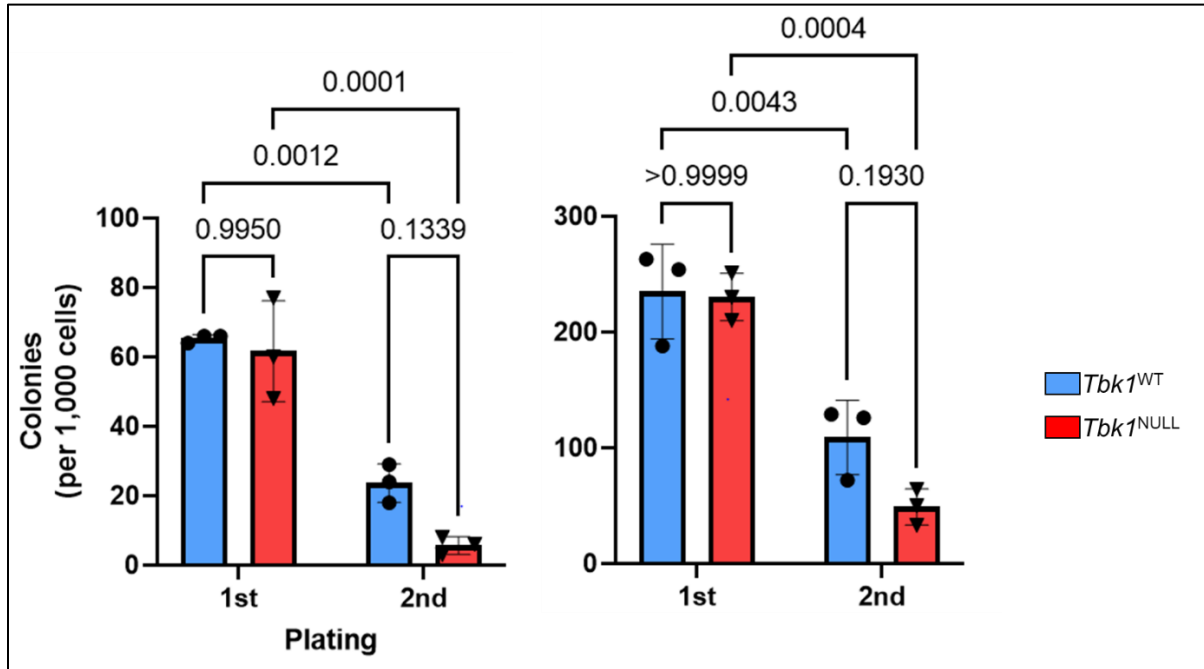


Figure 35. *Tbk1*^{NULL} MLL-AF9⁺ Cells Show a Trend Toward Reduced Clonogenicity. To determine if *Tbk1* influences the clonogenicity of MLL-AF9⁺ cells, 3,000 MLL-AF9⁺ cells either *Tbk1*^{NULL} or *Tbk1*^{WT} were isolated from liquid media, transferred to M3434, and aliquoted (n = 2, with 3 replicates each). Colonies were manually counted at 7-days-post-seeding and washed, then cultured overnight and replated similarly in a 2nd CFU assay. Two-way ANOVA was used for each analysis (comparing means +/- standard deviation), as it was desired to know (1) how *Tbk1*^{WT} and *Tbk1*^{NULL} groups compared to each other at both timepoints (inter-group comparison) as well as (2) how the groups compared to themselves across both timepoints (intra-group comparison).

As such, subsequent experiments by Wei Wei of our group indicated that *Tbk1*^{NULL} MLL-AF9⁺ cells do show significantly decreased clonogenicity compared to *Tbk1*^{WT} counterparts; this suggests that *Tbk1* does in fact promote the clonogenicity of MLL-AF9⁺ cells (data not shown).

***Tbk1*^{NULL} *MLL-AF9*⁺ HSPCs are Sensitized to Serum Starvation**

Serum starvation is a widely employed laboratory technique used to study autophagy, apoptosis, and to synchronize cells at G0/G1 [361]. As a type of nutrient stress, mammalian cells will activate autophagy/mitophagy and p27^{Kip1}-quiescence in response to serum starvation [362]. As *Tbk1* is a critical regulator of mitophagy, we sought to determine if *Tbk1*^{NULL} *MLL-AF9*⁺ cells showed any alterations in their sensitivity to serum starvation [363].

To this end, *Tbk1*^{NULL} *MLL-AF9*⁺ cells were transduced with the *MSCV-YFP* retrovirus and yellow fluorescent protein (YFP)-expressing (YFP⁺) cells were selected for via FACS. Following selection, *Tbk1*^{NULL} *MLL-AF9*⁺ YFP⁺ and *Tbk1*^{WT} *MLL-AF9*⁺ cells were mixed in an approximate 1/1 ratio (which was ultimately ~70% *Tbk1*^{NULL}). 6.0 x 10⁴ cells were seeded (3 replicates) in RPMI-1640 with (control/serum-replete conditions [Serum⁺]) or without 10% FBS (starved/serum-depleted conditions [Serum⁻]). 24 hours later, YFP-positivity was checked via FACS and analyzed as percentage of TNCs. With this method, any change in the YFP⁺ percentage indicates a net effect on *Tbk1*^{NULL} cells.

It was observed that the percent of TNCs that were YFP⁺ decreased significantly ($p < 0.0001$) in serum-starved conditions compared to control, serum-replete conditions (**Figure 36A**). This finding suggests that *Tbk1*^{NULL} *MLL-AF9*⁺ cells are significantly more sensitive to this type of nutrient stress than *Tbk1*^{WT} counterparts. However, this analysis cannot determine whether the change in YFP-positivity was due to increased cell death,

decreased proliferation, or a combination of both in *Tbk1*^{NULL} *MLL-AF9*⁺ cells. Further analysis of the data revealed that YFP-positivity did not significantly increase in control conditions (**Figure 36B**).

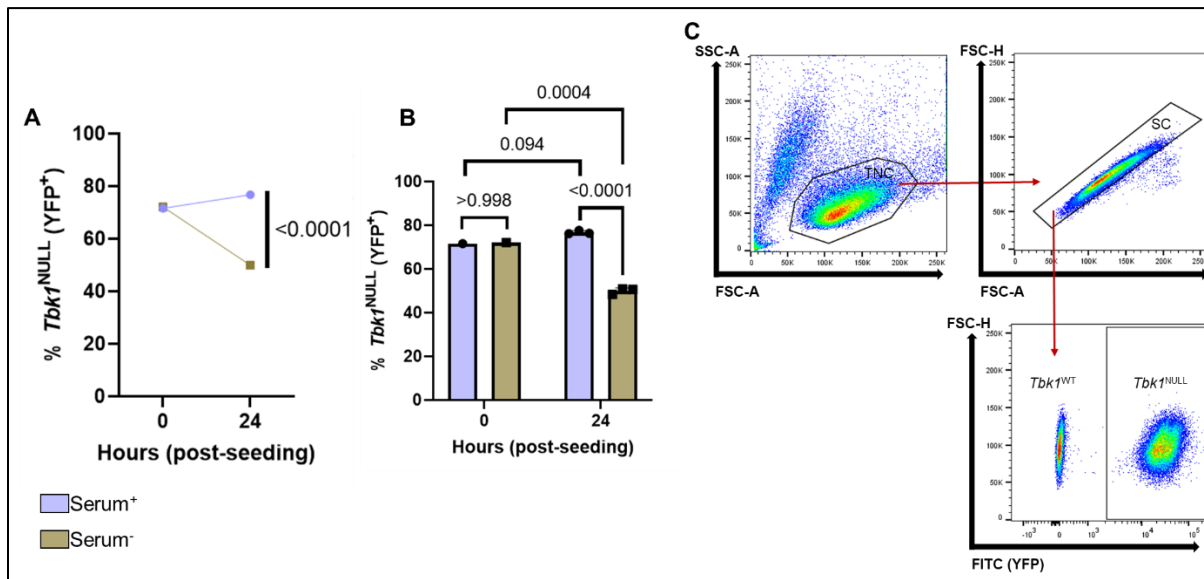


Figure 36. *Tbk1*^{NULL} *MLL-AF9*⁺ Cells are Sensitized to 24-hour Serum Starvation. To determine if *Tbk1* regulates the survival of *MLL-AF9*⁺ cells amid nutrient stress, serum starvation was performed on a co-culture of *Tbk1*^{WT} and *Tbk1*^{NULL} YFP⁺ cells (n = 1, with 3 replicates). The *Tbk1*^{NULL} percentage of the co-culture was assessed via FACS (as YFP-positivity) before and after 24-hour serum starvation. (A) YFP-positivity is significantly decreased (p < 0.0001) compared to serum-replete control conditions following 24-hour serum starvation; unpaired t-test used for statistical analysis. (B) YFP-positivity did not significantly increase over 24 hours in control conditions; two-way ANOVA used for statistical analysis (comparing means +/- standard deviation; inter- and intra-group comparisons). (C) Representative gating strategies for FACS analysis.

This finding indicates that without nutrient stress, *Tbk1*^{WT} *MLL-AF9*⁺ cells do not outcompete *Tbk1*^{NULL} counterparts in liquid media within 24 hours; moreover, any survival deficit caused by the loss of *Tbk1* is exacerbated by nutrient stress. However, it

is still unknown how the loss of *Tbk1* sensitizes *MLL-AF9*⁺ cells to serum starvation. Representative gating strategy is shown (**Figure 36C**); gating on TNC and SC is representative of that used in all FACS analyses of *MLL-AF9*⁺ cells.

c-Kit⁺Flt3⁺ *MLL-AF9*⁺ HSPCs are Resistant to DNO but Not Ara-C.

A 2013 study by our lab group demonstrated that mouse *MLL-AF9*⁺ LSCs (c-Kit⁺CD11b^{lo} [least differentiated]) are resistant to DNO and Ara-C, compared to the *MLL-AF9*⁺ mitotic (c-Kit⁺CD11b^{hi} [mid-differentiation]) and post-mitotic (c-Kit⁺CD11b^{hi} [most differentiated]) blast cells [271]. It was determined *MLL-AF9*⁺ LSCs are p27^{Kip1}-quiescent and therefore less sensitive to the cytotoxic effects of CTx. In the same study, it was shown that expression of p27^{Kip1} is induced by activation of c-Kit and Flt3; however, it was not determined whether c-Kit⁺Flt3⁺ *MLL-AF9*⁺ cells are similarly resistant to CTx. As such, we sought to determine if c-Kit⁺Flt3⁺ *MLL-AF9*⁺ cells are also drug-resistant. To this end, 5.0 x 10⁴ *Tbk1*^{WT} *MLL-AF9*⁺ and *Tbk1*^{NULL} counterparts (genetic control) were treated for 24 hours with varying dosages of either DNO (20-100nM) or Ara-C (0.5-30uM). The number of c-Kit⁺Flt3⁺ cells were then measured as percentage of *MLL-AF9*⁺ TNCs, and representative FACS gating strategies are shown (**Figure 37C**; FACS plots from *Tbk1*^{WT} groups are shown to illustrate *Tbk1*-dependent shift in cell populations). Cells were seeded with 3 replicates.

It was observed that *Tbk1*^{WT} c-Kit⁺Flt3⁺ *MLL-AF9*⁺ cells are resistant to DNO but NOT Ara-C, as only treatment with DNO caused a significant enrichment for c-Kit⁺Flt3⁺ cells (**Figure 37A** and **37B**).

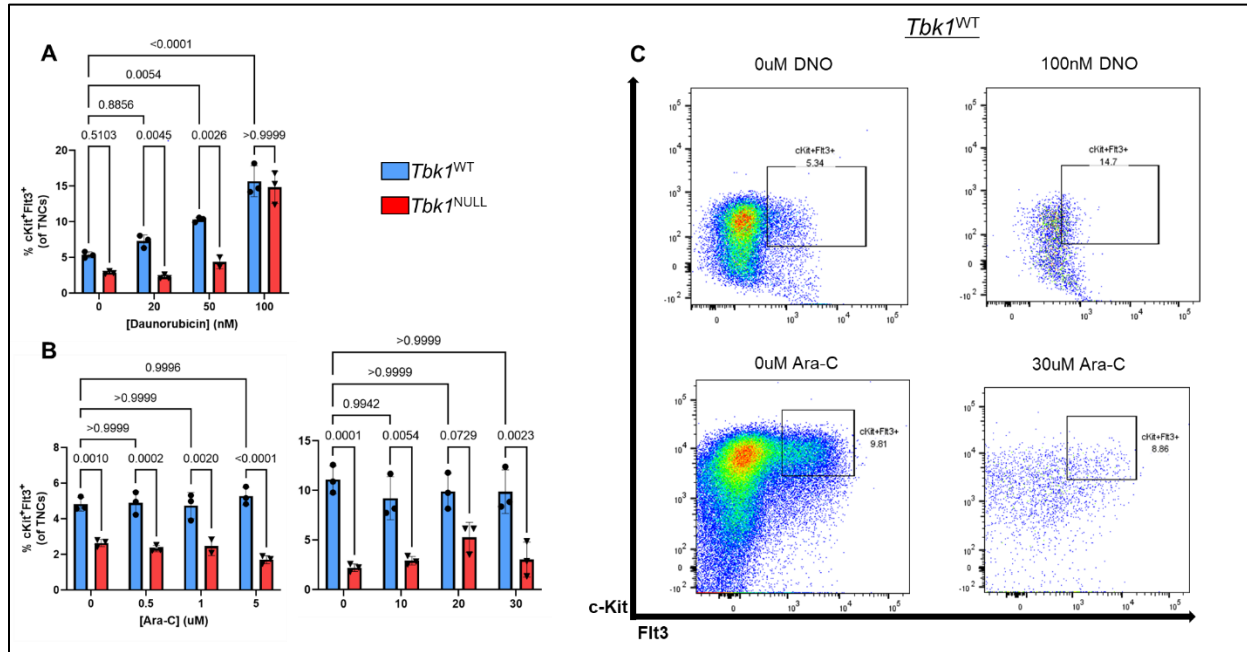


Figure 37. Treatment with Daunorubicin but Not Ara-C Enriches for c-Kit⁺Flt3⁺ MLL-AF9⁺ Cells. To determine if c-Kit⁺Flt3⁺ MLL-AF9⁺ cells are resistant to chemotherapy, bulk MLL-AF9⁺ cells were treated with increasing dosages of DNO and Ara-C (n = 1, with 3 replicates). Following treatment, the percentage of c-Kit⁺Flt3⁺ cells was determined; a significant increase from control group suggests these cells are chemotherapy-resistant. Quantification of c-Kit⁺Flt3⁺ MLL-AF9⁺ cells following DNO or Ara-C treatment and statistical analyses performed using two-way ANOVA (comparing means +/- standard deviation; inter- and intra-group comparisons). (A) ddH₂O- and DNO-treated groups. (B) ddH₂O- and Ara-C-treated groups. (C) Representative FACS gating strategies for analysis of c-Kit⁺Flt3⁺ MLL-AF9⁺ cells are shown; plots of *Tbk1*^{WT} cells are shown to illustrate change, if applicable, in c-Kit⁺Flt3⁺ population in response to either DNO or Ara-C. *Tbk1*^{NULL} cells serve as genetic control.

Moreover, a striking reduction in the amount of c-Kit⁺Flt3⁺ cells was observed in the ddH₂O-treated control *Tbk1*^{NULL} groups. Specifically, the c-Kit⁺Flt3⁺ population was significantly reduced following the loss of *Tbk1* in MLL-AF9⁺ cells across all Ara-C treatment groups (but only certain DNO treatment groups, which is attributed to

culturing variabilities). Oddly, it was noted that 100nM DNO causes an enrichment in *Tbk1*^{NULL} c-Kit⁺Flt3⁺ population, for which no explanation is yet available; it could be that the π -conjugated, aromatic structure of DNO (which causes its bright red color) may confound FACS analysis when high doses such as 100nM are used.

Additionally, in relation to the study by Zhang, et al., it was desired to know if several of the involved genes are of prognostic significance in AML. Microarray data from *BloodSpot* (GSE13159) were examined to determine if median gene expression was correlated with probability of OS (**Table 5**; encoded protein listed in parenthesis if naming differs significantly from gene name) [332, 335, 336].

Table 5. Select Genes, P-value, Correlation with Probability of OS in AML (if Applicable), and Microarray Probe Used [332, 335, 336].

Gene	p-value	Correlation	Probe
<i>CDKN1B</i> (p27 ^{Kip1})	0.837	None	209112_at
<i>FLT3</i>	0.040	Negative	206674_at
<i>FLT3LG</i> (FLT3 ligand)	0.184	None	206980_s_at
	0.073	None (trend toward negative)	210607_at
<i>KIT</i>	0.058	None (trend toward positive)	205051_s_at
<i>KITLG</i> (SCF)	0.3	None	207029
	0.779	None	211124_s_at
	0.704	None	226534_at
<i>ITGAM</i> (CD11b)	0.78	None	205785_at
	0.008	Negative	205786_s_at

Unexpectedly, most genes did not correlate with probability of OS. Even more surprising was the finding that *ITGAM* mRNA levels either did not correlate or even predicted worse survival, depending on the probe used. As *ITGAM* encodes a marker positively associated with differentiation (CD11b), it was anticipated that increased *ITGAM* expression would almost invariably portend a higher probability of OS, as more differentiated cancers tend to be less aggressive [358, 359]. Equally surprising was the finding that, while not significant, *KIT* expression trended towards a positive correlation with OS. In contrast to *ITGAM*, *KIT* encodes a surface receptor negatively associated with differentiation. Thus, it was hypothesized that *KIT* correlation would be opposite that of *ITGAM*.

While microarray data is valuable, it is limited by the fact that mRNA levels do not inherently indicate protein expression. In fact, mRNA levels can differ greatly from actual protein expression, such as is the case with basal expression of *TP53* mRNA compared to p53 protein [364]. These studies illustrate the importance of functional studies when investigating the role of a gene/protein in predicting prognosis.

***Tbk1* Regulates *MLL-AF9*⁺ LSCs**

Based on the findings in the previous experiment, we sought to confirm that *Tbk1* indeed maintains the c-Kit⁺Flt3⁺ pool of *MLL-AF9*⁺ cells. Additionally, we sought to determine if *Tbk1* regulates the c-Kit⁺CD11b^{lo} subset previously identified by our lab (Zhang, *et al.*) to be resistant to DNO and Ara-C [271]. To this end, ~1 million *Tbk1*^{NULL} *MLL-AF9*⁺ and *Tbk1*^{WT} counterparts were isolated from maintenance in liquid media and analyzed for c-Kit, Flt3, and CD11b expression via FACS. The size of each population

was measured as percentage of TNCs. Four samples were taken from each liquid culture (4 replicates), so statistics could not be performed.

It was observed that the loss of *Tbk1* seemed to shift *MLL-AF9*⁺ cells from the c-Kit⁺CD11b^{lo} to the c-Kit⁺CD11b^{hi} immunophenotype (**Figure 38A**). Strikingly, it was found that *Tbk1* deletion almost completely ablates the c-Kit⁺Flt3⁺ population (**Figure 38B**). However, with n = 1, further validation of these findings are necessary. Though, if true, these observations would be consistent with previous data, such as increased growth rate and morphology changes, that suggest *Tbk1*^{NULL} *MLL-AF9*⁺ cells are more differentiated than *Tbk1*^{WT} counterparts. Representative FACS gating strategies are shown (**Figure 38C**).

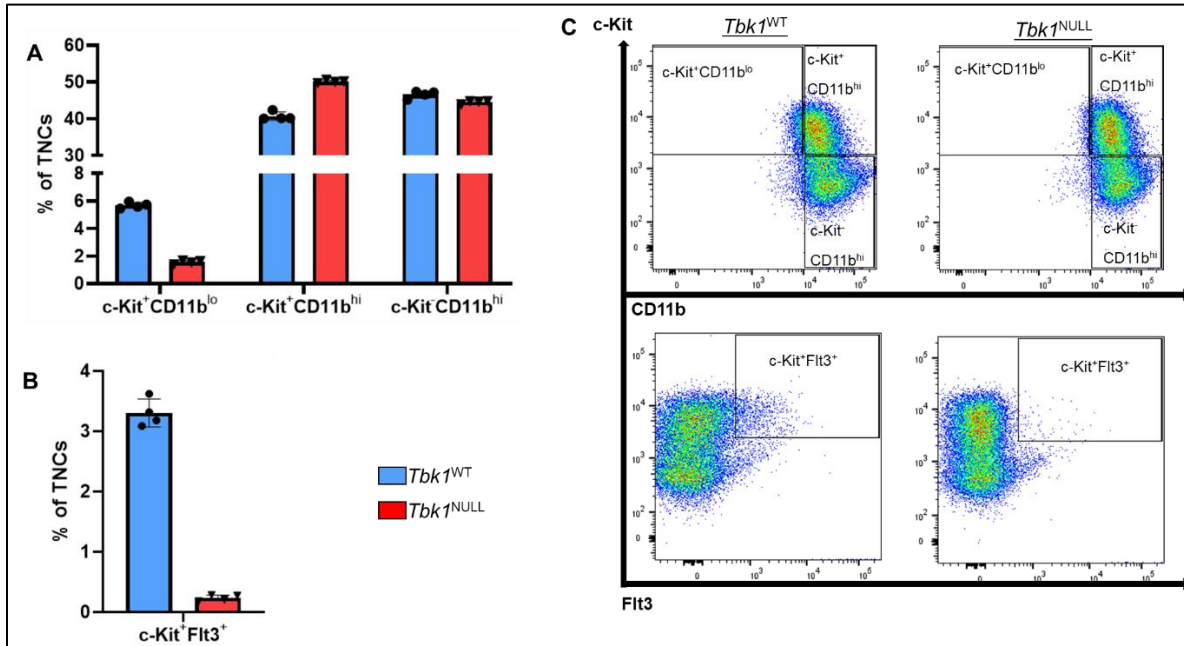


Figure 38. Loss of *Tbk1* Hampers the c-Kit⁺Flt3⁺ and c-Kit⁺CD11b^{lo} LSC Subsets of MLL-AF9⁺ cells. In accordance with a gating strategy indicated by Zhang, *et al.*, the c-Kit/Flt3 and c-Kit/CD11b immunophenotypes of our MLL-AF9⁺ cells were analyzed via FACS. Cells were isolated from liquid media (n = 1), stained, and subsets analyzed as percentage of TNCs. (A) Quantification of c-Kit⁺CD11b^{lo}, c-Kit⁺CD11b^{hi}, and c-Kit⁻CD11b^{hi} MLL-AF9⁺ LSCs. (B) Quantification c-Kit⁺Flt3⁺ MLL-AF9⁺ LSCs. (C) Representative FACS gating for c-Kit/CD11b and c-Kit/Flt3, separated by *Tbk1*^{WT} and *Tbk1*^{NULL} cells.

c-Kit⁺Flt3⁺ MLL-AF9⁺ Cells are Promoted by AMX

Deletion of *Tbk1* in MLL-AF9⁺ cells reduces the size of the c-Kit⁺Flt3⁺ and c-Kit⁺CD11b^{lo} LSC pools, which suggests that *Tbk1* is a target for the basis of AML treatment. However, as this is a genetic model, a means of clinical translation still has yet to be determined. To this end, we sought to determine if treatment with AMX, a TBK1/IKKε inhibitor, can elicit effects similar to genetic ablation of *Tbk1*. and analyzed its effect on the MLL-AF9⁺ LSC pools. Representative FACS gating strategy is shown (Figure 41).

To this end, 5.0×10^4 $Tbk1^{WT}$ $MLL-AF9^+$ and $Tbk1^{NULL}$ counterparts (genetic control) were treated for 24 hours with varying dosages of AMX (50-300uM), and the size of each population was measured as percentage of TNCs. Much to our surprise, it was found that high-dose (300uM) AMX causes an increase in the size of the c-Kit⁺Flt3⁺ population (**Figure 39A**); in terms of the c-Kit⁺CD11b^{lo} population, AMX had no effect (**Figure 39B**). These data suggest that AMX would be contraindicated in $MLL-AF9^+$ AML patients and that pharmacologic blockade of TBK1/IKK ϵ causes a compensatory upregulation of c-Kit⁺Flt3⁺ population in $Tbk1^{WT}$ $MLL-AF9^+$ cells. While the involvement of IKK ϵ is not yet known, $Tbk1$ certainly regulates the c-Kit⁺Flt3⁺ population as no significant changes were seen with AMX treatment in any $Tbk1^{NULL}$ cells (**Figure 39**). While IKK ϵ regulation of the c-Kit⁺Flt3⁺ population of $MLL-AF9^+$ cells cannot yet be ruled out, $Tbk1$ must be ruled-in.

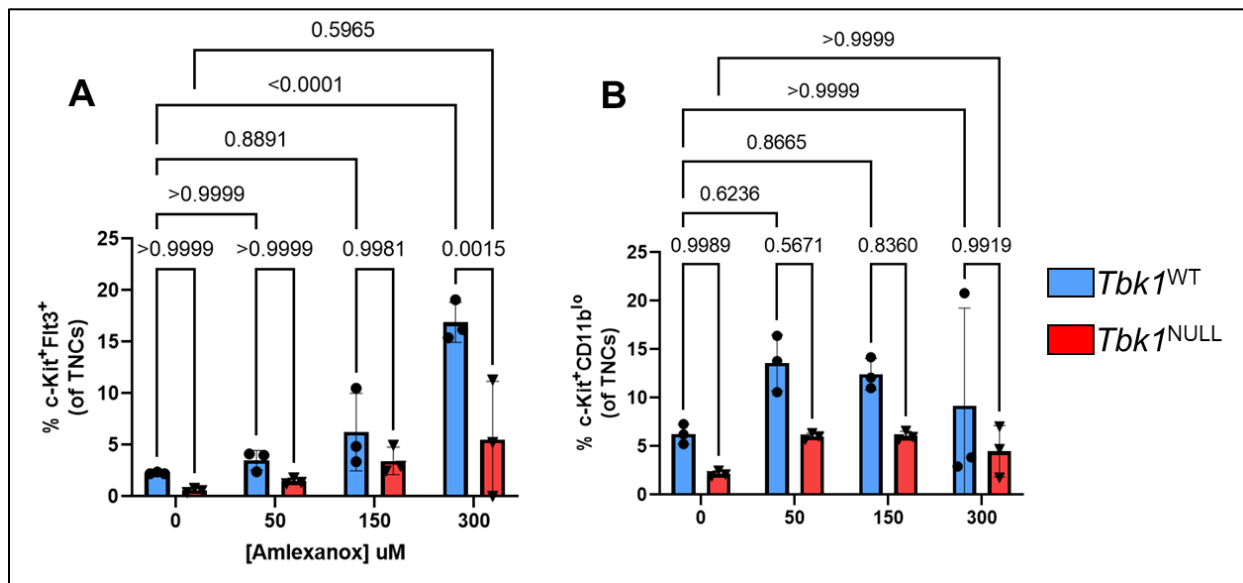


Figure 39. c-Kit⁺Flt3⁺ MLL-AF9⁺ Cells are Increased by High-dose AMX. To determine if AMX alters the size of the c-Kit⁺Flt3⁺ and c-Kit⁺CD11b^{lo} subsets of *MLL-AF9*⁺ cells, cells were treated with increasing dosages of AMX for 24 hours, and the size of the c-Kit⁺Flt3⁺ and c-Kit⁺CD11b^{lo} compartments were determined as percentage of TNCs via FACS (n = 1, with 3 replicates). Cells were isolated/washed and stained following drug treatment, analyzed via FACS; the data were quantified, and statistical analyses performed using two-way ANOVA (comparing means +/- standard deviation; inter- and intra-group comparisons). (A) Size of the c-Kit⁺Flt3⁺ population is shown. (B) Size of the c-Kit⁺CD11b^{lo} population is shown.

GSK8612 has Variable Effects on *MLL-AF9*⁺ LSCs

Following the results of the AMX treatment, we sought to determine if pharmacologic blockade of Tbk1 alone can mirror those following genetic ablation. While we wish to determine how pharmacologic IKK ϵ blockade affects these cells, IKK ϵ -selective inhibitors are not yet available. To this end, 5.0×10^4 *Tbk1*^{WT} *MLL-AF9*⁺ and *Tbk1*^{NULL} counterparts (genetic control) were treated for 24 hours with varying dosages (1-4 μ M) of GSK8612, a bromine-containing small molecule that strongly blocks the action of Tbk1 only. The size of each population was measured as percentage of TNCs, and representative FACS gating strategy is shown (**Figure 41**).

In contrast to AMX, it was observed that 2 μ M and 4 μ M GSK8612 dose-dependently decreases the size of the c-Kit⁺CD11b^{lo} pool of *MLL-AF9*⁺ cells (**Figure 40B**). Strangely, 1 μ M and 2 μ M GSK8612 causes an increase in the size of the c-Kit⁺Flt3⁺ pool; this increase, however, is lost with 4 μ M GSK8612 treatment.

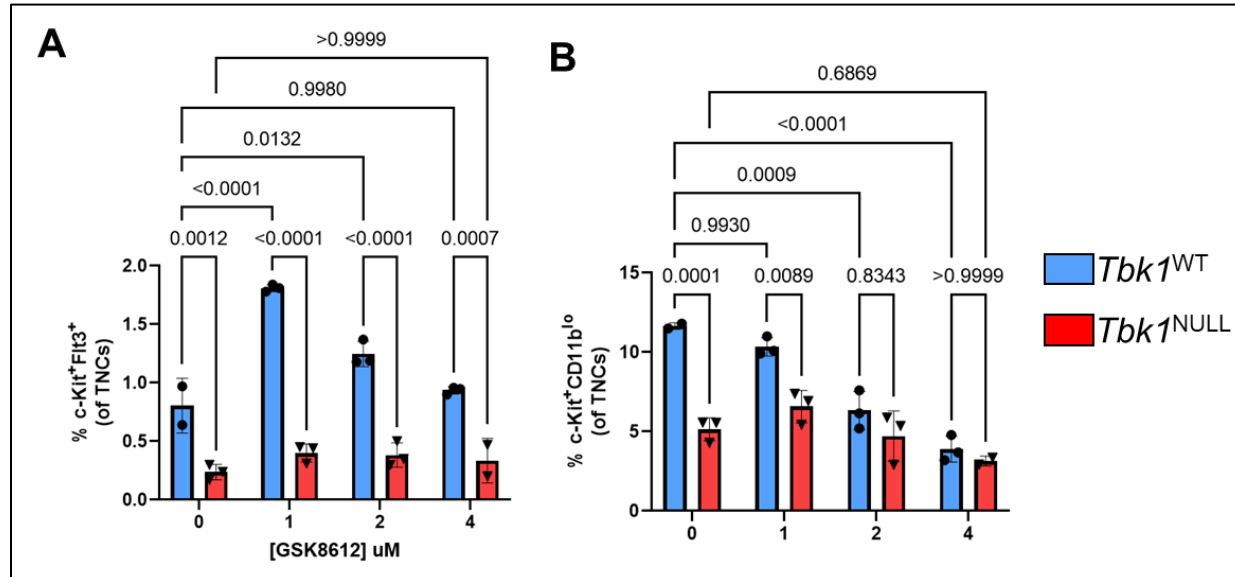


Figure 40. *c-Kit*⁺*Flt3*⁺ *MLL-AF9*⁺ Cells are Increased with Low-dose GSK8612 and *c-Kit*⁺*CD11b*^{lo} Cells are Decreased with GSK8612 in a Dose-dependent Manner. To determine if GSK8612 alters the size of the *c-Kit*⁺*Flt3*⁺ and *c-Kit*⁺*CD11b*^{lo} subsets of *MLL-AF9*⁺ cells, cells were treated with increasing dosages of GSK8612 for 24 hours, and the size of the *c-Kit*⁺*Flt3*⁺ and *c-Kit*⁺*CD11b*^{lo} compartments were determined as percentage of TNCs via FACS (n = 1, with 3 replicates). Cells were isolated/washed and stained following drug treatment, analyzed via FACS; the data were quantified, and statistical analyses performed using two-way ANOVA (comparing means +/- standard deviation; inter- and intra-group comparisons). (A) Size of the *c-Kit*⁺*Flt3*⁺ population is shown. (B) Size of the *c-Kit*⁺*CD11b*^{lo} population is shown.

Unfortunately, these data do not provide clear information on the effect of GSK8612 on *MLL-AF9*⁺ cells; while low-dose GSK8612 seems it could exacerbate AML, high-dose GSK8612 may have the opposite effect. However, much is still unknown and these data require further interpretation and validation. While AMX and GSK8612 do not seem to have significant off-target effects (as *Tbk1*^{NULL} cells were largely unaffected by both), it is possible that off-target effects in the presence of functional *Tbk1* exist and thus, complicate the clinical translation of *Tbk1* deletion.

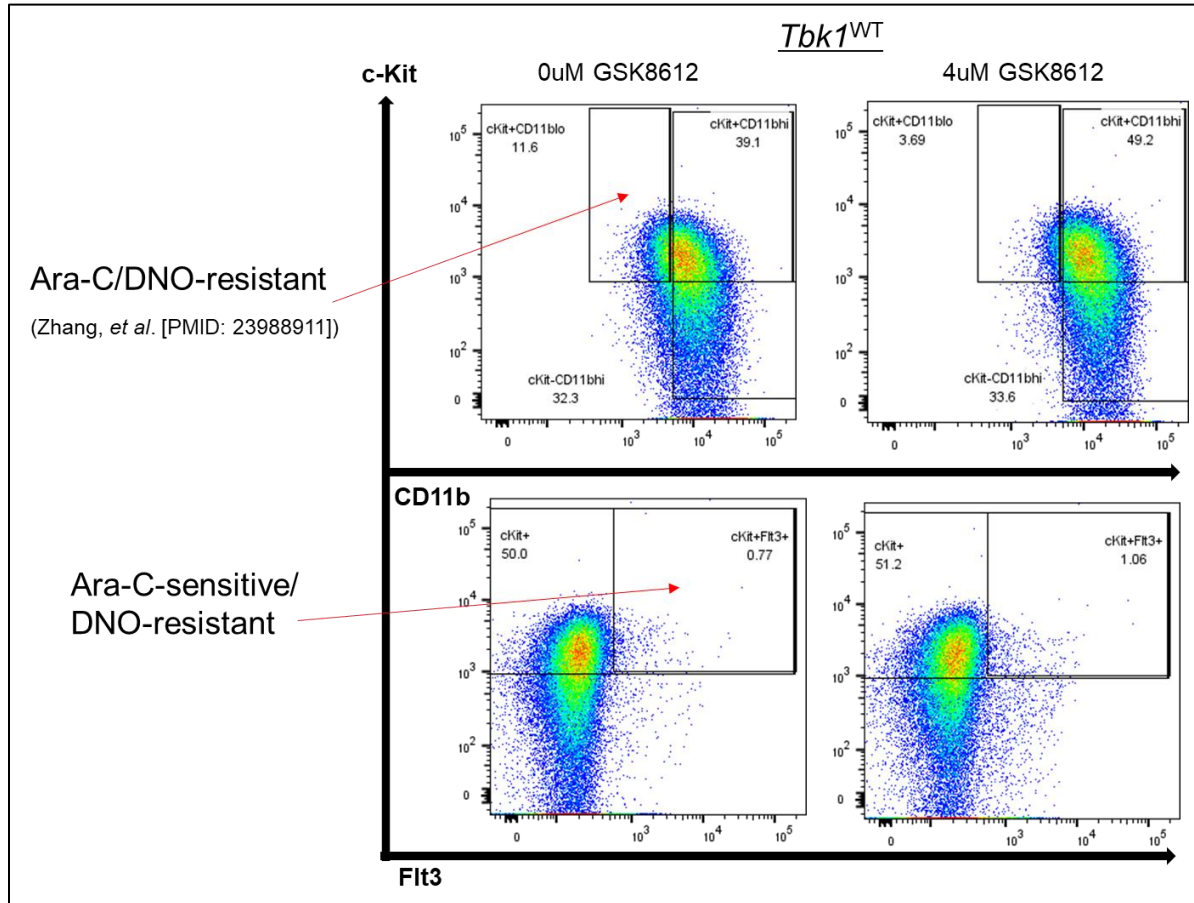


Figure 41. Representative Gating Strategies for FACS Analysis of AMX- or GSK8612-treated MLL-AF9⁺ Cells. Drug-resistant populations are indicated by red arrows and drug sensitives are indicated in accordance with those determined by Zhang, *et al.* and my analysis. Populations of MLL-AF9⁺ cells are separated by c-Kit^{+/−}CD11b^{lo/hi} and c-Kit⁺Flt3^{+/−}.

Loss of *Tbk1* Causes Increased Expression of c-Fms on MLL-AF9⁺ HSPCs

The c-FMS proto-oncogene protein (c-FMS; CD115/CSF1R/macrophage-colony stimulating (M-CSF) receptor [M-CSFR]), is a receptor tyrosine kinase that binds M-CSF and IL-34; c-FMS is the human analog of the *v-Fms* gene of the feline sarcoma virus-McDonough strain (SM-FeSV) [365, 366]. c-FMS is required for normal development of the mammalian embryo, skeleton, brain, and hematopoietic system. Specifically, c-FMS

is a differentiation marker that is expressed increasingly with differentiation towards the monocyte/macrophage fate [367]. In the AML setting, however, c-FMS^{WT} is overexpressed, especially cases that are *inv(16)*⁺ or of the M5 subtype; moreover, mutations in *CSFR1* drive AML and other myeloid neoplasms [368-370]. Clinically, c-FMS is a target of the multi-kinase inhibitor PLX3397 (pexidartinib [*Turalio*®], Plexxikon/Daiichi Sankyo]).

Mechanistically, as found in an *MLL-AF10*⁺ AML mouse model, PU.1 is co-opted by *MLL-AF10* to induce expression of c-Fms [371]. c-Fms^{hi} *MLL-AF10*⁺ cells were found to possess greater leukemogenicity compared to c-Fms^{lo} counterparts, indicating that the upregulation of c-Fms potentiates AML progression, despite being a marker of differentiation. As c-FMS is expressed on human AML cells and is being investigated as a therapeutic target in R/R *FLT3-ITD*⁺ AML (NCT01349049 [pexidartinib (*Turalio*®)]), we sought to determine whether c-Fms expression is altered by *Tbk1* blockade in our *MLL-AF9*⁺ model [372].

To this end, *Tbk1*^{WT} *MLL-AF9*⁺ and *Tbk1*^{NULL} counterparts (genetic control) were treated for 24 hours with varying dosages of AMX (50-300uM) and GSK8612 (1-4uM), or DMSO as vehicle control, and the amount of c-Fms^{hi} cells was measured as percentage of TNCs; representative gating strategy for FACS analysis is shown (**Figure 42**).

Firstly, it was noticed that deletion of *Tbk1* alone causes a dramatic increase in c-Fms expression on *MLL-AF9*⁺ cells (**Figure 42**). Specifically, in both DMSO-treated groups, it was observed that the c-Fms^{hi} population was significantly larger in the

Tbk1^{NULL} cells compared to *Tbk1*^{WT} cells—this finding is depicted in Figure 43 and quantified in Figure 44A and 44B). Notably, these data indicate that *Tbk1* is a negative regulator of c-Fms expression in *MLL-AF9*⁺ cells.

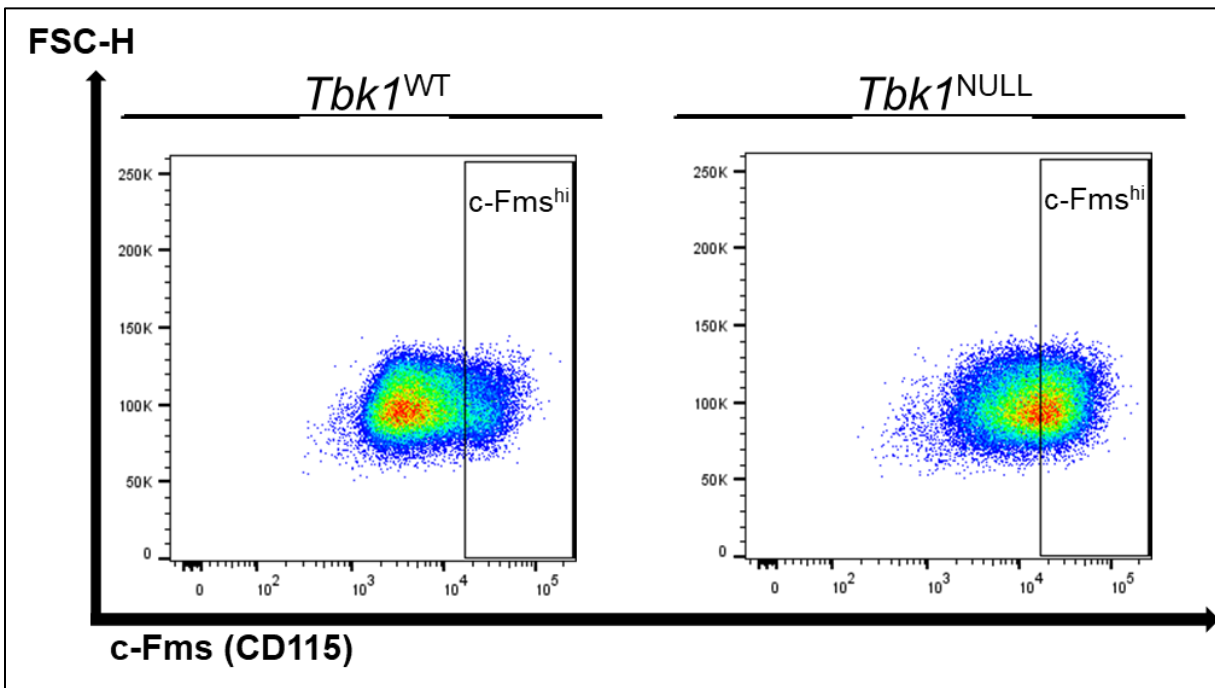


Figure 42. *Tbk1* Negatively Regulates c-Fms Expression on *MLL-AF9*⁺ Cells. To determine if the loss of *Tbk1* affects c-Fms expression, c-Fms expression was compared via FACS between DMSO-treated *Tbk1*^{WT} and *Tbk1*^{NULL} (n = 2, with 3 replicates each). FACS data were analyzed using FSC-H/c-Fms (CD115) gating and a significant right-shift was observed in *Tbk1*^{NULL} cells, indicating increased c-Fms expression.

c-Fms Upregulation Occurs Independently of c-Kit Status on *Tbk1*^{NULL} *MLL-AF9*⁺ HSPCs

It was observed that the loss of *Tbk1* causes increased c-Fms expression on *MLL-AF9*⁺ cells. However, it was not known whether the c-Fms^{hi} population was

comprised mostly of either c-Kit⁺ or c-Kit⁻ cells, or if it contained a relatively equal mixture of both. Thus, we sought to determine the c-Kit profile of the c-Fms^{hi} population.

To this end, the data from **Figure 42** were re-examined, and cells were separated by c-Kit and c-Fms (**Figure 43B**). It was determined that the increased c-Fms expression, while somewhat more apparent in c-Kit⁺ cells, was mostly independent of c-Kit status (**Figure 43A**). Thus, c-Fms appears to be increased on both c-Kit⁺ *MLL-AF9*⁺ cells and c-Kit⁻ counterparts following *Tbk1* deletion.

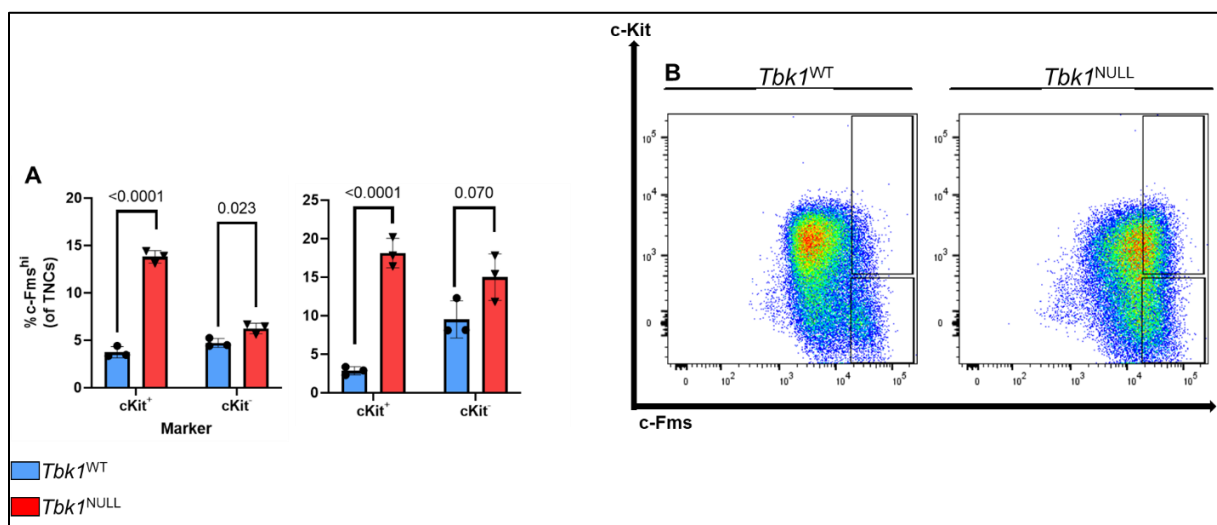


Figure 43. Increased c-Fms Expression Following *Tbk1* Deletion Occurs in Both c-Kit⁺ and c-Kit⁻ *MLL-AF9*⁺ Cells. To determine if the increased c-Fms expression correlated with c-Kit expression, c-Kit/c-Fms gating was used to analyze the FACS data collected from the DMSO-treated cells of the AMX and GSK8612 experiments. Unpaired t-test was used for both statistical analyses (n = 2, with 3 replicates each). (A) Quantification of FACS data, indicating significantly increased expression of c-Fms on c-Kit⁺ cells and a strong trend towards increased c-Fms expression on c-Kit⁻ cells. (B) Representative FACS gating strategies depict increased c-Fms expression in *Tbk1*^{NULL} cells, relatively independent of c-Kit status, though the increase in c-Kit⁻ cells did not reach significance in the second biological replicate.

Tbk1 and IKK ϵ May Act Oppositely in Regulating c-Fms expression on *MLL-AF9*⁺ HSPCs

While deletion of *Tbk1* causes significantly increased expression of c-Fms on *MLL-AF9*⁺ cells, the effect of pharmacologic blockade is not as clear. Interestingly, 24-hour treatment AMX and GSK8612 appears to elicit opposing effects, which suggests that IKK ϵ is involved in regulating c-Fms expression. In fact, Tbk1 and IKK ϵ seem to oppose the function of one another in regulating c-Fms expression: while Tbk1 restricts c-Fms levels, these data suggest IKK ϵ promotes it.

Treatment with AMX has largely no effect on *Tbk1*^{WT} cells, whereas AMX causes a dose-dependent reduction in c-Fms expression in *Tbk1*^{NULL} cells (**Figure 44A**). As AMX inhibits both TBK1 and IKK ϵ , this suggests that IKK ϵ is involved in governing c-Fms expression on *MLL-AF9*⁺ cells.

Treatment with GSK8612 has the opposite effect that AMX does and affects both *Tbk1*^{WT} and *Tbk1*^{NULL} cells (**Figure 44B**). As GSK8612 inhibits only Tbk1, the increase seen in the *Tbk1*^{NULL} group likely represents off-target effects, as only high-dose GSK8612 elicited any change. However, in the *Tbk1*^{WT} *MLL-AF9*⁺ cells, GSK8612 dose-dependently increased the size of the c-Fms^{hi} population, with even low-dose (1 μ M) having an effect ($p = 0.015$).

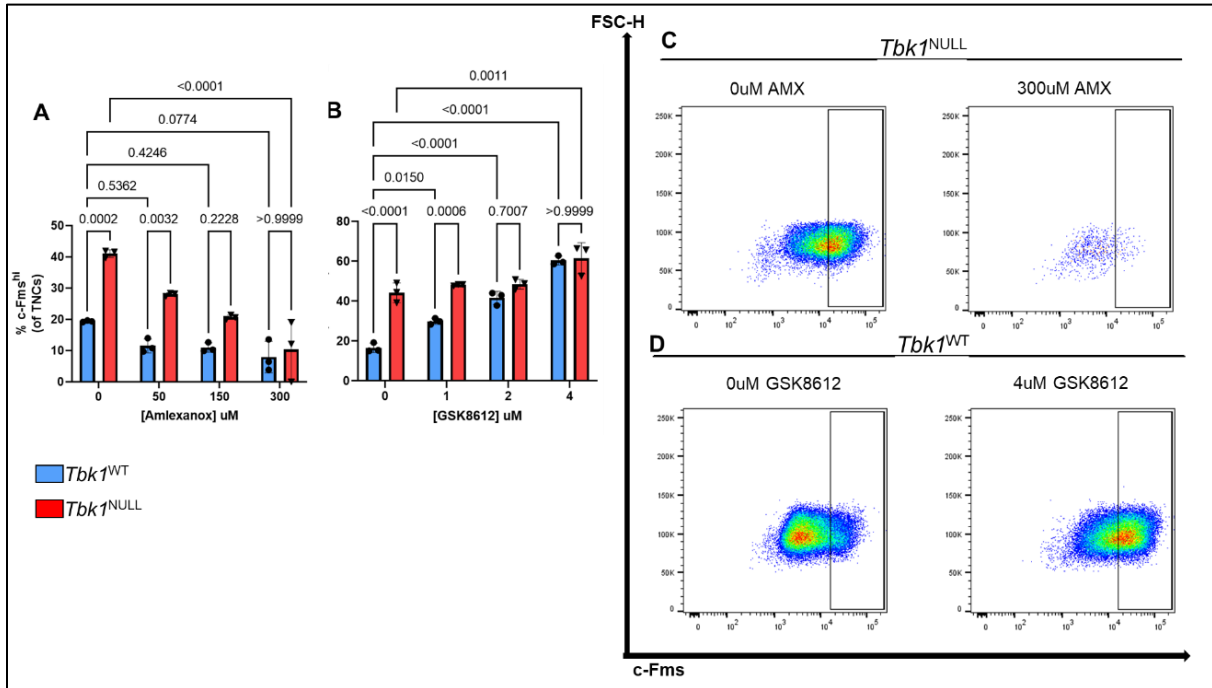


Figure 44. TBK1 and IKK ϵ May Act in Opposition in Regulating c-Fms Expression. To determine if pharmacologic Tbk1 blockade can recapitulate the increased c-Fms expression seen with genetic loss of *Tbk1*, *MLL-AF9*⁺ cells were treated for 24 hours with increasing dosages of either AMX or GSK8612 (n = 1 for each, with 3 replicates each). Following treatment, cells were isolated/washed, and analyzed via FACS. The data were quantified and two-way ANOVA used for statistical analyses (comparing means +/- standard deviation; inter- and intra-group comparisons). Treatment with AMX has an effect only in *Tbk1*^{NULL} cells, where it dose-dependently decreases c-Fms expression, which suggests IKK ϵ involvement; in contrast, GSK8612 causes an effect only in *Tbk1*^{WT} cells, where it dose-dependently increases c-Fms expression (FSC-H/c-Fms used to separate cells). (A) AMX treatment. (B) GSK8612 treatment. (C) AMX-treated *Tbk1*^{NULL} cells, dosages indicated. (D) GSK8612-treated *Tbk1*^{WT} cells, dosages indicated.

GSK8612 Promotes the c-Kit⁺Flt3⁺c-Fms^{hi} Population of *MLL-AF9*⁺ HSPCs

It was determined that *Tbk1* negatively regulates c-Fms expression on *MLL-AF9*⁺ cells; specifically, *Tbk1* strongly regulates c-Fms expression on c-Kit⁺ cells and seems to do so roughly equally in c-Kit⁻ counterparts, although the latter requires further validation (**Figure 43A and 43B**).

In conjunction with the observation that *Tbk1* is required for the maintenance of c-Kit⁺Flt3⁺ *MLL-AF9*⁺ cells, we sought to determine how *Tbk1* regulates the c-Kit⁺Flt3⁺ subset of c-Fms^{hi} *MLL-AF9*⁺ cells. To this end, FACS data from the AMX (**Figure 45A**) and GSK8612 (**Figure 45B**) treatments were analyzed; the size of the c-Kit⁺Flt3⁺c-Fms^{hi} population of *MLL-AF9*⁺ cells determined as percentage of TNCs.

It was learned that the loss of *Tbk1* alone did not significantly affect the size of the c-Kit⁺Flt3⁺c-Fms^{hi} population of *MLL-AF9*⁺ cells. However, treatment of *Tbk1*^{WT} *MLL-AF9*⁺ cells with GSK8612 caused a significant increase in the amount of c-Kit⁺Flt3⁺c-Fms^{hi} cells with all doses of GSK8612 (1-4uM). Whether GSK8612 dose-dependently increases c-Fms expression on c-Kit⁺Flt3⁺ cells is not clear.

These data indicate that 1-4uM GSK8612 causes an undesirable effect in *MLL-AF9*⁺ cells. However, we believe that the increase in the c-Kit⁺Flt3⁺c-Fms^{hi} population is not directly due to *Tbk1* blockade, but rather is a result of the killing of the more abundant Flt3⁻ cells, which are more sensitive to CTx; this enrichment of Flt3⁺ cells was also seen with DNO treatment (**Figure 37**). Doses above 4uM GSK8612 may be required to kill Flt3⁺ *MLL-AF9*⁺ cells.

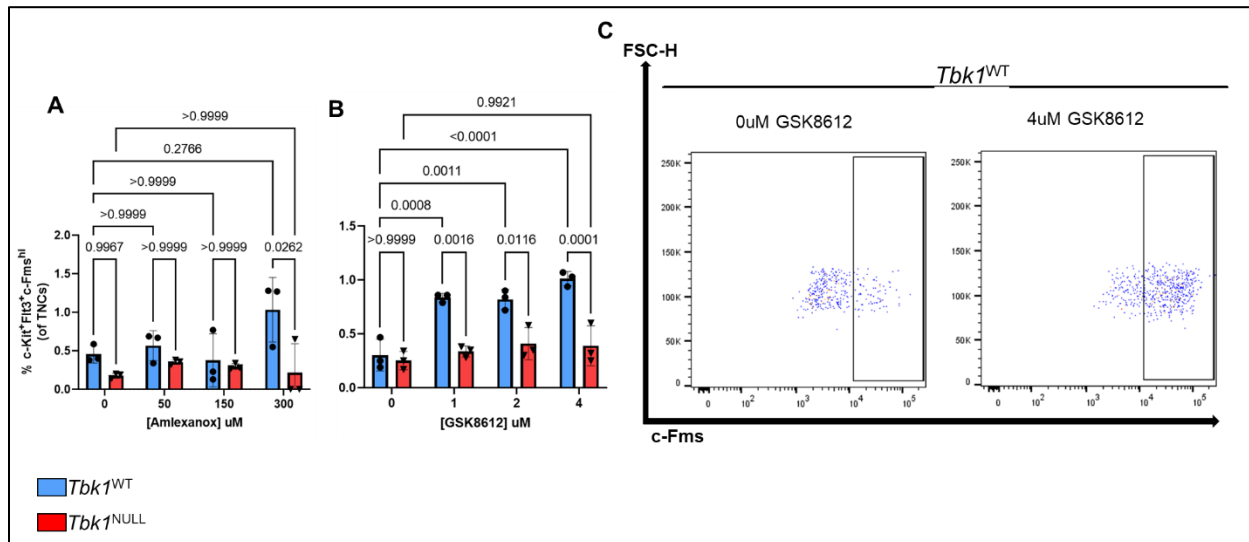


Figure 45. GSK8612 Upregulates the c-Kit⁺Flt3⁺c-Fms^{hi} Population of MLL-AF9⁺ Cells. To determine if pharmacologic *Tbk1* blockade can recapitulate the increased c-Fms expression seen with genetic loss of *Tbk1*, MLL-AF9⁺ cells were treated for 24 hours with increasing dosages of either AMX or GSK8612 (n = 1 of each, with 3 replicates each). Following treatment, cells were isolated/washed, and analyzed via FACS. The data were quantified, and two-way ANOVA used for statistical analyses (comparing means +/- standard deviation; inter- and intra-group comparisons). Treatment with AMX has an effect only in *Tbk1*^{NULL} cells, where it dose-dependently decreases c-Fms expression, which suggests IKKε involvement; in contrast, GSK8612 causes an effect only in *Tbk1*^{WT} cells, where it dose-dependently increases c-Fms expression (FSC-H/c-Fms used to separate cells). (A) AMX treatment. (B) GSK8612 treatment. (C) GSK8612-treated *Tbk1*^{WT} cells, dosages indicated.

Loss of *Tbk1* in Transplanted *MLL-AF9*⁺ HSPCs Causes Chloroma in B6 Mice

Our data suggest that *Tbk1* blockade could be a means of antagonizing *MLL-AF9*⁺ LSCs. We believe that targeting LSCs is required to maintain CR in AML but remains a clinically challenging endeavor. While our data suggest that *Tbk1* blockade would be beneficial in the treatment of AML, the *in vivo* significance of our findings had not been determined.

As the cells of the AML liquid tumor are highly heterogeneous, comprised of LSCs and blast cells, an *in vivo* model that investigated the role of *Tbk1* in both cell types was required (**Figure 46**). To this end, a model was developed where mice would be given *Tbk1*^{fx/fx}; *Rosa26-CreER*^{T2+} *MLL-AF9*⁺ cells and would undergo the tamoxifen regimen at two different timepoints.

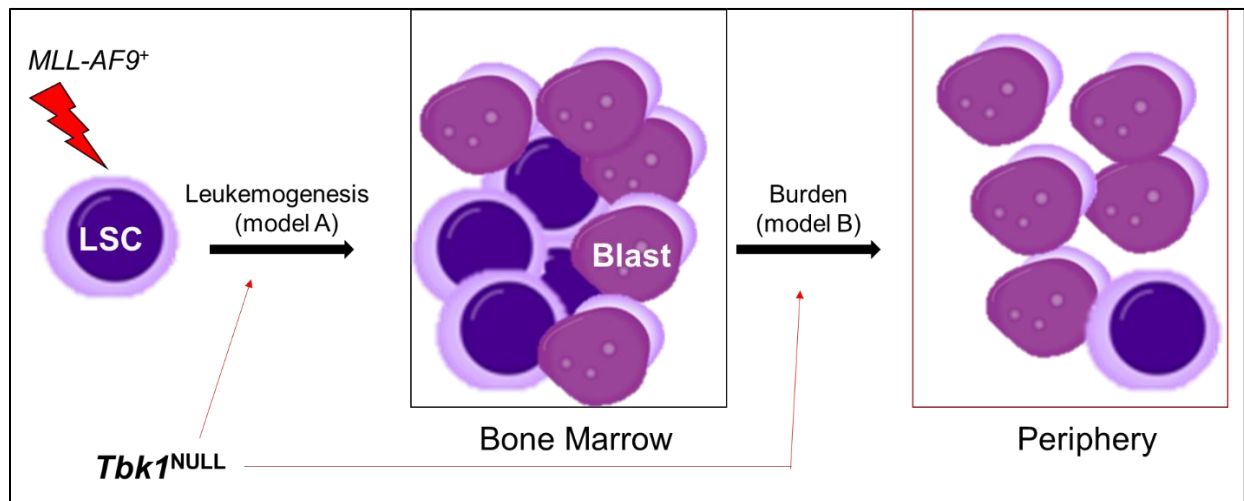


Figure 46. Schematic Depicting Models A and B in the In Vivo AML Study. The AML disease course consists of two, distinct stages: leukemogenesis (model A) and progression/disease burden (model B). To study the role of *Tbk1* in the disease course of AML, *Tbk1* deletion should be done at timepoints relevant to each stage in. Thus, we designed a model where *Tbk1* is deleted at timepoints corresponding to which stage the disease is mostly likely to be in. In model A, *Tbk1* is deleted shortly after transplant of *MLL-AF9*⁺ cells; in model B, *Tbk1* is deleted shortly before anticipated onset of symptoms. *Figures from Wikimedia Commons, reproduced under the GNU Free Documentation License and CC BY-SA 3.0 license.*

As LSCs are responsible for disease initiation (leukemogenesis), *Tbk1* would be deleted in one group of mice shortly after delivery of *MLL-AF9*⁺ cells, just after the transplanted cells were expected to have engrafted (**Figure 47**). At this stage, we believe that most AML cells are LSCs and thus, seek to determine if deletion of *Tbk1* at this stage can delay symptom onset (leukemogenesis model/model A). As blast cells are responsible for symptoms (disease burden), *Tbk1* would be deleted in another group of mice shortly before AML symptoms were expected to develop (**Figure 47**). At this stage, we believe blast cells are most abundant and thus, seek to determine if deletion of *Tbk1* at this stage can extend OS (burden model/model B).

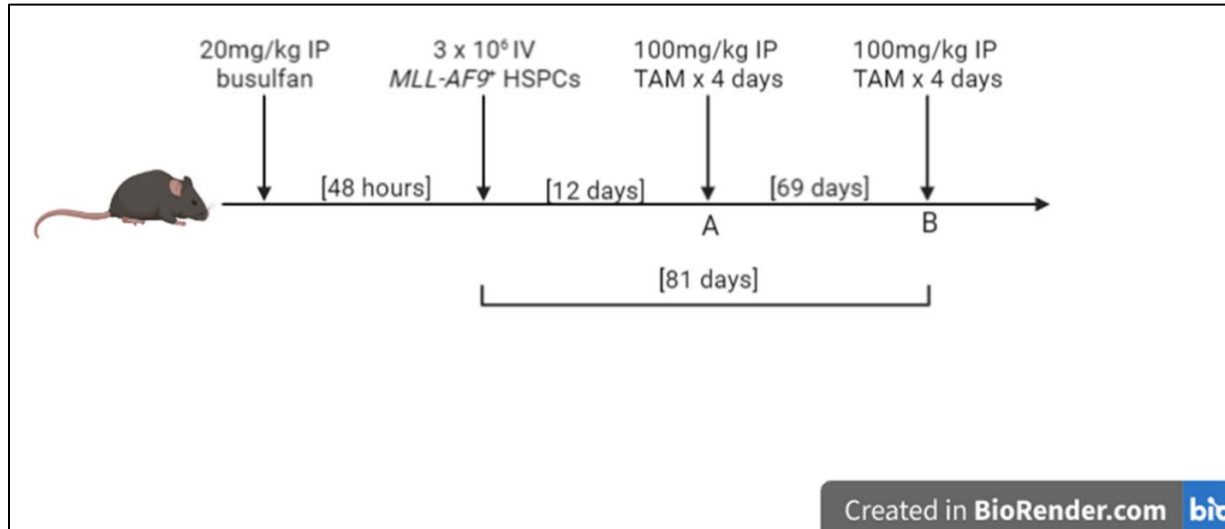


Figure 47. Schematic Depicting Conditioning and Transplant Protocol for our In Vivo Model of MLL-AF9⁺ AML; created with BioRender.com.

To this end, a syngeneic mouse model was used wherein 3.0×10^6 MLL-AF9⁺ cells were delivered to 8-week-old, CD45.2⁺/wild-type male mice that had undergone sublethal, 20mg/kg IP busulfan (*Busulfex*[®]) conditioning 48 hours prior. Four groups of mice were used: 2 groups that received *Tbk1*^{fx/fx};*Rosa26*-CreER^{T2+} cells (n = 8) and 2 groups that received *Tbk1*^{fx/fx} control cells (n = 7). In model A, half of the mice underwent the tamoxifen regimen ~2 weeks post-transplant, shortly after the transplanted cells were expected to have engrafted (n = 4 CreER^{T2+} + 4 control). In model B, the remaining mice (n = 4 CreER^{T2+} + 3 control) underwent the tamoxifen regimen ~80 days post-transplant, when AML symptoms were expected to develop. Unfortunately, 1 CreER^{T2+} and 1 control mouse from model A died from suspected tamoxifen toxicity, and 1 CreER^{T2+} mouse from model A had to be euthanized due to injury.

Nearing 3 months post-transplant, on the same day, 2 of the 3 mice remaining in the control group of model A were found dead. The timing of death and severe ascites found in both mice during necropsy suggested AML, but a lack of splenomegaly in both mice negated a post-mortem diagnosis of AML (tissue morbidity/decomposition precluded FACS, blood smear, and *HemaVet*[®] analyses). *The remaining mouse in the control group of model A displayed no signs of disease and was sacrificed.*

Several days later, it was observed that 1 of the 2 mice remaining in the CreER^{T2+} group of model A (hereafter, referred to as the “*Tbk1*^{NULL}_A mouse”) displayed difficulty moving. Upon further examination, it was revealed that the mouse’s mobility was likely limited due to the presence of a large, cumbersome mass in the pelvic cavity; ulceration through the ventral skin, near/atop the bladder, was evident. The mouse was euthanized, and necropsy revealed a white, encapsulated tumor situated at the ventral aspect of the sacrum. In addition, the spleen was noted to be pale and severely enlarged (splenomegaly), and the BM was also observed to be pale upon flushing. The sacral tumor, BM, spleen, liver, and PB were harvested for FACS analysis and/or H&E staining. Following previous analyses, FACS staining included c-Kit, CD11b, c-Fms, and Flt3. *The remaining mouse in the CreER^{T2+} group of model A displayed no signs of disease and was sacrificed.*

Approximately two weeks later, a mouse in the control group of model B (n = 4; hereafter, referred to as the “*Tbk1*^{WT}_B mouse”) was observed to be lethargic, kyphotic, and hypothermic after several days of the tamoxifen regimen. The mouse was euthanized due to suspected tamoxifen toxicity, but necropsy revealed a pale,

moderately enlarged spleen, so hematopoietic tissues were collected and analyzed to determine if the animal had AML. The BM of the *Tbk1*^{WT_B} mouse was also abnormally pale and, compared to the *Tbk1*^{NULL_A} mouse, the liver was appreciably darker and redder in color. BM, spleen, PB, and liver were harvested for FACS analysis and H&E staining; however, only FSC-A/SSC-A could be assessed from FACS analysis due to technical difficulties (**Figure 48A**). *The remaining 3 mice in the control group of model B displayed no signs of disease and were sacrificed.*

Based on forward scatter-area (FSC-A) and side scatter-area (SSC-A) alone, excessive myeloid infiltration consistent with AML was observed in the BM, spleen, and PB of both mice (**Figure 48A-B**).

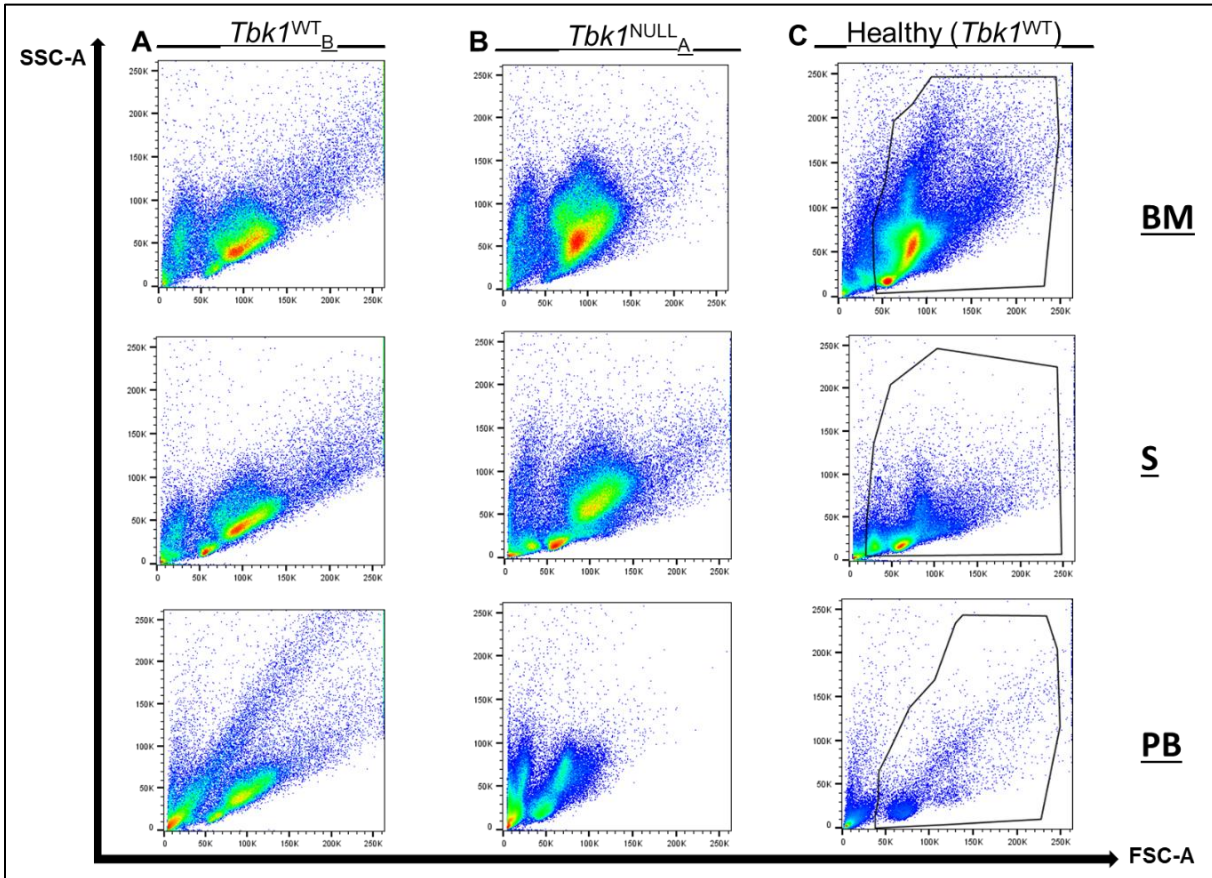


Figure 48. Deletion of *Tbk1* Does Not Prevent *MLL-AF9*⁺ AML. BM, S, and PB were isolated from *Tbk1*^{WT}_B (n = 1) and *Tbk1*^{NULL}_A (n = 1) mice with suspected AML, and tissues from a healthy mouse were used for comparison. Based on SSC-A/FSC-A alone, AML is evident in *Tbk1*^{WT}_B and *Tbk1*^{NULL}_A mice, indicated by excessive myeloid cells in all tissues. (A) *Tbk1*^{WT}_B. (B) *Tbk1*^{NULL}_A. (C) Healthy, *Tbk1*^{WT} mouse.

In the *Tbk1*^{NULL}_A mouse, antibody staining revealed flow cytometry profiles consistent with AML (**Figure 49**). Notably, 0.3% of BM-TNCs were c-Kit⁺Flt3⁺ (LMPP-like cells; red arrow in Figure 49), in sharp contrast to the 3-5% expected in mice with *MLL-AF9*⁺ AML (per Jiwang Zhang, MD/PhD). This finding confirms that *Tbk1* maintains the c-Kit⁺Flt3⁺ population of *MLL-AF9*⁺ AML cells. c-Kit⁺-CD11b^{lo/hi} and c-Kit⁺c-Fms^{-lo/hi} populations were analyzed, but conclusions could not be made given the lack of FACS

data from mice with *Tbk1*^{WT} *MLL-AF9*⁺ AML. Moreover, the biological significance of increased c-Fms expression following *Tbk1* deletion in *MLL-AF9*⁺ cells is not yet known. Notwithstanding, these data are shown to serve as the first-known FACS profiles of *Tbk1*^{NULL} *MLL-AF9*⁺ cells in adult, male B6 mice.

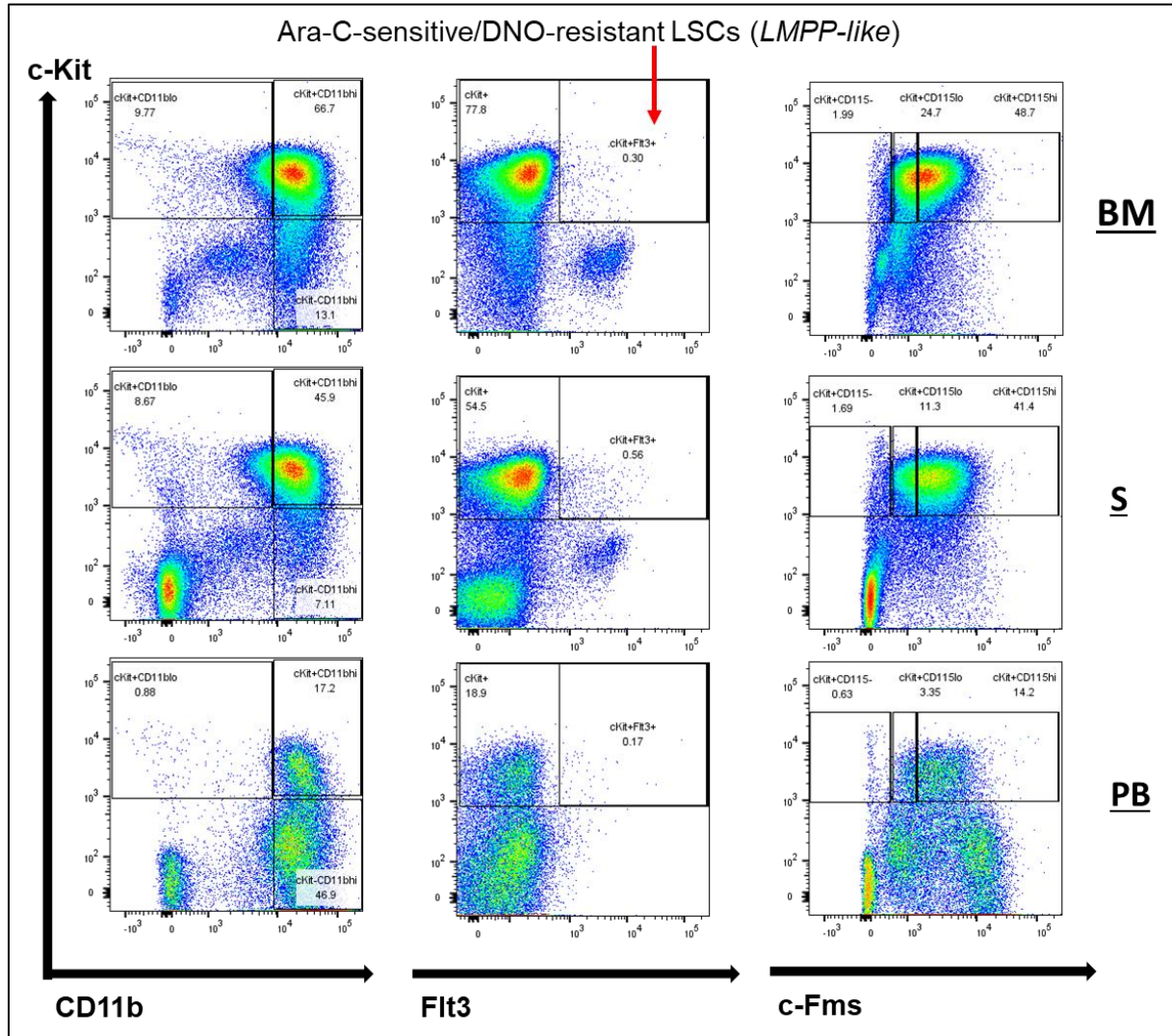
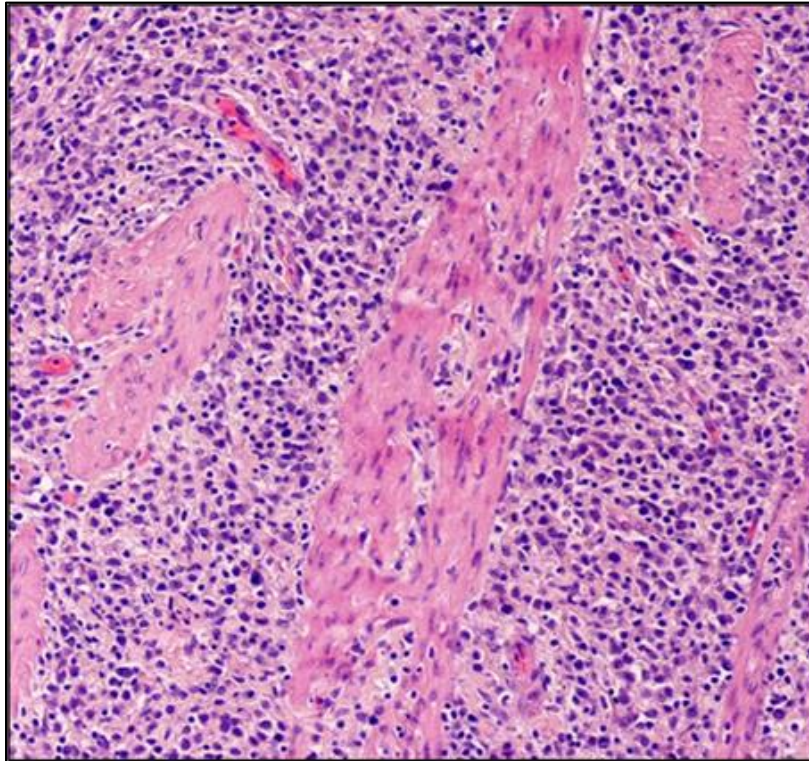


Figure 49. Deletion of *Tbk1* Ablates the c-Kit⁺Flt3⁺ Population of *MLL-AF9*⁺ Cells In Vivo. To determine the immunophenotype of *MLL-AF9*⁺ cells from our *Tbk1*^{NULLA} mouse, tissues were analyzed via FACS and relevant populations (c-Kit⁺Flt3⁺, c-Kit⁺-CD11b^{lo/hi} and c-Kit⁺c-Fms^{-/lo/hi}) were assessed. Notably, the c-Kit⁺Flt3⁺ population in the bone marrow is markedly lower than the 3-5% expected with *MLL-AF9*⁺ AML, supporting our previous *in vitro* finding that *Tbk1* is required for the maintenance of this population of *MLL-AF9*⁺ cells.

H&E staining was performed on the isolated hematopoietic tissues from both mice. Regarding the sacral tumor (Figure 51), histology was deemed consistent with

published reports of IHC-verified chloroma/MS (**Figures 50**) [373]. However, IHC/IF for CD68-KP1 (expressed in nearly all cases of chloroma), MPO, and/or c-Kit would be required to confirm the diagnosis [374]. While rare, chloroma development can occur in AML (specifically in M2/4/5 subtypes) as blasts cells proliferate at extramedullary sites, perhaps homing to neural cell adhesion molecule (NCAM; CD56) [242, 375]. Two case studies have reported *RUNX1-ETO*⁺ pediatric AML patients who displayed sacral chloromas and abdominal chloromas have been reported in children with *MLL1*-rearranged leukemia [376-378].



[Alexiev, et al. Myeloid sarcomas: a histologic, immunohistochemical, and cytogenetic study. *Diagn Pathol.* 2007; 2:42. PMID: 17974004.]

Figure 50. Monocytic Chloroma of the Gallbladder by Alexiev, et al. To support the diagnosis of chloroma in our *Tbk1*^{NULL}_A mouse, an H&E-stained, 100X-magnified section of a CD43⁺CD68⁺ monocytic chloroma of the gallbladder published by Alexiev, et al. is shown for comparison. *OpenAccess article reproduced with permission under BioMed Central Ltd.'s Creative Commons Attribution License.*

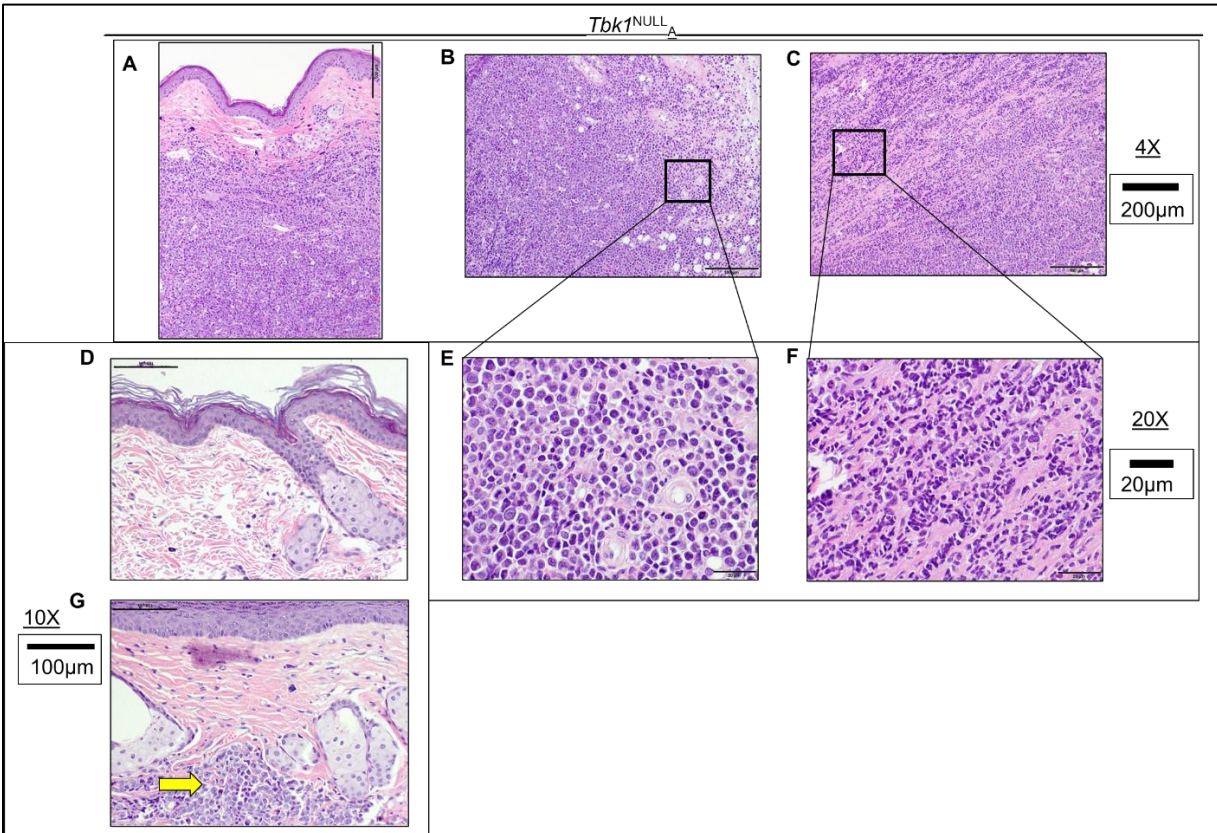


Figure 51. $Tbk1^{NULL_A}$ Mouse Developed a Likely Chloroma, Secondary to MLL-AF9⁺ AML. The sacral/pelvic mass was isolated from our $Tbk1^{NULL_A}$ mouse (n = 1) and fixed in zinc formalin then stored in 70% EtOH. After fixation, the mass was H&E-stained and histologic analysis was performed. While IHC for MPO, c-Kit, and/or CD68 is needed to confirm a diagnosis of chloroma, the H&E staining of our isolated tissue is consistent with published reports of IHC-confirmed (CD43⁺CD68⁺) chloroma (Alexiev, *et al.*). Objective magnification indicated with scale bars. (A) 4X-magnified section showing epidermis (top) with subcutaneous infiltration of AML blasts. (B-C) 4X-magnified sections showing the extent of AML-cell infiltration within the connective tissue of the integument. (D) 10X-magnified section showing normal adjacent epidermis (top)/subcutaneous tissue. (E-F) 20X-magnified sections of Figure B and C, respectively [black squares], further displaying AML-cell infiltration of the integument. (G) 10X-magnified section showing epidermis (top) and subcutaneous infiltration of AML cells, for comparison with Figure D; yellow arrow indicates AML cells.

Further supporting diagnoses of AML, myeloblasts were observed in the PB (**Figure 52**), livers (**Figure 53**), and spleens (**Figure 54**) of both mice. Notably, loss of *Tbk1* did not prevent infiltration of AML cells in the livers and spleens of both mice. While the *Tbk1*^{NULL_A} mouse seemed to display less AML burden in the liver, this may simply reflect a difference in disease progression, unrelated to *Tbk1* deletion. Furthermore, normal spleen and follicular architecture was lost in both mice due to infiltration of AML cells, and while fewer blast cells were visualized in the PB smear from the *Tbk1*^{NULL_A} mouse, *HemaVet*[®] analysis nor quantification were performed to confirm the WBC count.

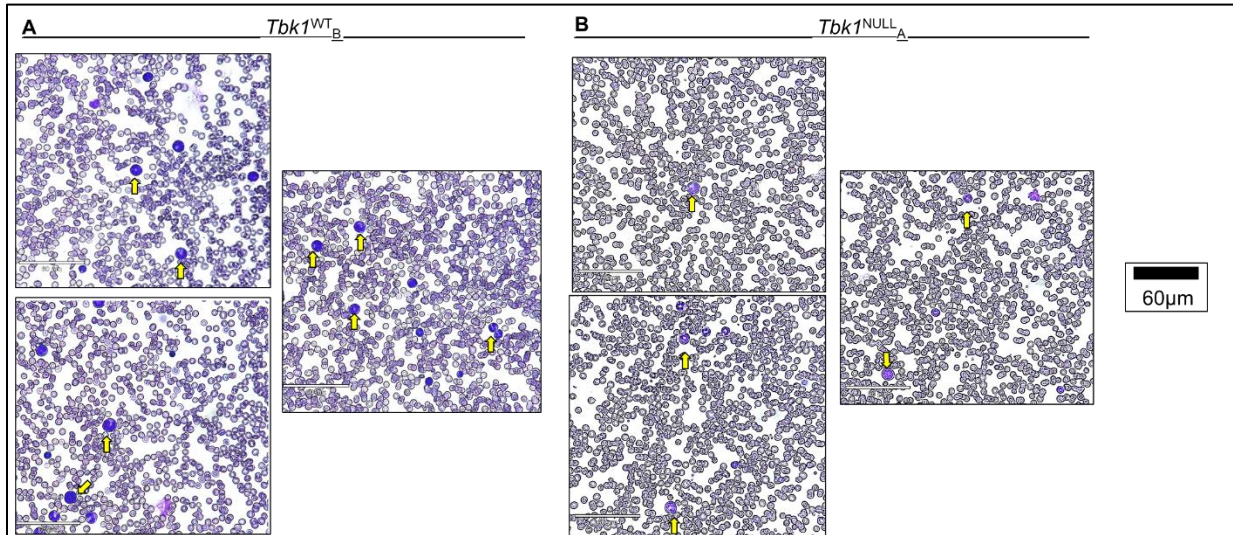


Figure 52. *Tbk1* Deletion in AML Cells May Cause Decreased Blasts in the PB of Mice with MLL-AF9⁺ AML. AML is characterized by the infiltration of malignant blasts in the bloodstream, and PB smear is used clinically to diagnose AML. To confirm the diagnosis of AML and to determine if *Tbk1* deletion caused a change in the frequency of AML blasts in the bloodstream, PB was isolated from mice with suspected AML, methanol-fixed and H&E-stained (*Hema 3*[®] kit, Fisher). Following H&E staining, histologic analysis was performed. *Tbk1* deletion may cause a reduced frequency of MLL-AF9⁺ cells in the bloodstream, though the observations were not quantified. Yellow arrows indicate suspected myeloblasts. (A) *Tbk1*^{WT}_B (n = 1). (B) *Tbk1*^{NULL}_A (n = 1). Objective magnification indicated with scale bars.

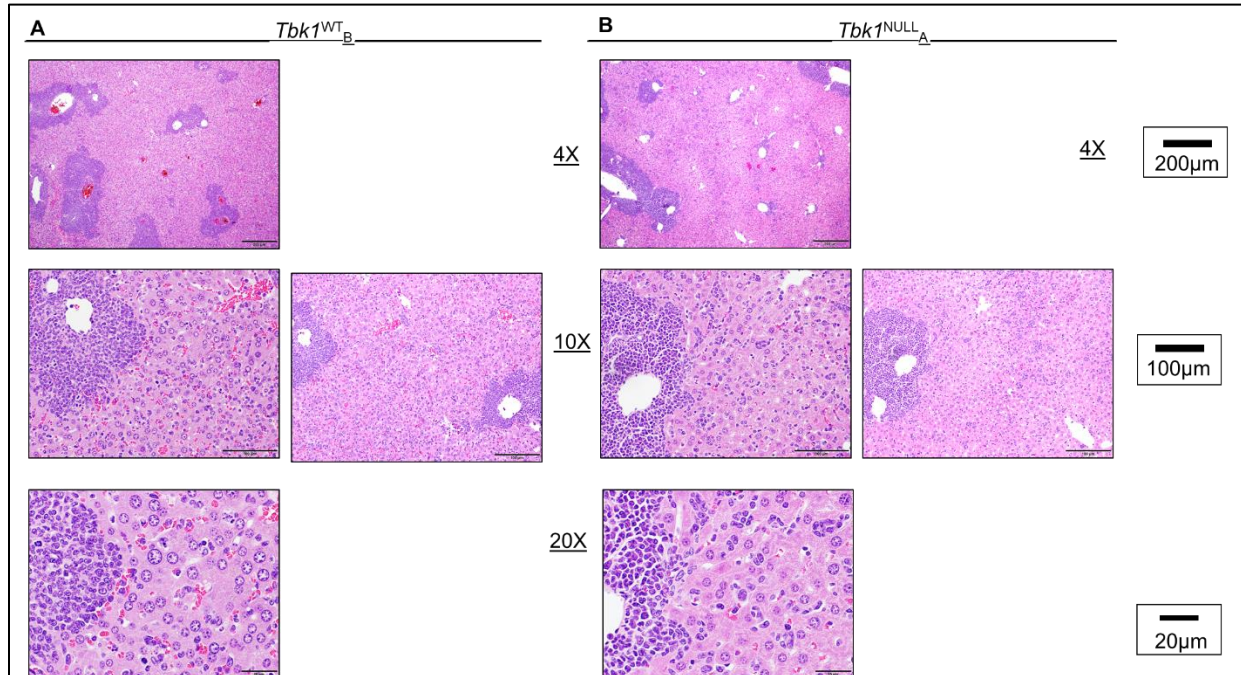


Figure 53. Loss of *Tbk1* Does Not Prevent Hepatic Infiltration by AML Cells. As the liver is commonly infiltrated by AML cells, livers of mice with suspected AML were harvested. Following H&E staining, histologic analysis was performed to determine if *Tbk1* deletion prevents *MLL-AF9*⁺ cells from infiltrating the liver. *Tbk1* deletion does not prevent liver infiltration by *MLL-AF9*⁺ cells. (A) *Tbk1*^{WT}_B (n = 1). (B) *Tbk1*^{NULL}_A (n = 1). Objective magnification indicated with scale bars.

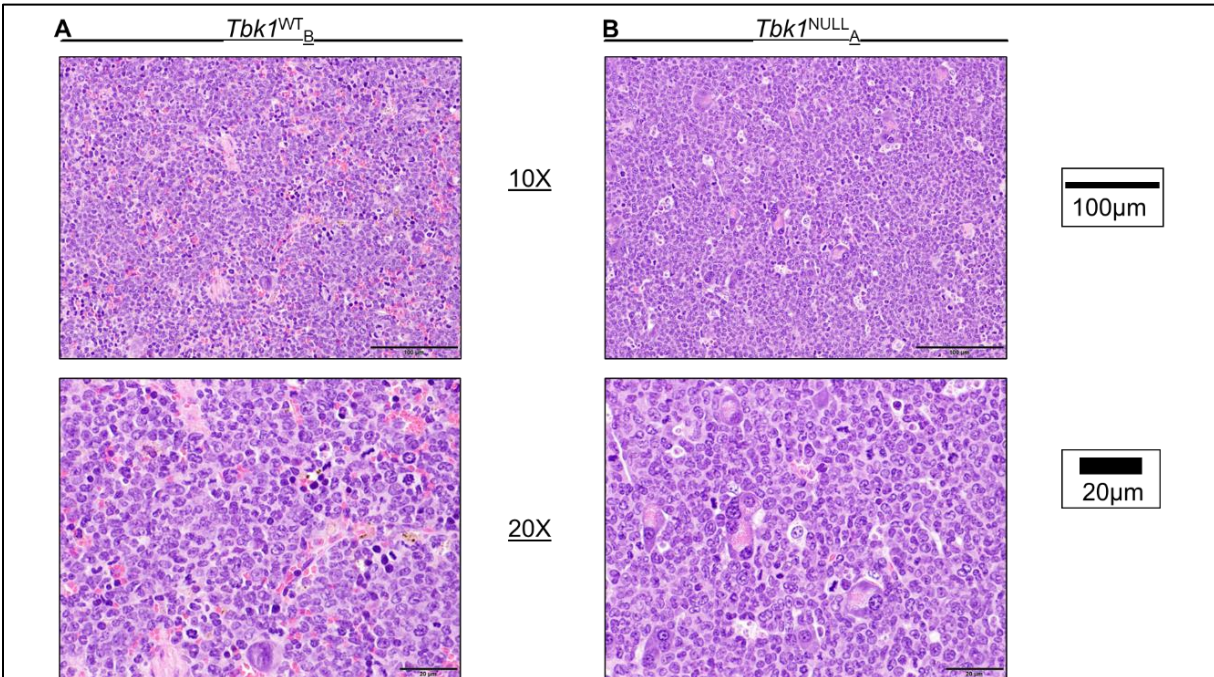


Figure 54. Loss of *Tbk1* Does Not Prevent Splenic Destruction by AML Cells. As the spleen is commonly infiltrated by AML cells, spleens of mice with suspected AML were harvested. Following H&E staining, histologic analysis was performed to determine if *Tbk1* deletion prevents *MLL-AF9*⁺ cells from infiltrating the spleen. *Tbk1* deletion does not prevent splenic/follicular destruction by *MLL-AF9*⁺ cells. (A) *Tbk1*^{WT_B} (n = 1). (B) *Tbk1*^{NULL_A} (n = 1). Objective magnification indicated with scale bars.

Around 100 days-post-transplant (~20 days-post-tamoxifen), 1 of the 2 mice remaining in the *Tbk1*^{NULL} group of model B was found dead, and a cause of death could not be determined due to tissue morbidity/decomposition. Approximately 3 weeks later (~40 days-post-tamoxifen), the remaining mouse in the *Tbk1*^{NULL} group of model B (hereafter, referred to as the “*Tbk1*^{NULL_B} mouse”) began to display slight difficulty moving. Upon further examination, a small, ulcerated lesion—reminiscent of the *Tbk1*^{NULL_A} mouse—was discovered on the ventral aspect of the mouse in the left

inguinal region (**Figure 55**). The $Tbk1^{NULL_B}$ mouse was euthanized, and necropsy revealed a white, encapsulated tumor situated within the pelvic cavity, similar though significantly smaller than the mass previously isolated from the $Tbk1^{NULL_A}$ mouse. In addition, a pale and severely enlarged spleen (splenomegaly) was evident, and the BM was observed to be pale upon flushing. While the isolated lesion is *strongly* suspected to be an $MLL-AF9^+$ chloroma, H&E staining is currently pending and IHC/IF would still be needed to confirm. The sacral tumor, liver, BM, spleen, kidney, liver, and PB were harvested for FACS analysis and/or H&E staining. Following previous analyses, FACS staining included c-Kit, c-Fms, CD11b, and Flt3, though time did not allow for the incorporation of these data in this thesis. Photos of the $Tbk1^{NULL_B}$ mouse (taken by Rohit Thalla, BS) are included and represent the type of lesion also seen in the $Tbk1^{NULL_A}$ mouse (**Figure 55**).



Figure 55. $Tbk1^{NULL_B}$ Mouse Developed a Likely Chloroma, Secondary to $MLL-AF9^+$ AML. Representative image of the ventral aspect of a 9-month-old, 20-30g male mouse that was given 3.0×10^6 $Tbk1^{fx/fx}; Rosa26-CreER^{T2+} MLL-AF9^+$ HSPCs ~120 days prior and underwent tamoxifen regimen ~40 days prior to euthanasia and photographing. Images depicts a lesion identified in the left inguinal region that is representative of a similar but larger lesion observed 1-2 months earlier in the $Tbk1^{NULL_A}$ mouse. The identified lesions are believed to be due to integumentary destruction by infiltrating $Tbk1^{NULL} MLL-AF9^+$ AML cells. Blue square depicts a close-up image of the lesion. Photos taken by Rohit Thalla, BS of our group.

Strikingly, despite severe splenomegaly and actively progressing solid tumors, neither the $Tbk1^{NULL_A}$ nor $Tbk1^{NULL_B}$ mouse displayed the characteristic symptoms of murine AML (e.g., lethargy, kyphosis, and hind-limb immobility), whereas the $Tbk1^{WT_B}$ mouse did. While the significance of these observations is unknown, they may suggest that even though $Tbk1$ deletion does not prevent the development of AML, loss of $Tbk1$ may lessen the disease severity and extend OS, as mice with $MLL-AF9^+$ AML usually deteriorate rapidly, often within days of exhibiting symptoms [379, 380]. Regardless, our *in vivo* study is not sufficiently powered to draw conclusions. Notwithstanding, we observed that the mice given $Tbk1^{NULL} MLL-AF9^+$ cells who showed evidence of AML ($Tbk1^{NULL_A}$ and $Tbk1^{NULL_B}$) did so in the form of extramedullary disease (EMD), specifically as what are likely pelvic/abdominal chloromas; in contrast, the control mouse that developed AML ($Tbk1^{WT_B}$) displayed the characteristic symptoms of murine AML, showed no signs of EMD/chloroma, and was moribund.

One confounding variable is the fact that the *Tbk1*^{NULL_A} and *Tbk1*^{WT_B} mice underwent the tamoxifen regimen several weeks apart, and it is not known if tamoxifen influences the development of EMD in *MLL-AF9*⁺ AML; though, the *Tbk1*^{NULL_B} and *Tbk1*^{WT_B} mice underwent the tamoxifen regimen at the same time, so these mice can be compared appropriately. As such, considering the insufficient sample size of our study, it seems that *Tbk1* deletion in *MLL-AF9*⁺ cells induces the formation of EMD and extends OS in B6 mice, though this interpretation must be met with caution due to our insufficient sample size and these data must be replicated.

Aim 2 Conclusion: *Tbk1* is Required by c-Kit⁺Flt3⁺ *MLL-AF9*⁺ HSPCs and May Prevent Chloroma in *MLL-AF9*⁺ AML

Deletion of *Tbk1* causes a near-total ablation of the c-Kit⁺Flt3⁺ subset of *MLL-AF9*⁺ cells; this is expected to be desirable in terms of eradicating LSCs. However, loss of *Tbk1* simultaneously causes an increase in c-Fms expression on *MLL-AF9*⁺ cells, which may be less desirable in terms of treating AML, though the *in vivo* significance of this finding is unknown. As well, deletion of *Tbk1* in *MLL-AF9*⁺ AML cells appears to cause blasts to extravasate from the PB and form a chloroma at the sacrum. While chloroma-formation is of unknown significance, and only occurred in a single mouse, it could suggest that *Tbk1*^{NULL} *MLL-AF9*⁺ AML cells are more differentiated and consequently more responsive to CTx. While typically responsive to DA or other anthracycline- or Ara-C-based CTx regimens, chloromas are largely of indeterminate prognostic significance [381, 382]. However, chloromas portend a poorer prognosis when detected in patients with *RUNX1-ETO*⁺ AML [383, 384]. Nonetheless, it appears

that deletion of *Tbk1* causes *MLL-AF9*⁺ cells to cause EMD in the form of chloroma, an uncommon presentation of AML, which warrants further investigation.

CHAPTER 5

DISCUSSION

Summary

Our study herein primarily sought to determine whether TBK1 should continue to be pursued as a molecular target for the basis of AML therapy. However, the role of TBK1 in normal hematopoiesis also required elucidation, as a treatment modality should not be pursued if the possible untoward effects have not been explored thoroughly.

In terms of life-sustaining/homeostatic hematopoiesis (*i.e.*, production of WBCs, RBCs, Hb, and Plts) in the adult B6 mouse, *Tbk1* plays little role. This was determined simply by the observation that no *Tbk1*^{NULL} mice died from anything other than what was attributed to tamoxifen toxicity—that is, any *Tbk1*^{NULL} mice that died did so during the tamoxifen regimen or within 1 week of its completion. However, the deletion of *Tbk1* is not without effect on hematopoiesis: it was observed that the global loss of *Tbk1* causes a significant increase in the number of circulating neutrophils and the size of the MPP3 population of HSPCs.

It is unknown whether the increase in the MPP3 population is a true differentiation block, which would be expected to eventually lead to decreased output of mature hematopoietic cells (e.g., WBCs, RBCs/Hb, and platelets) over time; however, overt hematologic abnormalities were not detected in *Tbk1*^{NULL} mice for up to 6 months following deletion, so the altered size of the MPP3 compartment may simply be a benign increase.

Additionally, the loss of *Tbk1* seemed to cause increased mononuclear cell infiltration in the liver, reminiscent of Marchlik, *et al.*'s 129S5 global *Tbk1*^{NULL} model wherein mononuclear and granulomatous infiltrates were seen in various tissues (e.g., lungs, liver, kidney, eyes, spleen, and skin) and increased circulating monocytes were noted [127]. However, in our WBM-intrinsic deletion of *Tbk1*, increased circulating monocytes were noted. Additionally, proliferation of the mesangial cells in the kidney of a *Tbk1*^{NULL} mouse was noted, which could indicate some renal pathology underway. Thus, global deletion of *Tbk1* is not entirely benign regarding its effect on hematopoiesis. However, it must be noted that, at least in the oncologic/AML setting, most treatments are of finite duration. Thus, TBK1 blockade as means of anticancer treatment would likely be transient, so the finding that genetic deletion was tolerable by mice suggests that temporary, pharmacologic blockade of TBK1 would be tolerable in humans. To this notion, hematological adverse events were not observed with oral AMX up to 50mg TID for 10 weeks (NCT01842282) [50].

Future Directions

In terms of experimental design, several optimizations would be made. Firstly, mice would be sex-matched in all studies. While mice were age-matched in comparisons and sex-matched in the WBM deletion of *Tbk1*, mice were not sex-matched in the global *Tbk1*^{NULL} model. It is not known how sex may affect the *Tbk1*^{NULL} phenotype, but it is known that male mice have been observed to display a different LSK/LK cell ratio (unpublished observations, Zhang lab) and male humans have an approximately a 1/3rd-increased lifetime risk of AML. Thus, sex should be controlled for in all studies.

Secondly, while most studies utilizing the Cre-*loxP* system use floxed;Cre⁻ mice as controls, it is my opinion that non-floxed;Cre⁺ mice should also be used, following a recent study by Rossi, *et al* [385]. The authors determined that that 75mg/kg IP tamoxifen on postnatal days 9, 10, and 11 causes myelotoxicity in non-floxed;*Rosa26*-CreER^{T2+} B6 mice. Notably, control mice did not display the severe reaction to tamoxifen seen in *Rosa26*-CreER^{T2+} mice. This suggests that CreER^{T2} may act promiscuously, at least in neonatal mice, recombining gDNA at “cryptic” or “pseudo-*loxP*” sites when no alleles are floxed. Additionally, most groups (including ours) seem to use floxed;*Rosa26*-CreER^{T2-} controls and do not employ non-floxed;*Rosa26*-CreER^{T2+} mice [152, 385]. Thus, it is my opinion that inclusion of non-floxed;*Rosa26*-CreER^{T2+} mice is optimal.

While some of our data herein is of unknown significance, such as the increased c-Fms expression imparted by *Tbk1* deletion and drug treatment, we believe that TBK1 blockade warrants further exploration as a means of anti-AML treatment. Our belief is supported by the data in this thesis, those of Cannova, 2018, and those from a *Map3k7/Tak1*^{NULL} mouse model (unpublished observations, Zhang lab) [32]. In fact, specifically following the observation that *Tbk1* deletion ablates the c-Kit⁺Flt3⁺ population of *MLL-AF9*⁺ cells, it is our recommendation that RNA-seq be performed on *Tbk1*^{WT} *MLL-AF9*⁺ cells and *Tbk1*^{NULL} counterparts to determine what genes are differentially expressed. We hypothesize that *Tbk1*^{NULL} *MLL-AF9*⁺ cells will show decreased expression of AML-associated genes, such as *MEIS1* and *HOXA9*. Mechanistically, we believe that the role TBK1 in regulating mitophagy is of particular interest in targeting the LSC.

In terms of future models, we recommend that GSK8612 be tested for its anti-AML abilities. While it is unlikely GSK8612 alone would suffice as an effective CTx, GSK8612 should still be tested as monotherapy, though we hypothesize it is better suited as an augmentation agent for standard DA. As such, we propose an experimental setup wherein mice with *Tbk1*^{WT} *MLL-AF9*⁺ AML be treated with either [DMSO +/- DA] or [GSK8612 +/- DA], to determine if GSK8612 can (1) act as monotherapy and/or (2) enhance the efficacy of standard DA, ideally allowing for a dose-reduction of DA without sacrificing efficacy. Moreover, given the increased c-Fms expression on *Tbk1*^{NULL} *MLL-AF9*⁺ cells, the anti-AML efficacy of c-Fms blockade warrants investigation. For example, c-Fms^{hi} *MLL-AF9*⁺ cells may be more sensitive to

pexidartinib (*Turalio*[®]); however, the biological significance of increased c-Fms expression in *Tbk1*^{NULL} *MLL-AF9*⁺ cells is not yet known. An experimental setup wherein mice with *Tbk1*^{WT} *MLL-AF9*⁺ AML be treated with ether [DMSO +/- DA] or [pexidartinib + GSK8612 +/- DA] would be informative (GSK8612 is suggested herein to pharmacologically increase c-Fms expression on *Tbk1*^{WT} *MLL-AF9*⁺ cells [**Figure 44B**]).

Secondly, we recommend that an anti-mitochondrial agent be tested in combination with GSK8612 to determine whether this drug combination has greater anti-AML effects than either agent alone; while devimistat (CAC inhibitor) has been proposed, it has been suggested that electron transport chain (ETC) blockade be pursued alternatively if antagonizing mitochondrial metabolism is desired. Additionally, it would also be of interest to determine if GSK8612 displays synergy with revumenib in the *MLL-AF9*⁺ setting.

Thirdly, we recommend that *Tbk1* deletion in *MLL-AF9*⁺ AML be revisited. Specifically, we envision a repeat experiment wherein mice receive either *Tbk1*^{NULL} *MLL-AF9*⁺ cells or *Tbk1*^{WT} *MLL-AF9*⁺ cells. As EMD in the form of chloroma—an uncommon presentation of AML—was seen in a mouse given *Tbk1*^{NULL} *MLL-AF9*⁺ cells, we believe it should be determined whether this was due to *Tbk1* deletion in the AML cells or occurred simply by chance. As the mechanisms that govern chloroma-formation are still somewhat poorly-understood, it would be of interest to know how *Tbk1* restricts this presentation of EMD in *MLL-AF9*⁺ AML [384].

Fourthly, E-selection (CD62E), which harbors sialyl-Lewis^x (sLeX), has been implicated as a contributor to the chemoresistance of AML LSCs [386, 387]. LSCs produce cytokines to induce upregulation of CD62E on vascular endothelia. Engagement between LSCs and endothelial cells via CD62E promotes LSC survival by stimulating the NF- κ B/BCL-2 pathway within LSCs (see uproleselan by *GlycoMimetics, Inc.*) [388, 389].

It is the hope of all those involved in this project that this information will improve understanding of *MLL-AF9*⁺ LSC physiology. Specifically, we hope that our research regarding TBK1 will contribute to making AML treatment more tolerable and more effective, thereby allowing CR to be achieved (and maintained) more readily.

Closing

Using cDNA microarray analysis, our lab has previously determined that patients with MLL-r leukemia express high levels TLR- and TNF-related genes including *TLR2*, *TLR3*, *TLR4*, *CSF1R*, *TNFA*, *IL1B*, and *MYD88* [35, 36, 390]. The increased expression of TLRs, TNF-related receptors, and associated machinery likely leads to increased activation of TBK1, as TBK1 resides downstream of these receptors/pathways [32, 56]. Thus, we expect *MLL-AF9*⁺ cells to display increased *TBK1* activity. Furthermore, it is established that *CDKN1B* (p27^{Kip1}) is a target gene of MLL-r, including MLL-AF9, and is upregulated in AML cells, specifically in c-Kit⁺CD11b^{lo} *MLL-AF9*⁺ cells, as shown by our lab [271, 391, 392]. Mechanistically, p27^{Kip1} is co-opted by MLL-r to maintain quiescence, which confers resistance to chemotherapies like DNO and Ara-C [271]. The loss of *Tbk1* in our mouse model is observed to afflict the cells previously identified by

Zhang, *et al.* to be p27^{Kip1}-quiescent; as such, we suspect *Tbk1* promotes the stability of p27^{Kip1} in these cells, though by a mechanism not yet known.

As TBK1 is a critical regulator of mitophagy, and increased TBK1 activation is hyperactivates mitophagy, we expect *MLL-AF9*⁺ cells to display increased mitophagic flux [100, 102, 393]. As mitophagy is exploited by cancer cells to adopt an aggressive, CTx-resistant phenotype, an upregulation of mitophagy is likely at least partially responsible for the chemoresistance and aggressiveness observed in *MLL-AF9*⁺ AML cells [133, 139-145].

In conclusion, we believe that *MLL-AF9* co-opts the TLR/TNF-TBK1 axis to upregulate mitophagy, allowing *MLL-AF9*⁺ cells to maintain a quiescent, CTx-resistant, c-Kit⁺Flt3⁺ (LMPP-like) phenotype (**Figure 56**), as I found that *Tbk1* is required for the survival of c-Kit⁺Flt3⁺ *MLL-AF9*⁺ AML cells. It has been established that TAK1 restricts apoptosis/necroptosis induced by inflammatory cytokines by simultaneously blocking RIPK1-mediated cell death and promoting NF-κB/JNK-mediated expression of pro-survival genes, such as BCL2—Cannova found that *Tak1* is required for the survival of c-Kit⁺Flt3⁻ (GMP-like) *MLL-AF9*⁺ LSCs [32, 394-397].

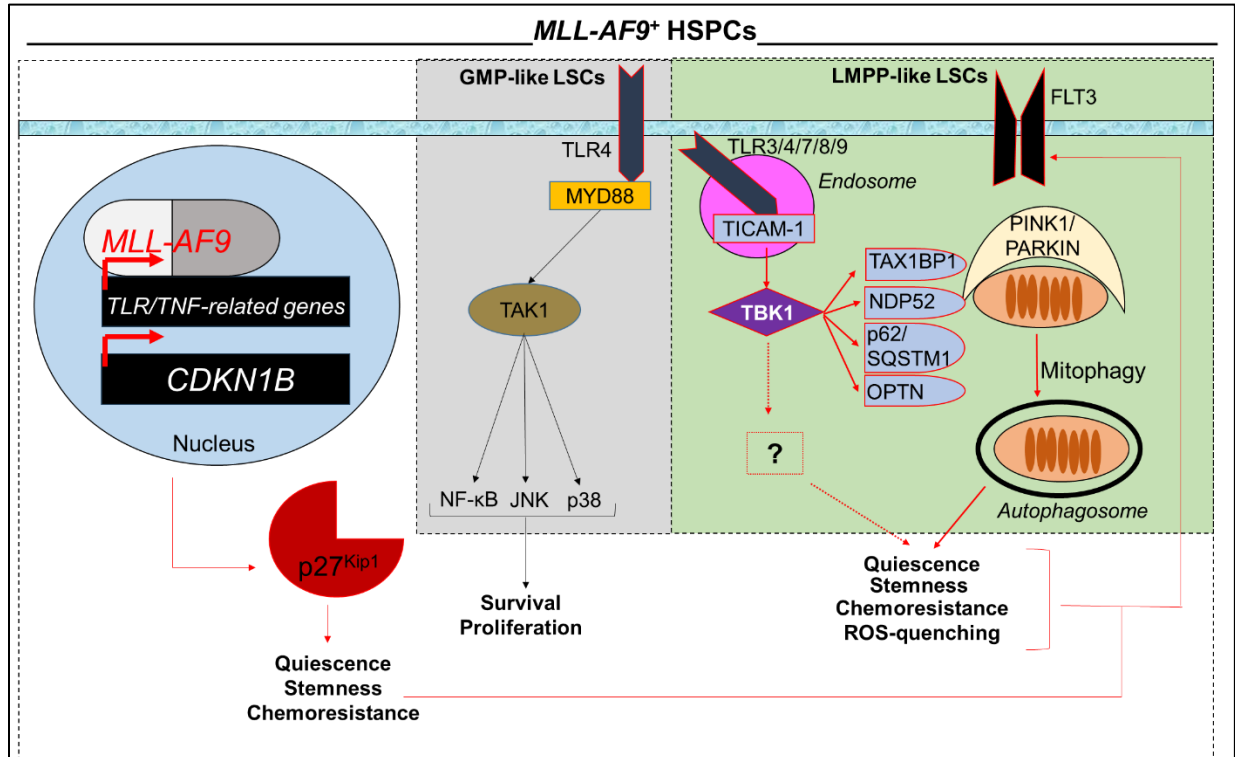


Figure 56. MLL-AF9 Exploits TLR/TNF-TBK1 Signaling to Upregulate Mitophagy. The increased mitophagy allows c-Kit⁺ MLL-AF9⁺ LSCs cells to counter the ROS-inducing effects of chemotherapy and maintain a stem-like/aggressive Flt3⁺ phenotype. Additionally, TBK1 may promote the stability of p27^{Kip1}, which is also upregulated by MLL-AF9. Together, MLL-AF9 co-opts TBK1 to promote mitophagy and maintain p27^{Kip1}-quiescence.

I hypothesize that, due to the upregulated TLR/TNF signaling induced by MLL-AF9, the TBK1-mitophagy axis is upregulated and LMPP-like/c-Kit⁺Flt3⁺ phenotype can be maintained in MLL-AF9⁺ LSCs.

CHAPTER 6

METHODS

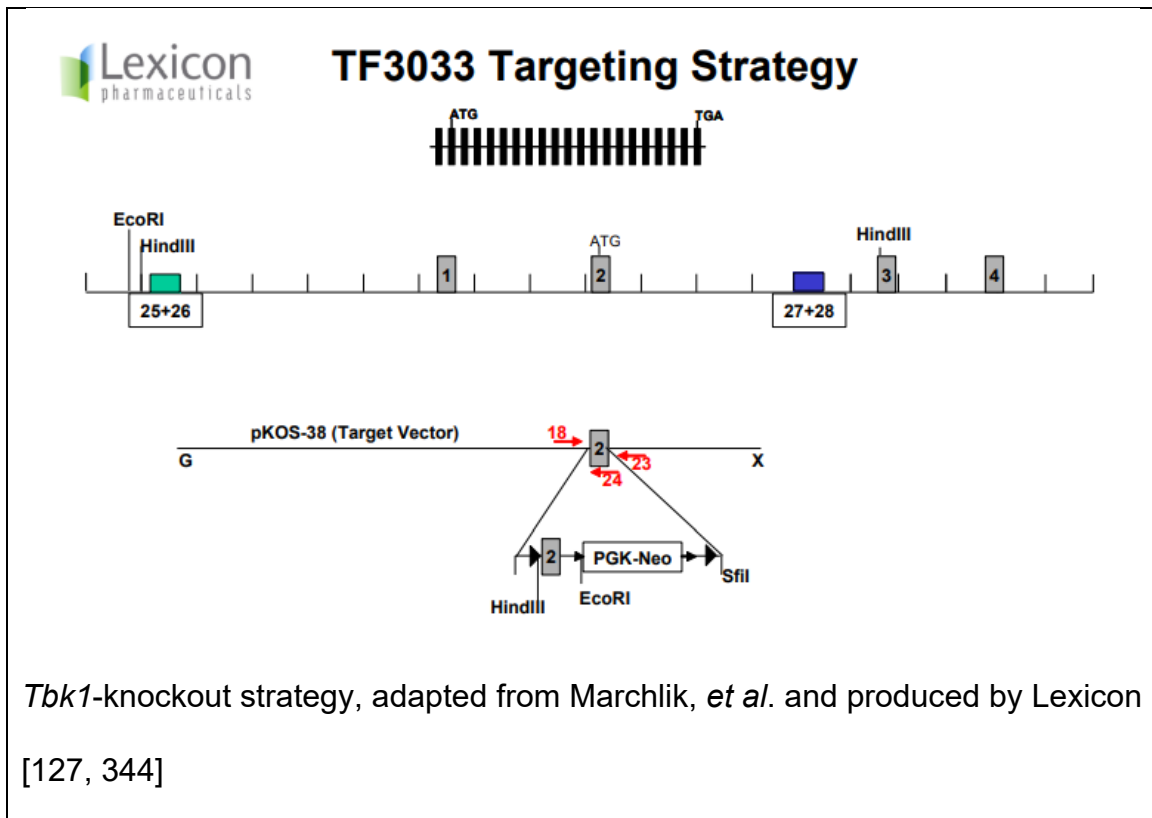
Mice

Mice were housed in accordance with the National Institutes of Health's *Guidelines for the Care and Use of Animals* in the Association for Assessment and Accreditation of Laboratory Animal Care (AAALAC)-certified, specific pathogen-free animal facility in the Cardinal Bernardin Cancer Center at LUMC [398]. Mice were exposed to 12-hour light/dark cycle and housed in microisolator cages/laminar flow system [399]. All procedures were performed in accordance with an Institutional Animal Care and Use Committee (IACUC)-approved protocol from Loyola University Chicago (IACUC protocol: 2020010).

Generation of *Tbk1^{fx/fx};Rosa26-CreER^{T2+}* Mice

All mice were maintained on B6 background. *Tbk1*-knockout strategy involved flanking exon 2 of *Tbk1* with *loxP* sites (indicated previously by Marchlik, *et al.*) [127]. Loss of exon 2 ablates the kinase activity of *Tbk1*, as exon 2 encodes the translation-initiating methionine and a G-Q-G-A-T-A amino acid sequence that coordinates ATP and Mg^{2+} in the kinase domain [127]. *Tbk1^{fx/fx}* mice were purchased from Lexicon

Pharmaceuticals (The Woodlands, TX, USA). *Casp8^{fx/fx};Rosa26-CreERT²⁺* (*Casp8^{NULL}*) mice were previously available to our lab, and as *Rosa26-CreERT²⁺* was desired for this model, *Casp8^{NULL}* mice were crossed with *Tbk1^{fx/fx}* mice until *Tbk1^{fx/fx};Rosa26-CreERT²⁺* progeny were attained; extensive backcrossing was required to eliminate the *Casp8^{fx}* allele. *Rosa26-CreERT²⁺* mice (stock #: 008463) were previously purchased from Jackson Labs (JAX; Bar Harbor, ME, USA) [400]. All genotypes and gene deletion were confirmed via PCR using gDNA. CD45.1⁺ recipient (stock #: 002014) and CD45.2⁺ donor mice (stock #: 000664) used in transplantation studies were also purchased from JAX [401, 402].



In vivo* Deletion of *Tbk1

200mg/mL stock of tamoxifen (B5965, ApexBio) was prepared by mixing tamoxifen in 100% ethanol (EtOH; 2701, Decon Labs). The 200mg/mL tamoxifen stock was then diluted 10-fold with corn oil (901414, MP Biomedicals) to achieve a working solution of 20mg/mL tamoxifen. The solution was vortexed vigorously, wrapped in foil to protect from light, and placed in 37°C, 250RPM-shaking incubator for ~24 hours. After incubation, the solution was kept protected from light and stored in 4°C for up to 6 days. To induce CreER^{T2}-mediated deletion of *Tbk1*, mice were weighed and tamoxifen was delivered intraperitoneally (IP) at a dosage of 100mg/kg for 4 consecutive days [348].

Example dose calculation (extra days and volume included, to account for spillage):

(8 mice · 5 days · 200uL) = 8mL of 20mg/mL tamoxifen working solution required;
 → 8mL / 10 = 0.8mL EtOH · 200mg tamoxifen = 160mg tamoxifen in 800uL EtOH;
 → 8mL – 0.8mL = 7.2mL corn oil added to tamoxifen-EtOH mixture to achieve 10-fold dilution.

Isolation of CD117/c-Kit⁺ Mouse BM Cells (HSPCs)

CD117/c-Kit⁺ mouse BM cells (hematopoietic stem/progenitors [HSPCs]) were isolated from the total BM eluate using *EasySep*TM Mouse CD117 (c-Kit) Positive Selection Kit (18757, STEMCELL Technologies), in accordance with the manufacturer's protocol. HSPCs were isolated and cultured overnight in standard culture conditions with 8-10% 4GFS (see ***Ex Vivo* Culture of Mouse HSPCs**).

Mouse Pre-transplant Conditioning Regimen

CD45.1⁺ recipient mice undergoing competitive *Tbk1*^{NULL} WBMT were lethally conditioned (myeloablation) with 1 dose of 40mg/kg IP busulfan (71288-116-11, Meitheal Pharmaceuticals; 1,4-butanediol dimethanesulfonate/*Busulfex*[®], Otsuka America Pharmaceutical, Inc.) 48 hours before tail-vein delivery of 1.0 x 10⁶ WBM cells in 200uL 1X PBS [403]. NOTE: it is our recommendation 2 doses of 20mg/kg IP busulfan (delivered 24 hours apart) be used instead of a single, 40mg/kg dose—subsequent studies from our lab have suggested that the halved regimen (40mg/kg cumulative) is as effective but better tolerated. CD45.2⁺/wild-type recipient mice undergoing adaptive *MLL-AF9*⁺ HSPC transplant (**Figure 47/In vivo AML Mouse Model**) were sublethally conditioned with 1 dose of 20mg/kg IP busulfan (non-myeloablation) 48 hours before tail-vein delivery of 3.0 x 10⁶ *MLL-AF9*⁺ cells (NO support cells delivered) [404, 405].

Mouse Post-transplant Antibiotic Prophylaxis

Enrofloxacin (E0786, TCI America; *Baytril*[®], Elanco) was added to mouse drinking water to prevent opportunistic infection during count recovery following busulfan conditioning. Every other day, 5mL of 16mg/mL enrofloxacin was added to a full, 450mL water bottle.

16mg/mL Enrofloxacin	Ratio
Enrofloxacin	0.8g
ddH ₂ O	50mL

***In Vivo* AML Mouse Model**

Following non-myeloablative/sublethal conditioning, 3.0×10^6 *MLL-AF9*⁺ HSPCs were delivered in 200uL 1X PBS via tail-vein injection to conditioned, CD45.2⁺/wild-type, 8-week-old male mice. HSPCs were either *Tbk1*^{fx/fx};*Rosa26-CreER*^{T2+} (*Tbk1*^{NULL}) or *Tbk1*^{fx/fx} (control) cells. Tamoxifen was then delivered to half of the *Tbk1*^{NULL} & control mice at ~2 weeks post-transplant (model A/leukemogenesis) and the other half of *Tbk1*^{NULL} & control mice at ~12 weeks post-transplant (model B/progression).

Harvest of Mouse BM

Mice were euthanized with CO₂ and subsequent cervical dislocation. Following euthanasia, femur(s) and tibia(s) were harvested; following harvest of leg bones, marrow was flushed with 1X PBS (10X PBS Buffer pH 7.4; AM9625, Thermo-Fisher) using a 1mL syringe. Marrow clumps were dissociated with 1mL syringe, then marrow was filtered into 50mL conical tube(s) using 40uM filter.

Harvest of Mouse PB

Within 1-3 minutes from cervical dislocation, PB was collected by using a 1mL syringe to pierce the heart at the apex and extract blood. Blood was deposited into lavender collection tube(s) (20.1278.100, Sarstedt). Prior to heart puncture, syringes were washed with 0.5M, pH 8.0 ethylenediamine tetra-acetic acid (EDTA; BP2482, Fisher) to coat the barrel, and 20uL EDTA was added to each lavender tube(s).

Agarose Gel Electrophoresis

Desired amount of agarose (15510-019, Life Technologies) was transferred to a glass flask and 1X TAE buffer swirled in. Mixture was microwaved for 1-3 minutes on high until agarose was fully dissolved. Mixture was allowed to cool for 2 minutes before 3uL of 10mg/mL ethidium bromide (EthBr) was added per 50mL 1X TAE buffer. After mixing in EthBr, gel was poured and allowed to cool for at least 45 minutes before loading samples and running. 4uL GeneRuler DNA Ladder Mix, ready to use (SM0333, Fisher Scientific) was used. 120V for ~1 hour.

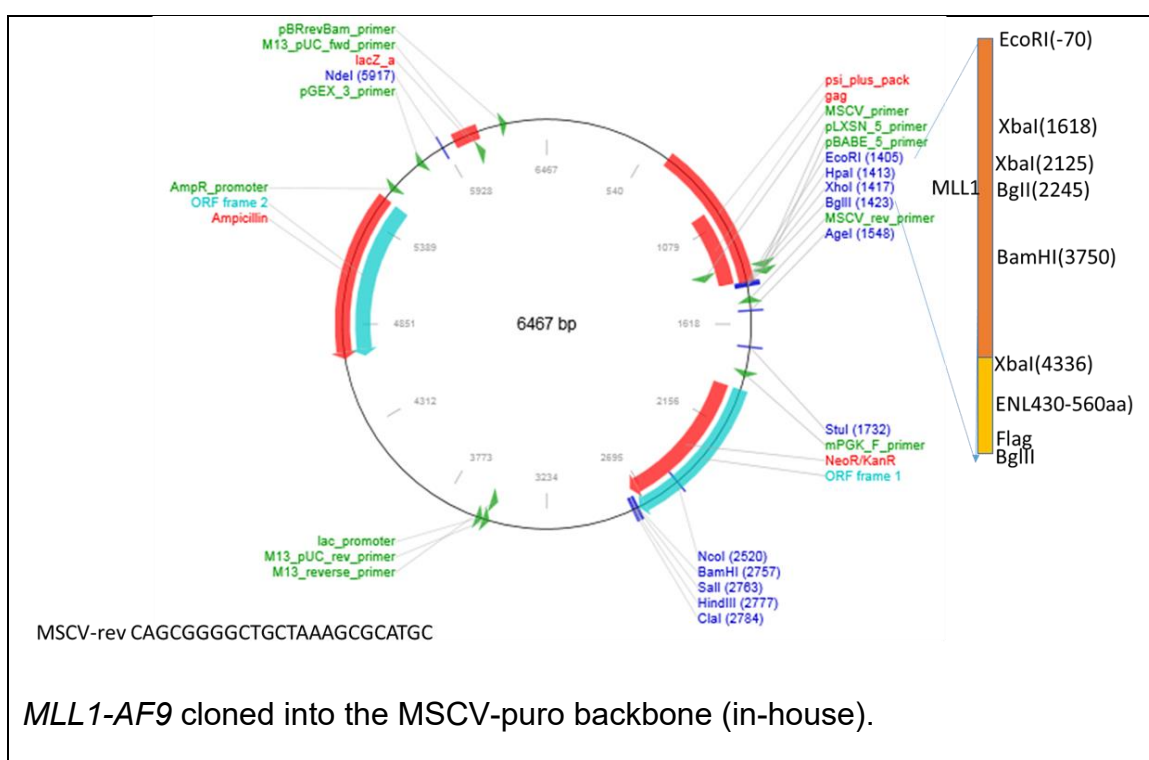
50X TAE Buffer Stock	Ratio
Tris-Base (BP152-1, Fisher)	242g
Glacial Acetic Acid	57.1mL
0.5M, pH 8.0 EDTA (BP2482, Fisher)	100mL
ddH ₂ O	1L

1X TAE buffer working solution was made by diluting 0.3L 50X TAE buffer stock in 14.7L MilliQ ddH₂O.

Bacterial Transformation and Plasmid Isolation

~50uL DH5a chemically-competent E. coli (New England Biolabs) were thawed on ice in a microcentrifuge tube(s). Upon thawing, 2uL of either MSCV-puro-MLL-AF9 (*MLL1-AF9* was cloned into the MSCV-puro backbone [68469, Addgene] in-house) or Gag/Pol plasmid (14887, Addgene) was added to tube(s). The mixture was incubated for 30 minutes on ice, then heat-shocked at 42°C for 30 seconds, then 200uL Miller's

Luria Broth (LB) Agar (MBPE-3060, GrowCells.com) was added to tube(s) and tube(s) transferred to a 37°C 250RPM-shaker for 1 hour. After shaking, 50uL of the mixture was plated on LB-Ampicillin⁺ plates and incubated in 37°C/5%CO₂/100% humidity overnight. The next day, colonies were selected for use with either PureYield™ Plasmid Midiprep System or PureYield™ Plasmid Maxiprep System (A2492/A2392, Promega) in accordance with manufacturer's protocol.



Creation of 293T Transfection Reagent

Opti-MEM™ (31985062, Thermo-Fisher) was added to 5mL polystyrene tube(s) in the biosafety hood. While vortexing, Gag/Pol plasmid was added to tube(s), then DNA-of-interest (e.g., MSCV-puro-MLL-AF9 or MSCV-YFP), and then PEI MAX® (NC1038561, Fisher Scientific) was added. NOTE: addition of reagents should follow in

the order as described. After addition of all reagents, tube(s) capped and allowed to incubated at RT in the hood for 15 minutes.

Reagent	Ratio
DNA-of-Interest	6ug
Gag/Pol	6ug
1ug/uL PEI MAX®	50ug
Opti-MEM™	450uL

293T Transfection and Collection of Retroviral Supernatant

12 hours before transfection, 3.0×10^6 293T cells were plated on a 10cm² tissue culture dish in 8mL DMEM-High Glucose media (SH30022.01, HyClone/GE) with 10% FBS and 1%P/S, then incubated in 37°C/5%CO₂/100% humidity. After incubation, transfection reagent was added dropwise to 293T cells, carefully, down the side of the tissue culture plate, as not to disturb the 293T cells. 293T cells were incubated for 18 hours before DMEM media was exchanged; after media was swapped, cells were incubated for 48 hours before the DMEM media (now harboring the retroviral supernatant) was collected. Retroviral supernatant was aliquoted to cryotube(s), snap-frozen (allowed to sit on dry ice for 30 minutes), then transferred to storage in -80°C.

Retroviral Transduction (Spinduction/Spinoculation) of Mouse HSPCs

1.0×10^5 mouse HSPCs were transferred to 5mL polystyrene tube(s) and centrifuged at 1800RPM for 5 minutes. Supernatant was discarded and replaced with 3mL of 293T-produced retroviral supernatant (e.g., *MSCV-puro-MLL-AF9*). 4uL of

4ug/uL polybrene (TR-1003, Sigma) was then added. The mixture was vortexed vigorously before being allowed to incubate in the biosafety hood at RT for 10 minutes. After incubation, mixture was centrifuged at 32°C at 2200RPM for 4 hours. After centrifugation, supernatant was discarded and cells were resuspended in usual culture conditions at 37°C/5%CO₂/100% humidity. Puromycin selection was initiated 48 hours later (allowing for transcription/translation of *pac*), wherein 1mg/mL puromycin (ant-pr-1, Invivogen) was added to the cells for a final concentration of 1X. The same protocol was used for transduction with *MSCV-YFP*; although, selection of YFP⁺ HSPCs was performed 48 hours later via FACS (FACSAria III, BD Biosciences).

***Ex Vivo* Culture of Mouse HSPCs**

Following c-Kit⁺ selection and *MSCV-puro-MLL-AF9* transduction, mouse HSPCs were cultured in RPMI-1640 with L-glutamine (SH30027.01, Cytiva) with 10% FBS and 1% Penicillin-Streptomycin (30-002-CI, Corning). Our proprietary mixture of IL-3, IL-6, SCF, and GM-CSF (4GFS; generated in-house) was added for a final concentration of 3-10% of the total media volume, based on experimental requirements; for simply maintaining cultures, 3.75% was determined empirically to be appropriate. Cells were incubated at 37°C/5%CO₂/100% humidity. Copper(II) sulfate pentahydrate (C8027, Sigma-Aldrich) was added to incubator water for a final concentration of 3% (60g in 2L of ddH₂O). Cell cultures were maintained in 3mL RPMI-1640/3.75% 4GFS in one well of a 6-well plate; *in vitro* FACS/growth curve analyses were conducted using 2mL RPMI-1640/3.75% 4GFS in one well of a 12-well plate.

In Vitro* Knockout of *Tbk1

1mg/mL 4-hydroxytamoxifen (4-OHT [afimoxifene]; H7904, Sigma-Aldrich) was added to healthy, media-replete cultures of both *Tbk1^{fx/fx};Rosa26-CreER^{T2+} MLL-AF9⁺* and *Tbk1^{fx/fx} MLL-AF9⁺* (control) mouse HSPCs for a final concentration of 1uM. Cells were incubated at 37°C/5%CO₂/100% humidity for 48 hours. Cells were then isolated and centrifuged at 1800RPM for 5 minutes; after pelleting, media was discarded and cells were resuspended in fresh RPMI-1640/8% 4GFS and re-plated. 1mg/mL 4-OHT was then re-added for a final concentration of 1uM. Cells were incubated for an additional 48 hours before being transferred to fresh RPMI-1640/3.75% 4GFS. PCR-genotyping and downstream analyses were performed 48 hours later.

Growth Curve Analysis

Adapted from Fisher Scientific/Mather, *et al.* [406]. 5.0×10^4 *MLL-AF9⁺* mouse HSPCs were plated in 2.175mL (2.1mL RPMI-1640/3.75% 4GFS) on a 12-well plate. Cells incubated at 37°C/5%CO₂/100% humidity and counted via trypan blue-exclusion every 24 hours. At 48 and 72 hours post-seeding, cultures were homogenized and 1.5mL was removed from each well, then 1.5mL RPMI-1640/3.75% 4GFS re-added (to prevent overgrowth/media exhaustion). The same volume of media was removed from each well, which would ensure that any difference in cell numbers was maintained between *Tbk1^{WT}* and *Tbk1^{NULL}* cells.

Serum Starvation

Tbk1^{NULL} YFP⁺ MLL-AF9⁺ and *Tbk1^{fx/fx} (YFP⁻) MLL-AF9⁺* cells were isolated from bulk cultures and mixed in ~1/1 ratio; subsequent FACS analysis revealed mixture was

closer to ~70% YFP⁺ (*Tbk1*^{NULL}). 6.0×10^4 cells from the mixture were seeded in 3mL RPMI-1640 (with or without 10% FBS)/5% 4GFS on a 6-well plate (3 replicates) and incubated at 37°C/5%CO₂/100% humidity. 24 hours later, YFP-positivity was checked via FACS.

Clonogenicity Assay

3.0×10^4 *MLL-AF9*⁺ mouse HSPCs were isolated from bulk culture and plated (3 replicates, $\sim 1 \times 10^4$ cells per well) in MethoCult™ GF M3434 (03434, STEMCELL Technologies) in accordance with manufacturer's protocol. Cells were incubated at 37°C/5%CO₂/100% humidity for 6-7 days, depending on experimental requirements.

70% EtOH Fixation and Cell Cycle Analysis

Protocol provided by Bert Ladd. 1.0×10^6 cultured *MLL-AF9*⁺ mouse HSPCs were transferred to 15mL conical tube(s) and pelleted via centrifugation at 1800RPM for 5 minutes. Media was discarded and 1mL of 70% EtOH was added dropwise while vortexing gently; the EtOH-fixed cells were then stored at -20°C for 7 days. On the day of analysis, a mastermix of 1X PBS, 100ug/mL propidium iodide (PI; P1304MP, Invitrogen), and 100ug/mL RNase A (EN0531, ThermoFisher), and was created. EtOH-fixed cells were then re-pelleted via centrifugation at 2500RPM for 5 minutes and EtOH was discarded. 1×10^6 cells were resuspended in 1mL mastermix, vortexed vigorously, then aliquotted to 5mL polystyrene tube(s). Samples were incubated at 4°C for 30-60 minutes before FACS analysis.

Polymerase Chain Reaction (PCR)

PCR was used to determine the *Tbk1*, *Casp8*, and *Rosa26-CreER^{T2}* status of mice and cultured cells. Reactions employed 10mM dNTP Mix (18427013, Life Technologies) and reagents from Promega: 5X Green GoTaq[®] Flexi Buffer (M891A), GoTaq[®] Flexi DNA Polymerase (M829B), 25mM MgCl₂ (A351H).

To assess *loxP* sites, PCRs were setup using the following parameters:

<i>Tbk1/Casp8</i> (<i>loxP</i> assessment)	Ratio
ddH ₂ O	13.075
5X Green GoTaq [®] Flexi Buffer	5
25mM MgCl ₂	2.6
10mM dNTP	0.2
10uM 5' Primer (J1091/J0875)	1
10uM 3' Primer (J1092/0876)	1
GoTaq [®] Flexi DNA Polymerase	0.125
Template DNA	2

To assess CreER^{T2}-mediated deletion of *Tbk1*, PCRs were setup using the following parameters:

<i>Tbk1</i> (post-tamoxifen/4-OHT)	Ratio
ddH ₂ O	13.075
5X Green GoTaq [®] Flexi Buffer	5
25mM MgCl ₂	2.6

10mM dNTP	0.2
10uM 5' Primer (J1091)	1
10uM 3' Primer (J1092)	0.5
10uM 3' Primer (J1093)	0.5
GoTaq® Flexi DNA Polymerase	0.125
Template DNA	2

To determine *Rosa26-CreER^{T2}* status, PCR reactions were setup using the following parameters:

<i>Rosa26-CreER^{T2}</i>	Ratio
ddH ₂ O	14.075
5X Green GoTaq® Flexi Buffer	5
25mM MgCl ₂	2.6
10mM dNTP	0.2
10uM 5' Primer (J0807)	0.5
10uM 3' Primer (J0808)	0.5
10uM 5' Control Primer (J0001)	0.2
10uM 3' Control Primer (J0002)	0.2
GoTaq® Flexi DNA Polymerase	0.125
Template DNA	2

Primers ordered from Integrated DNA Technologies (IDT).

<i>Tbk1</i> (sequences indicated by Lexicon Pharmaceuticals and purchased from IDT)		
Lexicon # (IDT ID)	Sequence	Band Size
#18 (J1091)	5'-GCCAGATATCCCTGTAACCTCACC-3'	332bp (<i>Tbk1</i> ^{WT})
#24 (J1092)	5'-CAGATGGTTGGAGGTGCTCTGCAT-3'	419bp (<i>Tbk1</i> ^{fx})
#23 (J1093)	5'-CCTACAGCTGCAGACGGCCTCGTAC-3'	775bp (<i>Tbk1</i> ^{PGK-Neo}); 323bp (<i>Tbk1</i> ^{NULL})

<i>Rosa26-CreER</i>^{T2}		
IDT ID	Sequence	Band Size
J0807	5'-CGGAGATCATGCAAGCTGGT-3'	~600bp (<i>Rosa26-CreER</i> ^{T2+})
J0808	5'-TCTCCACCATGCCCTCTACA-3'	~600bp (<i>Rosa26-CreER</i> ^{T2+})

<i>Il2</i> (reaction control for use with <i>Rosa26-CreER</i> ^{T2} PCR-genotyping [murine interleukin 2])		
IDT Name	Sequence	Band Size
J0001	5'-CTAGGCCACAGAATTGAAAGATCT-3'	324bp (<i>Il2</i> ^{WT})
J0002	5'-GTAGGTGGAAATTCTAGCATCATCC-3'	324bp (<i>Il2</i> ^{WT})

Mouse Tcrb rearrangement (Provided <i>graciously</i> by Dr. Thorsten Feyerabend & Dr. Hans-Reimer Rodewald [407, 408])		
IDT Name [nickname]	Sequence	Band Size
J1112 [Dβ1:Jβ1-F]	5'-GGGGTAGACCTATGGGAGGG-3'	[408]
J1113 [Dβ1:Jβ1-R]	5'-CCAAGACCATGGTCATCCAAC-3'	
J1114 [Dβ2:Jβ2-F]	5'-GTAGGCACCTGTGGGGAAGAAACT-3'	[407]
J1115 [Dβ2:Jβ2.7-R]	5'-TGAGAGCTGTCTCCTACTATCGATT-3'	

PCR-genotyping thermocycle:

PCR Thermocycle		
94°C	5 minutes	
94°C	30 seconds	10 cycles
65°C	45 seconds	
72°C	30 seconds	
94°C	30 seconds	
60°C	45 seconds	30 cycles
72°C	30 seconds	
72°C	5 minutes	
4°C	Hold	

RNA Isolation

Isolated cells were pelleted in microcentrifuge tube(s) via centrifugation at 1800RPM for 5 minutes and resuspended in 1mL TRIzol™ (15596026, Invitrogen). Tube(s) centrifuged at 1800RPM for 5 minutes and the supernatant was transferred to separate microcentrifuge tube(s). 20uL of 5M acetic acid was added to the supernatant, then mixture was inverted, vortexed, and allowed to rest, undisturbed, at RT for 5 minutes. 100uL of 1-bromo-3-chloropropane (B9673, Sigma) was then added and mixture was vortexed again, vigorously, for 15 seconds before being allowed to rest at RT again for an additional 5 minutes. Mixture was then centrifuged in at 4°C at 13,000RPM for 15 minutes. After centrifugation, the aqueous phase was carefully extracted, with care taken not to agitate the organic phase. The extracted solution was transferred to separate microcentrifuge tube(s), then 500uL isopropanol (A451-4, Fisher) was added. Mixture was vortexed vigorously, then 1uL glycogen (G1767-1VL, Sigma-Aldrich) was added and mixture was transferred to -20°C for ~18 hours. Mixture was then allowed to warm at RT for 10 minutes before centrifugation at 13,000RPM for 10 minutes. Supernatant was discarded, then 250uL diethyl pyrocarbonate (DEPC)-treated water was added followed by 750uL ice-cold 100% EtOH (75% EtOH final concentration). Mixture was vortexed before being centrifuged again at 13,000RPM for 5 minutes. Supernatant was discarded and pelleted RNA was allowed to air-dry at RT for 5 minutes. 30uL DEPC-treated ddH₂O was added and tube(s) incubated in 65°C-dry bath for 30 minutes before being transferred to -80°C.

DNase I Treatment and Reverse Transcriptase PCR (RT-PCR)

High-Capacity cDNA Reverse Transcription Kit (4368814, Applied Biosystems)

was used for cDNA synthesis from isolated RNA.

DNase I mastermix was setup:

DNase I Treatment	Ratio
RNA	2ug
10X DNase I Buffer	1uL
DNase I (1U/uL)	1uL
DEPC-treated ddH ₂ O	[Bring volume to 10uL]

DNase I thermocycle:

DNase I Thermocycle	
37°C	30 minutes
Add 1uL 50mM EDTA	-
65°C	10 minutes
4°C	Hold

Following DNase I treatment, RT-PCR mastermix was setup:

RT-PCR Mixture	Ratio
RNA	2 ug [up to 10uL]
10X RT Buffer	2uL
dNTP	0.8uL

10X RT Random Primers	2uL
Reverse Transcriptase	1uL
ddH ₂ O	[Bring volume to 20uL]

RT-PCR thermocycle:

RT-PCR Thermocycle	
25°C	10 minutes
37°C	120 minutes
85°C	8 seconds
4°C	Hold

Quantitative PCR (qPCR)

qPCR reactions were setup using the following parameters:

qPCR Mixture	Ratio	Example: x7 samples
cDNA (WT ^{c-Kit+} or <i>MLL-AF9</i> ⁺)	4uL	28uL
2X Buffer	14uL	98uL
Control Gene probe (<i>ActB</i> [VIC]; Mm.PT.39a.22214843.g, Integrated DNA Technologies)	1uL	7uL
Gene-of-Interest probe (<i>Tbk1</i> [FAM]; Mm00451150_m1, Thermo-Fisher)	1uL	7uL
Reaction Volume	20uL	-

qPCR Thermocycle		
95°C	3 minutes	Hold
95°C	5 seconds	40 cycles
60°C	30 seconds	
4°C	Hold	

TaqMan[®] reagents and comparative C_T ($\Delta\Delta C_T$) method used for multiplex qPCR. *QuantStudio*[™] *Real-Time PCR Software* (Applied Biosystems) and *Microsoft Excel*[®] (Microsoft) were used to perform $2^{-\Delta\Delta C_T}$ data analysis.

NOTE: to use qPCR to check for *Tbk1* deletion in our mouse model, a *TaqMan*[®] probe that encompasses exon 2 is required. As probe Mm00451150_m1 includes exons 3-5, it is not suitable for assessment of *Tbk1* exon 2 excision, and thus may yield a false negative result when attempting to confirm *Tbk1* deletion.

Isolation of gDNA from Mouse Tails

At 2-3 weeks of age, ~3mm of the distal tail was biopsied from desired mice and kept in microcentrifuge tube(s). NOTE: the ossification of tail vertebrae necessitates anesthesia for tail biopsies performed on mice greater than 3 weeks of age [409]. 500uL of 1X tail lysis buffer and 7uL of 20mg/mL proteinase K were added to tube(s) and tube(s) vortexed vigorously, then placed in 65°C water bath for ~18 hours. Tube(s) vortexed vigorously for at least 10 seconds and tail digestion was assessed; if incomplete digestion, an additional 3uL of 20mg/mL proteinase K was added and

tube(s) returned to 65°C water bath for an additional ~3 hours. Once tail digestion was confirmed, tube(s) centrifuged at 13,000RPM for 10 minutes and the supernatant was collected, then transferred to fresh microcentrifuge tube(s). 500uL isopropanol was added to the supernatant and tube(s) centrifuged similarly. After centrifugation, supernatant was discarded and 800uL ice-cold 70% EtOH was added to the tube(s). Tube(s) then centrifuged at 13,000RPM for 5 minutes. Supernatant was discarded and tube(s) inverted and placed on paper towel, allowed to air-dry at RT for 20 minutes. Once EtOH had evaporated, 200uL ddH₂O was added to each tube and tube(s) vortexed, then placed in 37°C water bath for 30 minutes. Following incubation in water bath, DNA was quantitated or stored at -20°C until quantitation; following quantitation, DNA was stored in -20°C. NOTE: Precedent suggests that the total amount of template gDNA (with an OD_{260/280} ratio near 1.8) should be at least 10ng but not exceed 130ng for a 25uL reaction [410]. My recommendation is to quantitate DNA and dilute accordingly, prior to performing PCR; in the unlikely event the quantitation reveals the template gDNA to be too dilute, see “**DNA Precipitation from H₂O**” and attempt to concentrate gDNA before obtaining a new tail biopsy.

10X tail lysis buffer stock requires the following reagents:

100mM Tris-HCl, pH 8.5
5mM EDTA
0.2% SDS (L3771-1KG, Sigma)
200mM NaCl (S271, Fisher)

NOTE: Tris-HCl, pH 8.5 was prepared using Tris Base (BP152-1, Fisher) and Hydrochloric Acid (HCl; A144-212, Fisher).

Example preparation:

10X Tail Lysis Buffer	Ratio
1M Tris-HCl, pH 8.5	20mL
0.5M EDTA (BP2482, Fisher)	2mL
20% SDS	2mL
5M NaCl	8mL
ddH ₂ O	168mL

DNA Quantitation

DNA was quantitated using NanoDrop (Thermo-Fisher); 2uL ddH₂O used as blank and 2uL DNA used for quantitation.

DNA Precipitation from H₂O

Adapted from Qiagen [411]. 3M sodium acetate (NaOAc) was added to DNA stock at 0.1X the volume of water, then ice-cold 100% EtOH was added at 2.5X the (initial) volume of water. Mixture was vortexed vigorously placed in -20°C for at least 3 hours. After cooling, mixture was centrifuged at 13,000RPM at 4°C for 15 minutes. Supernatant was then discarded and microcentrifuge tube(s) filled maximally with ice-cold 70% EtOH, then centrifuged similarly. Supernatant was discarded and tube(s) inverted and placed on paper towel, allowed to air-dry at RT for 20 minutes. After EtOH

had evaporated, 10uL ddH₂O was added, tube(s) vortexed, then placed in 37°C water bath for 30 minutes. After water bath, tube(s) stored in -20°C. NOTE: 5M NaCl can be used in place of 3M NaOAc.

Statistical Analyses

Quantification of results and statistical analyses performed using *GraphPad Prism* 9.3.1 [412]. Unpaired (Student's/independent) t-test used when comparing 1 independent variable across 2 unrelated groups; paired t-test not applicable for our analyses. Two-way ANOVA used when comparing 2+ independent variables across 2 different groups assumed to have equal variances for (e.g., comparing *Tbk1*^{WT} and *Tbk1*^{NULL} cells both treated with 4 different drug dosages).

Cell Counting

After mixing in 1/1 ratio with trypan blue, cells were counted using the T10 Automated Cell Counter (1450001, BioRad) and accompanying dual-chamber counting slides (1450011, BioRad).

Western blot/Immunoblot

Performed by Allan Youmaran, BS.

Reagent	Catalog #, Manufacturer
10X PBS pH 7.4, RNase-free	AM9625, Ambion
10X Cell Lysis Buffer (contains phosphatase	9803, Cell Signaling Technology

inhibitors; 5mL in 45mL ddH ₂ O for 1X working solution)	
cOmplete™ ULTRA Tablets, Mini, EDTA-free, EASYpack Protease Inhibitor Cocktail (1 tablet per 50mL 1X Cell Lysis Buffer)	05892791001, Roche
40% Acrylamide/Bis Solution 29:1	HC2040, Fisher
Sodium dodecyl sulfate (SDS)	L3771-1KG, Sigma
10% ammonium persulfate (APS)	A3678-25G, Sigma (in ddH ₂ O)
N,N,N',N'-Tetramethylethylenediamine (TEMED)	T9281, Sigma-Aldrich

Bicinchoninic acid (BCA)/Smith assay	23225, Thermo Fisher
Loading dye	
10X electrophoresis/running buffer, pH 8.3	30.3g Tris Base + 144.0g glycine (M103-5KG, Amresco) + 10.0g SDS + 1L ddH ₂ O
Trans-Blot Turbo 5X Transfer Buffer	10026938, BioRad
NaCl	S271, Fisher
Tris base	BP152, Fisher
Tween-20	2287, Sigma Aldrich
Trans-Blot Turbo RTA Midi 0.2 μ m Nitrocellulose Transfer Kit	1704271, Bio-Rad
Bovine serum albumin (BSA)	A7906, Sigma-Aldrich (in ddH ₂ O)
TBK1/NAK (E8I3G) Rabbit mAb	38066, Cell Signaling Technologies

Anti-rabbit IgG, horseradish peroxidase (HRP)-linked Antibody	7074P2, Cell Signaling Technologies
WesternBright Quantum Kit	K-12042-D10, Advansta
PageRuler Plus Prestained Protein Ladder, 250 uL	26619, Thermo

Hematology Analysis of Mouse PB

Assistance provided by Nick Achille. *HemaVer*[®] 950FS (Drew Scientific, Inc.) was used for analysis of mouse PB.

Photographs

Assistance provided by Dr. Xianzhong Ding and Dr. Mitch Denning. Photos were taken using Revolve R4 microscope (ECHO/Bico) and Olympus BX41 microscope/Olympus DP21 camera with cellSens software.

Histology

Assistance provided by Lourdcy Pazhampally, Dr. Maria Picken, and Dr. Xianzhong Ding. Isolated tissue(s) were kept in conical tube(s) filled with 10% zinc formalin (313-095, Fisher Healthcare) and placed on gyrating rocker for 2-3 days, until delivery to the LUMC Department of Pathology & Laboratory Medicine.

Sectioning/cutting, embedding, and H&E staining was performed by Lourdcy Pazhampally. Samples transferred to 70% EtOH after zinc formalin-fixation for long-term storage.

Cytocentrifuge

45uL was sampled from cell culture and “spun” onto glass slides using the EpreDia™ Cytospin™ 4 Cytocentrifuge (A78300003, Thermo-Fisher).

Hema 3® Kit

After cytocentrifugation, cells were fixed and stained using the *Hema 3*® kit (Fisher). Following fixation and both staining steps, slides were briefly submerged in RT ddH₂O to rinse.

Order of Use	Reagent	Duration	Serial #
1 st	Fixative	30 seconds	122-929
2 nd	Solution I	30 seconds	122-937
3 rd	Solution II	15 seconds	122-952

Figures

Where applicable, figures/schematics created with *GraphPad Prism* (version 9.3.1 for Windows, GraphPad Software, San Diego, California USA, www.graphpad.com) and/or *BioRender.com* (*BioRender.com* Basic Plan is suitable for publication of this thesis on *ProQuest*[®], confirmed with Mayet of *BioRender.com* on 05/23/2023) and/or *Microsoft PowerPoint*[®] [412, 413].

Created in **BioRender.com** 

Drug Treatments

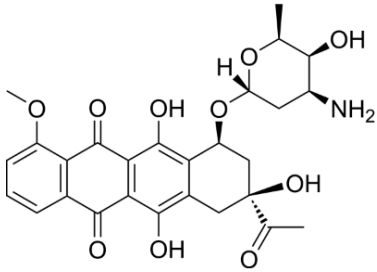
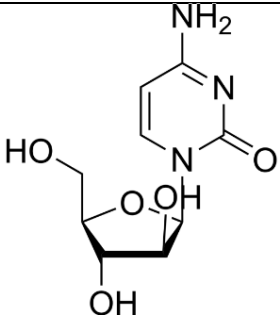
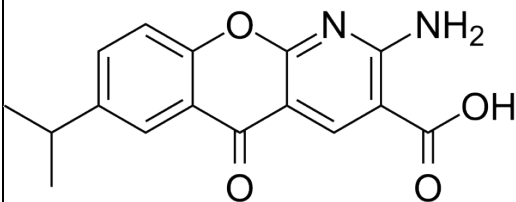
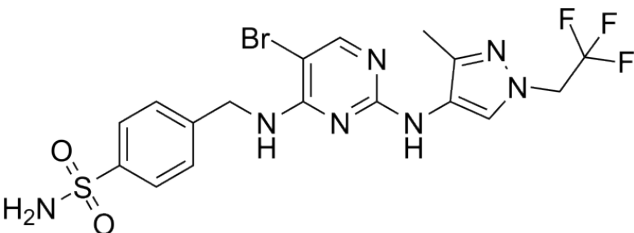
For *in vitro* drug treatments (DNO, Ara-C, AMX, and GSK8612), 5.0×10^4 *MLL-AF9*⁺ cells were seeded using 100uL liquid media (RPMI-1640/10% FBS/1% Penicillin-Streptomycin) into each well of a 12-well plate. Then, 75uL of 4GFS and an additional 2mL liquid media were added, bringing the total volume in each well to 2.175mL. After seeding, cells were incubated for 24 hours before drug treatment. The $[C_1V_1 = C_2V_2]$ equation was used to calculate the volume of drug to add for the desired final concentration; cells were treated for 24 hours before being collected, washed in 1X PBS, and prepped for FACS analysis.

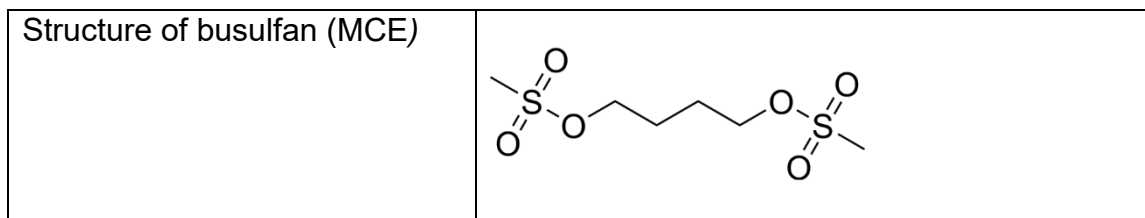
Drugs

Daunorubicin (HY-13062A [*Cerubidine*[®]]) and Ara-C (HY-13605 [*Cytosar-U*[®]]) were purchased from MedChemExpress (MCE) and resuspended in ddH₂O. Amlexanox (HY-B0713) and GSK8612 (HY-111941) were also purchased from MCE but required resuspension in dimethyl sulfoxide (DMSO). Busulfan (71288-116-11, Meitheal

Pharmaceuticals [*Busulfex*[®]]) was provided *graciously* by Dr. Patrick Hagan and LUMC

[414].

Structure of daunorubicin (MCE)	 <p>The chemical structure of daunorubicin is a complex polycyclic molecule. It features a tetracyclic aglycone core with a methoxy group at C-7, hydroxyl groups at C-5 and C-12, and a ketone at C-11. Attached to the C-10 position is a D-glucopyranoside sugar ring, which has a hydroxyl group at C-2, a hydroxyl group at C-3, and an amino group at C-4.</p>
Structure of Ara-C (MCE)	 <p>The chemical structure of Ara-C (cytosine arabinoside) consists of a cytosine base attached to a D-arabinose sugar ring. The cytosine base has an amino group at C-4 and a carbonyl group at C-2. The arabinose sugar has hydroxyl groups at C-2 and C-3, and a hydroxymethyl group at C-4.</p>
Structure of amlexanox (MCE)	 <p>The chemical structure of amlexanox is a benzoxazine derivative. It features a benzene ring fused to a six-membered ring containing an oxygen atom and a nitrogen atom. The nitrogen atom is substituted with an amino group. The benzene ring has an isopropyl group at the 6-position and a carboxylic acid group at the 2-position.</p>
Structure of GSK8612 (MCE)	 <p>The chemical structure of GSK8612 is a complex heterocyclic molecule. It features a central pyrimidine ring substituted with a bromine atom at C-5 and a methyl group at C-2. This pyrimidine ring is linked via its N-1 and N-3 positions to a benzimidazole ring system. The benzimidazole ring has a methyl group at C-2 and a trifluoromethyl group at C-5. The benzimidazole ring is further substituted at its N-1 position with a p-toluenesulfonamide group.</p>



We thank Dr. Rolf Brekken (UT Southwestern Medical Center) for *graciously* providing details regarding Compound II.

Lysis of RBCs/Hemolysis

10X Hemolytic Buffer Stock	Ratio
NH ₄ Cl	83g
NaHCO ₃	10g
0.5M, pH 8.0 EDTA BP2482, Fisher)	0.37g
MilliQ ddH ₂ O	1L

1X working solution created by diluting 100mL 10X stock in 900mL MilliQ ddH₂O.

Fluorescence-activated Cell Sorting (FACS [Flow Cytometry]) Analyses

Assistance provided by Pat Simms/Corbin Pomykata/Bert Ladd [FACS core], Ryan Mack/Kanak Joshi/Wei Wei [Zhang lab], and Lola Badmus/Janani Prakash/Nick Achille [Zeleznik-Le lab]. FACS analyses were conducted using LSRFortessa™ (BD Biosciences) the flow cytometry data were analyzed and gating depicted using *FlowJo*™ v10.8 Software (BD Life Sciences) [415]. Antibody cocktails were created using 1X PBS in the following concentrations and stored using amber microcentrifuge tube(s):

$[0.5\text{uL Ab} \cdot (\#\text{samples} + 1)]$

$[50\text{uL 1X PBS} \cdot (\#\text{samples} + 1)]$

Example calculation is:

5 samples to be stained = 3uL desired Ab(s) in 300uL 1X PBS.

With room lights off, cells-to-be-stained were transferred to 5mL polystyrene tube(s) and centrifuged at 1800RPM for 5 minutes. After centrifugation, tube(s) inverted and supernatant allowed to drain; for blood samples, supernatant was vacuumed- or pipetted-off, taking care to leave 100-200uL of supernatant remaining. Tube(s) then flicked to resuspend cells in the 100-200uL residual supernatant. 50uL of desired Ab cocktail was then added to desired samples, tube(s) flicked again and transferred to 4°C for 30-60 minutes for staining. After staining, cells were washed twice with ~3mL 1X PBS via similar centrifugation and brought to FACS core at the Cardinal Bernardin Cancer Center for analysis.

Compensations were created using the following concentrations: 1 drop UltraComp eBeads™ Compensation Beads (01-2222-42, Invitrogen) per 3mL 1X PBS, aliquotting 200uL of the mixture to desired 5mL polystyrene tube(s):

1 drop beads + $[200 \cdot (\#\text{fluorophores} + 1)]\text{uL 1X PBS}$

Example calculation is:

5 fluorophores in panel = 1 drop beads in 1.2mL 1X PBS

→ aliquot 200uL to each 5mL polystyrene tube(s), including unstained control (6 tube(s) total).

Then, 0.5uL corresponding Ab was added to the 200uL bead-1X PBS mixture aliquotted to each tube(s); tube(s) protected from light and stored in 4°C until analysis.

All antibodies listed below are reactive against mouse antigens (anti-mouse).

Antigen-Fluorophore	Manufacturer	Catalog #
CD3e-BV421	BioLegend	100336
CD45R (B220)-APC	BioLegend	103212
CD11b (Mac-1)-BV650	BioLegend	101239
Ly6-C/Ly6-G (Gr1)-PE	BioLegend	108407
CD41-PerCP/Cyanine5.5	BioLegend	133918
Ter119-FITC	ThermoFisher	11-5921-85
CD45.1 (Ly5.1)-PE	ThermoFisher	12-0453-83
CD45.2 (Ly5.2)-FITC	BioLegend	109806
B220-PE/Cyanine 7	BioLegend	103221
CD19-BV785	BioLegend	115543
CD5-APC	BioLegend	100625
B220-APC	BioLegend	103212
CD1d-FITC	BioLegend	123508
CD3-PE/Cyanine 7	BioLegend	100320
IgM-BV421	BioLegend	406517
IgD-BV650	BioLegend	405721
CD23-PE/Dazzle	BioLegend	101634
CD21-APC	BioLegend	123412


CD95 (Fas)-BV605	BioLegend	152612
GL7-FITC	BioLegend	144604
CD138 (Syndecan 1)-PE	BioLegend	142503
CD27-APC/Cyanine 7	BioLegend	124226
OX40L-APC	BioLegend	108812
IgA-FITC	BD Biosciences	559354
IgG1-BV650	BioLegend	406629
CD3e-PE/Cyanine 7	BioLegend	100320
CD4-e450	ThermoFisher	48-0041-82
CD8a-APC	ThermoFisher	17-0081-83
TCR γ / δ -PE	BioLegend	118107
TCR β -FITC	BioLegend	109206
B220-BV711	BioLegend	103255
CD4-FITC	BioLegend	553055
CD8a-FITC	ThermoFisher	11-0081-85
CD3e-FITC	ThermoFisher	11-0031-85
CD45R (B220)-FITC	ThermoFisher	11-0452-85
Gr1-FITC	ThermoFisher	11-5931-85
Gr1-PE	BioLegend	108407
CD11b (Mac-1)-FITC	BioLegend	101206
Ter119-BV510	BioLegend	116237

CD25-BV785	BioLegend	102051
CD44-BV650	BioLegend	103049
CD24-PE	BioLegend	553262
CD117 (c-Kit)-APC	BioLegend	105812
CD11c-BV421	BioLegend	117330
MHC class II-FITC	ThermoFisher	11-5980-82
CD69-PerCP/Cyanine5.5	BioLegend	104522
CD62L-FITC	BioLegend	553150
CD135 (Flt3)-PerCP-eFluor710	ThermoFisher	46-1351-82
CXCR5-BV711	BioLegend	145529
PD1-APC/Cyanine 7	BioLegend	135224
CD278 (ICOS)-PE	ThermoFisher	12-9942-82
CD117 (c-Kit)-APC/eFluor780	ThermoFisher	47-1171-82
CD150 (Slam)-BV785	BioLegend	115937
Tbk1 (pS172)-PE	BD BioSciences	558604

MilliQ ddH₂O Water

Molecular biology-grade double distilled water (ddH₂O) was acquired using the MilliQ Direct Water Purification System (MilliQ; ZR0Q008WW, Sigma-Aldrich).

Open Researcher and Contributor ID (ORCID) iD

Austin P. Runde  <https://orcid.org/0000-0002-2583-9502>

REFERENCE LIST

1. Saultz, J.N. and R. Garzon, *Acute Myeloid Leukemia: A Concise Review*. J Clin Med, 2016. **5**(3).
2. Roboz, G.J. and M. Guzman, *Acute myeloid leukemia stem cells: seek and destroy*. Expert Rev Hematol, 2009. **2**(6): p. 663-72.
3. The American Cancer Society medical and editorial content team, A. *Key Statistics for Acute Myeloid Leukemia (AML)*. 2023 [cited 2023; Available from: <https://www.cancer.org/cancer/acute-myeloid-leukemia/about/key-statistics.html#:~:text=AML%20is%20generally%20a%20disease,occur%20in%20children%20as%20well>].
4. Thol, F. and A. Ganser, *Treatment of Relapsed Acute Myeloid Leukemia*. Curr Treat Options Oncol, 2020. **21**(8): p. 66.
5. Institute, N.C. *Cancer Stat Facts: Leukemia — Acute Myeloid Leukemia (AML)*. 2023; Available from: <https://seer.cancer.gov/statfacts/html/amyl.html>.
6. Thol, F., et al., *How I treat refractory and early relapsed acute myeloid leukemia*. Blood, 2015. **126**(3): p. 319-27.
7. Wang, E.S., *Treating acute myeloid leukemia in older adults*. Hematology Am Soc Hematol Educ Program, 2014. **2014**(1): p. 14-20.
8. Kantarjian, H., et al., *Intensive chemotherapy does not benefit most older patients (age 70 years or older) with acute myeloid leukemia*. Blood, 2010. **116**(22): p. 4422-9.
9. (ACS), A.C.S. *Cancer Facts & Figures 2022*. 2022 [cited 2023; Available from: <https://www.cancer.org/research/cancer-facts-statistics/all-cancer-facts-figures/cancer-facts-figures-2022.html>].
10. The American Cancer Society, A. *Typical Treatment of Acute Myeloid Leukemia (Except APL)*. 2023; Available from: <https://www.cancer.org/cancer/acute-myeloid-leukemia/treating/typical-treatment-of-aml.html>.
11. Tomita, A., H. Kiyoi, and T. Naoe, *Mechanisms of action and resistance to all-trans retinoic acid (ATRA) and arsenic trioxide (As₂O₃) in acute promyelocytic leukemia*. Int J Hematol, 2013. **97**(6): p. 717-25.
12. Huang, M.E., et al., *Use of all-trans retinoic acid in the treatment of acute promyelocytic leukemia*. Blood, 1988. **72**(2): p. 567-72.
13. (ACS), A.C.S., *Targeted Therapy Drugs for Acute Myeloid Leukemia (AML)*. 2022.
14. Totiger, T.M., et al., *Targeted Therapy Development in Acute Myeloid Leukemia*. Biomedicines, 2023. **11**(2).
15. Kim, E.S., *Midostaurin: First Global Approval*. Drugs, 2017. **77**(11): p. 1251-1259.

16. Cortes, J.E., et al., *Randomized comparison of low dose cytarabine with or without glasdegib in patients with newly diagnosed acute myeloid leukemia or high-risk myelodysplastic syndrome*. *Leukemia*, 2019. **33**(2): p. 379-389.
17. Norsworthy, K.J., et al., *FDA Approval Summary: Glasdegib for Newly Diagnosed Acute Myeloid Leukemia*. *Clin Cancer Res*, 2019. **25**(20): p. 6021-6025.
18. Heuser, M., et al., *Clinical benefit of glasdegib plus low-dose cytarabine in patients with de novo and secondary acute myeloid leukemia: long-term analysis of a phase II randomized trial*. *Ann Hematol*, 2021. **100**(5): p. 1181-1194.
19. Pollyea, D.A., et al., *Venetoclax for AML: changing the treatment paradigm*. *Blood Adv*, 2019. **3**(24): p. 4326-4335.
20. Cortes, J.E., et al., *Glasdegib plus intensive/nonintensive chemotherapy in untreated acute myeloid leukemia: BRIGHT AML 1019 Phase III trials*. *Future Oncol*, 2019. **15**(31): p. 3531-3545.
21. Jamieson, C., et al., *Hedgehog Pathway Inhibitors: A New Therapeutic Class for the Treatment of Acute Myeloid Leukemia*. *Blood Cancer Discov*, 2020. **1**(2): p. 134-145.
22. Issa, G.C., et al., *The menin inhibitor revumenib in KMT2A-rearranged or NPM1-mutant leukaemia*. *Nature*, 2023. **615**(7954): p. 920-924.
23. DeAngelo, D.J., et al., *Phase 1/2 study of uproleselan added to chemotherapy in patients with relapsed or refractory acute myeloid leukemia*. *Blood*, 2022. **139**(8): p. 1135-1146.
24. Perner, F., et al., *MEN1 mutations mediate clinical resistance to menin inhibition*. *Nature*, 2023. **615**(7954): p. 913-919.
25. van Gils, N., F. Denkers, and L. Smit, *Escape From Treatment; the Different Faces of Leukemic Stem Cells and Therapy Resistance in Acute Myeloid Leukemia*. *Front Oncol*, 2021. **11**: p. 659253.
26. Schneider, C., et al., *SAMHD1 is a biomarker for cytarabine response and a therapeutic target in acute myeloid leukemia*. *Nat Med*, 2017. **23**(2): p. 250-255.
27. Zhang, F., et al., *Stabilization of SAMHD1 by NONO is crucial for Ara-C resistance in AML*. *Cell Death Dis*, 2022. **13**(7): p. 590.
28. Walter, R.B., et al., *Acute myeloid leukemia stem cells and CD33-targeted immunotherapy*. *Blood*, 2012. **119**(26): p. 6198-208.
29. Runde, A.P., et al., *The role of TBK1 in cancer pathogenesis and anticancer immunity*. *Journal of Experimental & Clinical Cancer Research*, 2022. **41**(1): p. 135.
30. Jin, J., et al., *The kinase TBK1 controls IgA class switching by negatively regulating noncanonical NF- κ B signaling*. *Nat Immunol*, 2012. **13**(11): p. 1101-9.
31. Xiao, Y., et al., *The kinase TBK1 functions in dendritic cells to regulate T cell homeostasis, autoimmunity, and antitumor immunity*. *J Exp Med*, 2017. **214**(5): p. 1493-1507.
32. Cannova, J.M., *Divergent Pro-Leukemic Effects of MYD88 and TICAM-1/TRIF Mediated Toll-Like Receptor Signaling*, in *Molecular and Cellular Biochemistry Program 2018*, Loyola University Chicago: Dissertations of Loyola eCommons. p. 164.

33. Chen, S., et al., *TANK-binding kinase 1 inhibitor GSK8612 enhances daunorubicin sensitivity in acute myeloid leukemia cells via the AKT-CDK2 pathway*. Am J Transl Res, 2021. **13**(12): p. 13640-13653.
34. Liu, S., et al., *The kinases IKBKE and TBK1 regulate MYC-dependent survival pathways through YB-1 in AML and are targets for therapy*. Blood Adv, 2018. **2**(23): p. 3428-3442.
35. Volk, A., et al., *Co-inhibition of NF- κ B and JNK is synergistic in TNF-expressing human AML*. J Exp Med, 2014. **211**(6): p. 1093-108.
36. Xin, J., et al., *Sensitizing acute myeloid leukemia cells to induced differentiation by inhibiting the RIP1/RIP3 pathway*. Leukemia, 2017. **31**(5): p. 1154-1165.
37. Yu, T., et al., *The pivotal role of TBK1 in inflammatory responses mediated by macrophages*. Mediators Inflamm, 2012. **2012**: p. 979105.
38. Ikeda, F., et al., *Involvement of the ubiquitin-like domain of TBK1/IKK-i kinases in regulation of IFN-inducible genes*. EMBO J, 2007. **26**(14): p. 3451-62.
39. Larabi, A., et al., *Crystal structure and mechanism of activation of TANK-binding kinase 1*. Cell Rep, 2013. **3**(3): p. 734-46.
40. Oakes, J.A., M.C. Davies, and M.O. Collins, *TBK1: a new player in ALS linking autophagy and neuroinflammation*. Mol Brain, 2017. **10**(1): p. 5.
41. Ryzhakov, G. and F. Randow, *SINTBAD, a novel component of innate antiviral immunity, shares a TBK1-binding domain with NAP1 and TANK*. EMBO J, 2007. **26**(13): p. 3180-90.
42. Li, F., et al., *Structural insights into the ubiquitin recognition by OPTN (optineurin) and its regulation by TBK1-mediated phosphorylation*. Autophagy, 2018. **14**(1): p. 66-79.
43. Tojima, Y., et al., *NAK is an IkappaB kinase-activating kinase*. Nature, 2000. **404**(6779): p. 778-82.
44. Consortium, U. *UniProt Align*. Available from: <https://www.uniprot.org/align>.
45. Consortium, U., *UniProt: the Universal Protein Knowledgebase in 2023*. Nucleic Acids Res, 2023. **51**(D1): p. D523-D531.
46. Perry, A.K., et al., *Differential requirement for TANK-binding kinase-1 in type I interferon responses to toll-like receptor activation and viral infection*. J Exp Med, 2004. **199**(12): p. 1651-8.
47. Sharma, S., et al., *Triggering the interferon antiviral response through an IKK-related pathway*. Science, 2003. **300**(5622): p. 1148-51.
48. tenOever, B.R., et al., *Activation of TBK1 and IKKvarepsilon kinases by vesicular stomatitis virus infection and the role of viral ribonucleoprotein in the development of interferon antiviral immunity*. J Virol, 2004. **78**(19): p. 10636-49.
49. Fitzgerald, K.A., et al., *IKKepsilon and TBK1 are essential components of the IRF3 signaling pathway*. Nat Immunol, 2003. **4**(5): p. 491-6.
50. Oral, E.A., et al., *Inhibition of IKK ϵ and TBK1 Improves Glucose Control in a Subset of Patients with Type 2 Diabetes*. Cell Metab, 2017. **26**(1): p. 157-170.e7.
51. Lefranc, J., et al., *Discovery of BAY-985, a Highly Selective TBK1/IKK ϵ Inhibitor*. J Med Chem, 2020. **63**(2): p. 601-612.

52. McIver, E.G., et al., *Synthesis and structure-activity relationships of a novel series of pyrimidines as potent inhibitors of TBK1/IKK ϵ kinases*. *Bioorg Med Chem Lett*, 2012. **22**(23): p. 7169-73.
53. Chau, T.L., et al., *Are the IKKs and IKK-related kinases TBK1 and IKK-epsilon similarly activated?* *Trends Biochem Sci*, 2008. **33**(4): p. 171-80.
54. Balka, K.R., et al., *TBK1 and IKK ϵ Act Redundantly to Mediate STING-Induced NF- κ B Responses in Myeloid Cells*. *Cell Rep*, 2020. **31**(1): p. 107492.
55. Tenoever, B.R., et al., *Multiple functions of the IKK-related kinase IKKepsilon in interferon-mediated antiviral immunity*. *Science*, 2007. **315**(5816): p. 1274-8.
56. Runde, A.P., et al., *The role of TBK1 in cancer pathogenesis and anticancer immunity*. *J Exp Clin Cancer Res*, 2022. **41**(1): p. 135.
57. Mahajan, K. and N.P. Mahajan, *PI3K-independent AKT activation in cancers: a treasure trove for novel therapeutics*. *J Cell Physiol*, 2012. **227**(9): p. 3178-84.
58. Tu, D., et al., *Structure and ubiquitination-dependent activation of TANK-binding kinase 1*. *Cell Rep*, 2013. **3**(3): p. 747-58.
59. (NCBI), N.L.o.M.N.o.t.N.C.f.B.I. *TBK1 TANK binding kinase 1 [Homo sapiens (human)]*. 2023; Available from: <https://www.ncbi.nlm.nih.gov/gene/29110>.
60. Hu, Y.W., et al., *TANK-Binding Kinase 1 (TBK1) Isoforms Negatively Regulate Type I Interferon Induction by Inhibiting TBK1-IRF3 Interaction and IRF3 Phosphorylation*. *Front Immunol*, 2018. **9**: p. 84.
61. Information, N.C.f.B. *Tbk1 TANK-binding kinase 1 [Mus musculus (house mouse)]*. Gene ID: 56480]. Available from: <https://www.ncbi.nlm.nih.gov/gene?Db=gene&Cmd=DetailsSearch&Term=56480>.
62. Fagerberg, L., et al., *Analysis of the human tissue-specific expression by genome-wide integration of transcriptomics and antibody-based proteomics*. *Mol Cell Proteomics*, 2014. **13**(2): p. 397-406.
63. Deng, W., et al., *Negative regulation of virus-triggered IFN-beta signaling pathway by alternative splicing of TBK1*. *J Biol Chem*, 2008. **283**(51): p. 35590-7.
64. Chang, M.X. and J. Zhang, *Alternative Pre-mRNA Splicing in Mammals and Teleost Fish: A Effective Strategy for the Regulation of Immune Responses Against Pathogen Infection*. *Int J Mol Sci*, 2017. **18**(7).
65. Zhang, L., et al., *TBK1-like transcript negatively regulates the production of IFN and IFN-stimulated genes through RLRs-MAVS-TBK1 pathway*. *Fish Shellfish Immunol*, 2016. **54**: p. 135-43.
66. Castro-Mondragon, J.A., et al., *JASPAR 2022: the 9th release of the open-access database of transcription factor binding profiles*. *Nucleic Acids Res*, 2022. **50**(D1): p. D165-D173.
67. Rouillard, A.D., et al., *The harmonizome: a collection of processed datasets gathered to serve and mine knowledge about genes and proteins*. *Database (Oxford)*, 2016. **2016**.
68. Shu, C., et al., *Structural insights into the functions of TBK1 in innate antimicrobial immunity*. *Structure*, 2013. **21**(7): p. 1137-48.

69. Ma, X., et al., *Molecular basis of Tank-binding kinase 1 activation by transautophosphorylation*. Proc Natl Acad Sci U S A, 2012. **109**(24): p. 9378-83.
70. Kawai, T. and S. Akira, *TLR signaling*. Cell Death Differ, 2006. **13**(5): p. 816-25.
71. Ishikawa, H., Z. Ma, and G.N. Barber, *STING regulates intracellular DNA-mediated, type I interferon-dependent innate immunity*. Nature, 2009. **461**(7265): p. 788-92.
72. Barbie, D.A., et al., *Systematic RNA interference reveals that oncogenic KRAS-driven cancers require TBK1*. Nature, 2009. **462**(7269): p. 108-12.
73. Hamarsheh, S., et al., *Immune modulatory effects of oncogenic KRAS in cancer*. Nat Commun, 2020. **11**(1): p. 5439.
74. Hsia, H.C., J.E. Hutti, and A.S. Baldwin, *Cytosolic DNA Promotes Signal Transducer and Activator of Transcription 3 (STAT3) Phosphorylation by TANK-binding Kinase 1 (TBK1) to Restrain STAT3 Activity*. J Biol Chem, 2017. **292**(13): p. 5405-5417.
75. Fukasaka, M., et al., *Critical role of AZI2 in GM-CSF-induced dendritic cell differentiation*. J Immunol, 2013. **190**(11): p. 5702-11.
76. Saul, V.V., et al., *ULK1/2 Restricts the Formation of Inducible SINT-Speckles, Membraneless Organelles Controlling the Threshold of TBK1 Activation*. iScience, 2019. **19**: p. 527-544.
77. Gao, T., et al., *Myeloid cell TBK1 restricts inflammatory responses*. Proc Natl Acad Sci U S A, 2022. **119**(4).
78. Kemmoku, H., et al., *Specific association of TBK1 with the trans-Golgi network following STING stimulation*. Cell Struct Funct, 2022. **47**(1): p. 19-30.
79. Liu, S., et al., *Lck/Hck/Fgr-Mediated Tyrosine Phosphorylation Negatively Regulates TBK1 to Restrain Innate Antiviral Responses*. Cell Host Microbe, 2017. **21**(6): p. 754-768.e5.
80. Wu, S., et al., *HER2 recruits AKT1 to disrupt STING signalling and suppress antiviral defence and antitumour immunity*. Nat Cell Biol, 2019. **21**(8): p. 1027-1040.
81. Cooper, J.M., et al., *TBK1 Provides Context-Selective Support of the Activated AKT/mTOR Pathway in Lung Cancer*. Cancer Res, 2017. **77**(18): p. 5077-5094.
82. Zhu, L., et al., *TBKBP1 and TBK1 form a growth factor signalling axis mediating immunosuppression and tumorigenesis*. Nature Cell Biology, 2019. **21**(12): p. 1604-1614.
83. Kishore, N., et al., *IKK-i and TBK-1 are enzymatically distinct from the homologous enzyme IKK-2: comparative analysis of recombinant human IKK-i, TBK-1, and IKK-2*. J Biol Chem, 2002. **277**(16): p. 13840-7.
84. Clark, K., et al., *Novel cross-talk within the IKK family controls innate immunity*. Biochem J, 2011. **434**(1): p. 93-104.
85. Zhao, P., et al., *TBK1 at the Crossroads of Inflammation and Energy Homeostasis in Adipose Tissue*. Cell, 2018. **172**(4): p. 731-743.e12.
86. Zhao, Y., et al., *PPM1B negatively regulates antiviral response via dephosphorylating TBK1*. Cell Signal, 2012. **24**(11): p. 2197-204.

87. Xie, W., et al., *Selective autophagy controls the stability of TBK1 via NEDD4 to balance host defense*. *Cell Death Differ*, 2022. **29**(1): p. 40-53.
88. Lin, M., et al., *USP38 Inhibits Type I Interferon Signaling by Editing TBK1 Ubiquitination through NLRP4 Signalosome*. *Mol Cell*, 2016. **64**(2): p. 267-281.
89. Cui, J., et al., *NLRP4 negatively regulates type I interferon signaling by targeting the kinase TBK1 for degradation via the ubiquitin ligase DTX4*. *Nat Immunol*, 2012. **13**(4): p. 387-95.
90. Charoenthongtrakul, S., L. Gao, and E.W. Harhaj, *The NLRP4-DTX4 axis: a key suppressor of TBK1 and innate antiviral signaling*. *Cell Mol Immunol*, 2012. **9**(6): p. 431-3.
91. Zheng, Q., et al., *Siglec1 suppresses antiviral innate immune response by inducing TBK1 degradation via the ubiquitin ligase TRIM27*. *Cell Res*, 2015. **25**(10): p. 1121-36.
92. Song, G., et al., *E3 ubiquitin ligase RNF128 promotes innate antiviral immunity through K63-linked ubiquitination of TBK1*. *Nat Immunol*, 2016. **17**(12): p. 1342-1351.
93. Ye, J.S., et al., *Lysine 63-linked TANK-binding kinase 1 ubiquitination by mindbomb E3 ubiquitin protein ligase 2 is mediated by the mitochondrial antiviral signaling protein*. *J Virol*, 2014. **88**(21): p. 12765-76.
94. Wang, L., S. Li, and M.E. Dorf, *NEMO binds ubiquitinated TANK-binding kinase 1 (TBK1) to regulate innate immune responses to RNA viruses*. *PLoS One*, 2012. **7**(9): p. e43756.
95. Tang, J.L., et al., *Histone deacetylase 3 promotes innate antiviral immunity through deacetylation of TBK1*. *Protein Cell*, 2021. **12**(4): p. 261-278.
96. Yang, Q., et al., *Host HDAC4 regulates the antiviral response by inhibiting the phosphorylation of IRF3*. *J Mol Cell Biol*, 2019. **11**(2): p. 158-169.
97. Li, X., et al., *Methyltransferase Dnmt3a upregulates HDAC9 to deacetylate the kinase TBK1 for activation of antiviral innate immunity*. *Nat Immunol*, 2016. **17**(7): p. 806-15.
98. Saul, V.V., et al., *SUMO modification of TBK1 at the adaptor-binding C-terminal coiled-coil domain contributes to its antiviral activity*. *Biochim Biophys Acta*, 2015. **1853**(1): p. 136-43.
99. Liu, Q., et al., *GSNOR facilitates antiviral innate immunity by restricting TBK1 cysteine S-nitrosation*. *Redox Biol*, 2021. **47**: p. 102172.
100. Hu, L., et al., *TBK1 Is a Synthetic Lethal Target in Cancer with VHL Loss*. *Cancer Discovery*, 2020. **10**(3): p. 460-475.
101. Pillai, S., et al., *Tank binding kinase 1 is a centrosome-associated kinase necessary for microtubule dynamics and mitosis*. *Nat Commun*, 2015. **6**: p. 10072.
102. Richter, B., et al., *Phosphorylation of OPTN by TBK1 enhances its binding to Ub chains and promotes selective autophagy of damaged mitochondria*. *Proc Natl Acad Sci U S A*, 2016. **113**(15): p. 4039-44.

103. He, L., L. Chen, and L. Li, *The TBK1-OPTN Axis Mediates Crosstalk Between Mitophagy and the Innate Immune Response: A Potential Therapeutic Target for Neurodegenerative Diseases*. *Neurosci Bull*, 2017. **33**(3): p. 354-356.
104. Huh, J.Y., et al., *TANK-Binding Kinase 1 Regulates the Localization of Acyl-CoA Synthetase ACSL1 to Control Hepatic Fatty Acid Oxidation*. *Cell Metab*, 2020. **32**(6): p. 1012-1027.e7.
105. Zhang, C., et al., *Structural basis of STING binding with and phosphorylation by TBK1*. *Nature*, 2019. **567**(7748): p. 394-398.
106. Sarraf, S.A., et al., *PINK1/Parkin Influences Cell Cycle by Sequestering TBK1 at Damaged Mitochondria, Inhibiting Mitosis*. *Cell Rep*, 2019. **29**(1): p. 225-235.e5.
107. Heo, J.M., et al., *The PINK1-PARKIN Mitochondrial Ubiquitylation Pathway Drives a Program of OPTN/NDP52 Recruitment and TBK1 Activation to Promote Mitophagy*. *Mol Cell*, 2015. **60**(1): p. 7-20.
108. Matsumoto, G., et al., *TBK1 controls autophagosomal engulfment of polyubiquitinated mitochondria through p62/SQSTM1 phosphorylation*. *Hum Mol Genet*, 2015. **24**(15): p. 4429-42.
109. Nerurkar, L., et al., *The Systemic Response to Topical Aldara Treatment is Mediated Through Direct TLR7 Stimulation as Imiquimod Enters the Circulation*. *Sci Rep*, 2017. **7**(1): p. 16570.
110. Kim, M.H., et al., *The TRIF/TBK1/IRF-3 activation pathway is the primary inhibitory target of resveratrol, contributing to its broad-spectrum anti-inflammatory effects*. *Pharmazie*, 2011. **66**(4): p. 293-300.
111. Youn, H.S., et al., *Specific inhibition of MyD88-independent signaling pathways of TLR3 and TLR4 by resveratrol: molecular targets are TBK1 and RIP1 in TRIF complex*. *J Immunol*, 2005. **175**(5): p. 3339-46.
112. Thurston, T.L., et al., *The TBK1 adaptor and autophagy receptor NDP52 restricts the proliferation of ubiquitin-coated bacteria*. *Nat Immunol*, 2009. **10**(11): p. 1215-21.
113. Chang, C.H., et al., *TBK1-associated protein in endolysosomes (TAPE) is an innate immune regulator modulating the TLR3 and TLR4 signaling pathways*. *J Biol Chem*, 2011. **286**(9): p. 7043-51.
114. Yang, C., et al., *CXCL4 synergizes with TLR8 for TBK1-IRF5 activation, epigenomic remodeling and inflammatory response in human monocytes*. *Nat Commun*, 2022. **13**(1): p. 3426.
115. Kwa, M.Q., et al., *Interferon regulatory factor 6 differentially regulates Toll-like receptor 2-dependent chemokine gene expression in epithelial cells*. *J Biol Chem*, 2014. **289**(28): p. 19758-68.
116. Li, S., et al., *Fish IRF6 is a positive regulator of IFN expression and involved in both of the MyD88 and TBK1 pathways*. *Fish Shellfish Immunol*, 2016. **57**: p. 262-268.
117. Farlik, M., et al., *Contribution of a TANK-binding kinase 1-interferon (IFN) regulatory factor 7 pathway to IFN- γ -induced gene expression*. *Mol Cell Biol*, 2012. **32**(6): p. 1032-43.

118. Chang Foreman, H.C., et al., *Activation of interferon regulatory factor 5 by site specific phosphorylation*. PLoS One, 2012. **7**(3): p. e33098.
119. Loevenich, S., et al., *Human Metapneumovirus Induces IRF1*. Front Immunol, 2021. **12**: p. 563336.
120. Li, D., et al., *The E3 Ubiquitin Ligase TBK1 Mediates the Degradation of Multiple Picornavirus VP3 Proteins by Phosphorylation and Ubiquitination*. J Virol, 2019. **93**(23).
121. Lee, M.S.J., et al., *B cell-intrinsic TBK1 is essential for germinal center formation during infection and vaccination in mice*. J Exp Med, 2022. **219**(2).
122. Wei, C., et al., *Elevated expression of TANK-binding kinase 1 enhances tamoxifen resistance in breast cancer*. Proc Natl Acad Sci U S A, 2014. **111**(5): p. E601-10.
123. Muñoz, M.C., et al., *TANK-binding kinase 1 mediates phosphorylation of insulin receptor at serine residue 994: a potential link between inflammation and insulin resistance*. J Endocrinol, 2009. **201**(2): p. 185-97.
124. Quinn, P.M.J., et al., *PINK1/PARKIN signalling in neurodegeneration and neuroinflammation*. Acta Neuropathol Commun, 2020. **8**(1): p. 189.
125. Chen, H., et al., *Activation of STAT6 by STING is critical for antiviral innate immunity*. Cell, 2011. **147**(2): p. 436-46.
126. Korherr, C., et al., *Identification of proangiogenic genes and pathways by high-throughput functional genomics: TBK1 and the IRF3 pathway*. Proc Natl Acad Sci U S A, 2006. **103**(11): p. 4240-5.
127. Marchlik, E., et al., *Mice lacking Tbk1 activity exhibit immune cell infiltrates in multiple tissues and increased susceptibility to LPS-induced lethality*. J Leukoc Biol, 2010. **88**(6): p. 1171-80.
128. Cochran, B.H., A.C. Reffel, and C.D. Stiles, *Molecular cloning of gene sequences regulated by platelet-derived growth factor*. Cell, 1983. **33**(3): p. 939-47.
129. Kang, M.H., Y.H. Jin, and B.S. Kim, *Effects of Keratinocyte-Derived Cytokine (CXCL-1) on the Development of Theiler's Virus-Induced Demyelinating Disease*. Front Cell Infect Microbiol, 2018. **8**: p. 9.
130. Lin, Q., et al., *New insights into mitophagy and stem cells*. Stem Cell Res Ther, 2021. **12**(1): p. 452.
131. Kurihara, Y., et al., *Mitophagy plays an essential role in reducing mitochondrial production of reactive oxygen species and mutation of mitochondrial DNA by maintaining mitochondrial quantity and quality in yeast*. J Biol Chem, 2012. **287**(5): p. 3265-72.
132. Murphy, M.P., *How mitochondria produce reactive oxygen species*. Biochem J, 2009. **417**(1): p. 1-13.
133. Sullivan, L.B. and N.S. Chandel, *Mitochondrial reactive oxygen species and cancer*. Cancer Metab, 2014. **2**: p. 17.
134. De Gaetano, A., et al., *Mitophagy and Oxidative Stress: The Role of Aging*. Antioxidants (Basel), 2021. **10**(5).
135. Cairns, G., et al., *Mitophagy: A New Player in Stem Cell Biology*. Biology (Basel), 2020. **9**(12).

136. Ji, A.R., et al., *Reactive oxygen species enhance differentiation of human embryonic stem cells into mesendodermal lineage*. *Exp Mol Med*, 2010. **42**(3): p. 175-86.
137. Cieślak-Pobuda, A., et al., *ROS and Oxidative Stress in Stem Cells*. *Oxid Med Cell Longev*, 2017. **2017**: p. 5047168.
138. Chen, Y., et al., *The tango of ROS and p53 in tissue stem cells*. *Cell Death Differ*, 2018. **25**(4): p. 639-641.
139. Yan, C. and T.S. Li, *Dual Role of Mitophagy in Cancer Drug Resistance*. *Anticancer Res*, 2018. **38**(2): p. 617-621.
140. Luanpitpong, S., et al., *Mitochondrial superoxide mediates doxorubicin-induced keratinocyte apoptosis through oxidative modification of ERK and Bcl-2 ubiquitination*. *Biochem Pharmacol*, 2012. **83**(12): p. 1643-54.
141. Barrera, G., *Oxidative stress and lipid peroxidation products in cancer progression and therapy*. *ISRN Oncol*, 2012. **2012**: p. 137289.
142. Liou, G.Y. and P. Storz, *Reactive oxygen species in cancer*. *Free Radic Res*, 2010. **44**(5): p. 479-96.
143. Nakamura, H. and K. Takada, *Reactive oxygen species in cancer: Current findings and future directions*. *Cancer Sci*, 2021. **112**(10): p. 3945-3952.
144. Al-Aamri, H.M., et al., *Time dependent response of daunorubicin on cytotoxicity, cell cycle and DNA repair in acute lymphoblastic leukaemia*. *BMC Cancer*, 2019. **19**(1): p. 179.
145. Guan, Y., et al., *Mitophagy in carcinogenesis, drug resistance and anticancer therapeutics*. *Cancer Cell Int*, 2021. **21**(1): p. 350.
146. Lee, K.C., et al., *Formation and anti-tumor activity of uncommon in vitro and in vivo metabolites of CPI-613, a novel anti-tumor compound that selectively alters tumor energy metabolism*. *Drug Metab Lett*, 2011. **5**(3): p. 163-82.
147. Pardee, T.S., et al., *A Phase I Study of CPI-613 in Combination with High-Dose Cytarabine and Mitoxantrone for Relapsed or Refractory Acute Myeloid Leukemia*. *Clin Cancer Res*, 2018. **24**(9): p. 2060-2073.
148. Philip, P.A., et al., *A Phase III open-label trial to evaluate efficacy and safety of CPI-613 plus modified FOLFIRINOX (mFFX) versus FOLFIRINOX (FFX) in patients with metastatic adenocarcinoma of the pancreas*. *Future Oncol*, 2019. **15**(28): p. 3189-3196.
149. Wegner, J., et al., *Increased IKKε protein stability ensures efficient type I interferon responses in conditions of TBK1 deficiency*. *Front Immunol*, 2023. **14**: p. 1073608.
150. Bonnard, M., et al., *Deficiency of T2K leads to apoptotic liver degeneration and impaired NF-κB-dependent gene transcription*. *EMBO J*, 2000. **19**(18): p. 4976-85.
151. Xu, D., et al., *TBK1 Suppresses RIPK1-Driven Apoptosis and Inflammation during Development and in Aging*. *Cell*, 2018. **174**(6): p. 1477-1491.e19.
152. Yu, J., et al., *Regulation of T-cell activation and migration by the kinase TBK1 during neuroinflammation*. *Nat Commun*, 2015. **6**: p. 6074.

153. Cruz, V.H., et al., *Loss of Tbk1 kinase activity protects mice from diet-induced metabolic dysfunction*. Mol Metab, 2018. **16**: p. 139-149.
154. Duan, W., et al., *Deletion of Tbk1 disrupts autophagy and reproduces behavioral and locomotor symptoms of FTD-ALS in mice*. Aging (Albany NY), 2019. **11**(8): p. 2457-2476.
155. Duan, W., et al., *Myeloid TBK1 Deficiency Induces Motor Deficits and Axon Degeneration Through Inflammatory Cell Infiltration*. Molecular Neurobiology, 2021.
156. Hagan, R.S., J. Torres-Castillo, and C.M. Doerschuk, *Myeloid TBK1 Signaling Contributes to the Immune Response to Influenza*. Am J Respir Cell Mol Biol, 2019. **60**(3): p. 335-345.
157. Yang, J.Y., et al., *Intestinal Epithelial TBK1 Prevents Differentiation of T-helper 17 Cells and Tumorigenesis in Mice*. Gastroenterology, 2020. **159**(5): p. 1793-1806.
158. Harding, O., et al., *ALS- and FTD-associated missense mutations in TBK1 differentially disrupt mitophagy*. Proc Natl Acad Sci U S A, 2021. **118**(24).
159. Abreha, M.H., et al., *TBK1 interacts with tau and enhances neurodegeneration in tauopathy*. J Biol Chem, 2021. **296**: p. 100760.
160. Herman, M., et al., *Heterozygous TBK1 mutations impair TLR3 immunity and underlie herpes simplex encephalitis of childhood*. J Exp Med, 2012. **209**(9): p. 1567-82.
161. Fingert, J.H., et al., *Copy number variations on chromosome 12q14 in patients with normal tension glaucoma*. Hum Mol Genet, 2011. **20**(12): p. 2482-94.
162. Ritch, R., et al., *TBK1 gene duplication and normal-tension glaucoma*. JAMA Ophthalmol, 2014. **132**(5): p. 544-8.
163. Ahmad, L., et al., *Human TBK1: A Gatekeeper of Neuroinflammation*. Trends Mol Med, 2016. **22**(6): p. 511-527.
164. Gurfinkel, Y., et al., *Functional and structural consequences of TBK1 missense variants in frontotemporal lobar degeneration and amyotrophic lateral sclerosis*. Neurobiol Dis, 2022. **174**: p. 105859.
165. Taft, J., et al., *Human TBK1 deficiency leads to autoinflammation driven by TNF-induced cell death*. Cell, 2021. **184**(17): p. 4447-4463.e20.
166. Boeve, B. *ARTFL LEFFTDS Longitudinal Frontotemporal Lobar Degeneration (ALLFTD)* Available from: <https://clinicaltrials.gov/ct2/show/NCT04363684>.
167. Mørk, N., et al., *Mutations in the TLR3 signaling pathway and beyond in adult patients with herpes simplex encephalitis*. Genes Immun, 2015. **16**(8): p. 552-66.
168. Zhang, Q., et al., *Inborn errors of type I IFN immunity in patients with life-threatening COVID-19*. Science, 2020. **370**(6515).
169. Schmidt, A., et al., *TBK1 and TNFRSF13B mutations and an autoinflammatory disease in a child with lethal COVID-19*. NPJ Genom Med, 2021. **6**(1): p. 55.
170. Muller, H.J., *Further studies on the nature and causes of gene mutations*. 1932: *Proceedings of the 6th International Congress of Genetics*. p. 213-255.
171. Kawase, K., et al., *Confirmation of TBK1 duplication in normal tension glaucoma*. Exp Eye Res, 2012. **96**(1): p. 178-80.

172. Awadalla, M.S., et al., *Copy number variations of TBK1 in Australian patients with primary open-angle glaucoma*. *Am J Ophthalmol*, 2015. **159**(1): p. 124-30.e1.
173. Fingert, J.H., et al., *Tank-Binding Kinase 1* (Trans Am Ophthalmol Soc, 2016. **114**: p. T6.
174. Jiao, B., et al., *Rare TBK1 variants in patients with frontotemporal dementia and amyotrophic lateral sclerosis in a Chinese cohort*. *Transl Neurodegener*, 2018. **7**: p. 31.
175. Moore, A.S. and E.L. Holzbaur, *Dynamic recruitment and activation of ALS-associated TBK1 with its target optineurin are required for efficient mitophagy*. *Proc Natl Acad Sci U S A*, 2016. **113**(24): p. E3349-58.
176. Ye, J., et al., *Effects of ALS-associated TANK binding kinase 1 mutations on protein-protein interactions and kinase activity*. *Proc Natl Acad Sci U S A*, 2019. **116**(49): p. 24517-24526.
177. Thanos, D. and T. Maniatis, *Virus induction of human IFN beta gene expression requires the assembly of an enhanceosome*. *Cell*, 1995. **83**(7): p. 1091-100.
178. Servant, M.J., et al., *Identification of the minimal phosphoacceptor site required for in vivo activation of interferon regulatory factor 3 in response to virus and double-stranded RNA*. *J Biol Chem*, 2003. **278**(11): p. 9441-7.
179. Gijssels, I., et al., *Loss of TBK1 is a frequent cause of frontotemporal dementia in a Belgian cohort*. *Neurology*, 2015. **85**(24): p. 2116-25.
180. van der Zee, J., et al., *TBK1 Mutation Spectrum in an Extended European Patient Cohort with Frontotemporal Dementia and Amyotrophic Lateral Sclerosis*. *Hum Mutat*, 2017. **38**(3): p. 297-309.
181. The Cancer Genome Atlas Program (TCGA) Research Network, N.C.I.N., *TBK1 in Bone Marrow Cancers*, <https://www.cancer.gov/tcga>, Editor. 2023: Genomic Data Commons (GDC)
at https://portal.gdc.cancer.gov/exploration?cases_size=100&facetTab=genes&filters=%7B%22content%22%3A%5B%7B%22content%22%3A%7B%22field%22%3A%22cases.diagnoses.tissue_or_organ_of_origin%22%2C%22value%22%3A%5B%22blood%22%2C%22bone%20marrow%22%2C%22hematopoietic%20system%2C%20nos%22%2C%22reticuloendothelial%20system%2C%20nos%22%2C%22spleen%22%5D%7D%2C%22op%22%3A%22in%22%7D%2C%7B%22content%22%3A%7B%22field%22%3A%22cases.primary_site%22%2C%22value%22%3A%5B%22hematopoietic%20and%20reticuloendothelial%20systems%22%5D%7D%2C%22op%22%3A%22in%22%7D%2C%7B%22op%22%3A%22in%22%2C%22content%22%3A%7B%22field%22%3A%22genes.gene_id%22%2C%22value%22%3A%5B%22ENSG00000183735%22%5D%7D%7D%5D%2C%22op%22%3A%22and%22%7D.
182. The Cancer Genome Atlas Program (TCGA) Research Network, N., *TBK1 in Bone Marrow Cancers*, <https://www.cancer.gov/tcga>, Editor. 2023: Genomic Data Commons (GDC)
at https://portal.gdc.cancer.gov/exploration?cases_size=100&facetTab=genes&filters=%7B%22content%22%3A%5B%7B%22content%22%3A%7B%22field%22%3A%22cases.diagnoses.tissue_or_organ_of_origin%22%2C%22value%22%3A%5B%22blood%22%2C%22bone%20marrow%22%2C%22hematopoietic%20system%2C%20nos%22%2C%22reticuloendothelial%20system%2C%20nos%22%2C%22spleen%22%5D%7D%2C%22op%22%3A%22in%22%7D%2C%7B%22content%22%3A%7B%22field%22%3A%22cases.primary_site%22%2C%22value%22%3A%5B%22hematopoietic%20and%20reticuloendothelial%20systems%22%5D%7D%2C%22op%22%3A%22in%22%7D%2C%7B%22op%22%3A%22in%22%2C%22content%22%3A%7B%22field%22%3A%22genes.gene_id%22%2C%22value%22%3A%5B%22ENSG00000183735%22%5D%7D%7D%5D%2C%22op%22%3A%22and%22%7D.

- %3A%22cases.diagnoses.tissue_or_organ_of_origin%22%2C%22value%22%3A%5B%22blood%22%2C%22bone%20marrow%22%2C%22hematopoietic%20system%2C%20nos%22%2C%22reticuloendothelial%20system%2C%20nos%22%2C%22spleen%22%5D%7D%2C%22op%22%3A%22in%22%7D%2C%22value%22%3A%5B%22hematopoietic%20and%20reticuloendothelial%20systems%22%5D%7D%2C%22op%22%3A%22in%22%7D%2C%22op%22%3A%22in%22%2C%22content%22%3A%7B%22field%22%3A%22genes.gene_id%22%2C%22value%22%3A%5B%22ENSG00000183735%22%5D%7D%7D%5D%2C%22op%22%3A%22and%22%7D.
183. Cheng, C., et al., *Apthous ulcer drug inhibits prostate tumor metastasis by targeting IKK ϵ /TBK1/NF- κ B signaling*. *Theranostics*, 2018. **8**(17): p. 4633-4648.
 184. Cruz, V.H. and R.A. Brekken, *Assessment of TANK-binding kinase 1 as a therapeutic target in cancer*. *J Cell Commun Signal*, 2018. **12**(1): p. 83-90.
 185. Cruz, V.H., et al., *Axl-mediated activation of TBK1 drives epithelial plasticity in pancreatic cancer*. *JCI Insight*, 2019. **4**(9).
 186. Kim, J.Y., et al., *Dissection of TBK1 signaling via phosphoproteomics in lung cancer cells*. *Proc Natl Acad Sci U S A*, 2013. **110**(30): p. 12414-9.
 187. Muvaffak, A., et al., *Evaluating TBK1 as a therapeutic target in cancers with activated IRF3*. *Mol Cancer Res*, 2014. **12**(7): p. 1055-66.
 188. Alam, M., G.M. Hasan, and M.I. Hassan, *A review on the role of TANK-binding kinase 1 signaling in cancer*. *Int J Biol Macromol*, 2021. **183**: p. 2364-2375.
 189. Li, J., et al., *Selective TBK1/IKKi dual inhibitors with anticancer potency*. *Int J Cancer*, 2014. **134**(8): p. 1972-80.
 190. Jiang, Y., et al., *TANK-Binding Kinase 1 (TBK1) Serves as a Potential Target for Hepatocellular Carcinoma by Enhancing Tumor Immune Infiltration*. *Front Immunol*, 2021. **12**: p. 612139.
 191. Revach, O.Y., S. Liu, and R.W. Jenkins, *Targeting TANK-binding kinase 1 (TBK1) in cancer*. *Expert Opin Ther Targets*, 2020. **24**(11): p. 1065-1078.
 192. Ou, Y.H., et al., *TBK1 directly engages Akt/PKB survival signaling to support oncogenic transformation*. *Mol Cell*, 2011. **41**(4): p. 458-70.
 193. Shiozawa, Y., et al., *Human prostate cancer metastases target the hematopoietic stem cell niche to establish footholds in mouse bone marrow*. *J Clin Invest*, 2011. **121**(4): p. 1298-312.
 194. Kim, J.K., et al., *TBK1 regulates prostate cancer dormancy through mTOR inhibition*. *Neoplasia*, 2013. **15**(9): p. 1064-74.
 195. Jiang, Q., et al., *TBK1 promotes thyroid cancer progress by activating the PI3K/Akt/mTOR signaling pathway*. *Immun Inflamm Dis*, 2023. **11**(3): p. e796.
 196. Jin, S., et al., *The m6A demethylase ALKBH5 promotes tumor progression by inhibiting RIG-I expression and interferon alpha production through the IKK ϵ /TBK1/IRF3 pathway in head and neck squamous cell carcinoma*. *Mol Cancer*, 2022. **21**(1): p. 97.
 197. Wang, Y., et al., *The up-regulation of TANK-binding kinase 1 in head and neck squamous cell carcinoma* 2017: *Translational Cancer Research*. p. 679-686.

198. Newman, A.C., et al., *TBK1 kinase addiction in lung cancer cells is mediated via autophagy of Tax1bp1/Ndp52 and non-canonical NF- κ B signalling*. PLoS One, 2012. **7**(11): p. e50672.
199. Wang, X., et al., *Expression and prognostic role of IKBKE and TBK1 in stage I non-small cell lung cancer*. Cancer Manag Res, 2019. **11**: p. 6593-6602.
200. Carr, M., et al., *IKK ϵ and TBK1 in diffuse large B-cell lymphoma: A possible mechanism of action of an IKK ϵ /TBK1 inhibitor to repress NF- κ B and IL-10 signalling*. J Cell Mol Med, 2020. **24**(19): p. 11573-11582.
201. Liu, Y. and S.K. Barta, *Diffuse large B-cell lymphoma: 2019 update on diagnosis, risk stratification, and treatment*. Am J Hematol, 2019. **94**(5): p. 604-616.
202. Zhang, H., et al., *Identification of TBK1 and IKK ϵ , the non-canonical I κ B kinases, as crucial pro-survival factors in HTLV-1-transformed T lymphocytes*. Leuk Res, 2016. **46**: p. 37-44.
203. Cai, H., et al., *IFI16 promotes cervical cancer progression by upregulating PD-L1 in immunomicroenvironment through STING-TBK1-NF- κ B pathway*. Biomedicine & Pharmacotherapy, 2020. **123**: p. 109790.
204. Sun, Q., et al., *TBK1/Ikk ϵ Inhibitor Amlx Blocks Multiple Myeloma Cell Growth in Vitro and In Vivo*. 2018: Blood.
205. Yang, K.M., et al., *Loss of TBK1 induces epithelial-mesenchymal transition in the breast cancer cells by ER α downregulation*. Cancer Res, 2013. **73**(22): p. 6679-89.
206. Jiang, Z., et al., *Targeting HER2(+) breast cancer: the TBK1/IKK ϵ axis*. Oncoscience, 2014. **1**(2): p. 180-2.
207. Deng, T., et al., *shRNA kinome screen identifies TBK1 as a therapeutic target for HER2+ breast cancer*. Cancer Res, 2014. **74**(7): p. 2119-30.
208. (TCGA), G.D.C.G.D.P., *TBK1*.
209. Ancrile, B., K.H. Lim, and C.M. Counter, *Oncogenic Ras-induced secretion of IL6 is required for tumorigenesis*. Genes Dev, 2007. **21**(14): p. 1714-9.
210. Zhu, Z., et al., *Inhibition of KRAS-driven tumorigenicity by interruption of an autocrine cytokine circuit*. Cancer Discov, 2014. **4**(4): p. 452-65.
211. Bodur, C., et al., *The IKK-related kinase TBK1 activates mTORC1 directly in response to growth factors and innate immune agonists*. EMBO J, 2018. **37**(1): p. 19-38.
212. Dhillon, S., *Adagrasib: First Approval*. Drugs, 2023. **83**(3): p. 275-285.
213. Blair, H.A., *Sotorasib: First Approval*. Drugs, 2021. **81**(13): p. 1573-1579.
214. Kitajima, S., et al., *Overcoming Resistance to Dual Innate Immune and MEK Inhibition Downstream of KRAS*. Cancer Cell, 2018. **34**(3): p. 439-452.e6.
215. Yang, S., et al., *Autophagy Inhibition Dysregulates TBK1 Signaling and Promotes Pancreatic Inflammation*. Cancer Immunol Res, 2016. **4**(6): p. 520-30.
216. Jenkins, R.W., et al., *Profiling of PD-1 Blockade Using Organotypic Tumor Spheroids*. Cancer Discov, 2018. **8**(2): p. 196-215.
217. Sun, Y., et al., *Targeting TBK1 to overcome resistance to cancer immunotherapy*. Nature, 2023. **615**(7950): p. 158-167.

218. Mesa, R.A., et al., *SIMPLIFY-1: A Phase III Randomized Trial of Momelotinib Versus Ruxolitinib in Janus Kinase Inhibitor-Naïve Patients With Myelofibrosis*. J Clin Oncol, 2017. **35**(34): p. 3844-3850.
219. Padda, S.K., et al., *A phase 1b study of erlotinib and momelotinib for the treatment of EGFR-mutated, tyrosine kinase inhibitor-naïve metastatic non-small cell lung cancer*. Cancer Chemother Pharmacol, 2022. **89**(1): p. 105-115.
220. Bailly, C., *The potential value of amlexanox in the treatment of cancer: Molecular targets and therapeutic perspectives*. Biochem Pharmacol, 2021. **197**: p. 114895.
221. Khandwala, A., R.G. Van Inwegen, and M.C. Alfano, *5% amlexanox oral paste, a new treatment for recurrent minor aphthous ulcers: I. Clinical demonstration of acceleration of healing and resolution of pain*. Oral Surg Oral Med Oral Pathol Oral Radiol Endod, 1997. **83**(2): p. 222-30.
222. Liu, Y., et al., *Amlexanox, a selective inhibitor of IKBKE, generates anti-tumoral effects by disrupting the Hippo pathway in human glioblastoma cell lines*. Cell Death Dis, 2017. **8**(8): p. e3022.
223. Möller, M., et al., *The Specific IKKε/TBK1 Inhibitor Amlexanox Suppresses Human Melanoma by the Inhibition of Autophagy, NF-κB and MAP Kinase Pathways*. Int J Mol Sci, 2020. **21**(13).
224. Xiong, J., et al., *Amlexanox Enhances Temozolomide-Induced Antitumor Effects in Human Glioblastoma Cells by Inhibiting IKBKE and the Akt-mTOR Signaling Pathway*. ACS Omega, 2021. **6**(6): p. 4289-4299.
225. Vu, H.L. and A.E. Aplin, *Targeting TBK1 inhibits migration and resistance to MEK inhibitors in mutant NRAS melanoma*. Mol Cancer Res, 2014. **12**(10): p. 1509-19.
226. Clark, K., et al., *Use of the pharmacological inhibitor BX795 to study the regulation and physiological roles of TBK1 and IκappaB kinase epsilon: a distinct upstream kinase mediates Ser-172 phosphorylation and activation*. J Biol Chem, 2009. **284**(21): p. 14136-46.
227. Feldman, R.I., et al., *Novel small molecule inhibitors of 3-phosphoinositide-dependent kinase-1*. J Biol Chem, 2005. **280**(20): p. 19867-74.
228. Hasan, M., et al., *Cutting Edge: Inhibiting TBK1 by Compound II Ameliorates Autoimmune Disease in Mice*. J Immunol, 2015. **195**(10): p. 4573-7.
229. Perrior, T.R., et al., *Pyrimidine compounds as inhibitors of protein kinases IKK epsilon and/or TBK-1, processes for their preparation, and pharmaceutical compositions containing them*. 2015, Domainex Limited (GB): United States.
230. Thomson, D.W., et al., *Discovery of GSK8612, a Highly Selective and Potent TBK1 Inhibitor*. ACS Med Chem Lett, 2019. **10**(5): p. 780-785.
231. Asshoff, M., et al., *Momelotinib inhibits ACVR1/ALK2, decreases hepcidin production, and ameliorates anemia of chronic disease in rodents*. Blood, 2017. **129**(13): p. 1823-1830.
232. Barbie, D.A., et al., *Phase 1B Study of Momelotinib Combined With Trametinib in Metastatic, Kirsten Rat Sarcoma Viral Oncogene Homolog-Mutated Non-Small-Cell Lung Cancer After Platinum-Based Chemotherapy Treatment Failure*. Clin Lung Cancer, 2018. **19**(6): p. e853-e859.

233. Harrison, C.N., et al., *Momelotinib versus best available therapy in patients with myelofibrosis previously treated with ruxolitinib (SIMPLIFY 2): a randomised, open-label, phase 3 trial*. *Lancet Haematol*, 2018. **5**(2): p. e73-e81.
234. Ng, K., et al., *Phase 1 dose-escalation study of momelotinib, a Janus kinase 1/2 inhibitor, combined with gemcitabine and nab-paclitaxel in patients with previously untreated metastatic pancreatic ductal adenocarcinoma*. *Invest New Drugs*, 2019. **37**(1): p. 159-165.
235. Zheng, J., et al., *Pharmacokinetics and Disposition of Momelotinib Revealed a Disproportionate Human Metabolite-Resolution for Clinical Development*. *Drug Metab Dispos*, 2018. **46**(3): p. 237-247.
236. Richards, B.a.C.M.a.S.N.a.N.J.a.B.V.a.C.A.a.R.R.a.H.M.a.D.T.a.P.D.a.S., *Cellular and In Vivo Properties of MPI-0485520, a Novel and Potent Small Molecule Inhibitor of IKKe*. *The FASEB Journal*, 2010. **24**(S1): p. 753.6-753.6.
237. Richters, A., et al., *Identification and further development of potent TBK1 inhibitors*. *ACS Chem Biol*, 2015. **10**(1): p. 289-98.
238. Crew, A.P., et al., *Identification and Characterization of Von Hippel-Lindau-Recruiting Proteolysis Targeting Chimeras (PROTACs) of TANK-Binding Kinase 1*. *J Med Chem*, 2018. **61**(2): p. 583-598.
239. Emadi, A. and J.Y. Law. *Acute Myeloid Leukemia (AML)*. 2022 [cited 2023; Available from: <https://www.merckmanuals.com/professional/hematology-and-oncology/leukemias/acute-myeloid-leukemia-aml>].
240. ACS, *Tests for Acute Myeloid Leukemia (AML)*. 2018.
241. Arber, D.A., et al., *The 2016 revision to the World Health Organization classification of myeloid neoplasms and acute leukemia*. *Blood*, 2016. **127**(20): p. 2391-405.
242. Bakst, R.L., et al., *How I treat extramedullary acute myeloid leukemia*. *Blood*, 2011. **118**(14): p. 3785-93.
243. Porcu, P., et al., *Hyperleukocytic leukemias and leukostasis: a review of pathophysiology, clinical presentation and management*. *Leuk Lymphoma*, 2000. **39**(1-2): p. 1-18.
244. Trinkaus, M. *Decision Making in Emergency Critical Care SECTION 7 - Gastrointestinal and Hematological Critical Care 27 Acute Leukemia*. Available from: <https://doctorlib.info/therapy/emergency/28.html>.
245. Miller KB, D.P. and B.E. Hoffman R, Shattil SJ, et al., *Clinical Manifestations of Acute Myeloid Leukaemia*, in *Haematology: Basic Principles and Practice*. 2005, Elsevier. p. 1071-1097.
246. (ACS), A.C.S. *What Are Myelodysplastic Syndromes?* 2018 01/22/2018 [cited 2023; Available from: <https://www.cancer.org/cancer/myelodysplastic-syndrome/about/what-is-mds.html#:~:text=In%20about%201%20in%203,pre%2Dleukemia%20or%20smoldering%20leukemia>].
247. Ezoë, S., *Secondary leukemia associated with the anti-cancer agent, etoposide, a topoisomerase II inhibitor*. *Int J Environ Res Public Health*, 2012. **9**(7): p. 2444-53.

248. Mateos, M.K., et al., *Down syndrome and leukemia: insights into leukemogenesis and translational targets*. *Transl Pediatr*, 2015. **4**(2): p. 76-92.
249. Stabellini, N., et al., *Sex differences in adults with acute myeloid leukemia and the impact of sex on overall survival*. *Cancer Med*, 2022.
250. McHale, C.M., L. Zhang, and M.T. Smith, *Current understanding of the mechanism of benzene-induced leukemia in humans: implications for risk assessment*. *Carcinogenesis*, 2012. **33**(2): p. 240-52.
251. (ACS), A.C.S. *Risk Factors for Acute Myeloid Leukemia (AML)*. 2018 08/21/2018 [cited 2023; Available from: <https://www.cancer.org/cancer/acute-myeloid-leukemia/causes-risks-prevention/risk-factors.html>].
252. Appelbaum, F.R., et al., *Age and acute myeloid leukemia*. *Blood*, 2006. **107**(9): p. 3481-5.
253. Sekeres, M.A., et al., *Time from diagnosis to treatment initiation predicts survival in younger, but not older, acute myeloid leukemia patients*. *Blood*, 2009. **113**(1): p. 28-36.
254. (ASCO), A.S.o.C.O. *Leukemia - Acute Myeloid - AML: Statistics 2022 04/2022* [cited 2023; Available from: <https://www.cancer.net/cancer-types/leukemia-acute-myeloid-aml/statistics#:~:text=The%205%2Dyear%20survival%20rate%20for%20people%2020%20and%20older,see%20Subtypes%20for%20more%20information>).
255. ACS, *Acute Myeloid Leukemia (AML) Subtypes and Prognostic Factors*. 2018.
256. (ASCO), A.x.A.S.o.C.O., *Leukemia - Acute Myeloid - AML: Subtypes*. 2022: Cancer.net.
257. *Organization Emadi, A. and U. EW. Acute Myeloid Leukemia (AML)*. Available from: <https://www.merckmanuals.com/professional/hematology-and-oncology/leukemias/acute-myeloid-leukemia-aml>.
258. Vardiman, J.W., N.L. Harris, and R.D. Brunning, *The World Health Organization (WHO) classification of the myeloid neoplasms*. *Blood*, 2002. **100**(7): p. 2292-302.
259. Burns, A., *Observations on the surgical anatomy of the head and neck*. 1811: cesimadigital.pucsp.br.
260. King, A., *Case of Chloroma*. 1853, PMC/NIH: *Mon J Med Sci*. p. 97-104.
261. Lalayanni, C., et al., *Secondary Acute Myeloid Leukemia (sAML): Similarly Dismal Outcomes of AML After an Antecedent Hematologic Disorder and Therapy Related AML*. *Clin Lymphoma Myeloma Leuk*, 2022. **22**(4): p. e233-e240.
262. Capelli, D., et al., *Secondary Acute Myeloid Leukemia: Pathogenesis and Treatment*. 2022, Exon Publications: Leukemia
263. Walter, R.B., et al., *Significance of FAB subclassification of "acute myeloid leukemia, NOS" in the 2008 WHO classification: analysis of 5848 newly diagnosed patients*. *Blood*, 2013. **121**(13): p. 2424-31.
264. Angelescu, S., et al., *Value of multifaced approach diagnosis and classification of acute leukemias*. *Maedica (Bucur)*, 2012. **7**(3): p. 254-60.

265. Singh, G., *Acute Basophilic Leukemia: Recent Molecular and Diagnostic Update*. Cureus, 2022. **14**(6): p. e26054.
266. Kishtagari, A., R.L. Levine, and A.D. Viny, *Driver mutations in acute myeloid leukemia*. Curr Opin Hematol, 2020. **27**(2): p. 49-57.
267. Chopra, M. and S.K. Bohlander, *The cell of origin and the leukemia stem cell in acute myeloid leukemia*. Genes Chromosomes Cancer, 2019. **58**(12): p. 850-858.
268. Meyer, C., et al., *The MLL recombinome of acute leukemias in 2017*. Leukemia, 2018. **32**(2): p. 273-284.
269. Meyer, C., et al., *The MLL recombinome of acute leukemias in 2013*. Leukemia, 2013. **27**(11): p. 2165-76.
270. Stavropoulou, V., et al., *MLL-AF9 Expression in Hematopoietic Stem Cells Drives a Highly Invasive AML Expressing EMT-Related Genes Linked to Poor Outcome*. Cancer Cell, 2016. **30**(1): p. 43-58.
271. Zhang, J., et al., *p27kip1 maintains a subset of leukemia stem cells in the quiescent state in murine MLL-leukemia*. Mol Oncol, 2013. **7**(6): p. 1069-82.
272. Chang, P.Y., et al., *Binding of the MLL PHD3 finger to histone H3K4me3 is required for MLL-dependent gene transcription*. J Mol Biol, 2010. **400**(2): p. 137-44.
273. Schiller, G.J., *High-risk acute myelogenous leukemia: treatment today ... and tomorrow*. Hematology Am Soc Hematol Educ Program, 2013. **2013**: p. 201-8.
274. Gong, X.Y., et al., *[Characteristics and prognosis in adult acute myeloid leukemia patients with MLL gene rearrangements]*. Zhonghua Xue Ye Xue Za Zhi, 2018. **39**(1): p. 9-14.
275. Drynan, L.F., et al., *Mll fusions generated by Cre-loxP-mediated de novo translocations can induce lineage reassignment in tumorigenesis*. EMBO J, 2005. **24**(17): p. 3136-46.
276. Stubbs, M.C., et al., *MLL-AF9 and FLT3 cooperation in acute myelogenous leukemia: development of a model for rapid therapeutic assessment*. Leukemia, 2008. **22**(1): p. 66-77.
277. Gebru, M.T. and H.G. Wang, *Therapeutic targeting of FLT3 and associated drug resistance in acute myeloid leukemia*. J Hematol Oncol, 2020. **13**(1): p. 155.
278. Wu, M., C. Li, and X. Zhu, *FLT3 inhibitors in acute myeloid leukemia*. J Hematol Oncol, 2018. **11**(1): p. 133.
279. Kottaridis, P.D., R.E. Gale, and D.C. Linch, *Flt3 mutations and leukaemia*. Br J Haematol, 2003. **122**(4): p. 523-38.
280. Meshinchi, S. and F.R. Appelbaum, *Structural and functional alterations of FLT3 in acute myeloid leukemia*. Clin Cancer Res, 2009. **15**(13): p. 4263-9.
281. Daver, N., et al., *Targeting FLT3 mutations in AML: review of current knowledge and evidence*. Leukemia, 2019. **33**(2): p. 299-312.
282. Quentmeier, H., et al., *FLT3 mutations in acute myeloid leukemia cell lines*. Leukemia, 2003. **17**(1): p. 120-4.
283. Wooten, D.J., et al., *Data-Driven Math Model of FLT3-ITD Acute Myeloid Leukemia Reveals Potential Therapeutic Targets*. J Pers Med, 2021. **11**(3).

284. Hermetet, F., et al., *High-fat diet intensifies MLL-AF9-induced acute myeloid leukemia through activation of the FLT3 signaling in mouse primitive hematopoietic cells*. Sci Rep, 2020. **10**(1): p. 16187.
285. Zarrinkar, P.P., et al., *AC220 is a uniquely potent and selective inhibitor of FLT3 for the treatment of acute myeloid leukemia (AML)*. Blood, 2009. **114**(14): p. 2984-92.
286. Ono, R., et al., *Dimerization of MLL fusion proteins and FLT3 activation synergize to induce multiple-lineage leukemogenesis*. J Clin Invest, 2005. **115**(4): p. 919-29.
287. Lavallée, V.P., et al., *The transcriptomic landscape and directed chemical interrogation of MLL-rearranged acute myeloid leukemias*. Nat Genet, 2015. **47**(9): p. 1030-7.
288. Joshi, K., et al., *Leukemia Stem Cells in the Pathogenesis, Progression, and Treatment of Acute Myeloid Leukemia*. Adv Exp Med Biol, 2019. **1143**: p. 95-128.
289. Bewersdorf, J.P. and A.M. Zeidan, *Hyperleukocytosis and Leukostasis in Acute Myeloid Leukemia: Can a Better Understanding of the Underlying Molecular Pathophysiology Lead to Novel Treatments?* Cells, 2020. **9**(10).
290. Parmar, A., et al., *Medical emergency team involvement in patients hospitalized with acute myeloid leukemia*. Leuk Lymphoma, 2013. **54**(10): p. 2236-42.
291. The American Cancer Society, A. *Treatment of Acute Promyelocytic Leukemia (APL)*. 2018; Available from: <https://www.cancer.org/cancer/types/acute-myeloid-leukemia/treating/m3-leukemia.html>.
292. Lichtman, M.A., *A historical perspective on the development of the cytarabine (7days) and daunorubicin (3days) treatment regimen for acute myelogenous leukemia: 2013 the 40th anniversary of 7+3*. Blood Cells Mol Dis, 2013. **50**(2): p. 119-30.
293. Murphy, T. and K.W.L. Yee, *Cytarabine and daunorubicin for the treatment of acute myeloid leukemia*. Expert Opin Pharmacother, 2017. **18**(16): p. 1765-1780.
294. Momparler, R.L., *Optimization of cytarabine (ARA-C) therapy for acute myeloid leukemia*. Exp Hematol Oncol, 2013. **2**: p. 20.
295. Dombret, H. and C. Gardin, *An update of current treatments for adult acute myeloid leukemia*. Blood, 2016. **127**(1): p. 53-61.
296. Rowe, J.M., *The "7+3" regimen in acute myeloid leukemia*. Haematologica, 2022. **107**(1): p. 3.
297. Green, S.D. and H. Konig, *Treatment of Acute Myeloid Leukemia in the Era of Genomics-Achievements and Persisting Challenges*. Front Genet, 2020. **11**: p. 480.
298. Kim, K., et al., *Urgent cytoreduction for newly diagnosed acute myeloid leukemia patients allows acquisition of pretreatment genomic data and enrollment on investigational clinical trials*. Am J Hematol, 2022. **97**(7): p. 885-894.
299. Pastore, D., et al., *FLAG-IDA in the treatment of refractory/relapsed acute myeloid leukemia: single-center experience*. Ann Hematol, 2003. **82**(4): p. 231-5.

300. Schneidawind, D., et al., *Allogeneic hematopoietic cell transplantation with reduced-intensity conditioning following FLAMSA for primary refractory or relapsed acute myeloid leukemia*. *Ann Hematol*, 2013. **92**(10): p. 1389-95.
301. Anderson, E., et al., *Intracellular cytarabine triphosphate in circulating blasts post-treatment predicts remission status in patients with acute myeloid leukemia*. *Exp Hematol*, 2019. **74**: p. 13-18.e3.
302. van Pelt, K., et al., *Administration of low-dose cytarabine results in immediate S-phase arrest and subsequent activation of cell cycling in murine stem cells*. *Exp Hematol*, 2005. **33**(2): p. 226-31.
303. Di Francia, R., et al., *Response and Toxicity to Cytarabine Therapy in Leukemia and Lymphoma: From Dose Puzzle to Pharmacogenomic Biomarkers*. *Cancers (Basel)*, 2021. **13**(5).
304. Quigley, G.J., et al., *Molecular structure of an anticancer drug-DNA complex: daunomycin plus d(CpGpTpApCpG)*. *Proc Natl Acad Sci U S A*, 1980. **77**(12): p. 7204-8.
305. Pang, B., et al., *Drug-induced histone eviction from open chromatin contributes to the chemotherapeutic effects of doxorubicin*. *Nat Commun*, 2013. **4**: p. 1908.
306. Pommier, Y., et al., *DNA topoisomerases and their poisoning by anticancer and antibacterial drugs*. *Chem Biol*, 2010. **17**(5): p. 421-33.
307. Niu, J., D. Peng, and L. Liu, *Drug Resistance Mechanisms of Acute Myeloid Leukemia Stem Cells*. *Front Oncol*, 2022. **12**: p. 896426.
308. Voso, M.T., et al., *MRD in AML: The Role of New Techniques*. *Front Oncol*, 2019. **9**: p. 655.
309. Pollyea, D.A., et al., *Acute Myeloid Leukemia, Version 3.2023, NCCN Clinical Practice Guidelines in Oncology*. *J Natl Compr Canc Netw*, 2023. **21**(5): p. 503-513.
310. Lachowiez, C.A., et al., *Comparison and validation of the 2022 European LeukemiaNet guidelines in acute myeloid leukemia*. *Blood Adv*, 2023. **7**(9): p. 1899-1909.
311. Wang, A.J., et al., *NPM1c impedes CTCF functions through cytoplasmic mislocalization in acute myeloid leukemia*. *Leukemia*, 2020. **34**(5): p. 1278-1290.
312. Sallman, D.A., et al., *Eprenetapopt (APR-246) and Azacitidine in*. *J Clin Oncol*, 2021. **39**(14): p. 1584-1594.
313. Monlish, D.A., S.T. Bhatt, and L.G. Schuettelpelz, *The Role of Toll-Like Receptors in Hematopoietic Malignancies*. *Front Immunol*, 2016. **7**: p. 390.
314. Capitano, M.L., *Toll-like receptor signaling in hematopoietic stem and progenitor cells*. *Curr Opin Hematol*, 2019. **26**(4): p. 207-213.
315. Takizawa, H., S. Boettcher, and M.G. Manz, *Demand-adapted regulation of early hematopoiesis in infection and inflammation*. *Blood*, 2012. **119**(13): p. 2991-3002.
316. Ishimine, N., et al., *Combination of white blood cell count and left shift level real-time reflects a course of bacterial infection*. *J Clin Lab Anal*, 2013. **27**(5): p. 407-11.

317. Harada, T., et al., *Bandemia as an Early Predictive Marker of Bacteremia: A Retrospective Cohort Study*. Int J Environ Res Public Health, 2022. **19**(4).
318. Pession, A., et al., *MLL-AF9 oncogene expression affects cell growth but not terminal differentiation and is downregulated during monocyte-macrophage maturation in AML-M5 THP-1 cells*. Oncogene, 2003. **22**(54): p. 8671-6.
319. Brenner, A.K. and Ø. Bruserud, *Functional Toll-Like Receptors (TLRs) Are Expressed by a Majority of Primary Human Acute Myeloid Leukemia Cells and Inducibility of the TLR Signaling Pathway Is Associated with a More Favorable Phenotype*. Cancers (Basel), 2019. **11**(7).
320. Aluri, J., M.A. Cooper, and L.G. Schuettepelz, *Toll-Like Receptor Signaling in the Establishment and Function of the Immune System*. Cells, 2021. **10**(6).
321. Cannova, J., P. Breslin S J, and J. Zhang, *Toll-like receptor signaling in hematopoietic homeostasis and the pathogenesis of hematologic diseases*. Front Med, 2015. **9**(3): p. 288-303.
322. Liu, X., et al., *IMPDH inhibition activates TLR-VCAM1 pathway and suppresses the development of MLL-fusion leukemia*. EMBO Mol Med, 2023. **15**(1): p. e15631.
323. Rybka, J., et al., *The expression of Toll-like receptors in patients with acute myeloid leukemia treated with induction chemotherapy*. Leuk Res, 2015. **39**(3): p. 318-22.
324. Eriksson, M., et al., *Agonistic targeting of TLR1/TLR2 induces p38 MAPK-dependent apoptosis and NFκB-dependent differentiation of AML cells*. Blood Adv, 2017. **1**(23): p. 2046-2057.
325. Shindo, M., et al., *Toll-Like Receptor Agonists Induce Immunogenicity and Apoptosis of Acute Myeloid Leukemia Cells*. 2007: Blood. p. 160.
326. Liu, Y., et al., *RIP1/RIP3-regulated necroptosis as a target for multifaceted disease therapy (Review)*. Int J Mol Med, 2019. **44**(3): p. 771-786.
327. Liu, S., et al., *Phosphorylation of innate immune adaptor proteins MAVS, STING, and TRIF induces IRF3 activation*. Science, 2015. **347**(6227): p. aaa2630.
328. McWhirter, S.M., et al., *IFN-regulatory factor 3-dependent gene expression is defective in Tbk1-deficient mouse embryonic fibroblasts*. Proc Natl Acad Sci U S A, 2004. **101**(1): p. 233-8.
329. Wouters, B.J., et al., *Double CEBPA mutations, but not single CEBPA mutations, define a subgroup of acute myeloid leukemia with a distinctive gene expression profile that is uniquely associated with a favorable outcome*. Blood, 2009. **113**(13): p. 3088-91.
330. Valk, P.J., et al., *Prognostically useful gene-expression profiles in acute myeloid leukemia*. N Engl J Med, 2004. **350**(16): p. 1617-28.
331. Stirewalt, D.L., et al., *Identification of genes with abnormal expression changes in acute myeloid leukemia*. Genes Chromosomes Cancer, 2008. **47**(1): p. 8-20.
332. Bagger, F.O., S. Kinalis, and N. Rapin, *BloodSpot: a database of healthy and malignant haematopoiesis updated with purified and single cell mRNA sequencing profiles*. Nucleic Acids Res, 2019. **47**(D1): p. D881-D885.

333. BloodSpot. *Overall survival in TCGA AML dataset*. Available from: https://servers.binf.ku.dk/bloodspot/?gene=TBK1&dataset=normal_human_v2_with_AMLs.
334. BloodSpot. *Overall survival in TCGA AML dataset (IKBKE)*.
335. Haferlach, T., et al., *Clinical utility of microarray-based gene expression profiling in the diagnosis and subclassification of leukemia: report from the International Microarray Innovations in Leukemia Study Group*. *J Clin Oncol*, 2010. **28**(15): p. 2529-37.
336. Kohlmann, A., et al., *An international standardization programme towards the application of gene expression profiling in routine leukaemia diagnostics: the Microarray Innovations in LEukemia study prephase*. *Br J Haematol*, 2008. **142**(5): p. 802-7.
337. Gebru, M.T., et al., *Glucocorticoids enhance the antileukemic activity of FLT3 inhibitors in FLT3-mutant acute myeloid leukemia*. *Blood*, 2020. **136**(9): p. 1067-1079.
338. Ctortocka, C., et al., *Functional Proteomics and Deep Network Interrogation Reveal a Complex Mechanism of Action of Midostaurin in Lung Cancer Cells*. *Mol Cell Proteomics*, 2018. **17**(12): p. 2434-2447.
339. Peter, B., et al., *Target interaction profiling of midostaurin and its metabolites in neoplastic mast cells predicts distinct effects on activation and growth*. *Leukemia*, 2016. **30**(2): p. 464-72.
340. Amjad, M., A. Chidharla, and A. Kasi, *Cancer Chemotherapy*. 2023: StatPearls.
341. Lin, J., et al., *Ribosome-Targeting Antibiotics: Modes of Action, Mechanisms of Resistance, and Implications for Drug Design*. *Annu Rev Biochem*, 2018. **87**: p. 451-478.
342. Padma, V.V., *An overview of targeted cancer therapy*. *Biomedicine (Taipei)*, 2015. **5**(4): p. 19.
343. Choi, J., et al., *Haemopedia RNA-seq: a database of gene expression during haematopoiesis in mice and humans*. *Nucleic Acids Res*, 2019. **47**(D1): p. D780-D785.
344. *Lexicon Pharmaceuticals, Inc.* 2023; Available from: <https://www.lexpharma.com/>.
345. Feil, S., N. Valtcheva, and R. Feil, *Inducible Cre mice*. *Methods Mol Biol*, 2009. **530**: p. 343-63.
346. Kaczmarczyk, L., et al., *Slc1a3-2A-CreERT2 mice reveal unique features of Bergmann glia and augment a growing collection of Cre drivers and effectors in the 129S4 genetic background*. *Sci Rep*, 2021. **11**(1): p. 5412.
347. Al Shoyaib, A., S.R. Archie, and V.T. Karamyan, *Intraperitoneal Route of Drug Administration: Should it Be Used in Experimental Animal Studies?* *Pharm Res*, 2019. **37**(1): p. 12.
348. Zhong, Z.A., et al., *Optimizing tamoxifen-inducible Cre/loxP system to reduce tamoxifen effect on bone turnover in long bones of young mice*. *Bone*, 2015. **81**: p. 614-619.

349. Murakami, J. and Y. Shimizu, *Hepatic manifestations in hematological disorders*. Int J Hepatol, 2013. **2013**: p. 484903.
350. Haas, M., et al., *Consensus definitions for glomerular lesions by light and electron microscopy: recommendations from a working group of the Renal Pathology Society*. Kidney Int, 2020. **98**(5): p. 1120-1134.
351. (NCBI), N.L.o.M. *Mesangial hypercellularity*. MedGen UID: 924090; Concept ID: C4281741; HP:0012574]. Available from: <https://www.ncbi.nlm.nih.gov/medgen/924090>.
352. Yamakawa, Y., et al., *Accumulation of brown pigment-laden macrophages associated with vascular lesions in the lungs of cynomolgus monkeys (Macaca fascicularis)*. J Toxicol Pathol, 2016. **29**(3): p. 181-4.
353. Friel, J., et al., *Hierarchy of stroma-derived factors in supporting growth of stroma-dependent hemopoietic cells: membrane-bound SCF is sufficient to confer stroma competence to epithelial cells*. Growth Factors, 2002. **20**(1): p. 35-51.
354. Broudy, V.C., et al., *Interaction of stem cell factor and its receptor c-kit mediates lodgment and acute expansion of hematopoietic cells in the murine spleen*. Blood, 1996. **88**(1): p. 75-81.
355. Li, Q., et al., *Oncogenic Nras has bimodal effects on stem cells that sustainably increase competitiveness*. Nature, 2013. **504**(7478): p. 143-147.
356. Skinner, B.M. and E.E. Johnson, *Nuclear morphologies: their diversity and functional relevance*. Chromosoma, 2017. **126**(2): p. 195-212.
357. Gupta, D., et al., *Differentiation and characterization of myeloid cells*. Curr Protoc Immunol, 2014. **104**: p. 22F.5.1-22F.5.28.
358. Jögi, A., et al., *Cancer cell differentiation heterogeneity and aggressive behavior in solid tumors*. Ups J Med Sci, 2012. **117**(2): p. 217-24.
359. Yuan, S., R.J. Norgard, and B.Z. Stanger, *Cellular Plasticity in Cancer*. Cancer Discov, 2019. **9**(7): p. 837-851.
360. Somerville, T.C. and M.L. Cleary, *Identification and characterization of leukemia stem cells in murine MLL-AF9 acute myeloid leukemia*. Cancer Cell, 2006. **10**(4): p. 257-68.
361. Rashid, M.U. and K.M. Coombs, *Serum-reduced media impacts on cell viability and protein expression in human lung epithelial cells*. J Cell Physiol, 2019. **234**(6): p. 7718-7724.
362. Li, B., et al., *Autophagy mediates serum starvation-induced quiescence in nucleus pulposus stem cells by the regulation of P27*. Stem Cell Res Ther, 2019. **10**(1): p. 118.
363. Frank, M., et al., *Mitophagy is triggered by mild oxidative stress in a mitochondrial fission dependent manner*. Biochim Biophys Acta, 2012. **1823**(12): p. 2297-310.
364. Melanson, B.D., et al., *The role of mRNA decay in p53-induced gene expression*. RNA, 2011. **17**(12): p. 2222-34.
365. Stanley, E.R. and V. Chitu, *CSF-1 receptor signaling in myeloid cells*. Cold Spring Harb Perspect Biol, 2014. **6**(6).

366. Wheeler, E.F., et al., *The v-fms oncogene induces factor independence and tumorigenicity in CSF-1 dependent macrophage cell line*. *Nature*, 1986. **324**(6095): p. 377-80.
367. Rogers, P.B. and E.H. Schwartz, *Generation of Large Numbers of Myeloid Progenitors and Dendritic Cell Precursors from Murine Bone Marrow Using a Novel Cell Sorting Strategy*. *J Vis Exp*, 2018(138).
368. Dubreuil, P., et al., *c-fms expression is a molecular marker of human acute myeloid leukemias*. *Blood*, 1988. **72**(3): p. 1081-5.
369. Ridge, S.A., et al., *FMS mutations in myelodysplastic, leukemic, and normal subjects*. *Proc Natl Acad Sci U S A*, 1990. **87**(4): p. 1377-80.
370. Simonis, A., et al., *Disruption of CSF-1R signaling inhibits growth of AML with inv(16)*. *Blood Adv*, 2021. **5**(5): p. 1273-1277.
371. Aikawa, Y., et al., *Essential role of PU.1 in maintenance of mixed lineage leukemia-associated leukemic stem cells*. *Cancer Sci*, 2015. **106**(3): p. 227-36.
372. Smith, C.C., et al., *A phase 1/2 study of the oral FLT3 inhibitor pexidartinib in relapsed/refractory FLT3-ITD-mutant acute myeloid leukemia*. *Blood Adv*, 2020. **4**(8): p. 1711-1721.
373. Alexiev, B.A., et al., *Myeloid sarcomas: a histologic, immunohistochemical, and cytogenetic study*. *Diagn Pathol*, 2007. **2**: p. 42.
374. Pileri, S.A., et al., *Myeloid sarcoma: clinico-pathologic, phenotypic and cytogenetic analysis of 92 adult patients*. *Leukemia*, 2007. **21**(2): p. 340-50.
375. Singh, A., et al., *Unravelling chloroma: review of imaging findings*. *Br J Radiol*, 2017. **90**(1075): p. 20160710.
376. McCarty, S.M. and D.J. Kuo, *Persistent sacral chloroma in refractory acute myelogenous leukaemia*. *BMJ Case Rep*, 2017. **2017**.
377. Rodrigues, J.R., et al., *Sacral Myeloid Sarcoma Manifesting as Radiculopathy in a Pediatric Patient: An Unusual Form of Myeloid Leukemia Relapse*. *Case Rep Radiol*, 2018. **2018**: p. 4257012.
378. Johansson, B., et al., *Granulocytic sarcomas in body cavities in childhood acute myeloid leukemias with 11q23/MLL rearrangements*. *Genes Chromosomes Cancer*, 2000. **27**(2): p. 136-42.
379. Neff, T., et al., *Polycomb repressive complex 2 is required for MLL-AF9 leukemia*. *Proc Natl Acad Sci U S A*, 2012. **109**(13): p. 5028-33.
380. Chen, X., et al., *Publisher Correction: MLL-AF9 initiates transformation from fast-proliferating myeloid progenitors*. *Nat Commun*, 2020. **11**(1): p. 681.
381. Bisschop, M.M., et al., *Extramedullary infiltrates at diagnosis have no prognostic significance in children with acute myeloid leukaemia*. *Leukemia*, 2001. **15**(1): p. 46-9.
382. Kaur, V., et al., *Clinical characteristics, molecular profile and outcomes of myeloid sarcoma: a single institution experience over 13 years*. *Hematology*, 2018. **23**(1): p. 17-24.
383. Byrd, J.C., et al., *Extramedullary leukemia adversely affects hematologic complete remission rate and overall survival in patients with t(8;21)(q22;q22):*

- results from Cancer and Leukemia Group B 8461. *J Clin Oncol*, 1997. **15**(2): p. 466-75.
384. Byrd, J.C., et al., *Extramedullary myeloid cell tumors in acute nonlymphocytic leukemia: a clinical review*. *J Clin Oncol*, 1995. **13**(7): p. 1800-16.
385. Rossi, M., et al., *Warning regarding hematological toxicity of tamoxifen activated CreERT2 in young Rosa26CreERT2 mice*. *Sci Rep*, 2023. **13**(1): p. 5976.
386. GlycoMimetics, I. *Uproleselan*. 2023; Available from: <https://glycomimetics.com/pipeline/programs/uproleselan/>.
387. Barbier, V., et al., *Endothelial E-selectin inhibition improves acute myeloid leukaemia therapy by disrupting vascular niche-mediated chemoresistance*. *Nat Commun*, 2020. **11**(1): p. 2042.
388. Pezeshkian, B., et al., *Leukemia Mediated Endothelial Cell Activation Modulates Leukemia Cell Susceptibility to Chemotherapy through a Positive Feedback Loop Mechanism*. *PLoS One*, 2013. **8**(4): p. e60823.
389. Chiu, J.J., et al., *Mechanisms of induction of endothelial cell E-selectin expression by smooth muscle cells and its inhibition by shear stress*. *Blood*, 2007. **110**(2): p. 519-28.
390. Li, J., et al., *Sensitizing leukemia stem cells to NF- κ B inhibitor treatment in vivo by inactivation of both TNF and IL-1 signaling*. *Oncotarget*, 2017. **8**(5): p. 8420-8435.
391. Milne, T.A., et al., *Menin and MLL cooperatively regulate expression of cyclin-dependent kinase inhibitors*. *Proc Natl Acad Sci U S A*, 2005. **102**(3): p. 749-54.
392. Xia, Z.B., et al., *The MLL fusion gene, MLL-AF4, regulates cyclin-dependent kinase inhibitor CDKN1B (p27kip1) expression*. *Proc Natl Acad Sci U S A*, 2005. **102**(39): p. 14028-33.
393. Li, L., et al., *SQSTM1 is a pathogenic target of 5q copy number gains in kidney cancer*. *Cancer Cell*, 2013. **24**(6): p. 738-50.
394. Shinohara, H., et al., *TAK1 maintains the survival of immunoglobulin λ -chain-positive B cells*. *Genes Cells*, 2016. **21**(11): p. 1233-1243.
395. Podder, B., et al., *TAK1 suppresses RIPK1-dependent cell death and is associated with disease progression in melanoma*. *Cell Death Differ*, 2019. **26**(12): p. 2520-2534.
396. Geng, J., et al., *Regulation of RIPK1 activation by TAK1-mediated phosphorylation dictates apoptosis and necroptosis*. *Nat Commun*, 2017. **8**(1): p. 359.
397. Li, S., et al., *Inhibition of the sonic hedgehog pathway activates TGF- β -activated kinase (TAK1) to induce autophagy and suppress apoptosis in thyroid tumor cells*. *Cell Death Dis*, 2021. **12**(5): p. 459.
398. the, N.R.C.U.C.f.t.U.o.t.G.f. and C.a.U.o.L. *Animals, Guide for the Care and Use of Laboratory Animals*. 2011.
399. Zhang, L., et al., *Ripk3 signaling regulates HSCs during stress and represses radiation-induced leukemia in mice*. *Stem Cell Reports*, 2022. **17**(6): p. 1428-1441.

400. Ventura, A., et al., *Restoration of p53 function leads to tumour regression in vivo*. *Nature*, 2007. **445**(7128): p. 661-5.
401. Janowska-Wieczorek, A., et al., *Platelet-derived microparticles bind to hematopoietic stem/progenitor cells and enhance their engraftment*. *Blood*, 2001. **98**(10): p. 3143-9.
402. Paigen, B., et al., *Variation in susceptibility to atherosclerosis among inbred strains of mice*. *Atherosclerosis*, 1985. **57**(1): p. 65-73.
403. Montecino-Rodriguez, E. and K. Dorshkind, *Use of Busulfan to Condition Mice for Bone Marrow Transplantation*. *STAR Protoc*, 2020. **1**(3): p. 100159.
404. Almosaileakh, M. and J. Schwaller, *Murine Models of Acute Myeloid Leukaemia*. *Int J Mol Sci*, 2019. **20**(2).
405. Hsieh, M.M., et al., *Low-dose parenteral busulfan provides an extended window for the infusion of hematopoietic stem cells in murine hosts*. *Exp Hematol*, 2007. **35**(9): p. 1415-20.
406. Mather, J.P. and P.E. Roberts, *Introduction to Cell and Tissue Culture: Theory and Technique* 1ed. 1998: Springer. 258.
407. Anderson, S.J., et al., *Inhibition of T-cell receptor beta-chain gene rearrangement by overexpression of the non-receptor protein tyrosine kinase p56lck*. *EMBO J*, 1992. **11**(13): p. 4877-86.
408. Feyerabend, T.B., et al., *Deletion of Notch1 converts pro-T cells to dendritic cells and promotes thymic B cells by cell-extrinsic and cell-intrinsic mechanisms*. *Immunity*, 2009. **30**(1): p. 67-79.
409. Hankenson, F.C., et al., *Evaluation of tail biopsy collection in laboratory mice (Mus musculus): vertebral ossification, DNA quantity, and acute behavioral responses*. *J Am Assoc Lab Anim Sci*, 2008. **47**(6): p. 10-8.
410. Ramiro, T. and V.M. Kasimov. *Re: How much DNA template (5.7ng/ul) should I be using during 20ul PCR reaction?* 2018; Available from: https://www.researchgate.net/post/How_much_DNA_template_57ng_ul_should_I_be_using_during_20ul_PCR_reaction/5c1273cbaa1f09703932558a/citation/download.
411. Qiagen. *How do I perform a DNA precipitation to concentrate my sample?* [cited 2023; Available from: <https://www.qiagen.com/us/resources/faq?id=5d591b8b-968a-4a17-849f-9d0f719b40af&lang=en>].
412. GraphPad Software, L., *GraphPad Prism version 9.3.1 for Windows*. 2023: San Diego, California USA, www.graphpad.com.
413. BioRender. *BioRender.com*. 2023; Created with BioRender.com]. Available from: <https://www.biorender.com/>.
414. (MCE), M., *MedChemExpress (MCE)*. 2023.
415. Software, F., *FlowJo™ Software for Windows, Version 10.8.1* . Ashland, OR: Becton, Dickinson and Company; 2023. <https://www.flowjo.com/>.

VITA

The author, Austin Runde, was born in Aurora, IL on September 15, 1998 to Dan and Janet Runde. He attended Loyola University Chicago where he earned a Bachelor of Science, *cum laude*, in Molecular Biology in May of 2021. After graduation, Runde matriculated into the Loyola University Chicago Stritch School of Medicine master's degree (MS) program and began his graduate education in the Cellular and Molecular Oncology (CMO) program under the mentorship of Dr. Jiwang Zhang.

Runde's thesis work has served to support the Zhang lab's application for an R01 grant.

After completion of his graduate studies, Runde will matriculate into the Loyola University Chicago Stritch School of Medicine's Doctor of Medicine (MD) program, continuing to pursue his dream of becoming a pediatric hematologist-oncologist.